Abstract

Quantum dots (QDs) have attracted an increasing attention in the last decade over many conventional organic dyes. This is due to their unique optical properties including broad absorption spectra, high photostability, and size-tunable photoluminescence (PL). However, some toxicity concerns associated with traditional quantum dots have hindered their wide applicability. Interestingly, silicon quantum dots (SQDs) have been shown to be more advantageous than most of QDs thanks to their excellent biocompatibility and biodegradability, low cytotoxicity, and versatile surface functionalization capability. Thus, SQDs are promising candidates for various biological and biomedical applications such as bioimaging, biosensing, and photodynamic therapy. Unfortunately, only a few studies in literature investigated factors that impact the optical properties of SQDs. In this thesis, we studied the impact of functionalization of ultra-small SQDs (< 2 nm diameter) with different aromatic fluorophores and/or spacers as a means to control their optical properties. We first functionalized the SQDs with phenanthrene, pyrene, and perylene fluorophores through a conjugated spacer which led to an efficient energy transfer from the fluorophores to the SQDs core. As a result, the photoluminescence of the SQDs was red- or blue-shifted and its emission quantum efficiency (QE) was moderately enhanced depending on the fluorophore type. Furthermore, we investigated the impact of different spacers, e.g. N-propylurea and propylamine spacers, on controlling the optical properties of SQDs in which perylene dye was utilized as the capping agent. The nature of spacer played a vital role influencing the interaction of the aromatic dye with the electronic wave function of SQDs. Energy transfer was proven to be the predominant process when propylurea spacer was utilized, while propylamine spacer was found to facilitate electron transfer process. Finally, SQDs were functionalized with different fluorescein and rhodamine derivatives using different spacers that vary in length, chemical nature, and attachment position with the dye. This led to an efficient energy and/or electron transfer in all dyad systems leading to an enhanced QE and photostability for at least one year. To demonstrate the potential application of the functionalized SQDs for bioimaging applications, they were examined for fluorescent imaging of HeLa, HEK293, and U2OS cells.

Keywords

Quantum Dots - Silicon Quantum Dots – Energy Transfer – photoinduced Electron Transfer - Förster energy transfer – Quantum Confinement – Bioimaging – Surface States – HeLa Cells – U2OS cells

Summary for Lay Audience

Cancer is a complex group of individual diseases which differ in causes and effects. The Canadian Cancer Society sadly estimates that nearly 1 in 2 Canadians is expected to get cancer in their lifetime. All types of cancers start in our cells. Unfortunately, there is a lack of tools that can enable the early detection of very limited quantities of cancer inside the body and thus they are left without treatment for long time. As a result, cancer cells would spread into nearby tissues or organs. In this thesis, we have made a new suite of silicon nanocrystals (so called silicon quantum dots) and investigated their potential applications as biomarkers for the bioimaging of cancerous cells. We have also studied their photostability and cytotoxicity. Interestingly, the silicon quantum dots (SQDs) reported in this thesis showed promising results when used for *in vitro* fluorescent imaging of cervical cancerous HeLa cells and human bone cancerous U2OS cells. These SQDs were of low toxicity and exhibited a high photostability for at least one year. We are now aiming to further develop the properties of these SQDs using synthetic methods to allow for their use as photodynamic therapy agents for the apoptosis of cancer cells.

Co-Authorship Statement

Chapter 2. Tuning the Optical Properties of Silicon Quantum Dots via Surface Functionalization with Conjugated Aromatic Fluorophores.

This chapter has been published in Scientific Reports**,** volume 8, Article number: 3050 (2018).

Authors. Mohammed Abdelhameed, Diego Rota Martir, Shalimar Chen, William Z. Xu, Olabode O. Oyeneye, Subrata Chakrabarti, Eli Zysman-Colman & Paul A. Charpentier

Mohammed Abdelhameed performed the syntheses and characterization of all products. Diego Rota Martir and Eli Zysman-Colman performed the photophysical measurements and data interpretation of the photophysical data. Shalimar Chen and Subrata Chakrabarti helped in the cellular imaging study and the cytotoxicity assessment. **Mohammed Abdelhameed** and Paul A. Charpentier wrote the manuscript. William Z. Xu Olabode and O. Oyeneye edited and revised the manuscript. All authors reviewed the manuscript.

Chapter 3. Energy/Electron Transfer Switch for Controlling Optical Properties of Silicon Quantum Dots

This chapter has been published in Scientific Reports**,** Article number: 17068 (2018).

Authors. Mohammed Abdelhameed, Shawkat Aly, Jeremy T. Lant, Xiaoran Zhang & Paul Charpentier

Mohammed Abdelhameed and Shawkat Aly carried out the synthesis and photophysical characterization of the materials. Jeremy T. Lant performed the cellular imaging study. Xiaoran Zhang helped in the synthesis of the materials. **Mohammed Abdelhameed**, Shawkat Aly, and Paul Charpentier wrote the manuscript. All authors reviewed the manuscript.

Chapter 4. Impact of the Chemical Nature and Position of Spacers on Controlling the Optical Properties of Silicon Quantum Dots

This chapter has been published in Phys. Chem. Chem. Phys, , 2019,21, 17096-17108.

Authors. Mohammed Abdelhameed, Shawkat Aly, Partha Maity, Emad Manni, Omar F. Mohammed, Paul A. Charpentier

Mohammed Abdelhameed carried out the synthesis for all products. **Mohammed Abdelhameed** and Shawkat Aly performed the photophysical characterization of the materials and wrote the manuscript. Emad Manni performed the cellular imaging study. Partha Maity and Omar F. Mohammed carried out the Femto-Second Transient Absorption measurements.

Chapter 5. Controlling the Surface-defect-state Photoluminescence in Ultra-Small Silicon Quantum Dots Via Spacers

Authors. Mohammed Abdelhameed, Shawkat Aly, Partha Maity, Omar F. Mohammed, Paul A. Charpentier

Mohammed Abdelhameed carried out the synthesis for all products. **Mohammed Abdelhameed** and Shawkat Aly performed the photophysical characterization of the materials and wrote the manuscript. Partha Maity and Omar F. Mohammed carried out the Femto-Second Transient Absorption measurements.

Acknowledgments

I would like to thank Professor Paul Charpentier for giving me the opportunity to pursue my PhD in his laboratory. I especially thank him for his guidance and support. His advices given to me were greatly appreciated.

Special thanks to Dr. Shawkat Aly for his great help and advice during my graduate studies.

I would like to thank all of my colleagues and University staff, who all significantly contributed to my training and understanding of chemical research: Dr. William Z. Xu, Dr. Wei Wu, Dr. Anil Jahawar, David Hiscott, Devin Machin, Shidokht Nazari, Dr. Shalimar Chen, Dr. Subrata Chakrabarti, Dr. Omar F. Mohammed, Jeremy T. Lant, Xiaoran Zhang, Dr. Lee-Ann Briere, and Anouar Elofir.

I would like also to thank my family for their support during all of my studies. Finally, I would like to thank the University of Western Ontario for having admitted me to the Ph.D. program and to NSERC Discovery (Natural Sciences and Engineering Research Council) and OGS (Ontario Graduate Scholarships) for their financial support which was absolutely essential.

Table of Contents

List of Tables

List of Figures

List of Abbreviations

nm	Nanometer
ns	Nanosecond
QD	Quantum Dots
SQD	Silicon Quantum Dots
PL	Photoluminescence
S_0	singlet ground state
S_1	first singlet excited state
T_1	first triplet excited state
λ	wavelength
A	absorption
UV	ultraviolet
Φ	quantum yield
τ	lifetime
NIR	Near Infrared
TEM	Transmission electron microscopy
PET	Photoinduced electron transfer
ET	Energy Transfer
µs	microsecond
FRET	Förster resonance energy transfer
K	Kelvin
k_{ET}	rate of energy transfer
$τ_p$	phosphorescence lifetime
$τ_F$	fluorescence lifetime

Chapter 1

1 Background and Theory

1.1 Background

Nowadays, one of the big challenges the world faces is the rising demand for energy. The U.S. Energy Information Administration (EIA) predicts that that world energy consumption will grow by 28% between 2015 and 2040.[1] Currently most of the world's energy supply comes from fossil fuels, such as coal, gas and oil which leads to several environmental problems generated by burning these fuels. Alternatively, renewables are expected to be the fastest-growing energy source, with consumption increasing by an average 2.3% per year between 2015 and 2040. Some examples of renewable energy sources are solar energy, wind energy, hydropower, geothermal energy, and biomass energy. These sources are considered the most sustainable and promising energy solutions to overcome many of the environmental problems caused by using fossil fuels. Solar energy is of particular interest as one hour of the whole sun illumination is equivalent to the yearly energy consumption of our world today.[2] The sunlight is dispersed; hence the light needs to be captured, stored and converted to other forms of energy such as electrical or chemical to be useful. The latter process is similar to green plants in which they absorb the sunlight and the absorbed energy is converted into chemical energy via a complex series of electron and energy transfer processes. In the light of this concept, several biomedical and optoelectronic applications can be implemented and improved. To do so, we need to synthesize and optimize the optical properties of new materials that can utilize the sunlight efficiently and develop a full understanding of the photoinduced energy and electron transfer processes that occur.

Quantum dots (QDs), are semiconductor nanocrystals with average diameters in the range of 2-10 nanometers (10-50 atoms), have attracted an increasing attention in the last two decades because of their unique optoelectronic properties which made them ideal candidates for a wide range of potential applications including photovoltaics, light-emitting diodes (LEDs), bioimaging, photodynamic therapy, and biosensing. Quantum dots produce

monochromatic light, so they can be more efficient than light sources which must be color filtered.[3]

1.2   Fluorophores

Fluorophores are fluorescent materials that have the ability to absorb the light energy of a specific wavelength and re-emit it at a longer wavelength. The absorbed light wavelength, energy/electron transfer efficiency, and the time a fluorophore spends in the excited state before returning to the ground state by emitting a photon (fluorescence lifetime) depend on the fluorophore structure and interaction with surrounding molecules.

The most frequently used fluorophores today are organic dyes, which are widely used in several biological and biochemical applications.[4] Although there are several reviews in literature comparing the properties of quantum dots and organic dyes, a comparison between the two is not widely understood. In comparison to conventional organic dyes, fluorescent quantum dots are endowed with several attractive properties as shown in Table 1-1.[5,6,7]

Table 1-1 comparison between Organic dyes and SQDs

Property	Organic dyes	QDs
Absorption profile	Narrow, discrete bands, FWHM ranges from 35 nm to 80–100 nm	Broad, unsymmetrical profile, and increase steadily towards UV region
Emission profile	Asymmetric, FWHM 35 nm to 70–100 nm	Gaussian profile, FWHM, 30–90 nm
Stokes shift	Usually less than 50 nm	Usually less than 100 nm
Quantum yield	0.5–1 (visible), 0.05–0.2 (NIR)	0.1–0.8 (visible), 0.2–0.7 (NIR)
Fluorescent lifetimes	1–5 ns	5–100 ns, up to ms for some red QDs.
Photochemical stability	Sufficient in the visible region, but can be insufficient for NIR dyes	High, sufficient in both visible and NIR regions
Multiple colors	Possible by varying molecular structure	Adjustable by varying size

Quantum Dots

Quantum dots (QDs) have been shown to exhibit several unique optical properties which include strong absorption, size-tunable photoluminescent (PL) emission, high quantum yield (QY) and high stability against photobleaching.[4] This is assigned to the quantum confinement effect [5] which occurs due to changes in the atomic structure from the ultra-small length scale of the energy band structure.[7] As a result of the change in the size, electrons respond by adjusting their energy (Figure 1-1). This phenomenon is known as the quantum-size effect.
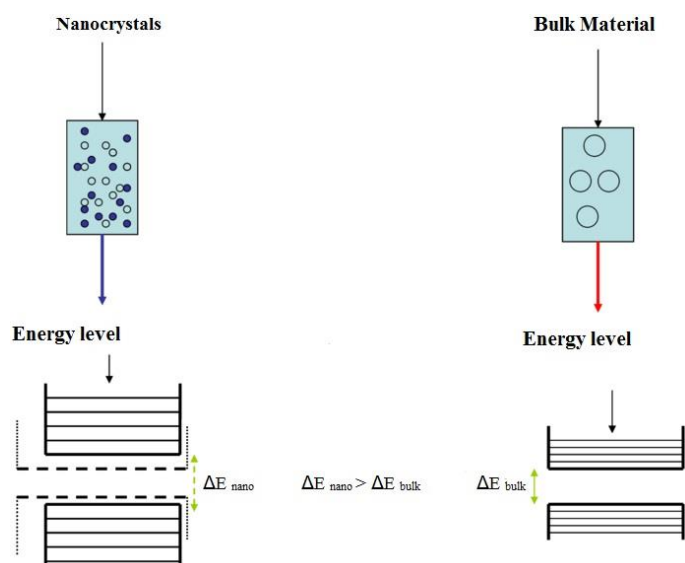
Figure 1-1. The quantum confinement effect is responsible for the increase of energy difference between energy states and band gap.

The quantization effects become most important when the particle size of a semiconductor is smaller than the semiconductor Bohr exciton radius which makes materials properties size dependent.[8] The Bohr radius of a particle (aB) is defined as:

$$a\text{B} = \varepsilon \frac{m}{m^*} \, a_0 \qquad\qquad \text{Equation 1}$$

where ε is the dielectric constant of the material, m* is the mass of the particle, m is the rest mass of the electron, and a_0 is the Bohr radius of the hydrogen atom.

Generally, as the size of the QDs decrease, the difference in energy between the highest valence band and the lowest conduction band increases. More energy would then be needed to excite the dot, and concurrently, more energy is released when the crystal returns to its ground state, resulting in a color shift from red to blue in the emitted light. As a result of this phenomenon, quantum dots can emit any color of light from the same material simply by changing the dot size (Figure 1-2). Additionally, because of the high level of control possible over the size of the nanocrystals produced, quantum dots can be tuned during manufacturing to emit any color of light.[9]
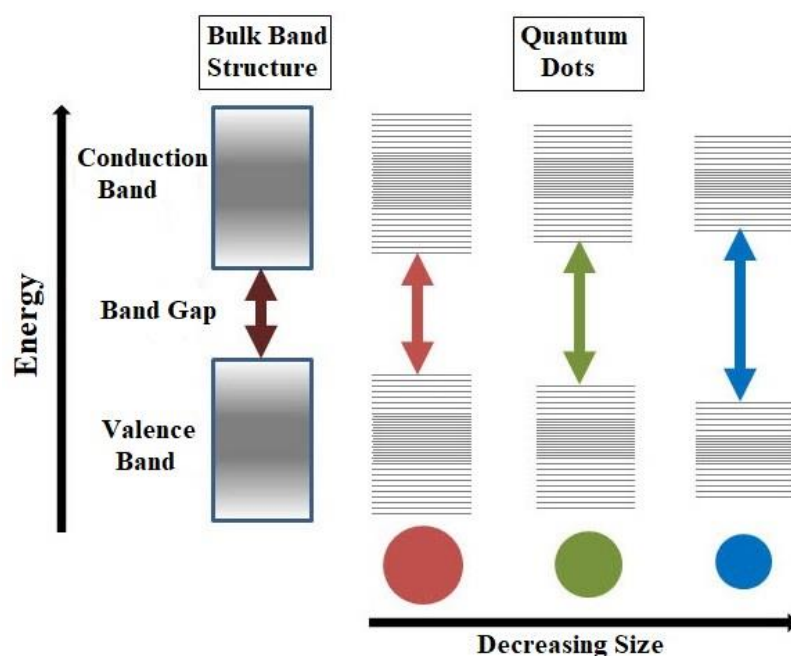
Figure 1-2. Splitting of energy levels in quantum dots due to the quantum confinement effect.

Silicon Quantum Dots (SQDs)

Nanocrystalline silicon quantum dots (SQDs) have recently attracted considerable interest as silicon is abundant, nontoxic and biodegradable.[10,11,12,13] The optical and electronic properties of SQDs are dramatically dependent on the diameter of the dots. The SQDs exhibit diameters less than the Bohr radius of exciton (~5 nm). Silicon Quantum Dots (SQDs) are more advantageous than most QDs due to their biocompatibility and

biodegradability which make them excellent candidates for several biomedical applications.

Effect of capping agents

Surface properties of SQDs are of particular importance in defining the photophysical properties of the SQDs because of the lack of a lattice-matched semiconductor barrier layer. The different potential barriers affect the photoluminescence (PL) properties, including the emission wavelength, quantum yield (QY), and fluorescence lifetime (τ_f). [14]

In terms of the emission profile, the absence of a semiconductor shell reduces the degree of exciton confinement in the core and broadens the emission peak. In practice, SQDs prepared via colloidal solution methods are predominantly blue-green in color, whilst red dots with broad emission can only be prepared via high temperature or etching related methods. In addition, there have been attempts to red-shift the emission profile of blue emitting SQDs by doping with substituent atoms.[15,16] Because of the small size of SQDs, any dopant atoms incorporated are present at concentrations that would be considered 'heavy doping', resulting in sub-populations of doped and undoped SQDs.[17,18]

In terms of quantum yield, the existence of defects and imperfections at the surface of SQDs can affect QY by providing alternative decay pathways. In most cases, additional decay pathways associated with surface capping ligands may become the dominant factor of causing a reduction in the QY,[19] and thus lead to the appearance of subsidiary blue/green emission peaks via surface-associated recombination.[14] Interestingly, certain electron donating groups including nitrogen containing species at the surface strongly enhance the QY of SQDs.[20] It was suggested that surface functionalization of SQDs with organic ligands has led to distortion of the electronic structure.[21] Oxidation of larger SQDs has been shown to affect the crystallinity and core diameter of the Si nanocrystals, reducing the QY and blue-shifting the wavelength of emission peak.[22] However, the functionalization of the SQDs surface with an organic monolayer can prevent the long-term oxidation, providing more photostability.[23]

In terms of lifetime, short fluorescence lifetimes (order of a nanosecond) in SQDs is often associated with core-related recombination.[24] Much longer lifetimes (order of milliseconds) in SQDs has been observed, which was suggested to be due to the existence of ultrafast trapping of excited carriers in surface states, preventing core recombination.[25]

1.3 Synthesis of SQDs

Many methods have been developed for preparing colloidal silicon quantum dots (SQDs). These methods can be classified into 'top-down' approaches in which silicon is broken down to smaller nanoscale pieces, or 'bottom-up' approach that rely on self-assembly processes using molecular silicon precursor species.

Etching of bulk silicon

This method is one of the most popular methods to prepare SQDs. It was first demonstrated by Sailor *et al*. with a mixture of HF and H_2O_2 in order to etch porous silicon electrochemically with the aid of ultrasound, and then create a luminescent colloidal suspension of silicon nanocrystals.[26] This method has been widely used because of its simplicity.[27,28] Recently, it was shown to produce silicon nanomaterials with controlled emission wavelengths by etching silicon powder with the assistance of ultrasound and a combination of HNO_3–HF.

Kang *et al.* developed the etching method where the color was tunable from blue to red as determined by the size of the particles (Figure 1-3). In this approach, a graphite rod was used as the anode and silicon wafer as the cathode. Polyoxometalates was a key in this method because of their ability to be an electron donor and acceptor simultaneously. Controlling the size of the nanoparticles was done by altering the current density upon HF/H_2O_2 etching, which produced size- and shape-controlled hydrogen terminated silicon nanoparticles with size ranging from 1–4 nm and emission peak between 450–700 nm.
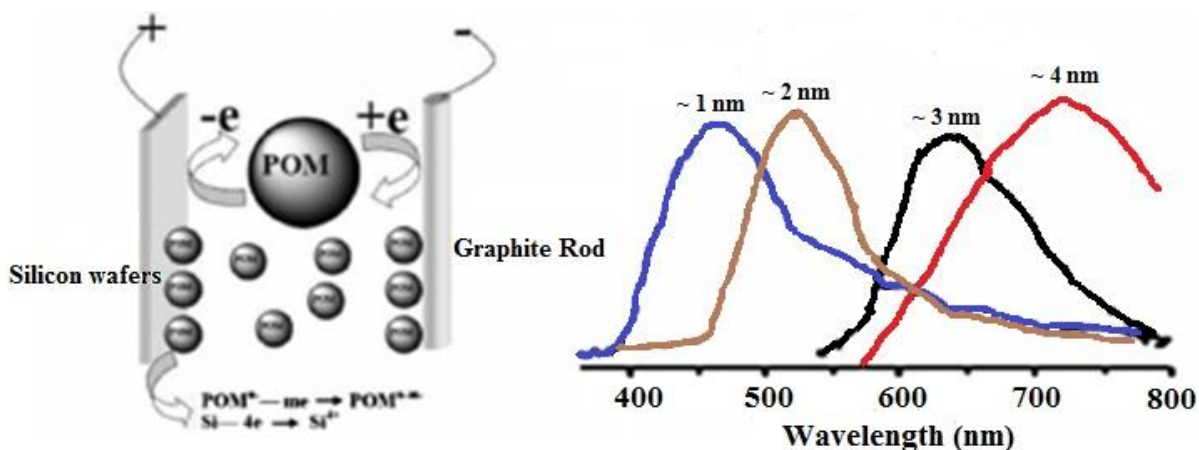
Figure 1-3. Electrochemical etching process of preparing colloidal Si NCs (modified from ref. 29)

The etching method was further modified for environmental considerations in which a mixture of H_2O_2 and ethanol replaced the HNO_3–HF. This method produced oxide coated silicon nanocrystals of 1–3 nm with a wide spectrum of colors were obtained.

Breaking down silicon rich oxides

This method is based on the breakdown of silicon rich oxides containing silicon nanocrystals (Figure 1-4). The strategy was first reported by Liu *et al.* where colloidal silicon nanocrystals were obtained by etching away the oxide layer from thermally annealed, amorphous, commercial SiO_x powder.[20,29] The size of the nanocrystals ranged from 2 to 16 nm depending on etching conditions as confirmed by TEM.
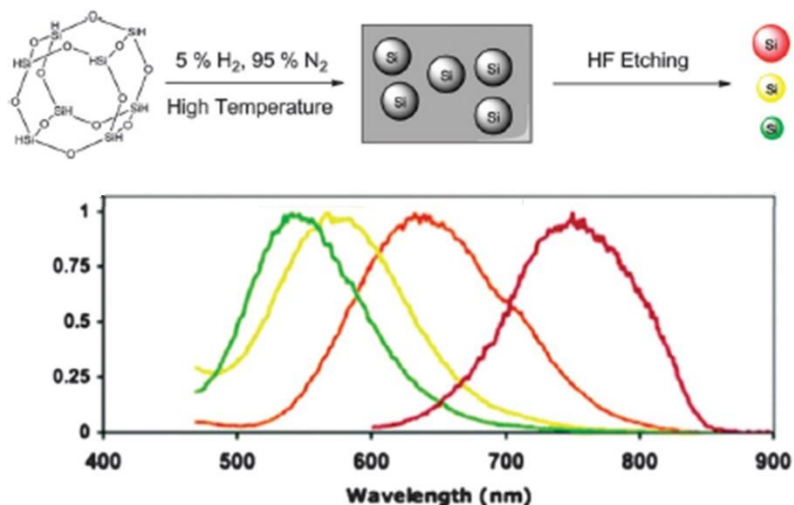
Figure1-4. Preparation of colloidal silicon nanocrystals by breaking down silicon rich oxides containing nanoparticles within them (modified from ref. 30)

Hessel *et al*. utilized thermal decomposition of hydrogen silsesquioxane to produce bulk amount of silicon rich oxides as thin films under high temperature.[30,31,32,33] This was followed by controlled HF etching to give colloidal, hydride terminated silicon quantum dots with emission wavelength tunable in the entire visible spectrum.

Advantages and drawbacks

Advantages: 1) good compatibility with studies of flat or porous silicon structures in terms of procedures used and techniques required. 2) good control of emission wavelength that cannot be easily achieved by other methods.

Drawbacks: 1) high concentration of HF (48% applied in some cases). 2) relative harsh conditions required for the heat treatment of silicon rich oxides is also critical for successful generation of nanoparticles within them before the etching step. Both issues impeded the progress towards large scale production or wide applicability, because of the high safety risk involved and specific techniques required for the processes.

The bottom-up approach

Solution based precursor reduction.

This method uses reducing agents in the presence of silane precursors in solution. It was first demonstrated by Heath *et al.* in 1992, in which polydispersed silicon nanoparticles were produced by mixing $SiCl_4$ and octyltrichlorosilane under high temperature and pressure.[34]

Because of the simplicity to produce silicon nanomaterials using this approach, numerous factors of this method have been established. For example, sodium naphthalenide was used as the reducing agent and $SiCl_4$ in glyme solution.[35] Additionally, sodium was a reducing agent and tetraethyl orthosilicate (TEOS) using several types of reactors (Figure 1-5).[36] The size of the silicon nanocrystals by both methods was in the range of several nanometers with visible blue luminescence. However, the poor control of the particle size was a main issue in this method, with particle diameter ranging over tens of nanometers. Surfactant molecules addition to the reaction mixture, to create inverse micelle environments assisted, assisted to control the size by reducing particle size distribution. This approach was first developed by Wilcoxon *et al.*,[37] and more recently advanced by Tilley *et al.[23,38]*

In a typical experiment, tetraoctylammonium bromide (TOAB), a phase transfer agent and surfactant, stabilized the halogenated silane precursors in toluene, allowing relatively homogeneous precipitation of silicon nanocrystals within the inverse micelle upon addition of lithium aluminum hydride. This method produced hydrogen terminated silicon nanocrystals with narrow size distribution. This method generally produces only blue emission nanocrystals.
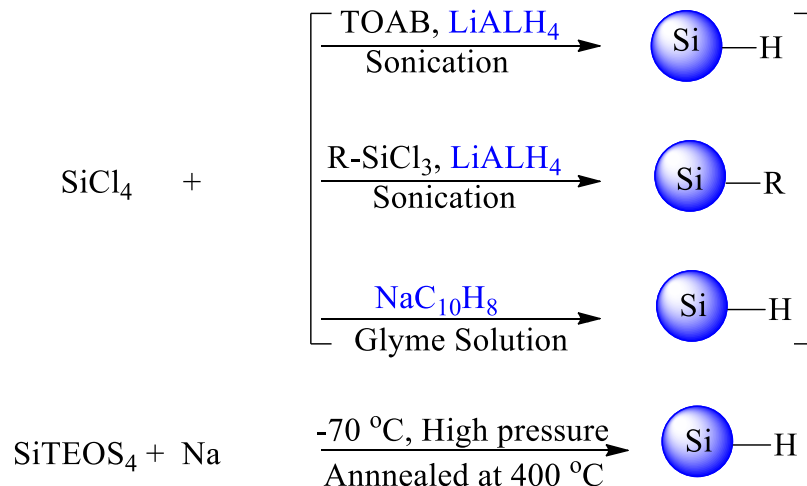
Figure 1-5. Preparation of colloidal silicon nanocrystals via solution-based precursor reduction.

Zintl salt-based approaches.

In this approach, silicon Zintl salts (i.e. ASix, A = Na, K, Mg etc.) are utilized to produce silicon nanocrystals. The silicon-Zintl salt is reacted with silicon halides, or bromine gas. Kauzlarich *et al.* prepared silicon nanocrystals via reactions between potassium silicide (KSi) and $SiCl_4$ in boiling glyme or diglyme solution (Figure 1-6).[39] Another method was developed by sodium silicide (NaSi) and ammonium bromide (NH_4Br). Both preparation methods gave blue luminescent silicon nanocrystals with average size of ~ 4– 5 nm.[40]
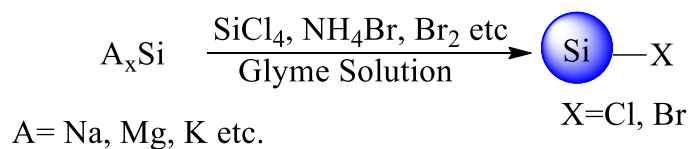
Figure 1-6. Zintl salts based synthetic methods of preparing Si QDs.

Advantages and drawbacks.

Advantages: 1) The bottom-up methods are more readily performed in solution. 2) Most of the used reagents and equipment needed for the preparation of the silicon nanoparticles are common and compatible with conventional bench top chemistry. 3) Surface chemistry of the particles was made more easily accessible which is important for the both preparation and characterization.

Drawbacks: 1) This method produces nanoparticles which emits only blue green colours. 2) The relatively low quantum yield of the nanomaterials prepared using bottom up approach usually is still considered a challenge with quantum yield rarely exceeding 15%.

Precursor decomposition and re-assembly

This class involves the decomposition precursor species containing silicon heteroatoms and re-assembly processes to form Si QDs. This method usually involves both the top-down and bottom-up steps.

Preparation in supercritical fluids

Korgel *et al.* developed a method to decompose precursor species and re-assemble residues to nanoparticles. Silicon nanocrystals preparation has been successful following this approach.[41,42] The alkoxy-coated crystalline silicon were typically prepared by allowing the degradation of diphenylsilane in a mixture containing octanol and hexane under high pressure and high temperature. This approach produced silicon nanocrystals with a good yield of 0.5-1.5%, and quantum yield of up to 5%. He *et al.* reported a method of silicon nanocrystals preparation in which the thermolysis process could be achieved by microwave heating, with silicon nanowires and glutaric acid as the precursor species. The silicon quantum dots prepared following this method had an average size of ~3.1 nm, good water dispersity, high pH and temperature stability, and excellent biocompatibility.[43]

Laser pyrolysis

This method was first demonstrated by Cannon *et al.,* utilizing a set-up that included the focus of a high-power laser beam on a stream of silane gas. The Laser irradiation induced

very high temperature of up to 1000 °C close to the point where the beam intersected with the gas, allowing formation of silicon nanocrystals in this area.[44]

Li *et al.* recently developed this method by first preparing silicon nanoclusters of up to 50 nm, achieved via CO_2 laser induced pyrolysis of SiH_4 gas in an aerosol reactor. This treatment was then followed by controlled etching using a mixture of hydrofluoric acid (HF) (48%) and nitric acid (HNO_3). This method produced silicon quantum dots with colour tunable in the entire visible spectrum, with a rate of ~20 – 200 mg per hour and quantum yield in the range between 2 – 15%.[45]

Advantages and drawbacks

Advantages: 1) The wide range of colours of particles obtained. This is particularly preferred for bio-applications because of the existence of tissue window in the range between ~650 nm to ~1000 nm. 2) High quantum yield.

Drawbacks: 1) The need for specialized apparatus. The high temperature, pressure, and toxic chemicals (e.g. HF) require a strict control of every step.

1.4 Objectives

The main goal of my PhD thesis is to develop and optimize the properties of SQDs to 1) control their optical properties while maintaining small-sized particles, 2) enhance their optical properties (e.g. improving their quantum yield) which facilitates the utilization of SQDS in a wide range of biomedical and optoelectronic applications, and 3) investigate the impact of the ligands on the optical properties of SQDs. Additionally, since SQDs tend to agglomerate and aggregate, there is an urgent need to improve their photostability. This can be achieved by incorporating covalently-linked aromatic capping agents to the surface of the SQDs and through the utilization of different spacers connecting the capping agents to the SQDs surface. The nature of the photophysical interactions between SQDs and their surface ligands fluorophores will be investigated within this thesis.

Different approaches are proposed to achieve the aforementioned goals. First, the functionalization of SQDs surface with different aromatic dyes through conjugated and non-conjugated spacers which is expected to have a great influence on the intramolecular interactions between SQDs and dyes. Secondly, the utilization of different spacers that vary in chemical nature and length to connect SQDs and aromatic dyes as well as attaching SQDs to different positions of the aromatic dyes is expected to impact the photoinduced energy and/or electron transfer process taking place through the dyad system. Thirdly, using different solvent for the synthesis of SQDs such as (glycerol, water, ethanol) in order to avoid potential aggregation.

The utilization of aromatic capping agents has been previously shown to enable the SQDs to be more dispersible in variety of solvents, including water. Since only a few studies in literature investigated the relationship between the optical properties and surface chemistry of SQDs,[73-77] this thesis will provide a better understanding of their photophysical behavior and different methods to control their optical properties.

Lastly, the suitability of SQDs for biomedical application will require biocompatible and non-toxic materials. Thus, the cytotoxicity of these materials will be assessed using different assays including TNF-α cytotoxicity assay and ATP-dependent viability assay.

1.5 Theory

This section presents the theory, the physical basis and techniques that are used to characterize the optical properties of SQDs assemblies including absorption, energy and electron transfer, excitation energy migration and emission without a chemical reaction which is known as photophysical behavior of the matter.

1.5.1. Electronic absorption and emission spectroscopy

When a molecule (M) absorbs a photon of light, the resulting molecule will then possess an excess amount of energy. The molecule then becomes excited and it is referred to as M^* (Equation 1.1). This molecule can simply emit the excess energy as the form of light to return back to its ground state (Equation 1.2).

$$M + h\upsilon \rightarrow M^* \hspace{4cm} [1.1]$$

$$M^* \rightarrow M + h\upsilon \hspace{4cm} [1.2]$$

The excited molecule (M^*) can transfer its excess energy to another acceptor molecule, A. This process is known as quenching (Equation 1.3).

$$M^* + A \rightarrow M + A^* \hspace{4cm} [1.3]$$

1.5.2. Excitation energy migration

If there are two molecules in close proximity, one with an absorption band at a wavelength shifted to a longer wavelength than the other molecule, light energy absorbed by the one absorbing at the shorter wavelength (i.e. higher energy) is often transferred to the one that absorbs at the longer wavelength (lower energy). One molecule would act as a donor, D, of excitation energy, and the other as an acceptor, A, of this energy. This transfer probably takes place by a resonance mechanism which is described in terms of quantum mechanics.

Excitation energy is in the form of an electron placed in the LUMO and a hole in the HOMO in the S_1 excited state of the molecule. This energy is transferred then from one fluorophore to another. This process is called **excitation energy migration** (Figure 1-7).
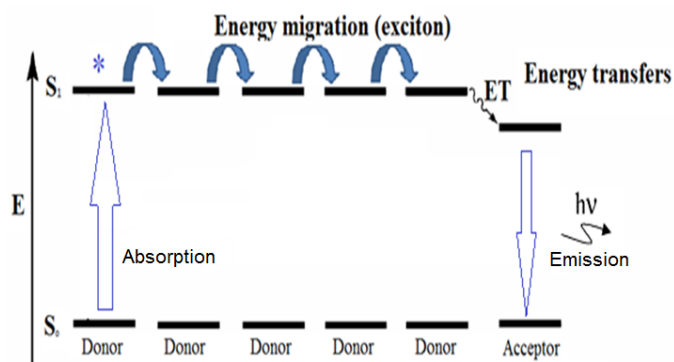
Figure 1-7. The exciton and energy transfer process (Modified from Reference 46).[46]

Energy transfer between different chromophore molecules is known as heterogeneous transfer, unlike the homogeneous transfer that occurs between identical molecules. The energy transfer can be repeated many times, giving rise to energy migration. Direct evidence of energy transfer between different chromophores is provided by sensitized fluorescence. Light quanta absorbed by molecules of one chromophore are transferred to molecules of another chromophore. When the first chromophore is excited, only fluorescence of the second is observed. This phenomenon of sensitized fluorescence is well known from studies on gases and solutions. The two possible mechanisms (Dexter and Förster) for this process are described below.

1.5.3. Electron transfer

The photoinduced electron transfer process (PET) is considered one of the most favorable way to convert light energy or to store it for further applications. This process takes place between a donor and an acceptor of electron after excitation resulting in the formation of a charge-separated state which relaxes to the ground state via an electron-hole recombination. The process (PET) involves an electron transfer within an electron donor-acceptor pair as shown in Figure 1-8.

$$D + A \xrightarrow{h\nu} D^* + A \xrightarrow[\text{transfer}]{\text{Electron}} D^{\cdot+} + A^{\cdot-} \xrightarrow[\text{recomination}]{\text{Electron}} D + A$$
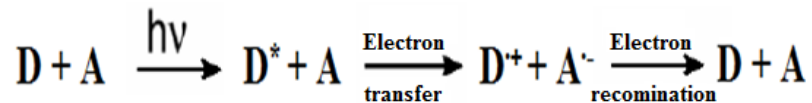
Figure 1-8. Photoinduced electron transfer process.

1.5.4. Light absorption

Light is an electromagnetic radiation that can be viewed as waves or particles. In the wave model, the electromagnetic radiation is considered as a wave emitted from a source and is characterized by (Equation 1.7):

$$\lambda = c/\nu \qquad\qquad [1.7]$$

where λ is the wavelength, c is the velocity of light (2.998×10^8 m/s) and ν is the frequency.

In the particles model, light is composed of particles which are called photons (particles that have no mass but only energy). Each photon has an energy of Plank's quantum, h c/ λ, where h is Plank's constant (h = 6.62×10^{-34} Js), c is the light velocity and λ is the wavelength of the radiation.

The photon absorption by a molecule (M) leads to photophysical or / and photochemical processes as it was stated by the Grotthus-Draper law.

Indeed, the optical transmittance, T, is a measure for how much light enters a sample and that is then absorbed (Equation 1.8).

$$T = I/I_o \qquad\qquad [1.8]$$

where I is the transmitted light intensity and I_o is the incident light intensity.

Absorbance, *A*, is the logarithm of the ratio of the intensity of the transmitted light to the intensity of the incident light (Equation 1.9).

$$A = \log (I/I_o) \qquad\qquad [1.9]$$

and hence

$$A = \log(1/T) = -\log T \tag{1.10}$$

Beer's law states that, the absorbance of a chromophore increases in proportion to the concentration of the latter (Equation 1.11).

$$A \, \alpha \, c \tag{1.11}$$

$$A = k \, c \tag{1.12}$$

where k is a constant.

Lambert's law stated that the absorbance is directly proportional to the path length (Equation 1.13).

$$A \, \alpha \, l \tag{1.13}$$

$$A = k' \, l \tag{1.14}$$

where l is the path length and k′ is a constant.

The Beer-Lambert law combines the two laws giving

$$A = \varepsilon \, l \, c \tag{1.15}$$

where ε is the molar absorption coefficient.

The absorption of a photon by a molecule at a certain wavelength leads to an excited molecule where the absorbed energy can be translated into rotational, vibrational and electronic modes. The quantized internal energy, E_{int}, of the molecule in both its ground and excited stated can be approximated by (Equation 1.16).

$$E_{int} = E_{el} + E_{vib} + E_{rot} \tag{1.16}$$

where E_{el}, E_{vib}, E_{rot} are the electronic, vibrational and rotational energies respectively.

According to the Born-Oppenheimer approximation, as the electronic transitions are very fast and occur in about 10^{-15}s compared to the characteristic time scale for molecular vibrations that occur in 10^{-12} s, the influence of the vibrational and the rotational motions are almost negligible.

The Frank-Condon principle indicates that the electronic transition occurs mostly without change in the position of the nuclei in the molecular entity and its environment and hence, it is possible to describe the molecular energy by a potential energy diagram (Figure 1-9).
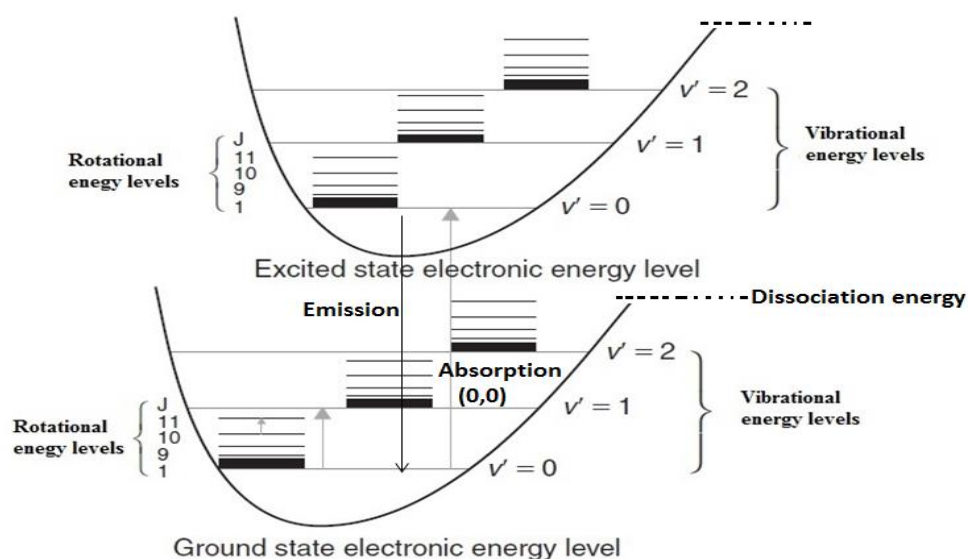
Figure 1-9. **The relative order of electronic, vibrational and rotational energy levels (modified from Reference 47).[47]**

The Frank-Condon principle shows that the vibrational and electronic transitions will be observed in the spectrum. According to this concept for a diatomic molecule, let's consider the example in Figure 1-10 below. According to the Boltzman distribution, at room temperature, most of the molecules are in the lowest vibrational level (v) of the ground state (i.e., $v = 0$). The absorption spectrum in Figure 1-10 exhibits a combination of both the pure electronic transitions (i.e., from $v = 0$ to $v' = 0$) and several vibronic peaks for which intensities depend on the relative position and shape of the potential curves of the ground and excited states.

In the example provided in Figure 1-10, the 0-2 peak has the highest intensity as going from $v = 0$ in the ground state to $v = 2$ in the excited sate is the most probable for vertical transitions as it falls on the highest point in the vibrational probability curve in the excited state.
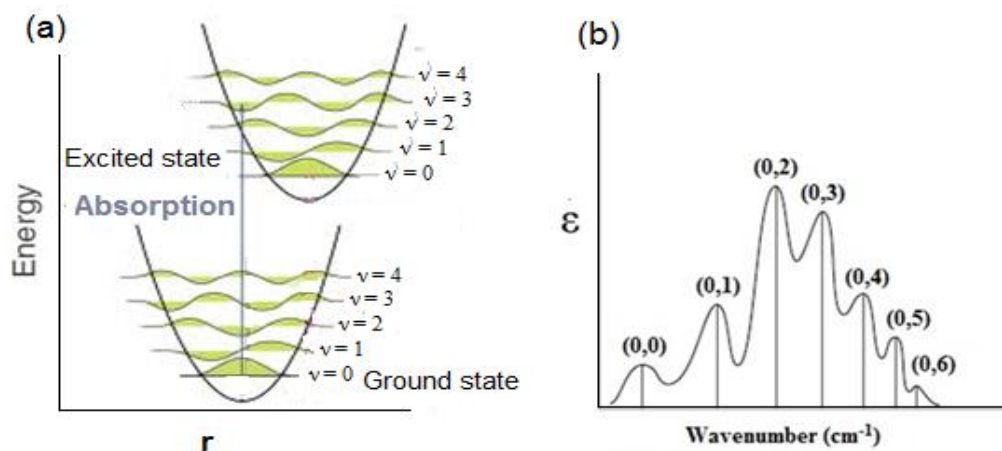
Figure 1-10. (a) Potential energy diagram for a diatomic molecule, illustrating the Frank-Condon excitation and, r is the nuclear coordinate. (b) Intensity distribution among vibronic bands as determined by the Frank-Condon principle. (Modified from Reference 48).[48]

The emission and excitation spectra are two types of distinct types of spectra, but they usually overlap. The excitation spectrum is normally known as the spectrum of light emitted by the material as a function of the excitation wavelength while the absorption spectrum is known as the spectrum of light absorbed by the material as a function of the wavelength. Usually, these two spectra, absorption and excitation, should overlap perfectly.

1.5.5. Photoluminescence

Generally, when a molecule absorbs a photon, it is described as an excited molecule (i.e. a molecule lying in an upper electronic excited state) and after a certain time, the excited state molecule can relax by two different pathways. The first type is fluorescence which shows photoluminescence as a result of singlet–singlet electronic relaxation. The typical

lifetime of fluorescence is the nanoseconds (ns) time scale. The second type is phosphorescence which shows photoluminescence as a result of triplet–singlet electronic relaxation. The typical lifetime of phosphorescence ranges from milliseconds to hours.

1.5.6. Jablonski diagram

It is an energy diagram that shows the different electronic states and transitions in molecules (Figure 1-11). S_0 represents the electronic ground state and S_1, S_2 represent the first and second singlet excited states, respectively. T_1 and T_2 represent the first and second triplet excited states, respectively. In the singlet states, all electrons spin are paired and the multiplicity of this state is 1 while in the triplet state, the electrons are no longer antiparallel and the electronic spin multiplicity is 3 as the total spin states can take values of -1, 0 and 1. The triplet state is more stable than the singlet state because of the Coulomb repulsion energy between the two electrons and the increase in degree of freedom of the magnetic spins.
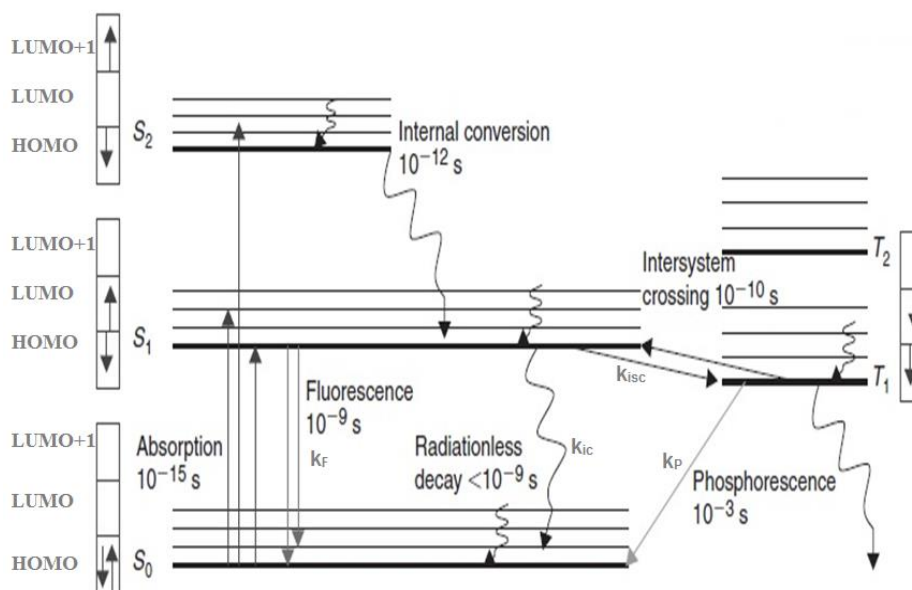
Figure 1-11. Jablonski diagram showing different states and transitions (Modified from Ref. 48).

In Figure 1-11, the arrows in the boxes represent the electron spins when they are paired in the singlet states and in the triplet states where electrons are no longer antiparallel. The subscript indicates the relative energetic position compared to other states of the same multiplicity. The symbols k_F, k_{isc}, k_{ic}, k_P represent the fluorescence, intersystem crossing, internal conversion and phosphorescence rate constants, respectively. Different processes in Jablonski diagram are shown including the absorption, vibrational relaxation and internal conversion, fluorescence, intersystem crossing and phosphorescence.

1.5.6.1. Absorption

The first transitional process in the Jablonski diagram is the absorption of a photon of a particular energy by the molecule (the characterization of this process has already been provided in section 1.3). This process is shown in the diagram by a straight arrow pointing up. The absorbance is a very fast transition which occurs on the order of 10^{-15} second.

1.5.6.2. Vibrational relaxation and internal conversion

Once the electron is excited, the molecule becomes in its excited state (S_1, S_2, ..,T_1, T_2, ..etc), there are several pathways by which the energy may be dissipated. The first option is through vibrational relaxation, a nonradiative process which is represented in the Jablonski diagram as curved arrows between vibrational levels. The vibrational relaxation is where the accumulated energy is released as kinetic energy (i.e. heat) and the molecule relaxes to a lower vibrational level of the same electronic state. The kinetic energy may stay within the same molecule or it could be transfered to other molecules around the excited molecule (i.e. the solvent for example). This process is very fast occuring on the order of 10^{-11}-10^{-14} second.

The second nonrdiative process is the internal conversion which is observed when the excited molecule relaxes to a lower excited state of the same multiplicity (i.e. $S_2 \rightarrow S_1$; $S_1 \rightarrow S_0$). It is mechanistically identical to the vibrational relaxation except it occurs between two different electronic states. It is indicated in the Jablonski diagram as a curved line between two vibrational levels in two different electronic states. This process occurs in the time scale of 10^{-12} second.

1.5.6.3. Fluorescence

This radiative process takes place between two electronic states (ground and excited states) of the same multiplicity (e.g., $S_1 \rightarrow S_0$ and $S_2 \rightarrow S_0$). The lifetime of the fluorescence is typically on the order of (10^{-8}-10^{-9} second for $S_1 \rightarrow S_0$). It is indicated in Jablonski diagram as a straight line going down on the energy axis between two different electronic states.

In general, the fluorescence band is a mirror image of the absorption band ($S_0 \rightarrow S_1$) (Figure 1-12). This is particularly true for rigid molecules (such as aromatics) as the Frank-Condon principle is applicable. The vibronic peaks are also expected to be present in both directions ($S_1 \rightarrow S_0$ and $S_0 \rightarrow S_1$) in the fluorescence band. There are some exceptions to this rule, when the molecule changes its geometry in the excited state. The difference in the wavelength between the (0,0) absorption and emission peaks is known as the **Stokes shift**.
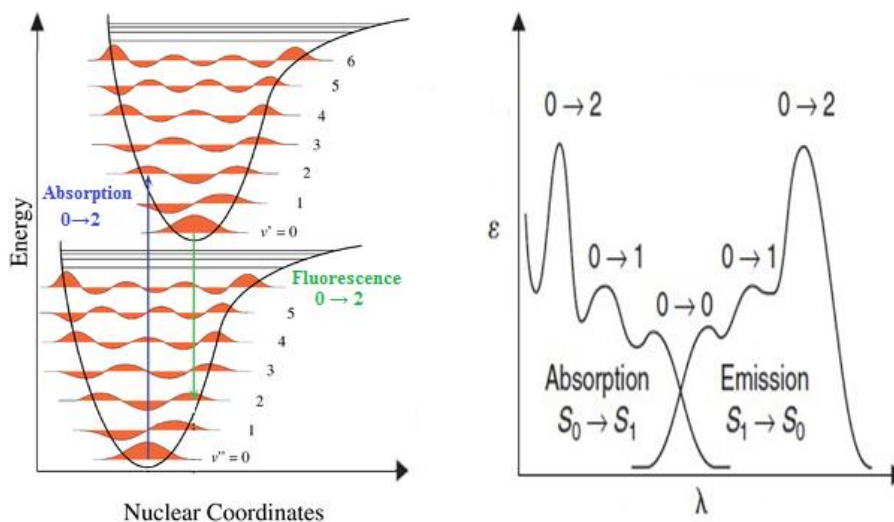
Figure 1-12. Potential energy curves and vibronic structures of fluorescence spectra (Modified from Reference 49).[49]

1.5.6.4. Intersystem crossing (ISC)

It is another non-radiative process which occurs when an excited molecule changes spin multiplicity from an excited singlet state to an excited triplet state or the inverse. This process occurs on a time scale of (10^{-6}-10^{-8} second) for organic molecules and 10^{-11} second for organometallics. This rate enhancement is due to spin-orbit coupling that is induced by

the presence of heavy atoms such as metal containing systems. This is an interaction between the spin angular momentum and the orbital angular momentum of S_n and T_n states and thus, singlet and triplet states are no longer "pure" as singlet or triplet.

1.5.6.5. Phosphorescence

This radiative process includes a relaxation of the molecule from the triplet state to the ground state. It usually exhibits longer lifetimes than fluorescence on time scale of 10^{-3} second for organic samples and (10^{-5}-10^{-7} second) for metal containing samples. The difference between the fluorescence and phosphorescence is due to the fact that it involves a spin-forbidden electronic transitions.

The phosphorescence bands are always more red-shifted than those for fluorescence due to the relative stability of the triplet state compared to the singlet state (Figure 1-13).
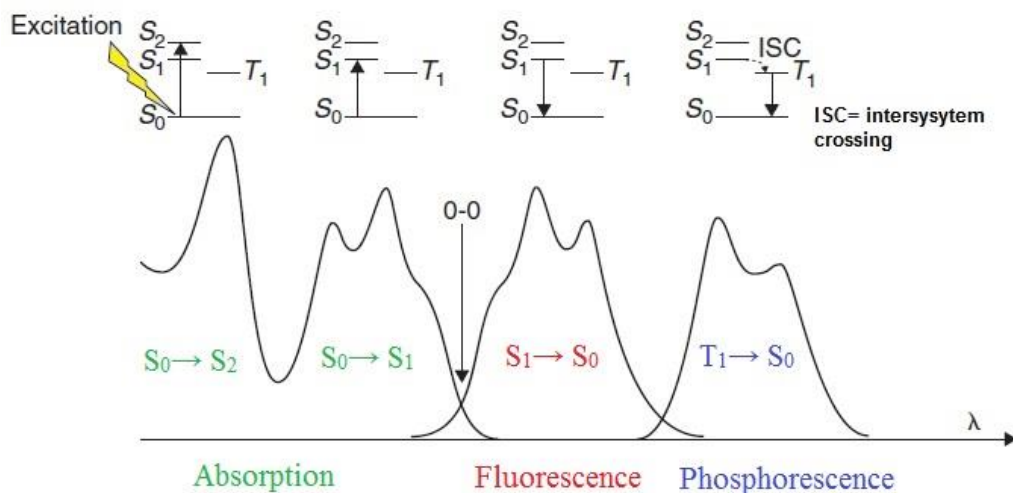
Figure 1-13. Relative positions of absorption, fluorescence and phosphorescence (Modified from Reference 49).

1.5.7. Emission lifetime

The emission lifetime is the average time that the molecules remain in its excited state before the photon is emitted. According to the viewpoint of the kinetics, the lifetime is the rate of depopulation of the excited state (singlet or triplet) states following an optical excitation from the ground state.

Luminescence generally follows first order kinetics as in Equation 1.17.

$$[S_1] = [S_1]_o \, e^{-k_F t} \qquad\qquad [1.17]$$

where $[S_1]$ is the concentration of the excited state molecules at time t, $[S_1]_o$ is the initial concentration and k_F is the decay rate.

The various radiative and nonradiative processes can decrease the excited state population, and so the overall decay rate is given as the sum of the radiative and nonradiative decay rates (Equation 1.18).

$$k_{total} = k_{radiative} + k_{nonradiative} \qquad\qquad [1.18]$$

Again, when a molecule, *A*, is excited, it is promoted from the ground state to the excited state (Equation 1.19).

$$A + h\upsilon \rightarrow A^* \qquad\qquad [1.19]$$

The excited molecule can relax to its ground state after losing its extra energy via radiative (Equation 1.20) and non-radiative processes (Equation 1.21).

$$A^* \rightarrow A + h\upsilon \quad \text{(radiative process, } k_r) \qquad\qquad [1.20]$$

$$A^* \rightarrow A + \text{heat} \quad \text{(nonradiative process, } k_{nr}) \qquad\qquad [1.21]$$
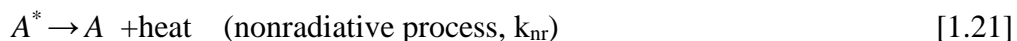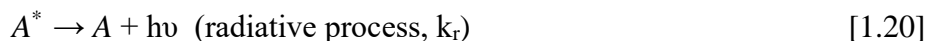
where k_r and k_{non} are the rate constants for the radiative and the nonradiative processes.

$$-\frac{d[A^*]}{dt} = (k_r + k_{nr})\,[A^*] = \frac{1}{\tau}[A^*] \qquad\qquad [1.22]$$

where $[A^*]$ is the concentration of the species A in its excited state at a given time t.

$$\ln \frac{[A^*]_t}{[A^*]_{t=0}} = -(k_r + k_{nr})\,t = -\frac{t}{\tau} \qquad [1.23]$$

Hence the mean emission lifetime (τ) of $[A^*]$ is given by

$$\tau = \frac{1}{(k_r + k_{nr})} \qquad [1.24]$$

The emission lifetime can be measured using a time-resolved experiment at which very short pulses excitation is made and followed by measuring the time-dependent intensity.

From a kinetic standpoint, the fluorescence and phosphorescence lifetimes τ_F and τ_P can be expressed respectively as the following (Equations 1.25, 1.26).

$$\tau_F = \frac{1}{k_F + k_{IC} + k_{ISC}} \qquad [1.25]$$

$$\tau_P = \frac{1}{k_P + k_{IC}} \qquad [1.26]$$

Thus, the measured unimolecular radiative lifetime is the reciprocal of the sum of the unimolecular rate constants for all the deactivation processes. The general form of the equation is given by:

$$\tau = \frac{1}{\sum_i k_i} \qquad [1.27]$$

where τ is the observed radiative lifetime and the rate constant k_i represents the unimolecular or pseudo-unimolecular processes that deactivate A^*.

1.5.8. Emission quantum yield (Φ)

Emission quantum yield represents the ratio of the number of photons emitted by the fluorophore to the number absorbed. It's useful as it provides information about the electronic excited state relaxation process (such as the rates of the radiative and non-radiative process).

The measurements of quantum yields are performed by preparing three different solutions of the same concentration of the sample and the standard for each photophysical datum quantum yields. The sample and standard concentrations are adjusted to obtain an absorbance of 0.05 or less. This absorbance is adjusted to be the same as much as possible for the standard and the sample. Each absorbance value is measured five times for better accuracy in the measurements of the quantum yields (Equation 1.28).

$$\Phi_u = \left[\frac{(A_s F_u n^2)}{(A_u F_s n_o^2)} \right] \Phi_s \qquad [1.28]$$

where, the subscript u refers to "unknown", and it refers to a comparative standard, Φ is the emission quantum yield, A is the absorbance at a certain excitation wavelength, F is the integrated emission area across the band of a spectrum plotted in a linear scale of energy (i.e. cm^{-1}), n and n$_o$ are the refractive indices of the solvent containing the unknown and the standard, respectively. From a kinetic standpoint, the fluorescence and phosphorescence quantum yield Φ_F and Φ_P can be expressed respectively as the following (Equations 1.29, 1.30).

$$\Phi_F = \frac{k_F}{k_F + k_{iC} + k_{ISC}} \qquad [1.29]$$

$$\Phi_P = \frac{k_P}{k_P + k_{ISC}} \qquad [1.30]$$

So,

$$k_F = \frac{\Phi_F}{\tau_F} \qquad [1.31]$$

$$k_P = \frac{\Phi_P}{\tau_P} \qquad [1.32]$$

1.5.9. Energy transfer

In the presence of an energy acceptor molecule of a lower energy, A, the excited donor, D^*, can be deactivated by a process called energy transfer which can be represented as in (Equations 1.33,1.34).

$$D + h\upsilon \rightarrow D^* \qquad\qquad [1.33]$$

$$D^* + A \rightarrow D + A^* \qquad\qquad [1.34]$$
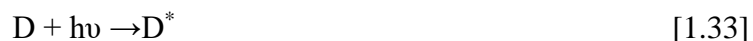
For the energy transfer to occur, the energy level of the excited state of the donor, D^*, has to be higher than that of the acceptor, A^*, and the time scale of the energy transfer process should be faster than the lifetime of the D^*.

There are two possible types of the energy transfer:

1.5.9.1. Radiative energy transfer which occurs when the extra energy in D^* is emitted in the form of luminescence and this radiation is absorbed by the acceptor, A, as in (Equations 1.35,1.36).

$$D + h\upsilon \rightarrow D^* \qquad\qquad [1.35]$$

$$A + h\upsilon \rightarrow A^* \qquad\qquad [1.36]$$

This interaction operates even when the distance between the donor and the acceptor is large (100Å). However, this process is not efficient since only a very small fraction of the emitted light is absorbed by the acceptor because the emission occurs in all directions.

1.5.9.2. Non-radiative energy transfer can be described according to Förster and Dexter mechanisms and both are very efficient, even occasionnally reaching close to 100% efficiency.

1.5.9.2.1. Förster mechanism (FRET)

Förster resonance energy transfer, FRET, involves the migration of energy by the resonant coupling of electrical dipoles from the donor molecule to the acceptor molecule. This process can occur over a long distance (30-100Å). As shown in Figure 1-14, the Förster

mechanism involves the migration (i.e. relaxation) of an electron from the excited donor that is placed in the LUMO to the HOMO and the released energy is transferred to the acceptor via Coulombic interactions and an electron in the HOMO of the acceptor is promoted to the LUMO. This mechanism operates mostly in the singlet states of both the donor and the acceptor.
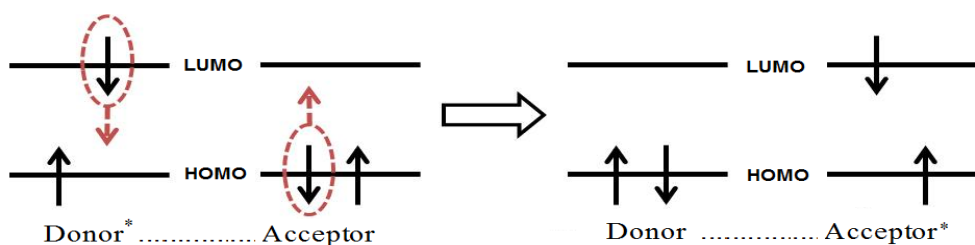
Figure1-14. Mechanism of the energy transfer according to Förster.

The rate of the energy transfer (k_{ET}) can be determined as in Equation 1.37.

$$k_{ET}=k_D R_F{}^6 (1/R)^6 \qquad [1.37]$$

where k_D is the emission rate constant of the donor in the absence of the acceptor, R is the center-to-center inter chromophore separation and R_F is the Förster radius. The Förster radius is defined as the distance between the donor and the acceptor at which 50% of the excited state decays by energy transfer. R_F is calculated by the overlap of the emission spectrum of the donor excited state (D^*) and the absorption spectrum of the acceptor (A).

$$R_F^6 = \frac{9000 \; \Phi_F \; (\ln 10) \hbar^2 J}{128 \; \pi^5 n^4 N_A} \qquad [1.38]$$

where Φ_F is the fluorescence quantum yield of the donor in the absence of the acceptor, $\hbar^2$ is the dipole orientation factor, n is the refractive index of the medium, N_A is Avogadro's number, and J is the spectral overlap integral which can be calculated as in Equation 1.39.

$$J = \int f_D \, (\lambda) \varepsilon_A \, (\lambda) \lambda^4 \; d\lambda \qquad [1.39]$$

where f_D is the normalized donor emission spectrum, and ε_A is the acceptor molar extinction coefficient.

Applications and limitations of FRET

FRET provides an efficient way to measure the distance between a donor and an acceptor chromophore. The energy transfer efficiency is highly influenced by the ratio of R and R_F because of the exponent 6. Thus, by measuring the FRET efficiency, one can easily get the precise distance between the donor and the acceptor. If choosing the donor and acceptor properly, this experiment can also be carried out *in vivo*. However, the FRET only gives the information about distances. If a dramatic conformational change happens, such as lengthening or kink, it is unable to know the exact movement of donor and the acceptor. Besides, attaching the chromophores to precise sites of a macromolecule is also important, both in quantity of chromophores and in position of a macromolecule, or the FRET might produce noise signals.

1.5.9.2.2. Dexter mechanism

This mechanism involves a double electron exchange between the donor and the acceptor (Figure 1-15). The Dexter mechanism involves the migration of one electron from the LUMO of the donor to the LUMO of the acceptor and at the same time, an electron from the HOMO of the acceptor moves to the HOMO of the donor. Both singlet-singlet and triplet-triplet transfers are possible, but the mechanism requires a close contact between the MO involved, either from the resonance structures (if any) of very close proximity in order to promote orbitals overlap favoring electron transfers.
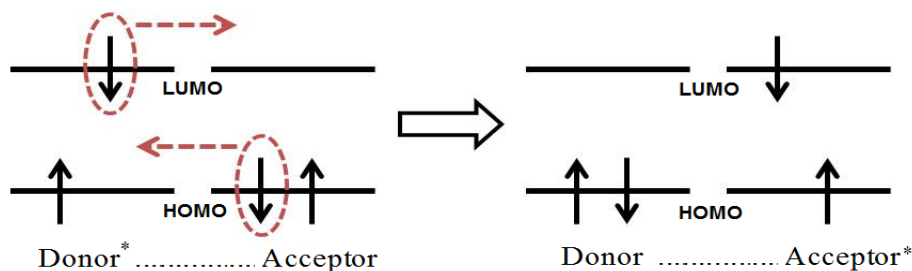
Figure 1-15. Mechanism of the energy transfer according to Dexter.

The rate of the energy transfer (k_{ET}) can be expressed as in Equation 1.26.

$$k_{ET} = \frac{2\pi}{h} V_0^2 J \exp\left(-\frac{2\,R_{DA}}{L}\right) \qquad [1.40]$$

where R_{DA} is the distance between the donor and acceptor, J is the internal spectral overlap between the donor and acceptor, L is the effective Bohr radius of the orbitals between which the electron is transferred, h is plank's constant, V_o is the electronic coupling matrix element between the donor and the acceptor at the contact distance.

The rate of the energy transfer can be determined experimentally using Equation 1.41.

$$k_{ET} = \frac{1}{\tau_F} - \frac{1}{\tau_F^0} \qquad [1.41]$$

where τ_F is the emission lifetime of the donor in the absence of the acceptor and τ_F^0 is the emission lifetime of the donor in the presence of the acceptor.

1.5.10. Transient absorption spectroscopy (Flash photolysis)

The phosphorescence process resulting from the triplet states is usually difficult to be detected in solutions at room temperature because of the high efficiency of the non-radiative pathway from long lived triplet states such as intermolecular collision with the solvent molecules.

This was a challenge for the development of triplet-state theory till the year 1949 when two scientists, Porter and Norris, introduced the flash photolysis technique. [24] This method allows the observation of the triplet states in solution by direct measurement of their absorption spectra. The long-lived nature of the triplet-states allow the buildup of the concentration of species residing in the T1 state and the fact that T1$\rightarrow$ Tn is a spin allowed transition making these transitions as intense as the S0 $\rightarrow$Sn. The basic principle of this concept is shown in Figure 1-16.
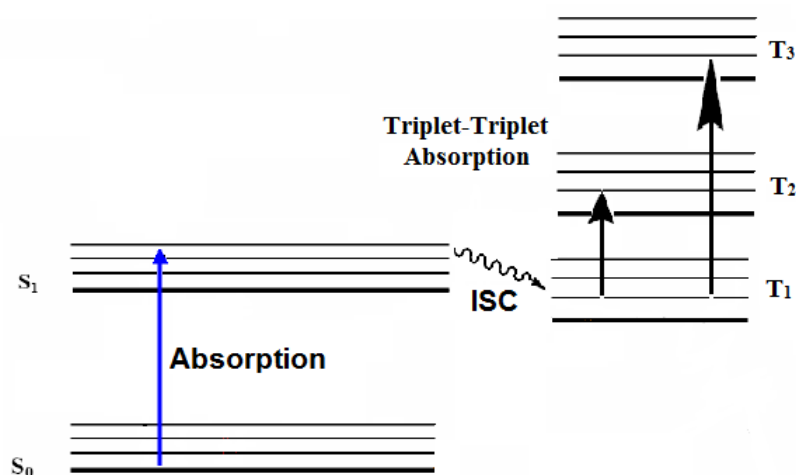
Figure 1-16. State diagram showing the pathway leading to T1-Tn absorption.

The basic principles of this technique involve the excitation of the molecule by the application of an intense flash (pump) which creates a high concentration of the singlet excited molecules, first in the S_1 state. Then two scenarios can occur depending on the width of the laser pulse (pump). If the laser pulse is very narrow (i.e. fs or ps) and that a second excitation (probe) is performed almost right away (delay time between the first and second pulse of fs or ps), then $S_0 \rightarrow S_n$ absorption is possible. At this time scale, the concentration of species lying on the S_1 state is still large since the time scale for the usually very fast inter-system crossing process is about 10^{-11} s. However for larger excitation pulse width (ns for example), then species lying on the S_1 state have the time to relax to the T_1 state. At this point, the concentration of these species is the highest. Hence, with an appropriate delay time after the pump and probe excitation (Figure 1-16) observation of $T_1 \rightarrow T_n$ absorption bands is possible.

1.6 Reference

1.   Administration, The U.S. Energy Information. "International Energy Outlook 2017." 2017.

2.   Morton, Oliver. "Silicon valley sunrise." <u>Nature</u> 443 (2006): 19-22.

3.   Resch-Genger, Ute; Grabolle, Markus; Cavaliere-Jaricot, Sara; Nitschke, Roland; and Nann, Thomas. "Quantum dots versus organic dyes as fluorescent labels." <u>Nature methods</u> 5 (2008): 763.

4.   Frangioni, John V. "In vivo near-infrared fluorescence imaging." <u>Current opinion in chemical biology</u> 7 (2003): 626-634.

5.   Brus, Louis. "Electronic wave functions in semiconductor clusters: experiment and theory." <u>The Journal of Physical Chemistry</u> 90 (1986): 2555-2560.

6.   Brus, Louis E. "Electron–electron and electron-hole interactions in small semiconductor crystallites: The size dependence of the lowest excited electronic state." <u>The Journal of chemical physics</u> 80 (1984): 4403-4409.

7.   Takagahara, Toshihide, and Takeda, Kyozaburo. "Theory of the quantum confinement effect on excitons in quantum dots of indirect-gap materials." <u>Physical Review B</u> 46 (1992): 15578.

8.   Yoffe, Abe D. "Low-dimensional systems: quantum size effects and electronic properties of semiconductor microcrystallites (zero-dimensional systems) and some quasi-two-dimensional systems." <u>Advances in Physics</u> 42 (1993): 173-262.

9.   Yoffe, Abraham D. "Semiconductor quantum dots and related systems: electronic, optical, luminescence and related properties of low dimensional systems." <u>Advances in physics</u> 50 (2001): 1-208.

10.   Alsharif, Naif H; Berger, Christine EM; Varanasi, Satya S; Chao, Yimin; Horrocks, Benjamin R; and Datta, Harish K. "Alkyl-capped silicon nanocrystals lack cytotoxicity and have enhanced intracellular accumulation in malignant cells via cholesterol-dependent endocytosis." <u>small</u> 5 (2009): 221-228.

11.   Ruizendaal, Loes; Bhattacharjee, Sourav; Pournazari, Kamyar; Rosso-Vasic, Milena; de Haan, Laura HJ; Alink, Gerrit M; Marcelis, Antonius TM; and Zuilhof, Han. "Synthesis and cytotoxicity of silicon nanoparticles with covalently attached organic monolayers." <u>Nanotoxicology</u> 3 (2009): 339-347.

12.   Bhattacharjee, Sourav; de Haan, Laura HJ; Evers, Nynke M; Jiang, Xue; Marcelis, Antonius TM; Zuilhof, Han; Rietjens, Ivonne MCM; and Alink, Gerrit M. "Role of surface charge and oxidative stress in cytotoxicity of organic monolayer-coated silicon nanoparticles towards macrophage NR8383 cells." <u>Particle and fibre toxicology</u> 7 (2010): 25.

13.   Park, Ji-Ho; Gu, Luo; Von Maltzahn, Geoffrey; Ruoslahti, Erkki; Bhatia, Sangeeta N; and Sailor, Michael J. "Biodegradable luminescent porous silicon nanoparticles for in vivo applications." <u>Nature materials</u> 8 (2009): 331.

14.   Takeoka, Shinji; Fujii, Minoru; and Hayashi, Shinji. "Size-dependent photoluminescence from surface-oxidized Si nanocrystals in a weak confinement regime." <u>Physical Review B</u> 62 (2000): 16820.

15.   Zhang, Xiaoming; Neiner, Doinita; Wang, Shizhong; Louie, Angelique Y; and Kauzlarich, Susan M. "A new solution route to hydrogen-terminated silicon nanoparticles: synthesis, functionalization and water stability." <u>Nanotechnology</u> 18 (2007): 095601.

16.   Sugimoto, Hiroshi; Fujii, Minoru; Imakita, Kenji; Hayashi, Shinji; and Akamatsu, Kensuke. "Phosphorus and boron codoped colloidal silicon nanocrystals with inorganic atomic ligands." <u>The Journal of Physical Chemistry C</u> 117 (2013): 6807-6813.

17.   Norris, David J; Efros, Alexander L; and Erwin, Steven C. "Doped nanocrystals." <u>Science</u> 319 (2008): 1776-1779.

18.   Mocatta, David; Cohen, Guy; Schattner, Jonathan; Millo, Oded; Rabani, Eran; and Banin, Uri. "Heavily doped semiconductor nanocrystal quantum dots." <u>Science</u> 332 (2011): 77-81.

19.   Mastronardi, Melanie L; Maier-Flaig, Florian; Faulkner, Daniel; Henderson, Eric J; Kübel, Christian; Lemmer, Uli; and Ozin, Geoffrey A. "Size-dependent absolute quantum yields for size-separated colloidally-stable silicon nanocrystals." <u>Nano letters</u> 12 (2011): 337-342.

20.   Liu, Shu-Man; Yang, Yang; Sato, Seiichi; and Kimura, Keisaku. "Enhanced photoluminescence from Si nano-organosols by functionalization with alkenes and their size evolution." <u>Chemistry of materials</u> 18 (2006): 637-642.

21.   Neumann, Philipp; Jakobi, Ingmar; Dolde, Florian; Burk, Christian; Reuter, Rolf; Waldherr, Gerald; Honert, Jan; Wolf, Thomas; Brunner, Andreas; and Shim, Jeong Hyun. "High-precision nanoscale temperature sensing using single defects in diamond." <u>Nano letters</u> 13 (2013): 2738-2742.

22.   Gupta, Anoop; Swihart, Mark T; and Wiggers, Hartmut. "Luminescent colloidal dispersion of silicon quantum dots from microwave plasma synthesis: exploring the photoluminescence behavior across the visible spectrum." <u>Advanced Functional Materials</u> 19 (2009): 696-703.

23.   Warner, Jamie H; Hoshino, Akiyoshi; Yamamoto, Kenji; and Tilley, Richard D. "Water-soluble photoluminescent silicon quantum dots." <u>Angewandte Chemie International Edition</u> 44 (2005): 4550-4554.

24. Chatterjee, Surajit, and Mukherjee, Tushar Kanti. "Spectroscopic investigation of interaction between bovine serum albumin and amine-functionalized silicon quantum dots." Physical Chemistry Chemical Physics 16 (2014): 8400-8408.

25. Dohnalová, Kateřina; Poddubny, Alexander N; Prokofiev, Alexei A; De Boer, Wieteke Dam; Umesh, Chinnaswamy P; Paulusse, Jos MJ; Zuilhof, Han; and Gregorkiewicz, Tom. "Surface brightens up Si quantum dots: direct bandgap-like size-tunable emission." Light: science & applications 2 (2013): e47.

26. Heinrich, Julie L; Curtis, Corrine L; Credo, Grace M; SAILOR, MICHAEL J; and KAVANAGH, KAREN L. "Luminescent colloidal silicon suspensions from porous silicon." Science 255 (1992): 66-68.

27. Nayfeh, Osama M; Antoniadis, Dimitri A; Mantey, Kevin; and Nayfeh, Munir H. "Uniform delivery of silicon nanoparticles on device quality substrates using spin coating from isopropyl alcohol colloids." Applied Physics Letters 94 (2009): 043112.

28. Sato, Keisuke; Tsuji, Hiroaki; Hirakuri, Kenji; Fukata, Naoki; and Yamauchi, Yusuke. "Controlled chemical etching for silicon nanocrystals with wavelength-tunable photoluminescence." Chemical Communications (2009): 3759-3761.

29. Liu, Shu-man; Sato, Seiichi; and Kimura, Keisaku. "Synthesis of luminescent silicon nanopowders redispersible to various solvents." Langmuir 21 (2005): 6324-6329.

30. Hessel, Colin M; Henderson, Eric J; and Veinot, Jonathan GC. "Hydrogen silsesquioxane: a molecular precursor for nanocrystalline Si− SiO2 composites and freestanding hydride-surface-terminated silicon nanoparticles." Chemistry of materials 18 (2006): 6139-6146.

31. Hessel, Colin M; Summers, Mark A; Meldrum, Al; Malac, Marek; and Veinot, Jonathan GC. "Direct Patterning, Conformal Coating, and Erbium Doping of Luminescent nc-Si/SiO2 Thin Films from Solution Processable Hydrogen Silsesquioxane." Advanced Materials 19 (2007): 3513-3516.

32. Hessel, Colin M; Reid, Dariya; Panthani, Matthew G; Rasch, Michael R; Goodfellow, Brian W; Wei, Junwei; Fujii, Hiromasa; Akhavan, Vahid; and Korgel, Brian A. "Synthesis of ligand-stabilized silicon nanocrystals with size-dependent photoluminescence spanning visible to near-infrared wavelengths." Chemistry of materials 24 (2011): 393-401.

33. Hessel, Colin M; Henderson, Eric J; and Veinot, Jonathan GC. "An investigation of the formation and growth of oxide-embedded silicon nanocrystals in hydrogen silsesquioxane-derived nanocomposites." The Journal of Physical Chemistry C 111 (2007): 6956-6961.

34. Heath, James R. "A liquid-solution-phase synthesis of crystalline silicon." <u>Science</u> 258 (1992): 1131-1133.

35. Baldwin, RK. "K. a. Pettigrew, E. Ratai, MP Augustine and SM Kauzlarich." <u>Chem. Commun</u> (2002): 1822-1823.

36. Arul Dhas, N; Raj, C Paul; and Gedanken, A. "Preparation of luminescent silicon nanoparticles: a novel sonochemical approach." <u>Chemistry of materials</u> 10 (1998): 3278-3281.

37. Wise, Frank W. "Lead salt quantum dots: the limit of strong quantum confinement." <u>Accounts of Chemical Research</u> 33 (2000): 773-780.

38. Tilley, Richard D, and Yamamoto, Kenji. "The microemulsion synthesis of hydrophobic and hydrophilic silicon nanocrystals." <u>Advanced Materials</u> 18 (2006): 2053-2056.

39. Yang, Chung-Sung; Bley, Richard A; Kauzlarich, Susan M; Lee, Howard WH; and Delgado, Gildardo R. "Synthesis of alkyl-terminated silicon nanoclusters by a solution route." <u>Journal of the American Chemical Society</u> 121 (1999): 5191-5195.

40. Manhat, Beth A; Brown, Anna L; Black, Labe A; Ross, JB Alexander; Fichter, Katye; Vu, Tania; Richman, Erik; and Goforth, Andrea M. "One-step melt synthesis of water-soluble, photoluminescent, surface-oxidized silicon nanoparticles for cellular imaging applications." <u>Chemistry of Materials</u> 23 (2011): 2407-2418.

41. Holmes, Justin D; Ziegler, Kirk J; Doty, R Christopher; Pell, Lindsay E; Johnston, Keith P; and Korgel, Brian A. "Highly luminescent silicon nanocrystals with discrete optical transitions." <u>Journal of the American Chemical Society</u> 123 (2001): 3743-3748.

42. English, Douglas S; Pell, Lindsay E; Yu, Zhonghua; Barbara, Paul F; and Korgel, Brian A. "Size tunable visible luminescence from individual organic monolayer stabilized silicon nanocrystal quantum dots." <u>Nano Letters</u> 2 (2002): 681-685.

43. He, Yao; Zhong, Yiling; Peng, Fei; Wei, Xinpan; Su, Yuanyuan; Lu, Yimei; Su, Shao; Gu, Wei; Liao, Liangsheng; and Lee, Shuit-Tong. "One-pot microwave synthesis of water-dispersible, ultraphoto-and pH-stable, and highly fluorescent silicon quantum dots." <u>Journal of the American Chemical Society</u> 133 (2011): 14192-14195.

44. Cannon, W Roger; Danforth, Stephen C; Haggerty, John S; and Marra, RA. "Sinterable ceramic powders from laser-driven reactions: II, powder characteristics and process variables." <u>Journal of the American Ceramic Society</u> 65 (1982): 330-335.

45. Li, Xuegeng; He, Yuanqing; and Swihart, Mark T. "Surface functionalization of silicon nanoparticles produced by laser-driven pyrolysis of silane followed by HF−HNO3 etching." Langmuir 20 (2004): 4720-4727.

46. Harvey, Pierre D; Stern, Christine; Gros, Claude P; and Guilard, Roger. "Comments on the through-space singlet energy transfers and energy migration (exciton) in the light harvesting systems." Journal of inorganic biochemistry 102 (2008): 395-405.

47. Marcus, Rudolph A. "Chemical and electrochemical electron-transfer theory." Annual review of physical chemistry 15 (1964): 155-196.

48. Valeur, B. "chapter 5, in" Molecular Fluorescence."WILEY-VCH Verlag GmbH, Weinheim, 2002.

49. Abdelhameed, Mohammed. "Transfert de Charge Et D'énergie Dans Les Dyades Et Oligomères de Porphyrine." Université de Sherbrooke, 2014.

Chapter 2 Tuning the Optical Properties of Silicon Quantum Dots via Surface Functionalization with Conjugated Aromatic Fluorophores

2.1 Introduction

Silicon Quantum Dots (SQDs) in the quantum-size range (2–10 nm) have recently attracted great interest due to their unique optoelectronic properties which include broad absorption spectra, high stability against photobleaching, and size-tunable photoluminescence (PL), ranging from visible to near-infrared, by changing their size[1]. These nanoparticles also have excellent biocompatibility [2], low cytotoxicity [3], and versatile surface modification capability, and are therefore promising candidates for various biological and biomedical applications, such as bioimaging [4] and photodynamic therapy [5].

A number of methods have been reported for the synthesis of SQDs, such as bulk silicon etching [6], laser pyrolysis [7], and preparation in supercritical fluids [8], which produce SQDs with wavelength-tunable emission by controlling their size. A simple solution-based reduction method [9,10,11,12,13] has been shown advantageous over previous syntheses methods due to its simplicity and ease with which the surface chemistry can be modified[14,15]. Interestingly, the use of aromatic fluorophores for the modification of the SQDs surface is an efficient pathway to both tune the optical properties and improve the colloidal stability of SQDs [16].

Despite some reports of aromatic fluorophores incorporated into SQDs that permit sensitization of the SQDs via energy transfer, there are still limited examples of luminescent SQDs covalently functionalized with conjugated emissive compounds obtained through a solution-based reduction method [17,18]. Bard *et al*. [19] used the electrochemical charge injection to induce the luminescence from SQDs passivated with a combination of hydrogen and alkoxide ligands; Rosso-Vasic *et al*. [20] reported up to 55% efficiency of energy transfer from SQDs to a Ru-based dye. Sommer *et al*. [21] reported very fast energy transfer in a system composed of SQDs functionalized with vinyl pyridine; Erogbogbo *et al*. [16] observed improvement in the emission efficiency of SQDs

functionalized by anthracene in the hydrophobic core of micelles as a result of energy transfer. Recently, Ceroni *et al*. investigated SQDs covalently linked with pyrene units through a nonconjugated bridge and observed efficient energy transfer from the donor pyrene moieties to the acceptor SQD core [22]. Using a conjugated bridge may offer even improved optical properties through photogenerated energy transfer.

Here, we report the synthesis and surface functionalization of SQDs using a conjugated bridging approach with 9-vinyl phenanthrene, 1-vinyl pyrene, and 3-vinyl perylene to produce SQD-phenanthrene, SQD-pyrene, and SQD- perylene, respectively. Phenanthrene, pyrene, and perylene fluorophores were chosen for the surface passivation of SQDs due to their high stability and excellent optical properties including high fluorescence quantum yield [23]. Functionalization of the SQDS with these fluorophores is expected to improve the quantum yield of SQDs and tunability of PL emission, which can be applied in many fields such as bioimaging. The functionalized SQDs were characterized by UV−Vis absorption spectroscopy, Fourier-transform infrared (FTIR) spectroscopy, steady-state and times-resolved emission spectroscopy, high-resolution transmission electronic microscopy (HRTEM), and X-ray photoelectron spectroscopy (XPS).

2.2 Results and discussions

SQDs functionalized with aromatic fluorophores were prepared following a solution-based reduction route as shown in Figure 2-1 [24]. Silicon tetrachloride ($SiCl_4$) was used as the silicon source and was reduced by a strong reducing agent (LAH). The resultant H-terminated SQDs were passivated with organic molecules in the presence of a Pt catalyst.
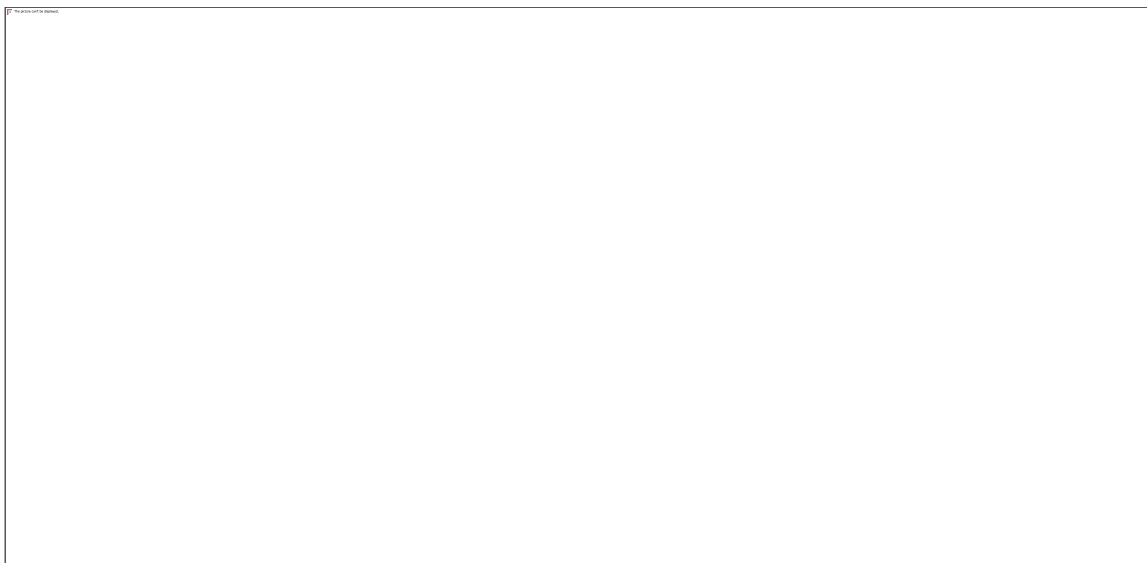
Figure 2-1. Synthesis route of H-terminated SNPs (A) and surface passivation using different ligands (B).

2.2.1 Size and structure

Figure 2-2 shows the TEM, size distribution histograms, and HR-TEM of the synthesized SQD-heptene, SQD-phenanthrene, SQD-pyrene, and SQD-perylene assemblies. The TEM images demonstrate that the functionalized SQDs are quasi-spherical without obvious agglomeration and aggregation. The size distributions indicate that the average diameter for SQD-heptene, SQD-phenanthrene, SQD-pyrene, and SQD-perylene are 1.68 ± 0.71, 2.14 ± 1.06, 1.94 ± 0.89, and 1.73 ± 0.62 nm, respectively, after the analysis of more than 150 dots from different regions of the grids. The HR-TEM images display the high crystallinity of the SQDs, as evidenced by the distinct lattice fringes with 0.30 nm interplanar spacing, which is consistent with the (111) plane of diamond silicon [14,25]. It should be mentioned that the low contrast of the TEM and HR-TEM images is due to the extreme small dimensions of SQDs and also the low atomic weight of silicon compared to metallic or semiconductor quantum dots, which results in poor visualization [12,26].
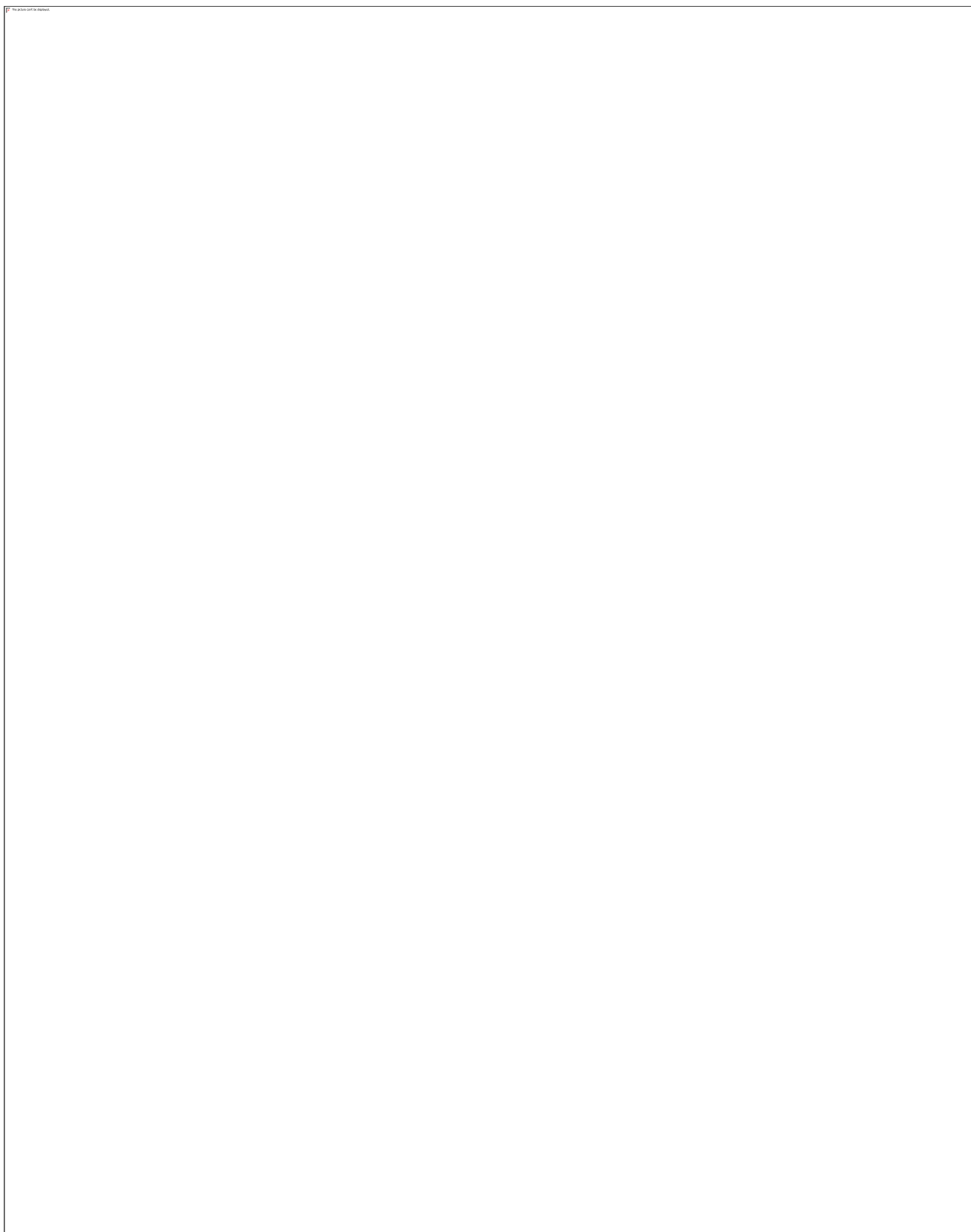
Figure 2-2. TEM (left), diameter distributions (middle) and HR-TEM images (right) of SQD-heptene (A), SQD-phenanthrene (B), SQD-pyrene (C), and SQD-perylene (D).

To confirm aromatic ligand binding to the surface of SQDs, both FTIR and XPS spectroscopy were performed. Figure 2-3 shows the FTIR spectra of SQD-phenanthrene, SQD-pyrene, and SQD-perylene. The broad peak at 3010–3680 cm^{-1} can be attributed to OH stretching [27], and the peak at 1000–1100 cm^{-1} indicates the presence of Si-O-Si stretching. This provides evidence for the oxidation of the surface of the SQDs [28]. The peaks at 3010–2850 and 1416–1480 cm^{-1} are attributed to aromatic fluorophores C-H stretching and bending, respectively [29]. The wide peak at 1630 cm^{-1} is assigned to the stretching vibrations of (-C=C), which was also observed in analogous systems [30,31]. Furthermore, the characteristic peaks of the ($\equiv$C-H) and (C$\equiv$C) stretching vibrations at 3230–3330 and 2115–2040 cm^{-1}, respectively observed for the free alkynyl fluorophores (Figure 2-8), as well as the stretching vibration peak of (Si–H) at 2100–2250 cm^{-1} [32], are absent in the spectra of the functionalized SQDs. This indicates complete reaction of the alkynyl fluorophores with the H-terminated SQDs.
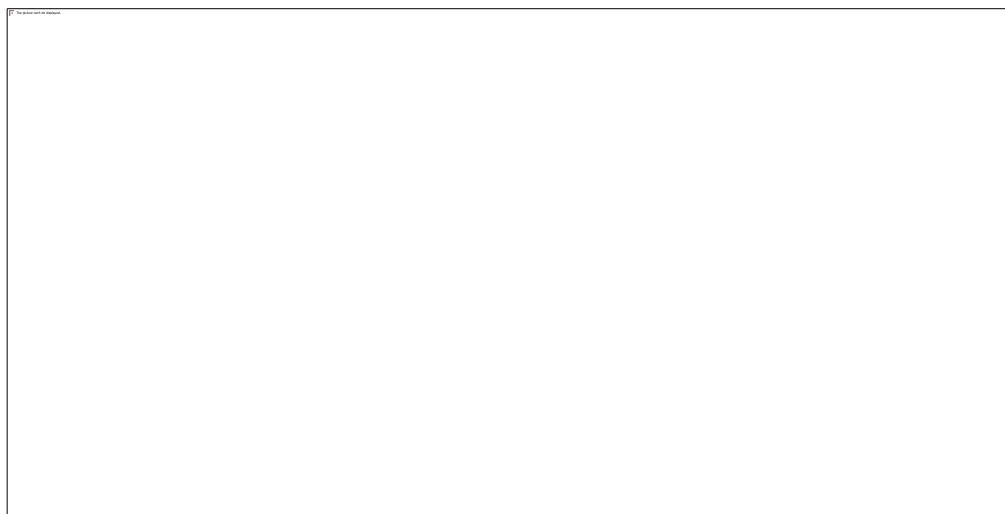
Figure 2-3. FTIR spectra of SQD-perylene (a), SQD-phenanthrene (b), and SQD-pyrene (c).

The dye-terminated SQDs were further investigated using high resolution XPS spectroscopy. Figure 2-4 shows high resolution XPS spectra of Si 2p for SQD-phenanthrene (a), SQD-pyrene (b), and SQD-perylene (c). The Si 2p spectra in Figure 2-4 were fitted with two peaks and one Shirley background. The deconvoluted peaks centered at 102.48, 102.37, and 102.19 eV are attributed to Si-C [33,34], which confirms that the

SQDs surface changed from H- to organic dye termination. The components at 103.50 and 103.30 eV are assigned to Si-O, indicating that the surface of the SQDs has been partially oxidized under ambient conditions [34]. XPS spectrum of C 1 s for SQD-pyrene (Figure 2-9) shows multiple peaks binding energy assigned to C-Si, $C=C$, CO_3, $O-C=O$, $C=O$, along with a key feature located at 291.4 eV, which is attributed to the characteristic shake-up peak, exhibited by the conjugated system or aromatic groups [35]. This further confirms the bonding of pyrene to SQDs through a conjugated linkage. These XPS results are in agreement with the FTIR results, confirming that the passivation of the SQDs has been successfully achieved and the aromatic fluorophores are covalently bonded to SQDs through a conjugated linkage.
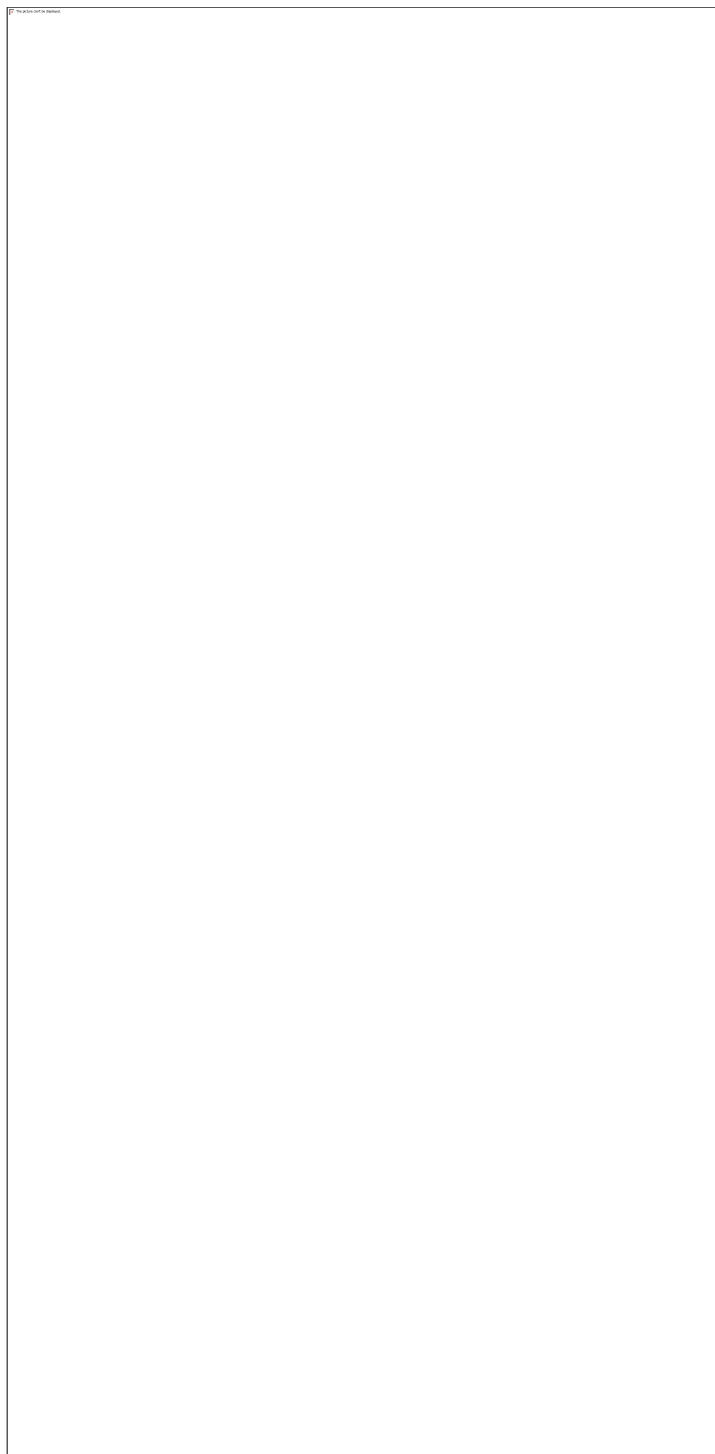
Figure 2-4. XPS spectra of Si 2p for SQD-phenanthrene (a), SQD-pyrene (b), and SQD-perylene (c).

2.2.2 Photophysical properties

The photophysical properties, including emission lifetime (τ_e), quantum efficiency, (Φ_{PL}) and emission and excitation spectra of the SQD-phenanthrene, SQD-perylene, SQD-pyrene, reference SQD-heptene, and chromophores phenanthrene, perylene and pyrene were investigated in DCM and are summarized in Table 2-1.

Table 2-1. Photophysical properties collected in DCM at 298 K.

	λ_{ex} nm	λ_{em} nm (RI)[a]	Φ_{PL}[b] %[a,c]	τ_e ns(pe)[f]
perylene	360	465 (1), 489 (0.95), 530 (0.41)	89	4.4
pyrene	360	384 (1), 404 (0.39), 431 (0.13)	61	2.2 (9), 17.9 (91)
phenanthrene	315	358 (0.74), 367 (0.94), 376 (1), 387 (0.69), 392 (0.48)	14	1.4 (67), 6.3 (33)
SQD-heptene	360	446	8	1.8 (27), 6.07 (73)
SQD-heptene	315	374	—	—
SQD-perylene	360	515	18[c]	2.5 (38), 6.6 (62)
SQD-pyrene	360	396 (1), 415 (0.95), 482 (0.52)	11[d]	1.9 (46), 7.7 (54)
SQD-phenanthrene	315	439	8[e]	1.8 (58), 6.9 (42)

[a]RI = relative intensity of the emission peak. [b]Quinine sulfate employed as the external reference (Φ_{PL} = 54.6% in 0.5 M H_2SO_4 at 298 K, λ_{exc} = 360 nm) [41]. [c]λ_{ex} = 440 nm, [d]λ_{ex} = 330 nm, [e]λ_{ex} = 310 nm. [f]pe = pre-exponential weighting factor, in relative % intensity, of the emission decay kinetics (λ_{ex} = 378 nm).

SQD-perylene and SQD-pyrene exhibited broad, red- and blueshifted emission maxima at λ_{max} = 515 and 396 nm, respectively with modestly higher photoluminescence quantum yields, Φ_{PL}, (SQD-perylene: Φ_{PL} = 18%, SQD-pyrene: Φ_{PL} = 11%) compared to the

heptene-capped control counterpart SQDs (SQD-heptene: $\lambda_{max} = 446$ nm, $\Phi_{PL} = 8\%$), when excited at 360 nm. Similarly, the SQD-phenanthrene exhibited a red-shifted emission maximum at $\lambda_{max} = 439$ nm compared to SQD-heptene ($\lambda_{max} = 374$ nm) when excited at 315 nm, but with a Φ_{PL} of 8%, which is similar to that of SQD-heptene (Figure 2-5).
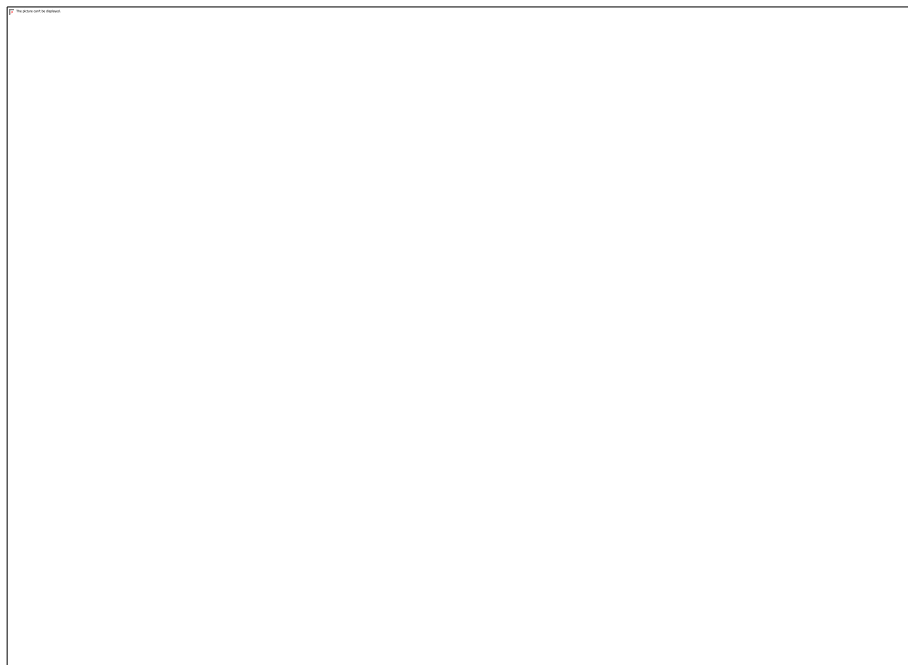
Figure 2-5. Emission spectra of SQD-heptene (dotted green line, $\lambda_{ex} = 315$ nm), SQD-phenanthrene (solid pink line, $\lambda_{ex} = 315$ nm), SQD-heptene (dotted black line, $\lambda_{ex} = 360$ nm), SQD-pyrene (solid blue line, $\lambda_{ex} = 360$ nm), and SQD-perylene (solid red line, $\lambda_{ex} = 360$ nm.

In water, both the SQD-pyrene and SQD-perylene exhibited emission peak maxima at 395 and 521 nm, respectively (Figure 2-20). Evidence of pyrene excimer emission at concentrations higher than 10 and 176 µM was observed for SQD-pyrene and free pyrene at 487 nm, respectively (Figures 2-18 and 2-19) [36]. It is also worth noting that SQD-phenanthrene, SQD-pyrene, and SQD-perylene exhibited red-shifted emissions comparing to their corresponding free aromatic fluorophores (Table 2-1 and Figures 2-12:2-14). Hence, depending on the surface functionalization of the SQD core, different emission maxima were observed, pointing to an ability of the chromophores to tune the emission properties of the nanoparticle.

Generally, any σ-π conjugation between Si atoms and π-conjugated fluorophores should increase the interaction of the aromatic fluorophores with the electronic wave functions of the SQDs [34], influencing the electronic structure of SQDs and inducing red-shifted emissions compared to fluorophore-free SQDs. This may account for the observed significant red-shifted emission of SQD-perylene and SQD-phenanthrene by 69 and 65 nm, respectively, compared to that of SQD-heptene. However, the emission of SQD-pyrene did not behave in an analogous manner. The deviation from the expected behavior may be attributed to the high ratio of Si-O$_x$ species, (SiO$_2$: Si-C ~ 1:1), on the silicon network, which seems crucial for influencing the optical properties. This is in good agreement with a previous report of blue shifting in the emission of SQDs that have a monolayer of organic molecules grafted to their surface via controlled thermal or photoinitiated surface oxidation [37]. From the XPS spectra, the ratio of SiO$_2$ on the silicon surface in SQD-pyrene and SQD-perylene was found to be (25:1), respectively. Thus, the blue shift in the emission of SQD-pyrene compared to that of SQD-heptene when excited at wavelength of 360 nm may have resulted from a greater surface oxidation.

The photoluminescence spectra for the SQD-perylene, SQD-pyrene, and SQD-phenanthrene assemblies were collected by photoexciting either at 360 nm, where the SQD core predominantly absorbs, or at 450 nm, 340 nm and 315 nm, where the perylene, pyrene or phenanthrene moieties, respectively, are predominantly photoexcited. Identical photoluminescence spectra without any contribution from the free perylene, pyrene or phenanthrene were observed (Figures 2-15:2-17). Thus, SQD-perylene, SQD-pyrene, and SQD-phenanthrene assemblies exhibit efficient energy transfer from the fluorophore to the SQD core upon photoexcitation. As no triplet states are involved in the energy transfer process between the fluorophore and the nanoparticle core as evident from the recorded lifetimes given in Table 2-1, and the PL spectra of all donor fluorophores exhibit spectral overlap with SQDs absorption (Figures 2-12:2-14), Förster energy transfer is the likely mechanism for energy transfer in these systems [38,39]. Photoluminescence excitation spectra measured by detecting the emissions of SQD-fluorophore are further consistent with energy transfer from the fluorophore to the SQD core, with the appearance of the corresponding perylene, pyrene and phenanthrene-based absorptions (Figures 2-12:2-14). Energy transfer from pyrene to SQDs in SQD-pyrene is also evidenced in the emission

lifetime decay monitored at 420 nm collected upon photoexcitation at 378 nm. Indeed, the bi-exponential emission lifetime of SQD-pyrene of 1.9 and 7.7 ns is similar to that of SQD-heptene ($\tau_e = 1.8$, 6.07 ns) and much shorter than that of the free pyrene fluorophore ($\tau_e = 2.2$ and 17.9 ns). The shorter lifetime of SQD-pyrene compared to free pyrene is consistent with energy transfer from the bound pyrene to the SQD core. Energy transfer from pyrene moieties covalently linked to silicon nanocrystals was also previously observed [22]. Similarly, SQD-perylene and SQD-phenanthrene exhibited respectively bi-exponential emission decays of $\tau_e = 2.5$, 6.6 ns and $\tau_e = 1.8$, 6.9 ns, which are correspondingly slightly shorter and longer compared to those of the free chromophores perylene ($\tau_e = 4.4$ ns) and phenanthrene ($\tau_e = 1.4$, 6.3 ns).

It is worth noting that because of the small size of the functionalized SQDs, the PL deviates significantly from the quantum confinement prediction. This is attributed to the non-radiative trapping of electrons in the higher excited states by surface states [24]. Thus, the nature of the fluorophore linked to the SQD surface, and the electronic communication between SQD core and fluorophores (through the σ-π conjugation) strongly influence the optical properties of the SQD core. This strategy is beneficial for producing SQDs with tunable emission wavelengths by modifying the surface with aromatic fluorophores and can be applied to overcome current synthetic limitations where only blue-emitting nanoparticles are predominantly obtained.

2.2.3 Fluorescent cellular imaging study

To demonstrate the suitability of SQD-perylene and SQD-pyrene assemblies for bioimaging application, they were used for *in vitro* fluorescent imaging of cancerous HeLa cells. The cells were incubated for 3 hours with SQD-perylene and SQD-pyrene, respectively. The nanoparticles were then excited at 405 nm using confocal microscopy to monitor the uptake of SQDs (Figure 2-6). The images were collected after 135 seconds of constant excitation to quench the cellular autofluorescence. Fluorescence imaging of HeLa cells without SQDs (panels A–C), with SQD-perylene (panels D–F), and SQD-pyrene (panels G–I) show bright fluorescence for cells incubated with SQD. The efficient uptake of nanoparticles by cells demonstrates the potential utility of SQDs for bioimaging studies.
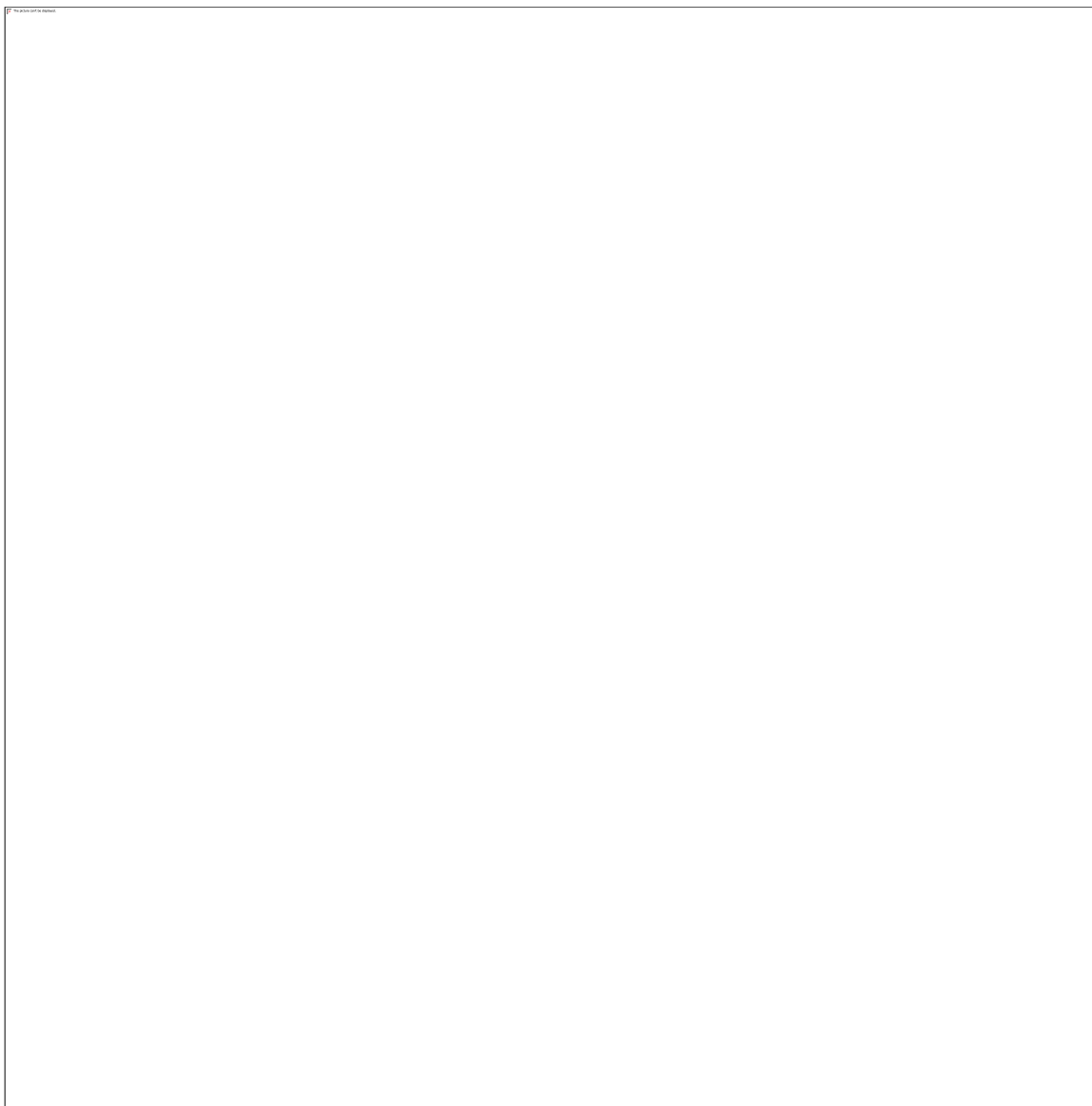
Figure 2-6. Confocal images of HeLa cells for DIC images (panels A, D, and G), fluorescence images (panels B, E, and H), and merged images (panels C, F, and I). Scale bar = 10 μm. Panels (A–C) are for control sample without SQDs, (D–F) and (G–I) are for cells incubated with SQD-perylene and SQD-pyrene, respectively.

2.2.4 Cytotoxicity Studies

The cytotoxicity of SQD-pyrene and SQD-perylene was assessed by TNF-α cytotoxicity assay to investigate whether the materials would be harmful when used for biomedical applications. Figure 2-7 shows the results of the TNF-α cytotoxicity assay for SQD-

perylene and SQD-pyrene at different concentrations. Over the concentration range in Figure 2-7, the cellular viability decreased by up to 40% of the control for SQD-perylene and SQD-pyrene. Hence, the nanoparticles SQD-perylene and SQD-pyrene were found to have low cytotoxicity, indicating the possibility of using SQDs for biolabeling applications.
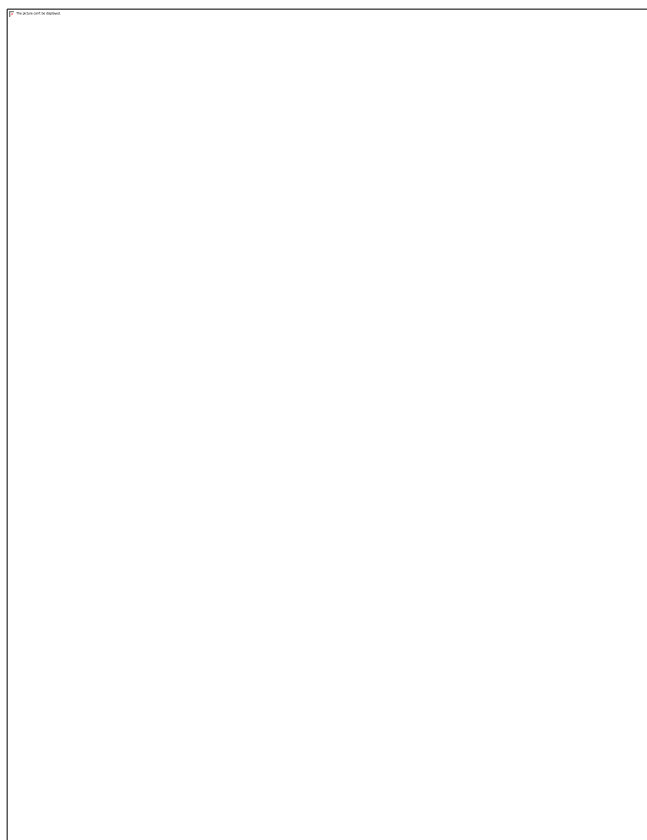
Figure 2-7. Cytotoxicity effect of the nanoparticles SQD-pyrene (A) and SQD-perylene (B) measured by TNF-α assay.

2.2.5 Conclusion

In summary, we have synthesized three families of SQDs covalently functionalized with phenanthrene, pyrene, and perylene chromophores. The PL of SQD core was red-shifted by 69 and 65 nm, and blue-shifted by 50 nm when perylene, phenanthrene, and pyrene were used as capping agents, respectively, compared to the counterpart model compound, SQD-heptene. The quantum efficiency was improved from 8% in SQD-heptene to 18% and 11% in SQD-perylene and SQD-pyrene, respectively. Therefore, the functionalization of the

SQD core with aromatic fluorophores is an efficient strategy to tune the optical properties of SQDs and improve their quantum efficiency. The nanoparticles SQD-perylene and SQD-pyrene showed promising results when used for fluorescent cellular imaging with low cytotoxicity, which enables the SQDs to be used as fluorescence probes in bioimaging. We are now aiming to apply this strategy to prepare SQDs that emit in the near-IR region and use them as photodynamic therapy agents for the apoptosis of cancer cells.

2.3 Methods

Materials

3-Ethynyl perylene, tetraoctylammonium bromide (98%, TOAB), silicon tetrachloride (99.998%, $SiCl_4$), hexachloroplatinic acid hexahydrate (Pt), lithium aluminum hydride solution (LAH, 1 M in THF), 1-ethynyl pyrene (pyrene), 3-ethynyl perylene (perylene), 9-ethynyl phenanthrene (97%, phenanthrene), and 1-heptyne (98%, heptyne) were used without additional purification. All solvents were dried by passing through MB SPS-800 (MBraun) solvent purification system with water content below 15 ppm.

Characterization

UV-Vis absorption spectra were measured using a Shimadzu UV-1800 double beam spectrophotometer. Steady-state emission and excitation spectra and time-resolved spectra were recorded at 298 K using an Edinburgh Instruments F980. The XPS analyses were carried out with a Kratos Axis Nova spectrometer using a monochromatic Al K(alpha) source (15 mA, 14 kV). The TEM/HRTEM images were recorded using Libra 200 MC operated at 200 kV. The FTIR spectra were obtained from a Nicolet 6700 FTIR spectrometer equipped with a smart iTR diamond horizontal attenuated total reflectance (ATR).

Photophysical measurements

All samples were prepared in HPLC grade dichloromethane with varying concentrations in the order of μM. Absorption spectra were recorded at room temperature using a Shimadzu UV-1800 double beam spectrophotometer. Molar absorptivity determination

was verified by linear least-squares fit of values obtained from at least four independent solutions at varying concentrations with absorbance ranging from 4.00×10^{-6} to 2.00×10^{-5} M.

The sample solutions for the emission spectra were prepared in HPLC-grade DCM and degassed *via* bubbling nitrogen for five minutes using a quartz cuvette designed in-house. Steady-state emission and excitation spectra and time-resolved emission spectra were recorded at 298 K using an Edinburgh Instruments F980. All samples for steady-state measurements were excited at 440 nm, 360 nm, 330 nm and 310 nm while samples for time-resolved measurements were excited at 378 nm using a PDL 800-D pulsed diode laser. Emission quantum yields were determined using the optically dilute method[40]. A stock solution with absorbance of *ca*. 0.5 was prepared and then four dilutions were prepared with dilution factors between 2 and 20 to obtain solutions with absorbances of *ca*. 0.095 0.065, 0.05 and 0.018, respectively. The Beer-Lambert law was found to be linear at the concentrations of these solutions. The emission spectra were then measured after the solutions were degassed *via* bubbling nitrogen for five minutes prior to spectrum acquisition. For each sample, linearity between absorption and emission intensity was verified through linear regression analysis and additional measurements were acquired until the Pearson regression factor (R^2) for the linear fit of the data set surpassed 0.9. Individual relative quantum yield values were calculated for each solution and the values reported represent the slope value. The equation $\Phi_s = \Phi_r(A_r/A_s)(I_s/I_r)(n_s/n_r)$[41] was used to calculate the relative quantum yield of each of the sample, where Φ_r is the absolute quantum yield of the reference, n is the refractive index of the solvent, A is the absorbance at the excitation wavelength, and I is the integrated area under the corrected emission curve. The subscripts s and r refer to the sample and reference, respectively. A solution of quinine sulfate in 0.5 M H_2SO_4 ($\Phi_r = 54.6\%$) was used as external ref.[42].

Synthesis and purification of functionalized SQDs

The synthesis of SQDs functionalized with conjugated aromatic linkages was carried out using Tilley's method[12,43]. All experiments were performed under argon atmosphere using a glovebox. In a typical experiment, 1.5 g of TOAB and 150 µL of $SiCl_4$ were dissolved in

100 mL of dry toluene by stirring for 45 minutes. An excess amount of lithium aluminum hydride (LAH) solution was then added, and the mixture was further stirred for 3 hours to produce H-terminated SQDs. Anhydrous methanol was then added to quench the excess of LAH until no further effervescence was observed. The passivation of H-terminated SQDs was carried out by reacting the SQDs with 4 mL of heptyne to produce SQD-heptene using 100 µL of 0.1 M Pt catalyst in methanol. The latter procedure was repeated using phenanthrene (500 mg), pyrene (500 mg), and perylene (500 mg) as capping agents to produce SQD-phenanthrene, SQD-pyrene, and SQD-perylene, respectively (Figure 2-1). The resulting capped SQDs were purified by dialysis against water to removed inorganic salts, and then DCM to remove organic impurities (MWCO of 1 KDa, Spectra/Por® 6 Standard RC Pre-wetted Dialysis Tubing, diameter 29 mm).

Fluorescent Imaging

The HeLa cells were cultured one day prior to imaging at a volume of 1×10^5 cells/well on a 6-well culture plate with the medium (Dulbecco's modified Eagle's medium (DMEM), 10% fetal calf serum and 4 mM L-glutamine) at 37 °C and 5% CO_2. On the day of imaging, cells were grown to 80% confluence and they were incubated with 50–100 µg/ml of functionalized SQDs dispersed in phosphate-buffered saline (PBS) for 3 hrs. Immediately before imaging, the medium was removed, and HeLa cells were washed $3 \times$ using fresh PBS solution. The cells were then imaged using a confocal microscope (Zeiss LSM 510 Duo Confocal).

Cytotoxicity (TNF-α)

TNF-α assay was performed to evaluate the cytotoxicity of SQD-pyrene and SQD-perylene. Cells were cultured in 96-well microplates in a humidified atmosphere (37 °C and 5% CO_2) to $70 - 80\%$ confluence. The cells were seeded at a concentration of 5×10^4 cells/well in 100 µl of culture medium (1 µg/ml of actinomycin C1 and various amounts of TNF-α) and different concentrations of SQDs. The cells were incubated for 24 hours at these conditions. Afterwards, 10 µl of Cell Proliferation Reagent WST-1 was added and incubated for another 4 hours, and they were finally shaken for 1 minute. The absorbance

of the sample was measured against the background control as blank using a microplate (ELISA) reader at wavelength of 450 nm.

2.4 Supporting Information
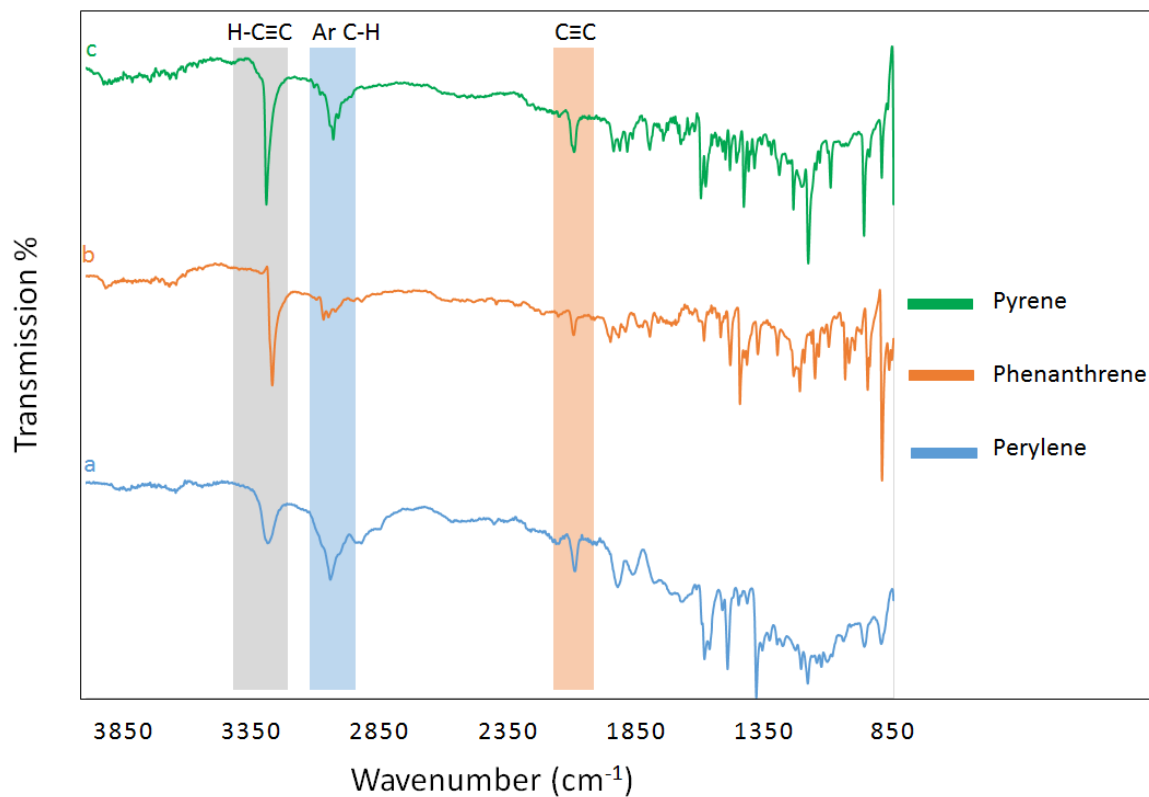
Figure 2-8. FTIR spectra of 3-Ethynylperylene(a), 9-Ethynylphenanthrene (b), and 1-Ethynylpyrene (c).
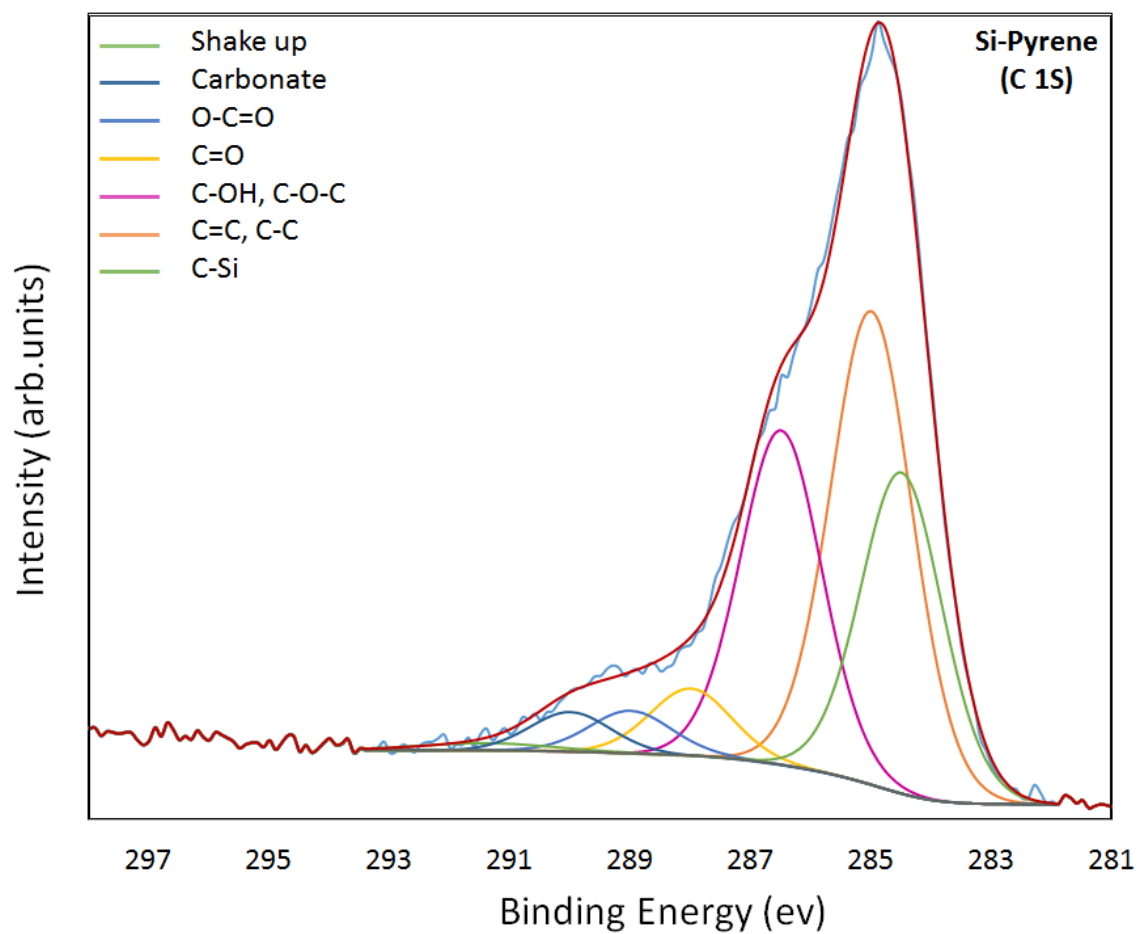
Figure 2-9. XPS spectra of C 1S for SQD-pyrene
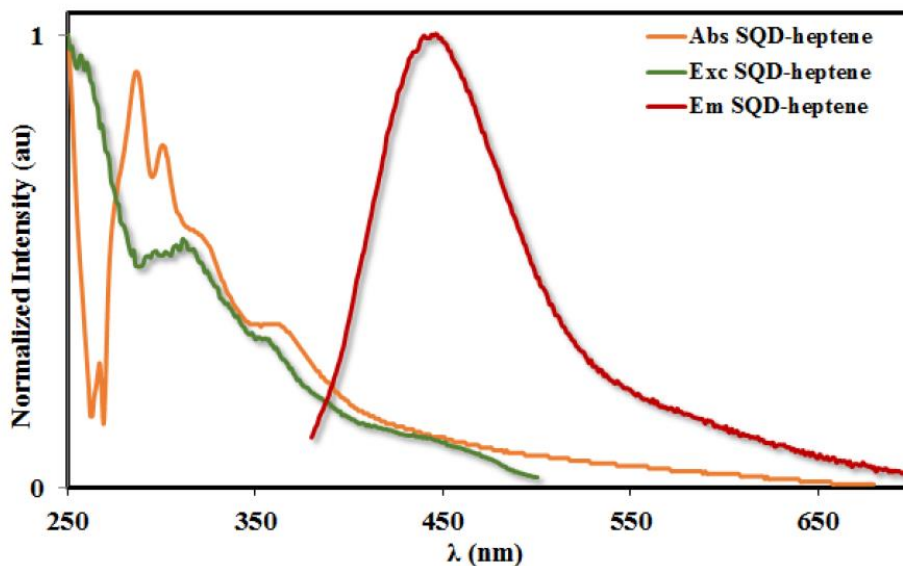
Figure 2-10. UV-Vis absorption, excitation (λ_{em} = 448 nm), and emission spectra of SQD-heptene collected in degassed DCM at 298 K (λ_{ex} = 360 nm).
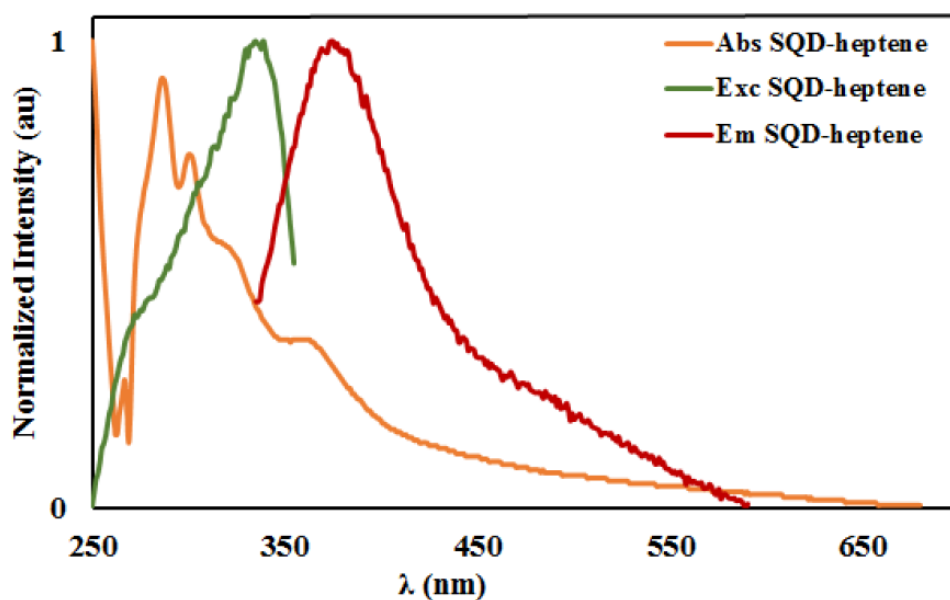
Figure 2-11. UV-Vis absorption, excitation (λ_{em} = 374 nm), and emission spectra of SQD-heptene collected in degassed DCM at 298 K (λ_{ex} = 315 nm).
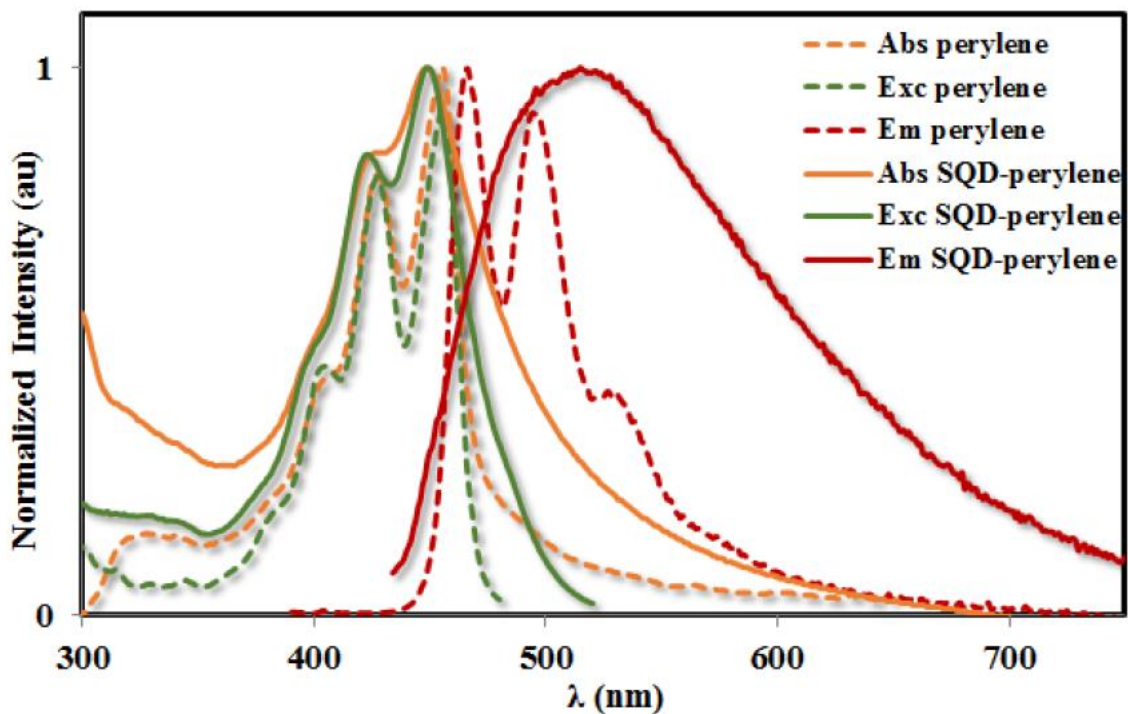
Figure 2-12. UV-Vis spectra of perylene (dotted orange line) and SQD-perylene (solid orange line); excitation spectra of perylene (dotted green line, λ_{em} = 467 nm) and SQD-perylene (solid green line, λ_{em} = 518 nm); and emission spectra of perylene (dotted red line) and SQD-perylene (solid red line) collected in degassed DCM at 298 K (λ_{ex} = 360 nm).
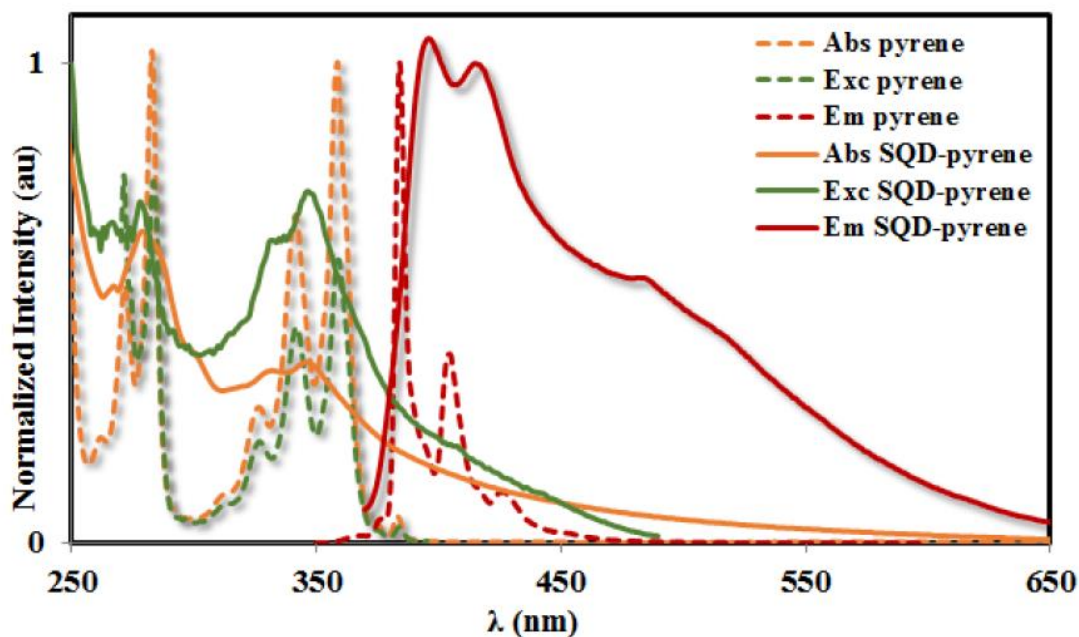
Figure 2-13. UV-Vis spectra of pyrene (dotted orange line) and SQD-pyrene (solid orange line); excitation spectra of pyrene (dotted green line, λ_{em} = 384 nm) and SQD-pyrene (solid green line, λ_{em} = 397 nm); and emission spectra of pyrene (dotted red line) and SQD-pyrene (solid red line) collected in degassed DCM at 298 K (λ_{ex} = 360 nm).
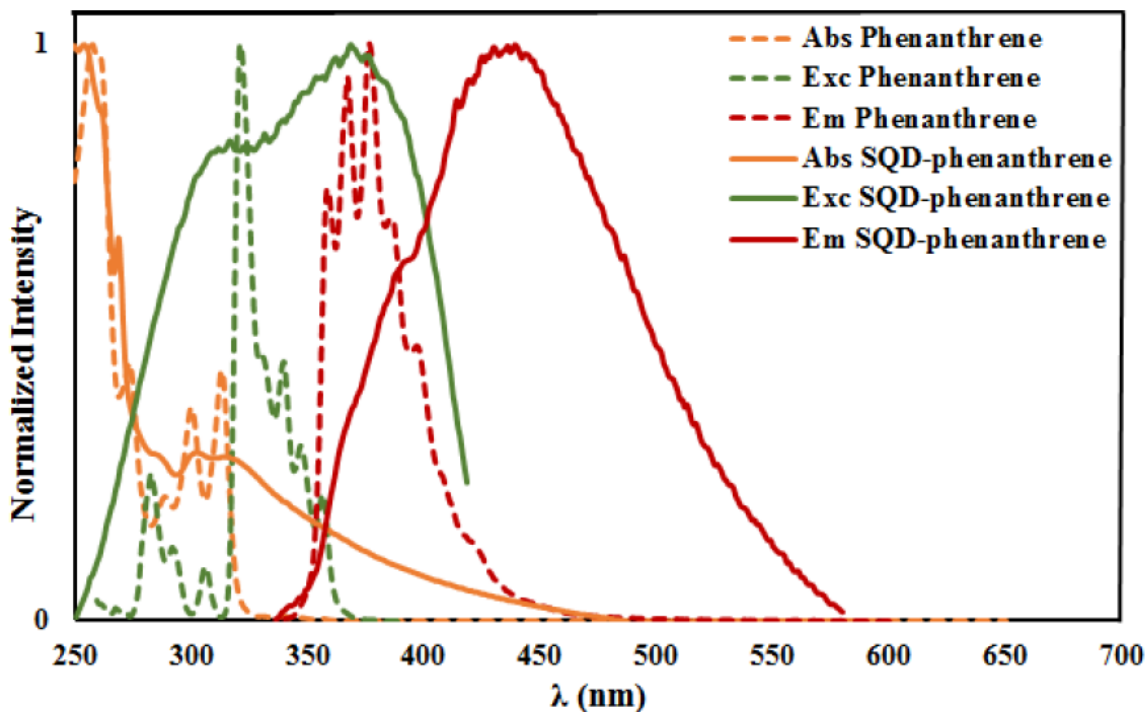
Figure 2-14. UV-Vis spectra of phenanthrene (dotted orange line) and SQD-phenanthrene (solid orange line); excitation spectra of Phenanthrene (dotted green line, λ_{em} = 377 nm) and SQD-phenanthrene (solid green line, λ_{em} = 447 nm); and emission spectra of phenanthrene (dotted red line) and SQD-phenanthrene (solid red line) collected in degassed DCM at 298 K (λ_{ex} = 315 nm).
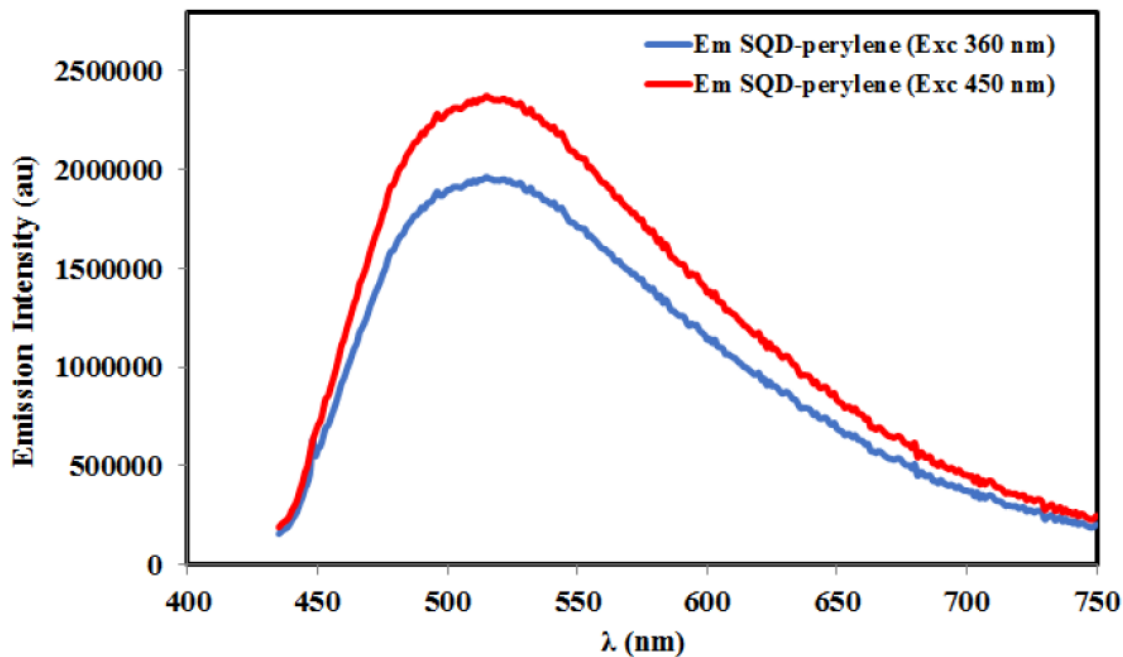
Figure 2-15. Emission spectra of SQD-perylene collected in degassed DCM at 298 K upon photoexcitation at 360 nm (light-blue line) and at 450 nm (red line).
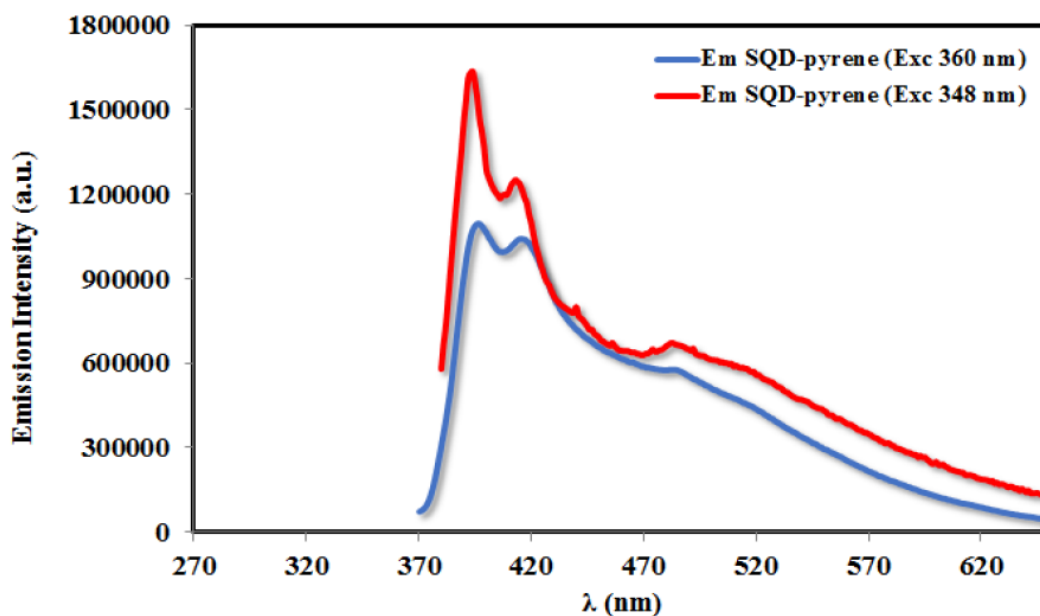
Figure 2-16. Emission spectra of SQD-pyrene collected in degassed DCM at 298 K upon photoexcitation at 360 nm (light-blue line) and at 348 nm (red line).
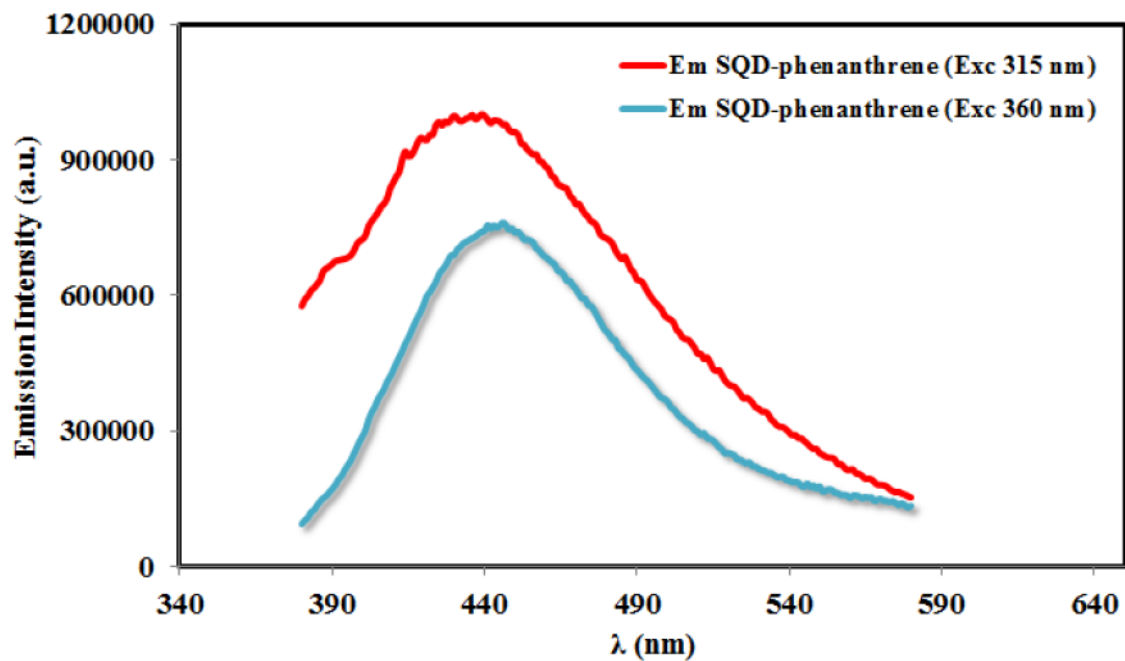
Figure 2-17. Emission spectra of SQD-phenanthrene collected in degassed DCM at 298 K upon photoexcitation at 360 nm (light-blue line) and at 315 nm (red line).
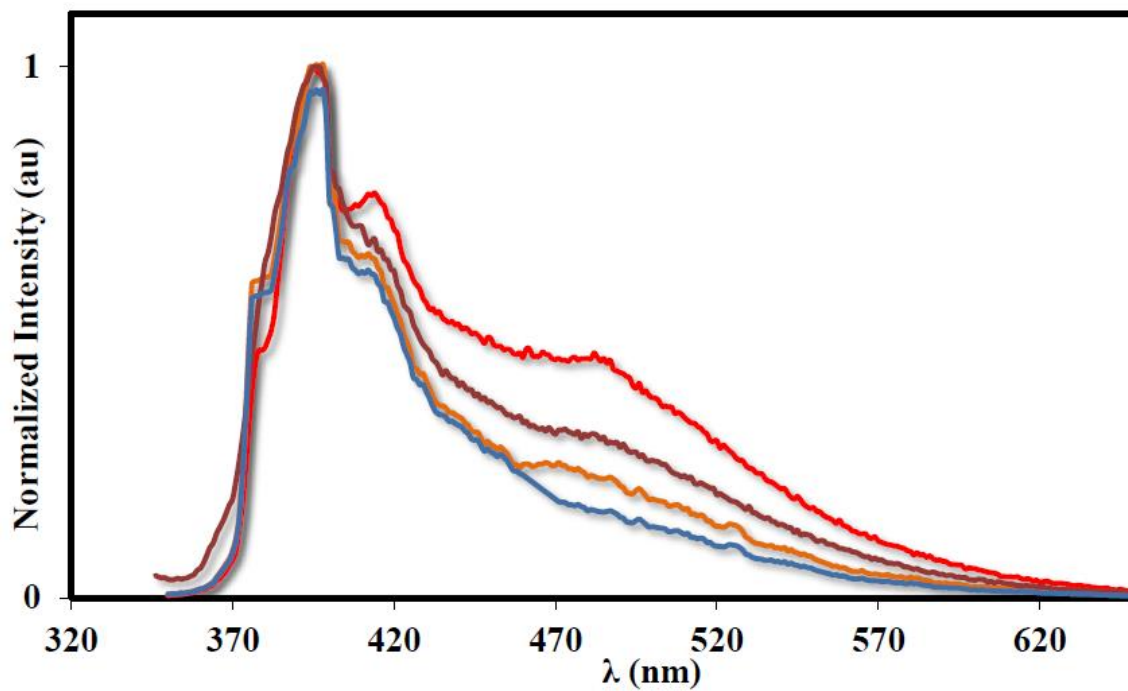
Figure 2-18. Emission spectra of SQD-pyrene collected in degassed DCM at 298 K at a concentration of 100 µM (red line), 50 µM (purple line), 10 µM (orange line) and 1 µM (blue line) (λ_{ex} = 360 nm).
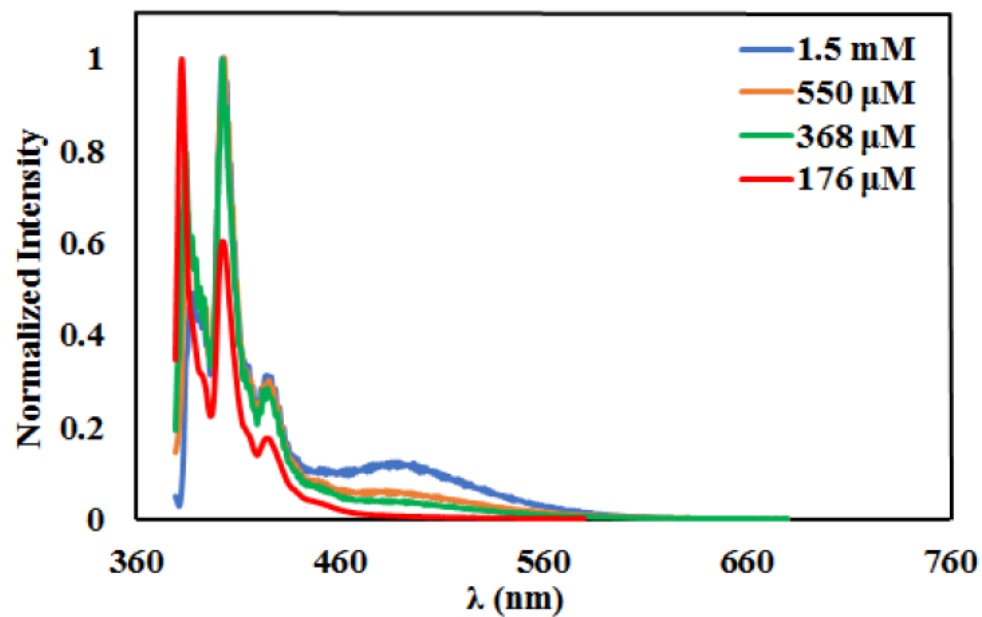
Figure 2-19. Emission spectra of pyrene collected in degassed DCM at 298 K at a concentration of 1.5 mM (blue line), 550 µM (orange line), 368 µM (green line) and 176 µM (red line) (λ_{ex} = 360 nm).
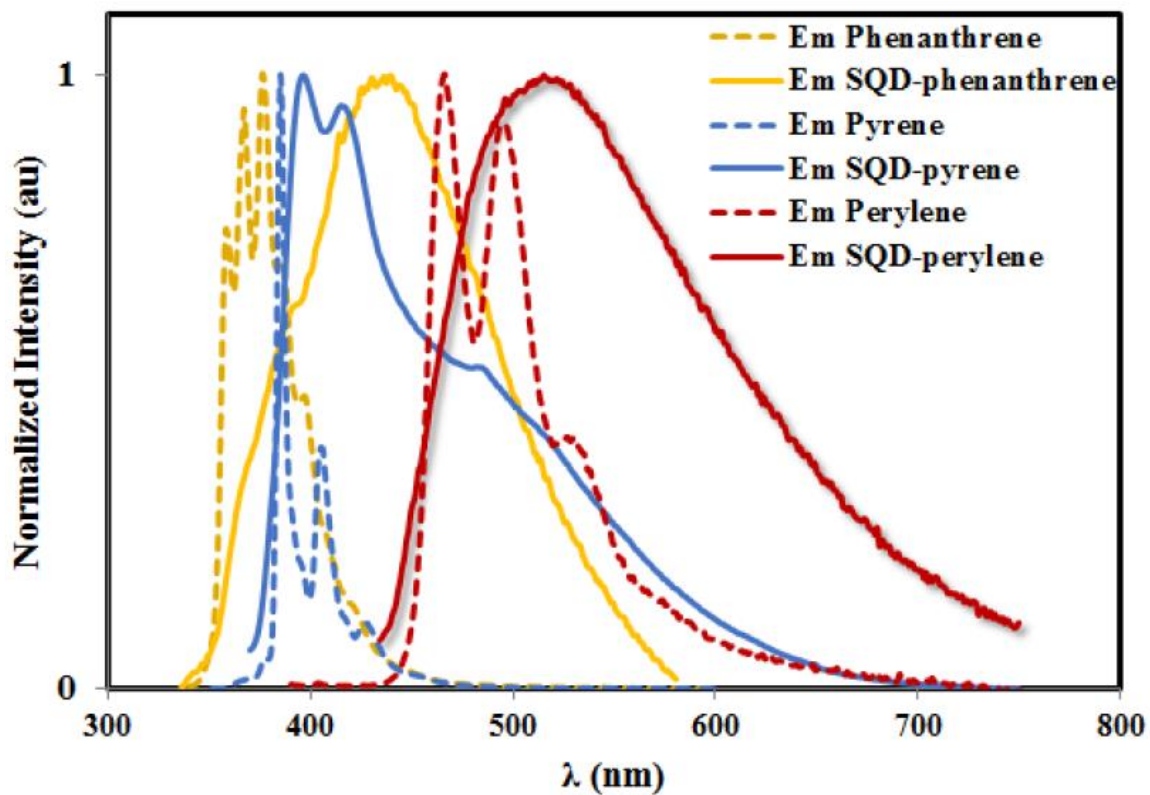
Figure 2-20. Emission spectra of perylene (λ_{ex} = 360 nm, dotted red line) and SQD-perylene (λ_{ex} = 360 nm, solid red line); pyrene (λ_{ex} = 360 nm, dotted blue line) and SQD-pyrene (λ_{ex} = 360 nm, solid blue-line); phenanthrene (λ_{ex} = 315 nm, dotted yellow line) and SQD-phenanthrene (λ_{ex} = 315 nm, solid yellow line) collected in degassed DCM at 298 K.
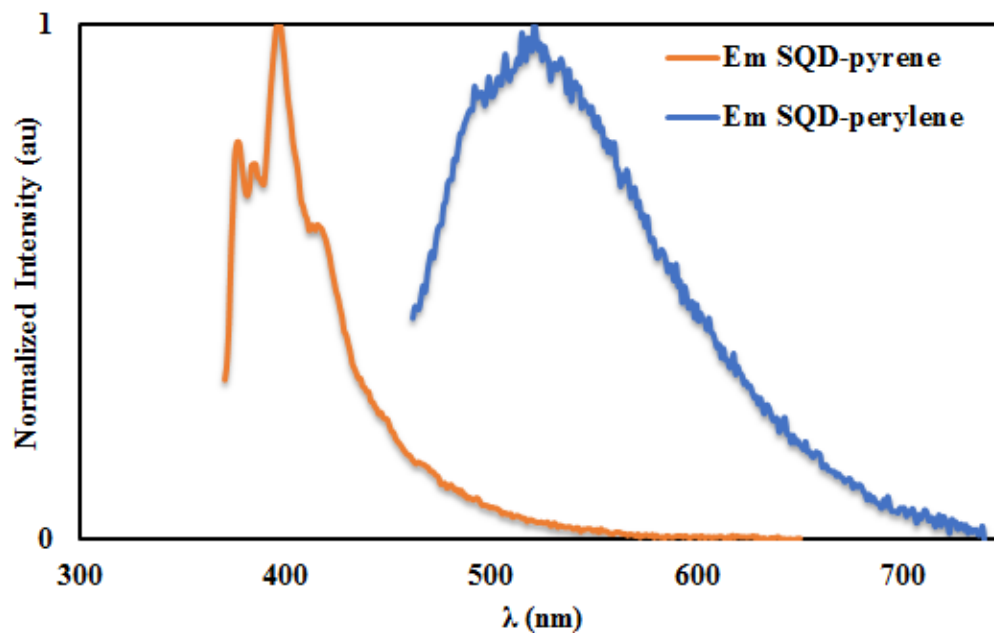
Figure 2-21. Emission spectra of SQD-perylene (λ_{ex} = 440 nm, blue) and SQD-pyrene (λ_{ex} = 350 nm, orange) in water.

2.5 Reference

1.   Alivisatos, A. P. "Perspectives on the Physical Chemistry of Semiconductor Nanocrystals." The Journal of Physical Chemistry 100 (1996/01/01 1996): 13226-13239.

2.   Erogbogbo, Folarin; Yong, Ken-Tye; Roy, Indrajit; Xu, GaiXia; Prasad, Paras N.; and Swihart, Mark T. "Biocompatible Luminescent Silicon Quantum Dots for Imaging of Cancer Cells." ACS Nano 2 (2008/05/01 2008): 873-878.

3.   Choi, Jonghoon; Zhang, Qin; Reipa, Vytas; Wang, Nam Sun; Stratmeyer, Melvin E.; Hitchins, Victoria M.; and Goering, Peter L. "Comparison of cytotoxic and inflammatory responses of photoluminescent silicon nanoparticles with silicon micron-sized particles in RAW 264.7 macrophages." Journal of Applied Toxicology 29 (2009): 52-60.

4.   Buriak, Jillian M. "Illuminating Silicon Surface Hydrosilylation: An Unexpected Plurality of Mechanisms." Chemistry of Materials 26 (2014/01/14 2014): 763-772.

5.   Beckman, James, and Ischenko, Anatoli. "Silicon nanoparticlefor photodynamic cancer treatment utilizing quantum dot optical properties."Google Patents, 2013.

6.   Kang, Zhenhui; Liu, Yang; Tsang, Chi Him A; Ma, Dorothy Duo Duo; Fan, Xia; Wong, Ning-Bew; and Lee, Shuit-Tong. "Water-soluble silicon quantum dots with wavelength-tunable photoluminescence." Advanced Materials 21 (2009): 661-664.

7.   Erogbogbo, Folarin; Chang, Ching-Wen; May, Jasmine L; Liu, Liwei; Kumar, Rajiv; Law, Wing-Cheung; Ding, Hong; Yong, Ken Tye; Roy, Indrajit; and Sheshadri, Mukund. "Bioconjugation of luminescent silicon quantum dots to gadolinium ions for bioimaging applications." Nanoscale 4 (2012): 5483-5489.

8.   Hessel, Colin M; Reid, Dariya; Panthani, Matthew G; Rasch, Michael R; Goodfellow, Brian W; Wei, Junwei; Fujii, Hiromasa; Akhavan, Vahid; and Korgel, Brian A. "Synthesis of ligand-stabilized silicon nanocrystals with size-dependent

photoluminescence spanning visible to near-infrared wavelengths." Chemistry of materials 24 (2011): 393-401.

9.   Heath, James R. "A liquid-solution-phase synthesis of crystalline silicon." Science 258 (1992): 1131-1133.

10.   Baldwin, Richard K; Pettigrew, Katherine A; Ratai, Eva; Augustine, Matthew P; and Kauzlarich, Susan M. "Solution reduction synthesis of surface stabilized silicon nanoparticles." Chemical communications (2002): 1822-1823.

11.   Arul Dhas, N; Raj, C Paul; and Gedanken, A. "Preparation of luminescent silicon nanoparticles: a novel sonochemical approach." Chemistry of materials 10 (1998): 3278-3281.

12.   Warner, Jamie H; Hoshino, Akiyoshi; Yamamoto, Kenji; and Tilley, Richard D. "Water-soluble photoluminescent silicon quantum dots." Angewandte Chemie International Edition 44 (2005): 4550-4554.

13.   Tilley, Richard D, and Yamamoto, Kenji. "The microemulsion synthesis of hydrophobic and hydrophilic silicon nanocrystals." Advanced Materials 18 (2006): 2053-2056.

14.   Dasog, Mita; Yang, Zhenyu; Regli, Sarah; Atkins, Tonya M; Faramus, Angelique; Singh, Mani P; Muthuswamy, Elayaraja; Kauzlarich, Susan M; Tilley, Richard D; and Veinot, Jonathan GC. "Chemical insight into the origin of red and blue photoluminescence arising from freestanding silicon nanocrystals." Acs Nano 7 (2013): 2676-2685.

15.   Wang, Rong; Pi, Xiaodong; and Yang, Deren. "First-principles study on the surface chemistry of 1.4 nm silicon nanocrystals: case of hydrosilylation." The Journal of Physical Chemistry C 116 (2012): 19434-19443.

16.   Erogbogbo, Folarin; Chang, Ching-Wen; May, Jasmine; Prasad, Paras N; and Swihart, Mark T. "Energy transfer from a dye donor to enhance the luminescence of silicon quantum dots." Nanoscale 4 (2012): 5163-5168.

17. Medintz, Igor L, and Mattoussi, Hedi. "Quantum dot-based resonance energy transfer and its growing application in biology." Physical Chemistry Chemical Physics 11 (2009): 17-45.

18. Beljonne, David; Curutchet, Carles; Scholes, Gregory D; and Silbey, Robert J. "Beyond Forster resonance energy transfer in biological and nanoscale systems." The journal of physical chemistry B 113 (2009): 6583-6599.

19. Bae, Yoonjung; Lee, Doh C; Rhogojina, Elena V; Jurbergs, David C; Korgel, Brian A; and Bard, Allen J. "Electrochemistry and electrogenerated chemiluminescence of films of silicon nanoparticles in aqueous solution." Nanotechnology 17 (2006): 3791.

20. Rosso-Vasic, Milena; De Cola, Luisa; and Zuilhof, Han. "Efficient energy transfer between silicon nanoparticles and a Ru− polypyridine complex." The Journal of Physical Chemistry C 113 (2009): 2235-2240.

21. Sommer, Anja; Cimpean, Carla; Kunz, Michael; Oelsner, Christian; Kupka, Hans J; and Kryschi, Carola. "Ultrafast excitation energy transfer in vinylpyridine terminated silicon quantum dots." The Journal of Physical Chemistry C 115 (2011): 22781-22788.

22. Locritani, Mirko; Yu, Yixuan; Bergamini, Giacomo; Baroncini, Massimo; Molloy, Jennifer K; Korgel, Brian A; and Ceroni, Paola. "Silicon nanocrystals functionalized with pyrene units: efficient light-harvesting antennae with bright near-infrared emission." The journal of physical chemistry letters 5 (2014): 3325-3329.

23. Crego-Calama, Mercedes, and Reinhoudt, David N. "New materials for metal ion sensing by self-assembled monolayers on glass." Advanced materials 13 (2001): 1171-1174.

24. Wen, Xiaoming; Zhang, Pengfei; Smith, Trevor A; Anthony, Rebecca J; Kortshagen, Uwe R; Yu, Pyng; Feng, Yu; Shrestha, Santosh; Coniber, Gavin; and Huang, Shujuan. "Tunability limit of photoluminescence in colloidal silicon nanocrystals." Scientific reports 5 (2015): 12469.

25.   Huisken, F; Hofmeister, H; Kohn, B; Laguna, MA; and Paillard, V. "Laser production and deposition of light-emitting silicon nanoparticles." Applied Surface Science 154 (2000): 305-313.

26.   Wu, Jinzhu; Dai, Jun; Shao, Yanbin; and Sun, Yanchun. "One-step synthesis of fluorescent silicon quantum dots (Si-QDs) and their application for cell imaging." RSC Advances 5 (2015): 83581-83587.

27.   Wu, Fu-Gen; Zhang, Xiaodong; Kai, Siqi; Zhang, Mengyi; Wang, Hong-Yin; Myers, John N; Weng, Yuxiang; Liu, Peidang; Gu, Ning; and Chen, Zhan. "One-Step Synthesis of Superbright Water-Soluble Silicon Nanoparticles with Photoluminescence Quantum Yield Exceeding 80%." Advanced Materials Interfaces 2 (2015): 1500360.

28.   Cheng, Xiaoyu; Lowe, Stuart B; Ciampi, Simone; Magenau, Astrid; Gaus, Katharina; Reece, Peter J; and Gooding, J Justin. "Versatile "click chemistry" approach to functionalizing silicon quantum dots: applications toward fluorescent cellular imaging." Langmuir 30 (2014): 5209-5216.

29.   Wang, Guan; Ji, Jianwei; and Xu, Xiangxing. "Dual-emission of silicon quantum dots modified by 9-ethylanthracene." Journal of Materials Chemistry C 2 (2014): 1977-1981.

30.   Baskaran, Xavierravi; Vigila, Antony Varuvel Geo; Parimelazhagan, Thangaraj; Muralidhara-Rao, Doulathabad; and Zhang, Shouzhou. "Biosynthesis, characterization, and evaluation of bioactivities of leaf extract-mediated biocompatible silver nanoparticles from an early tracheophyte, Pteris tripartita sw." International journal of nanomedicine 11 (2016): 5789.

31.   Stuart, Barbara H. Infrared Spectroscopy: Fundamentals and Applications: Wiley-VCH Verlag Gmbh & Co. KGaA, 2004.

32.   Wolkin, MV; Jorne, J; Fauchet, PM; Allan, G; and Delerue, C. "Electronic states and luminescence in porous silicon quantum dots: the role of oxygen." Physical Review Letters 82 (1999): 197.

33.   Wang, Qi; Ni, Hongjun; Pietzsch, Annette; Hennies, Franz; Bao, Yongping; and Chao, Yimin. "Synthesis of water-dispersible photoluminescent silicon nanoparticles and their use in biological fluorescent imaging." Journal of Nanoparticle Research 13 (2011): 405-413.

34.   Dung, Mai Xuan; Tung, Dao Duy; Jeong, Sohee; and Jeong, Hyun-Dam. "Tuning Optical Properties of Si Quantum Dots by π-Conjugated Capping Molecules." Chemistry–An Asian Journal 8 (2013): 653-664.

35.   Permatasari, Fitri Aulia; Aimon, Akfiny Hasdi; Iskandar, Ferry; Ogi, Takashi; and Okuyama, Kikuo. "Role of C–N configurations in the photoluminescence of graphene quantum dots synthesized by a hydrothermal route." Scientific reports 6 (2016): 21042.

36.   Hammarström, Per; Kalman, Björn; Jonsson, Bengt-Harald; and Carlsson, Uno. "Pyrene excimer fluorescence as a proximity probe for investigation of residual structure in the unfolded state of human carbonic anhydrase II." FEBS letters 420 (1997): 63-68.

37.   Hua, Fengjun; Erogbogbo, Folarin; Swihart, Mark T; and Ruckenstein, Eli. "Organically capped silicon nanoparticles with blue photoluminescence prepared by hydrosilylation followed by oxidation." Langmuir 22 (2006): 4363-4370.

38.   Benniston, Andrew C; Chapman, Glen M; Harriman, Anthony; and Mehrabi, Maryam. "Intramolecular Energy Transfer in Molecular Dyads Comprising Free-base Porphyrin and Ruthenium (II) Bis (2, 2 ': 6 ', 2 ''-terpyridine) Termini." The Journal of Physical Chemistry A 108 (2004): 9026-9036.

39.   Ito, Fuyuki; Ishibashi, Yukihide; Khan, Sazzadur Rahman; Miyasaka, Hiroshi; Kameyama, Kazuya; Morisue, Mitsuhiko; Satake, Akiharu; Ogawa, Kazuya; and Kobuke, Yoshiaki. "Photoinduced electron transfer and excitation energy transfer in directly linked zinc porphyrin/zinc phthalocyanine composite." The Journal of Physical Chemistry A 110 (2006): 12734-12742.

40.   Crosby, Glenn A, and Demas, James N. "Measurement of photoluminescence quantum yields. Review." The Journal of Physical Chemistry 75 (1971): 991-1024.

41.	Melhuish, WH. "Quantum efficiencies of fluorescence of organic substances: effect of solvent and concentration of the fluorescent solute1." The Journal of Physical Chemistry 65 (1961): 229-235.

42.	Brouwer, Albert M. "Standards for photoluminescence quantum yield measurements in solution (IUPAC Technical Report)." Pure and Applied Chemistry 83 (2011): 2213-2228.

43.	Chatterjee, Surajit, and Mukherjee, Tushar Kanti. "Spectroscopic investigation of interaction between bovine serum albumin and amine-functionalized silicon quantum dots." Physical Chemistry Chemical Physics 16 (2014): 8400-8408.

Chapter 3 Energy/Electron Transfer Switch for Controlling Optical Properties of Silicon Quantum Dots

This work was published in Scientific Reports, 8, 17068 (2018)

3.1 Introduction

Silicon Quantum Dots (SQDs) have recently attracted tremendous attention due to their unique optical properties, including wide absorption spectra, excellent stability against photobleaching compared to conventional dyes, and size-dependent tuneable photoluminescence (PL).[1] The SQDs have advantages over other quantum dots, including cadmium sulfide (CdS), due to their excellent biocompatibility and biodegradability, low toxicity, and the ease of their surface functionalization.[2] Thus, they are ideal candidates for a wide range of potential applications including bioimaging,[3] photodynamic therapy,[4] sensing,[5] photovoltaics,[6] and light-emitting diodes (LEDs).[7]

In general, the size-tuneable PL of SQDs is assigned to the quantum confinement effect where the PL is blue-shifted when the size of SQDs is more than ~ 3 nm. However, a deviation from this behaviour was observed for SQDs of size less than ~ 2 nm when the PL originates from surface relevant states.[8] The surface functionalization would then play a crucial role towards controlling the optical properties of SQDs.[9] It has been shown in previous studies that surface functionalization of SQDs with aromatic ligands helps tune their optical properties including their quantum yield and PL.[10,11] This strategy potentially can be utilized as a means to control the optical properties of SQDs. Moreover, the functionalization of SQDs with organic ligands increases their stability towards oxidation and prevents them from agglomeration and aggregation.[12]

Only a few reports in literature investigated the influence of aromatic fluorophores covalently linked to SQDs and the role of the spacer connecting the fluorophore on the optical properties of SQDs. Interestingly, the utilization of aromatic fluorophores as a capping agent was found to play a key role to control the optical properties of SQDs.[10,13,14,15,16]

Several methods have been reported in literature for preparing SQDs including laser pyrolysis,[17] the etching of bulk silicon,[18] nonthermal plasma,[19] and preparation in supercritical fluids.[20] In this work, a facile solution-based reduction method has been adopted with minor modifications to prepare SQDs.[21] Triethoxysilane derivatives and sodium citrate dihydrate were utilized as the silicon source and reducing agent, respectively while the synthesis was carried out in the glycerol green solvent at normal pressure and relatively high temperature (180 °C). Glycerol is a green solvent produced as a byproduct of biodiesel production, and with its high boiling point of 290 °C, and 3 available OH groups to help coordinate to the growing nanocrystals, is of interest for solvent engineering of SQDs.

Here, we report the synthesis of SQDs functionalized with perylene-3,4,9,10-tetracarboxylic acid diimide (PDI) through propylamine and N-propylurea spacers to produce Am-SQD-Per and Urea-SQD-Per, respectively. The PDI dye has been chosen for this study due to its excellent properties including high fluorescence quantum efficiency, high thermal and photochemical stability, and ease of processibility as well as scalability.[22] Additionally, the combination of the planar π-system of PDI and other electron withdrawing and donating groups within the system with SQDs could strongly affect the formed electronic interactions through a possible photoinduced energy and/or electron transfer processes. The latter processes are likely to change the optical properties of the assemblies. The products Am-SQD-Per and Urea-SQD-Per were characterized using high-resolution transmission electronic microscopy (HRTEM), Fourier-transform infrared (FTIR) spectroscopy, X-ray photoelectron spectroscopy (XPS), UV-Vis absorption spectroscopy, and steady-state and times-resolved emission spectroscopy.

3.2 Results and discussion

The nanoparticles SQDs and their surface functionalization were synthesized as shown in Figure 3-1. Both APTES and UPTES were used as the silicon source and were reduced by a citrate reducing agent. This reaction was carried out in glycerol as a high boiling point green solvent under atmospheric pressure and at 180 $^{\circ}$C using an oil bath. The resulting SQDs were then functionalized using PDA to produce Am-SQD-Per and Urea-SQD-Per.
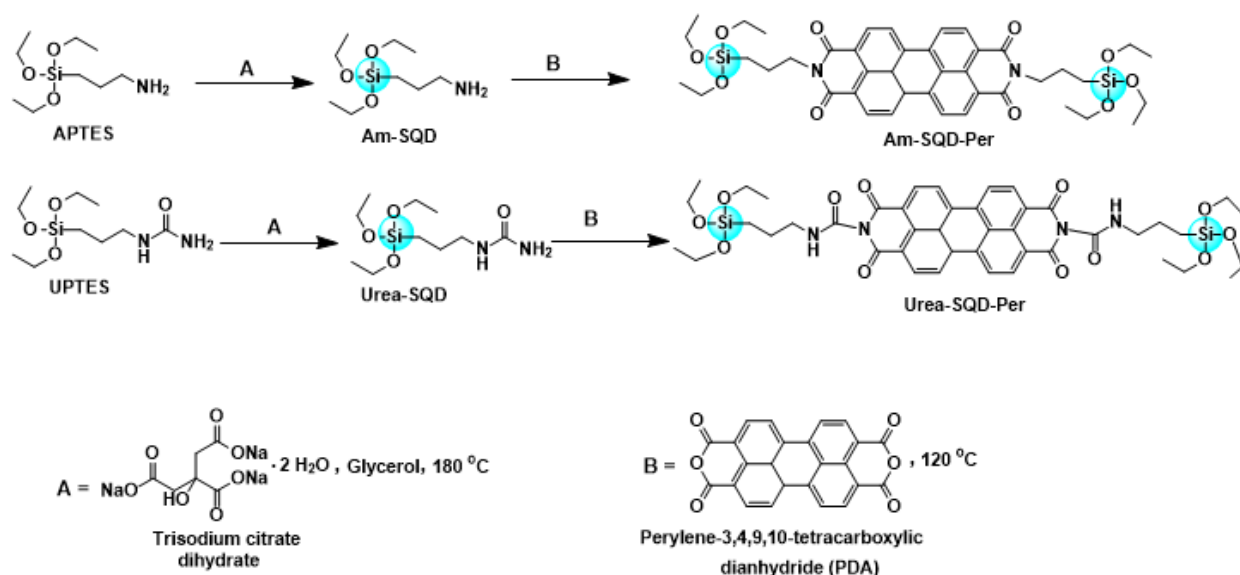
Figure 3-1. Synthesis route of SQDs (A) and their surface functionalization using perylene-3,4,9,10-tetracarboxylic dianhydride (B).

3.2.1 Size and structure

Figure 3-2 shows the TEM, HR-TEM, and size distribution images of the assemblies Am-SQD-Per and Urea-SQD-Per. The TEM images indicate that the functionalized SQDs are quasi-spherical particles with no obvious agglomeration or aggregation. The corresponding size distribution histograms obtained by analyzing of more than 300 dots from different regions of the grids showed that the diameter of these particles ranged from 0.9 to 3.3 nm. The average diameters of SQDs for the compounds Am-SQD-Per and Urea-SQD-Per are 1.61± 0.89 and 1.62 ± 0.81 nm, respectively. The functionalized SQDs exhibited high crystallinity which is evidenced by the distinct lattice fringes with 0.30 nm interplanar spacing, as shown in the HR-TEM insets of figure 3-2. This is in agreement with the (111) plane of diamond structured silicon.[23] It should be noted that the low resolution of the TEM and HR-TEM images is assigned to the ultra-small dimensions of these SQDs and the small atomic weight of the silicon atom compared to the counterpart metallic or semiconductor quantum dots, which is known to provide low-quality visualization.[10,24]
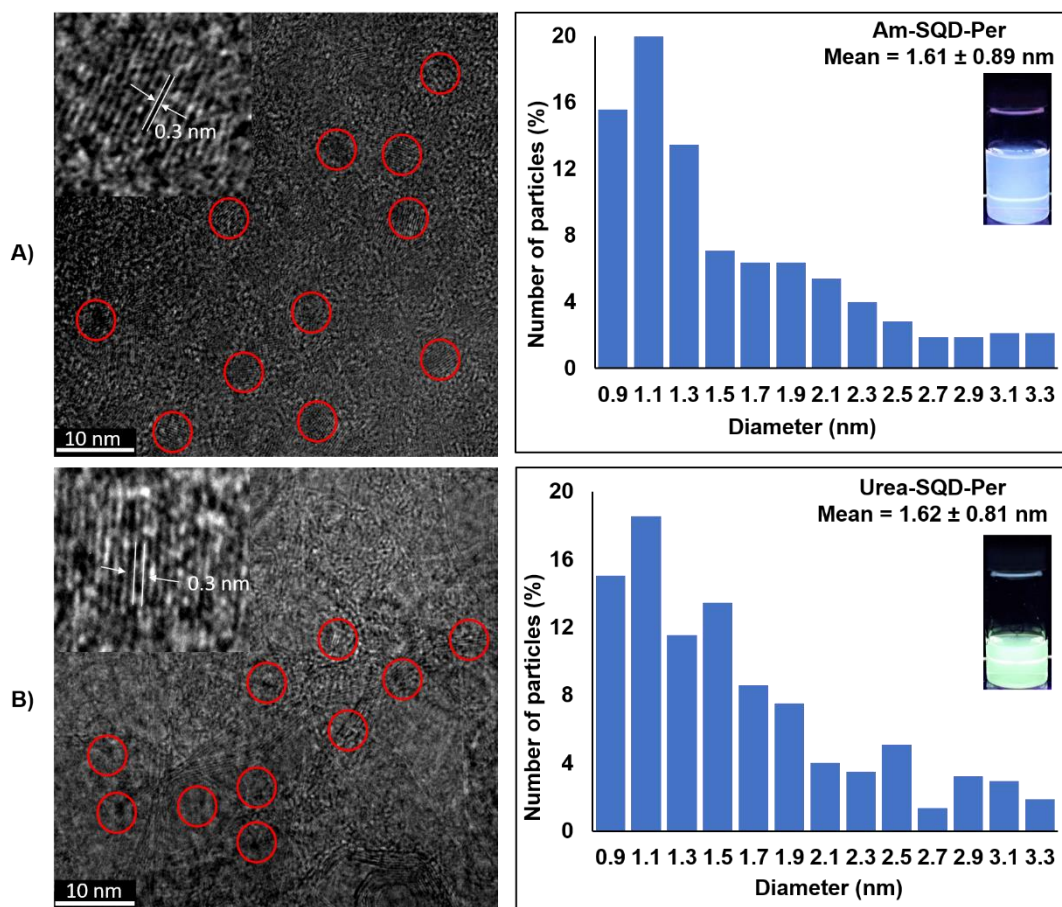
Figure 3-2. TEM together with HR-TEM (left) and diameter distribution with photographs for solutions under UV (365 nm) irradiation (right) for Am-SQD-Per (A) and Urea-SQD-Per (B).

To confirm the attachment of Am-SQD and Urea-SQD to the PDA dye to produce Am-SQD-Per and Urea-SQD-Per, respectively, FTIR and XPS spectroscopy were performed. Figure 3-3 displays the FTIR spectra of Am-SQD-Per and Urea-SQD-Per. The broad peak at $2980 - 3660$ cm^{-1} can be assigned to the stretching vibration of the O-H bond.[25] The intense peaks at 1019 and 970 cm^{-1} for Am-SQD-Per, and 1024 and 909 cm^{-1} for Urea-SQD-Per, are attributed to Si-O-Si/Si-O-C and Si-OH stretching, respectively.[26] The peaks at $2970 - 2808$ cm^{-1} correspond to the –CH stretching vibrations of the spacer and alkyl group.[27] Both peaks at 1685 and 1638 cm^{-1} for Am-SQD-Per, and 1692 and 1639 cm^{-1} for Urea-SQD-Per, are assigned to imidic C=O stretching (N-C=O).[26] The peaks at 1439 cm^{-1} in both compounds can be assigned to N-C stretching.[28] Furthermore, the

characteristic peaks of the anhydride carbonyl (O-C=O) in the free dye PDA at 1760 and 1720 cm^{-1} are absent in the FTIR spectra of Am-SQD-Per and Urea-SQD-Per. This indicates the success of SQDs binding to the dye.
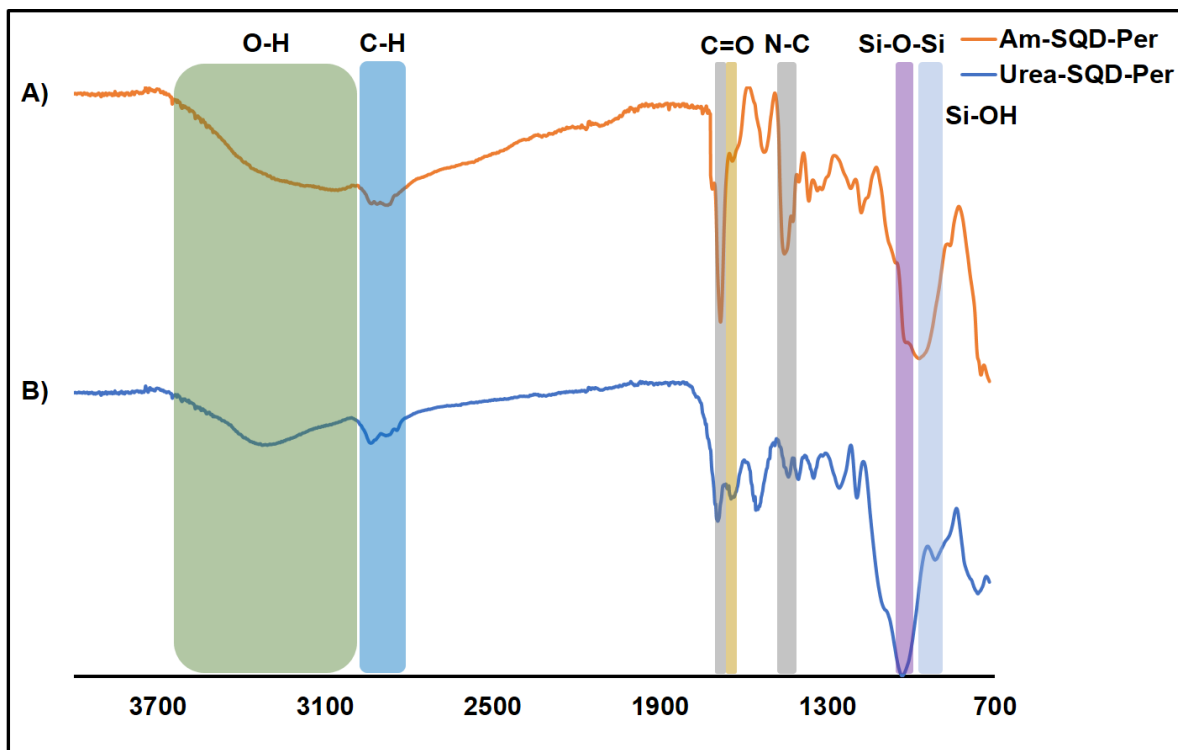
Figure 3-3. FTIR spectra of Am-SQD-Per (A) and Urea-SQD-Per (B).

To further confirm the binding of SQDs to the PDA dye, XPS spectroscopy was performed. Figure 3-4 displays the high resolution XPS spectra of O 1s, C 1s, N 1s, and Si 2p for Am-SQD-Per and Urea-SQD-Per. The deconvoluted peaks of O 1s appeared at 533.6, 532.3, and 530.9 eV for Am-SQD-Per, and 533.4, 532.1, 530.9 eV for Urea-SQD-Per. These can be assigned to C-O, Si-O, and amidic or imidic carbonyl (-N-C=O), respectively.[29,30,31] The C 1s binding energy peaks were present at 288.4, 286.4, and 285 eV for Am-SQD-Per, and 288.7, 286.3, and 284.8 eV for Urea-SQD-Per. These are attributed to C=O of imide or amide bonds (-N-C=O), C-O or C-OH, and Si-C or C=C of PDI kernel, respectively.[32,33,34,35] The XPS spectra of N 1s centered at 399.6 for Am-SQD-Per and 399.9 eV for Urea-SQD-Per signify the presence of N-C or N-C=O.[30,36] The Si 2p peak at 102.7 for Am-SQD-Per and 102.4 eV for Urea-SQD-Per can be assigned to Si-O-

C or Si-C.[33] The XPS data are consistent with the FTIR data, providing convincing evidence for successful functionalization of SQDs with PDI.
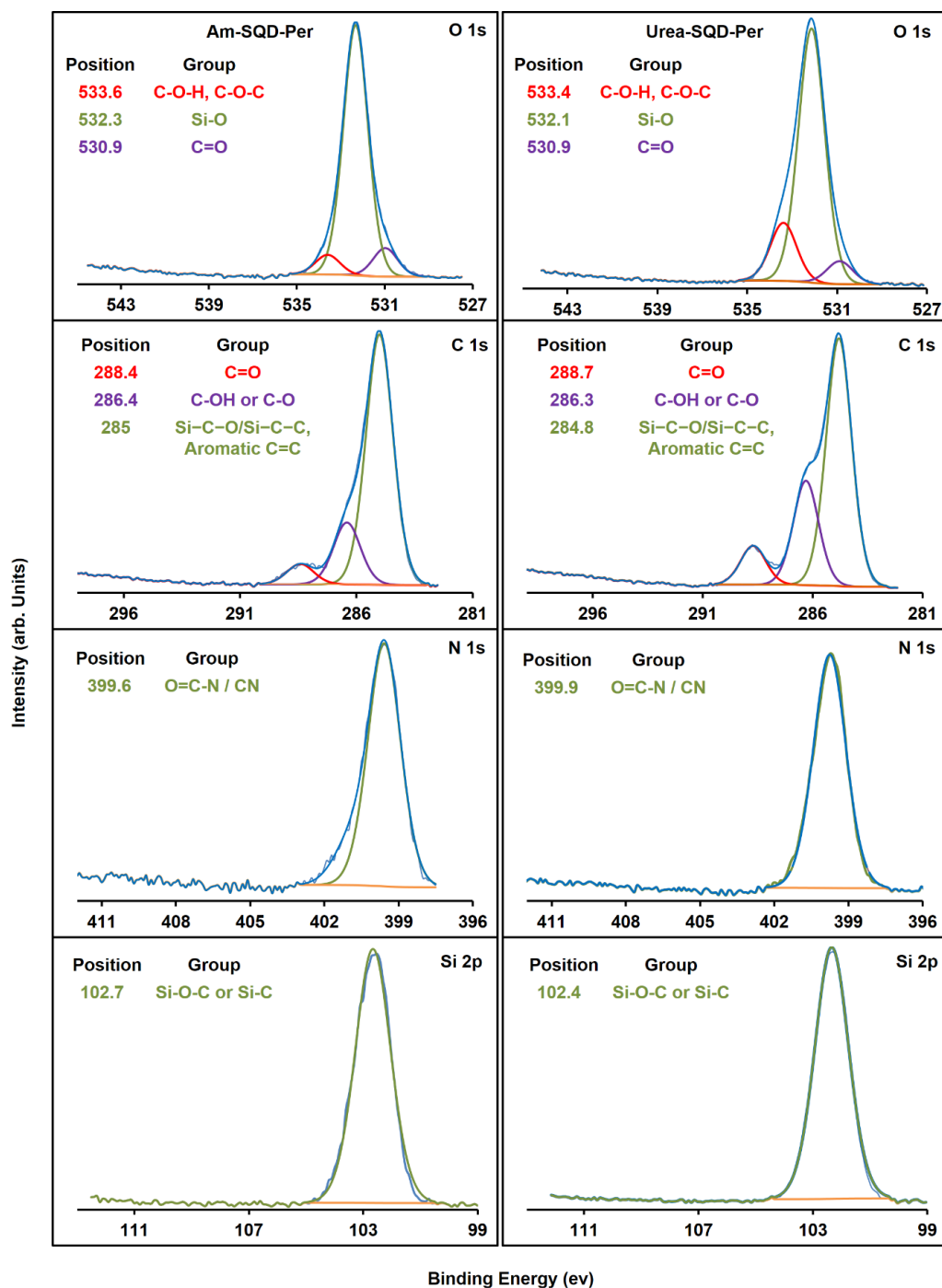
Figure 3-4. XPS spectra of O 1s, C 1s, N 1s, and Si 2p for Am-SQD-Per and Urea-SQD-Per.

3.2.2 Photophysical properties

Steady-state photoluminescence emission, absorption and excitation spectra for Urea-SQD, Urea-SQD-Per, Am-SQD and Am-SQD-Per in methanol (MeOH) at room temperature are given in Figure 3-5 (A&B).
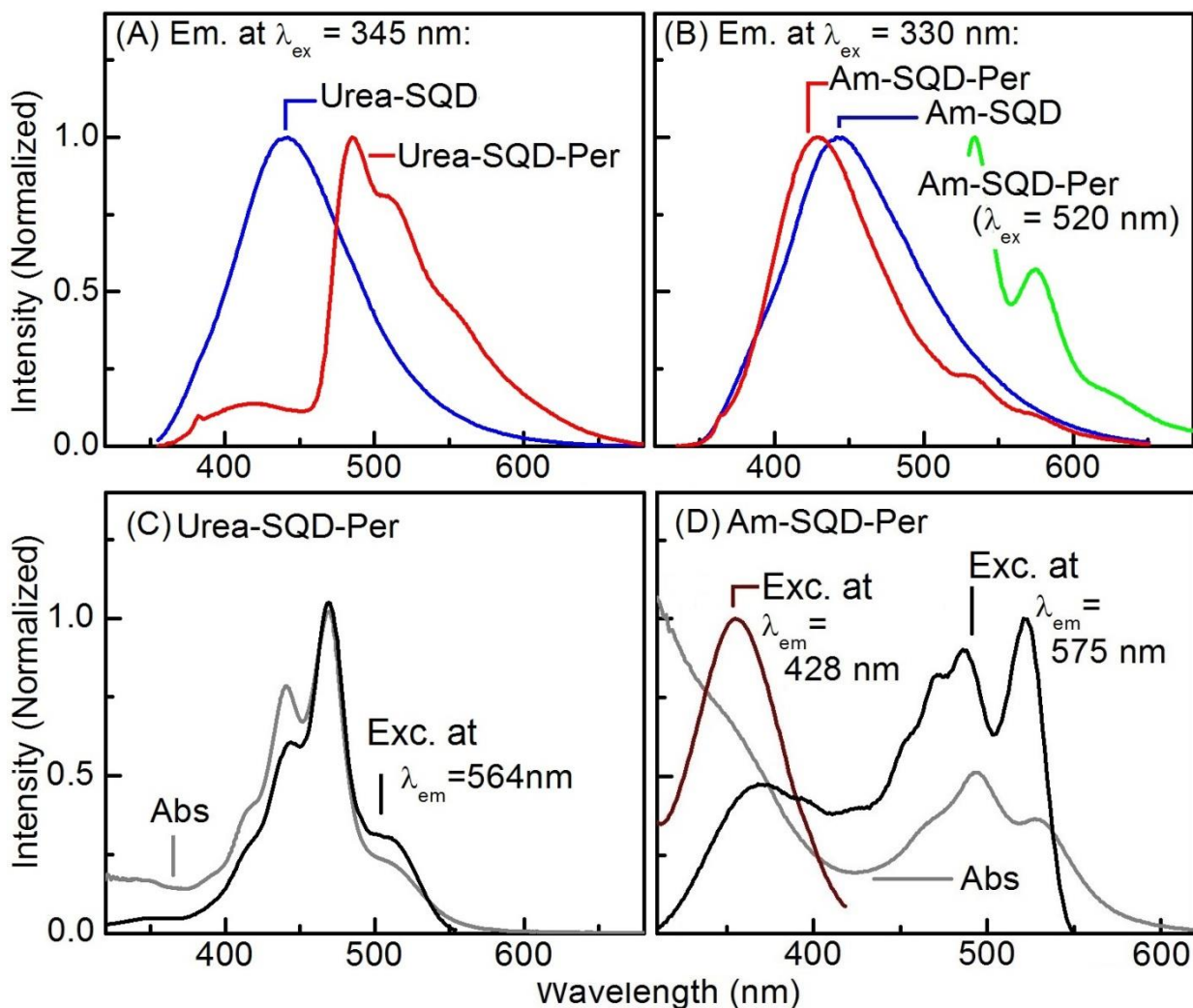
Figure 3-5. Emission spectra of (A) Urea-SQD (blue), Urea-SQD-Per (red) and (B) Urea-SQD (blue), Am-SQD-Per (red and green) as well as ground-state absorption (grey) and photoluminescence excitation spectra (black and brown) of (C) Urea-SQD-Per and (D) Am-SQD-Per collected at room temperature in methanol (excitation wavelength at which emission spectra collected and emission wavelengths at which excitation spectra collected are given on the graph).

Study of the emission spectrum recorded for the starting Urea-SQD (see Figure 3-5 A) revealed one broad spectrum extended over the spectral range of 350-650 nm, in agreement with reported literature data for amine-terminated silicon quantum dots.[37],[38] On the other hand, emission spectrum obtained for Urea-SQD-Per under the same experimental conditions exhibited two main bands (see Figure 3-5 A). The first emission band showed a resemblance with the starting Urea-SQD with a broad nature over the spectral range between 350-450 nm. An observable blue shift detected in the quantum dot emission in Urea-SQD-Per as compared to the starting Urea-SQD. Considering the average diameter for our SQDs to be 1.6 nm, such shift observed in the emission is likely to be assigned to surface chemistry and independent on quantum confinement. [8] This is in agreement with an earlier report where the emission properties for large QDs (d > ~ 3 nm) were found to be dominated by quantum confinement while those for smaller size quantum dots (d < ~ 2 nm) is associated with surface relevant states.[8] In this respect, the observed blue shift should be associated with surface polarity changes due to coupling of the organic dye to the quantum dot surface.[23,38,39,40,41,42,43] The second band detected in the emission of Urea-SQD-Per came as a relatively stronger band with spectral features extending over 450-650 nm where three main vibronic features detected at 488, 510 and 550 nm. Based on the structured nature of this band and literature data [44] we assign it to the organic dye, i.e. PDI. From the steady-state emission in Figure 3-5 A, it is evident that the emission of SQDs is of higher energy compared to that of PDI. An energy level diagram predicted from the lowest energy position of the emission spectra recorded for each of the lumophores constructing the investigated assemblies is given in the supporting information. This energy alignment together with the absorption overlap seen in the ground state absorption allows us to anticipate the possibility of energy transfer. Evidence for the anticipated energy transfer (ET) is found upon examining the PL excitation spectrum collected with emission monochromator fixed at 564 nm where emission is mainly due to the organic dye, (see Figure 3-5 C). The match found between the absorption and excitation spectra supporting the suggested ET process between the SQDs and the PDI.[45] Further evidences of the assigned ET are given in the time-resolved measurements as discussed below.

Interestingly, different behaviour was found on studying the steady-state emission spectra of Am-SQD-Per in methanol at room temperature (see Figure 3-5 B). Analysis of the

recorded steady-state emission of Am-SQD-Per revealed that spectrum mainly have the signature of SQD emission which suffered from blue shift as compared to its analogue of Am-SQD. Considering the average size of SQD, i.e. 1.6 nm, we confidently assign the observed shift to surface polarity changes associated with the PDI coupling in the same manner to that observed for Urea-SQD-Per.[43] The clear difference to that of Urea-SQD-Per came in the organic dye (PDI) emission vibronics that were absent or suffered from strong quenching in the recorded emission of Am-SQD-Per. Despite this absence or minor contribution of the organic dye in the emission profile, the excitation spectra collected at two different wavelengths revealed the spectral signatures of both the organic dye and the quantum dot; see Figure 3-5 B. Changing the excitation wavelength to 520 nm, corresponding to where the lowest energy (0-0) of the organic dye S_0-S_1 as obtained from absorption, allowed us to observe the PDI emission, see Figure 3-5 B. Being in the same respect, relatively strong quenching in the overall emission was indicated by the calculated PL quantum yield. (see Table 3-1). This overall photoluminescence quenching together with almost complete disappearance of the organic dye vibronic bands in the emission profile, as compared to its analogues of Urea-SQD-Per, strongly in favourite of photoinduced electron transfer (Pet). [46,47,48] [49,50,51] Additionally, the excitation spectra collected with emission monochromator fixed at two different wavelengths, one at SQDs emission (428 nm) and the other at PDI emission (575 nm) given in Figure 3-5 B. Examination of the obtained spectra revealed drastic changes in the relative contribution of the organic dye to the SQDs in the excitation spectrum at 575 nm as compared to their ratio in the absorption spectrum; thus supporting the suggested electron transfer mechanism.[51] Further differences between the two investigated systems of Urea-SQD-Per and Am-SQD-Per were found in the photoluminescence quantum yields calculated under the same experimental conditions; see Table 3-1.

Table 3-1. Emission quantum yields of SQDs assemblies in methanol at room temperature

% Φ^a	Sample			
	Am-SQD	Am-SQD-Per	Urea-SQD	Urea-SQD-Per
total	8.1	2.9	6.3	18.5
SQDs	-	-	-	1.7
Organic dye	-	quenched	-	16.8

[a] Reference used is 6-Aminochrysene and $\lambda_{ex} = 345$ nm

In general, the obtained quantum yield values (which are rather low) are comparable with those recently reported from our group for closely related systems [10] and in good agreement with literature. [41] While functionalizing SQDs with PDI improved the quantum yield for Urea-SQD-Per as compared to starting Urea-SQD; a large quenching was observed for Am-SQD-Per. The total quantum yield enhancement observed in Urea-SQD-Per can be attributed to the contribution of the organic dye (i.e. PDI, see Figure 3-5). On the other hand, the large decrease in quantum yield for Am-SQD-Per argues in favour of the energy loss associated with the suggested electron transfer between SQDs and PDI. Considering this possibility, the photoexcitation energy is anticipated to be lost in formation of the non-luminescent ion pair radical. Indeed, this can help explain the above observation of absence or strong quenching of organic emission in the emission profile displayed in Figure 3-5. Further evidence for the suggested (Pet) found in the time-resolved measurements discussed below.

Time-resolved single photon counting (TCSPC) measurements

To further decipher the different types of interaction between SQDs and PDI, the synthesized assemblies of Urea-SQD-Per, Am-SQD-Per, and their analogues Urea-SQD and Am-SQD were investigated using time-correlated single photon counting (TCSPC). TCSPC measurements were carried out in the nanosecond (ns) time scale at room temperature. Fluorescence lifetime measurements were collected at maximum emission

peaks (λ_{em}) as extracted from the steady-state measurements (Table 3-2). For both assemblies of Urea-SQD and Am-SQD, fluorescence decay traces can be fitted by double exponential functions (see Supporting Information SI 5 and SI 6). This may indicate the involvement of two competing fast and slow electron–hole recombination processes.[52] [53] On the other hand, kinetic traces for Urea-SQD-Per and Am-SQD-Per required equation with three lifetimes for the best fit.

Table 3-2. Fluorescence lifetimes (ns) at room temperature from TCSPC using laser excitation at 375 nm.

	Am-SQD	Am-SQD-Per	Urea-SQD	Urea-SQD-Per	
λ_{em} , nm	450	450	450	445	560
Time, ns (pre)	2.3±0.1 (63)	0.8±0.1 (52)	2.1±0.1 (48)	0.5±0.1 (47)	4.4±0.1
	11.6±0.3 (37)	2.9±0.1 (28)	9.4±0.1 (52)	2.6±0.1 (39)	
		10.6±0.2 (20)		8.9±0.2 (14)	

pre = pre-exponential weighting factor; IRF ≈ 250 ps (from LUDOX SM-30 colloidal silica solution)

For Urea-SQD-Per, two different kinetic profiles were detected: the first associated with PDI emission and the second corresponding to emission of SQDs. Kinetic traces for Urea-SQD-Per monitored at PDI emission were fit to a mono exponential equation where the extracted lifetime found to be ~ 4.4 ns. This finding is in good agreement with literature data for PDI-based compounds. [50] Kinetic traces corresponding to SQDs emission maxima revealed three components: one fast together with two of relatively longer lifetimes. The two relatively longer lifetimes are comparable with their analogous Urea-SQD, while the shorter lifetime was found to be in the picosecond (ps) time scale. Time resolved emission spectra (TRES) were done to further investigate the interaction mechanism. TRES collected over the first 500 ps revealed fast decay at emission bands of SQDs almost within the same time domain where those of organic dye are increasing in intensity, see Figure 3-6 A (inset). Furthermore, as the time delays extended up to 15 ns,

an overall decay detected as displayed in Figure 3-6 A and the kinetic traces in Figure 3-6 C where the kinetic traces monitored at the two wavelengths corresponding to quantum dot (430 nm) and PDI (525 nm). Kinetic traces are showing fast decay of the quantum dot emission peaks approximately within the same time domain for the rise of the PDI peaks. This rise/decay behavior is perfectly in line with the above suggested photoinduced energy transfer (PET): (Urea-SQD)*-Per → (Urea-SQD)-Per*. Indeed, fitting the kinetic traces showed that Urea-SQD-Per revealed a fast lifetime decay of ~0.5 ns while the lifetime corresponding to the rise of PDI emission found to be ~0.4 ns. Hence, we can estimate the rate of energy transfer to be ~2 x 10^9 s^{-1}; in good agreement with rates estimated for closely related systems in literature.[54]
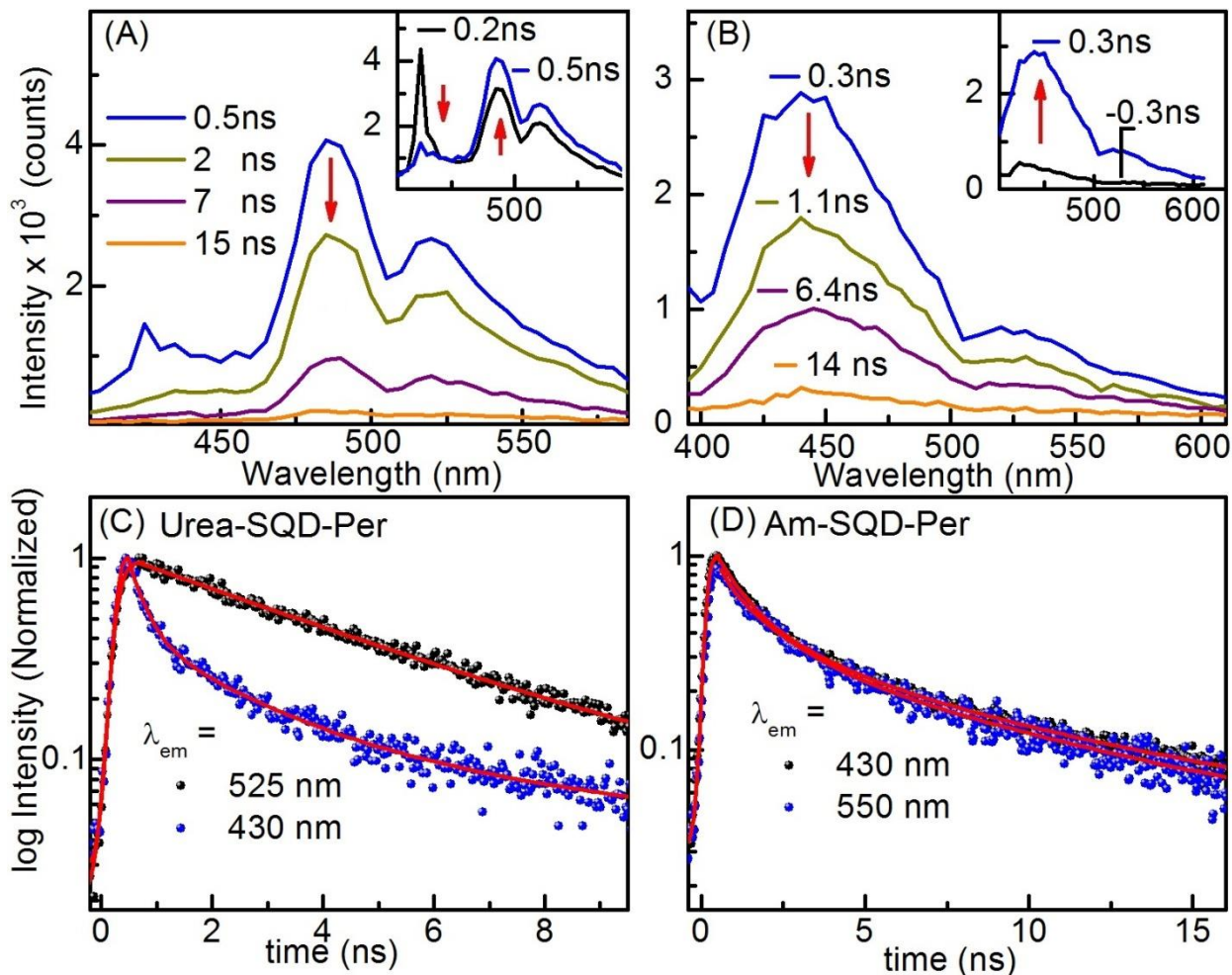
Figure 3-6. Time-resolved emission spectra of at different delay time of (A) Urea-SQD-Per (inset showing early time delay signals) and (B) Am-SQD-Per (inset showing early time delay signals) as well as kinetic traces of the decay at two different wavelengths of (C) Urea-SQD-Per and (D)Am-SQD-Per. Spectra collected using λ_{ex} = 375 nm in methanol at room temperature and delay times are indicated on the graph. (IRF ≈ 250 ps, red lines are fitted curves).

Another scenario found when studying the behavior of Am-SQD-Per as can be seen in the given spectra displayed in Figure 3-6 (B, D). TRES studied at the two sides of the laser signal (rise and decay of the laser pulse) are given in Figure 3-6 B (inset). The emission profile exhibited the signature of the quantum dots regardless of the delay time at which spectrum was collected, which is in line with the strong quenching for the PDI peaks found in the steady-state emission. This observation is in favour of the involvement of a process

faster than the temporal resolution of our measurement, i.e. ≤ 250 ps, responsible for the absence or strong quenching of the PDI emission. These findings together with the above overall weak PL quantum yield values given in Table 3-1 are indicative of the suggested photoinduced electron transfer process (Pet). Considering the disappearance of the PDI signature within the temporal resolution of our measurements, this allows us to estimate the rate to be $\geq 4 \times 10^9$ s^{-1}.

Confirmation of the charged nature for the interaction involved in Am-SQD-Per was further supported by the kinetic traces collected in different solvents. The charged radical nature of the ion pairs formed due to Pet which makes it sensitive to solvent polarity change (Figure 3-7). On the other hand, PET where no charge separation involved solvent change is expected to exhibit a less pronounced impact. Indeed, kinetic traces collected for Urea-SQD-Per revealed minor or no significant differences regardless the solvent used, see Figure 3-7. Fluorescence lifetimes extracted from the kinetic traces in different solvents given in Table 3-3 clearly showed the solvent nature to have a significant impact on the fluorescence kinetic trace for the case of Am-SQD-Per whereas minimum changes detected for that of Urea-SQD-Per. Thus, it is supporting our suggested type of interaction within each of the two systems.
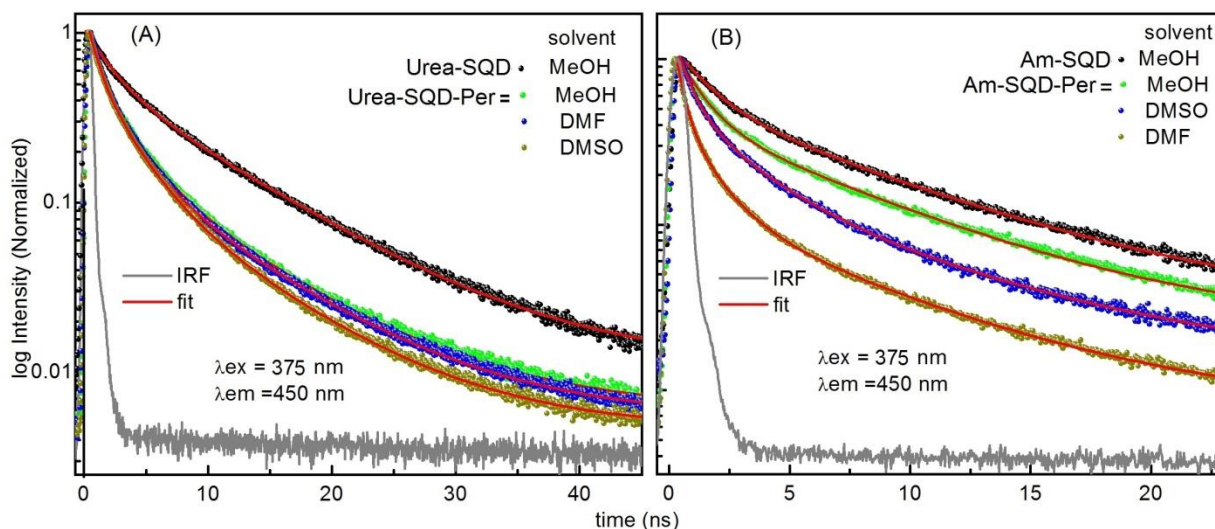
Figure 3-7. Solvent effect on kinetic traces of (A) Urea-SQD-Per and (B) Am-SQD-Per. Traces collected using λ_{ex} = 375 nm and emission wavelengths at which traces

collected as well as the solvents used are given on graph. (IRF ≈ 250 ps, and red lines are fitted curves)

Table 3-3. Solvent effect on fluorescence lifetimes of Am-SQD-Per at room temperature from TCSPC collected using laser excitation (λ_{ex}) at 375 nm

	Time, ns (pre)		
λ_{em} , nm	MeOH (PI = 5.1)	DMSO (PI = 7.2)	DMF (PI = 6.4)
450	0.8±0.1 (52)	0.6±0.1 (65)	0.4±0.1 (73)
	2.9±0.1 (28)	2.5±0.1 (26)	1.6±0.1 (21)
	10.6±0.2 (20)	8.5±0.3 (9)	8.3±0.3 (6)
560	0.9±0.1 (45)	0.5±0.1 (57)	0.4±0.1 (66)
	3.1±0.1 (37)	2.2±0.1 (30)	1.7±0.1 (27)
	10.2±0.3 (18)	8.7±0.2 (13)	7.9±0.2 (7)

pre = pre-exponential weighting factor; IRF ≈ 250 ps (from LUDOX SM-30 colloidal silica solution), PI= polarity index

Impact of the structure on the nature of the interaction.

In an earlier contribution, our group reported an efficient energy transfer to be active between SQDs and perylene dye [10], see Figure 3-8. In this specific system, coupling between the quantum dot and the organic dye achieved using an unsaturated alkyl chain provided an efficient energy transfer between the two luminophores. Herein and in continuation of our interest in tuning the photophysical properties of SQDs based systems, we synthesized two dyad systems built on SQDs and PDI where two different spacers are involved, see Figure 3-1. For Am-SQD-Per, with the bridge being a saturated alkyl chain, the two luminophores are expected to have minimum conjugation leaving the electronic system of the two luminophores separated.[55] In this manner; with PDI known to be an electron acceptor, [56] interaction is found to proceed mainly via electron transfer (Pet) as discussed above. It is worthy to indicate here that the possibility of energy transfer

interaction cannot be excluded in light of the strong spectral overlap. On the other hand for Urea-SQD-Per, having the hydrogen atom on the amine group closer to the oxygen of the diimide of PDI made hydrogen bond (HB) formation plausible, see Figure 3-8. With the PDI redox properties being sensitive to core modification [56] and energy levels of quantum dots being subtle to modify upon changing the surface chemical structure. [57] Such HB formation possibly rendered electron transfer to be less energetically active. Considering the strong spectral overlap between the absorption of PDI and emission of SQD energy transfer is in turn more likely to be responsible for the observed quenching of the SQD emission. This is supported by the negligible impact of the solvent on the fluorescence lifetime decay curve as discussed in the TSCPC section. Hence, we can pre-design the SQDs assemblies in a way to control the type of interaction permitted throughout and consequently their optical properties.
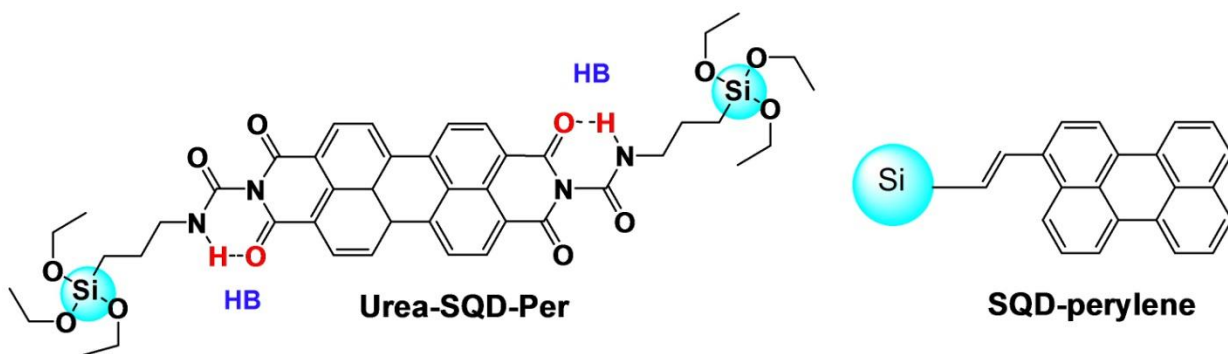
Figure 3-8. Hydrogen bond (HB) formation through Urea-SQD-Per (left) and earlier investigated SQD-perylene (right).

Effect of pH change on steady-state emission.

We extended our study to include the impact of pH changes on synthesized assemblies to better understand the charge-transfer mechanism, as well as the potential for biological applications [58,59] where pH is an important variable. The study carried out in aqueous solutions of the quantum dots where the pH values were changed while keeping the SQDs concentration constant. The Am-SQD-Per showed negligible changes in emission intensity with changing the pH, see Supporting Information. On the other hand, results revealed a large change in the emission profile of Urea-SQD-Per as function of pH change, see Figure

3-9. In general, the pronounced change in intensity detected in the spectral features assigned to PDI, whereas those peaks corresponding to SQD were subject to minor or neglected changes. For the PDI part of the spectrum, first change from the neutral condition to relatively acidic condition resulted in an initial increase of the intensity, see Figure 3-9 A. Such observed intensity increase with the pH decrease can be attributed to an emission recovery associated with removal charge transfer from the amine group to core of SQDs. [60] In solutions with relatively high pH values, lone pair on the nitrogen atom of the amine group is involved in relaxation processes resulting in a reduced emission. In relatively low pH values, the electron transfer between the amine moieties and the Si core is precluded, yielding higher emission intensity. [54] Further increase of the acid concentration showed a successive decrease in the emission intensity where sharp decrease in the PL intensity collected at 480 nm observed over pH range of 4 – 2.6, see Figure 3-9 (B,C). The changes found in the PL part of spectra assigned to the organic dye (i.e. PDI). Such changes can be understood considering that severe changes were earlier reported in literature for PDI emission as function of pH due to stacking or aggregate formation. [61]
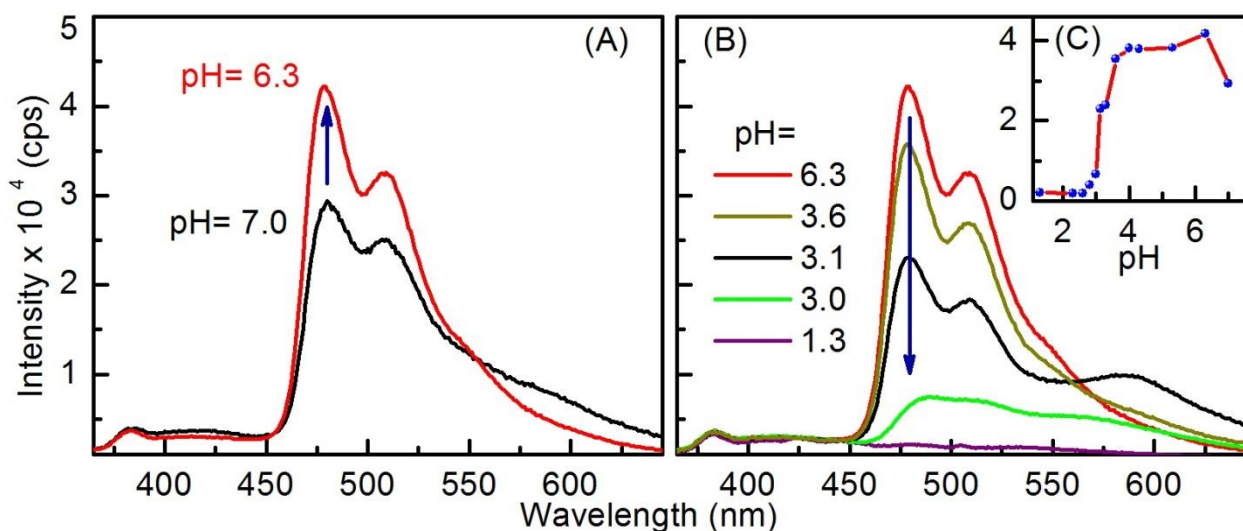
Figure 3-9. Effect of pH change on the emission of Urea-SQD-Per in water showing initial intensity increase (A), intensity decrease (B) and emission intensity at 480 nm as function of pH change (C).

3.2.3 Fluorescent cellular imaging study

To demonstrate the applicability of the Urea-SQD-Per assembly for bioimaging applications, they were utilized for *in vitro* fluorescent imaging of the human osteosarcoma U2OS and human embryonic kidney HEK293 cell lines. Figure 3-10 shows the U2OS and HEK293 cells that were incubated with Urea-SQD-Per, for which an excitation wavelength of 470 nm was used and the PL at 510 nm was monitored. The control images of both cell lines (Figures 3-10 A and 3-10 C) showed no fluorescence from the cells relative to the U2OS and HEK293 cells with the incorporated Urea-SQD-Per (Figures 3-10 B and 3-10 D). Thus, the green fluorescence observed in these cells is assigned to the emission from the functionalized SQDs and not autofluorescence from the cells. Therefore, the Urea-SQD-Per assembly are suitable for biological fluorescence imaging applications.
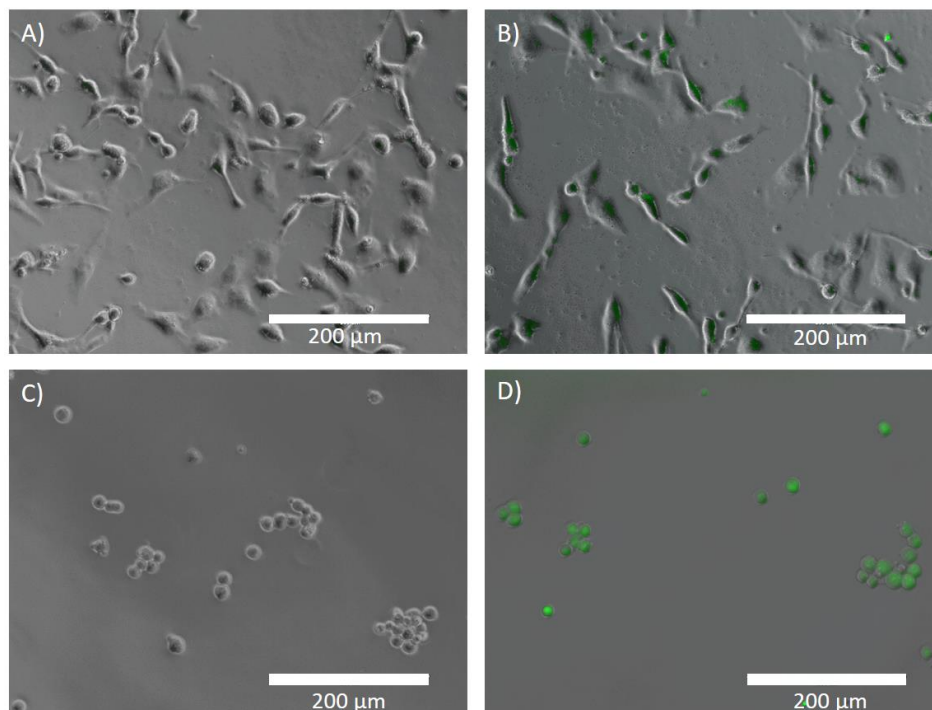
Figure 3-10. Overlay of the transmission and fluorescence microscope images of the U2OS in the absences of SQDs (A) and with functionalized Urea-SQD-Per incorporated inside the cells (B), and HEK293 cells with no SQDs (C) and with functionalized Urea-SQD-Per (D).

3.2.4 Impact of Urea-SQD-Per on cellular viability

Using a standard assay, cellular viability was assessed based on the production of ATP in metabolically active cells (see methods). U2OS cells were incubated with and without Urea-SQD-Per at a concentration representing double the concentration used for fluorescent imaging (see Figure 3-11), and in six replicates. The viability of cells incubated with Urea-SQD-Per was not significantly different from untreated cells, indicating no detectable cytotoxicity.

Cells	+	+	-	-	-
DMEM	+	+	+	+	+
CellGlo	+	+	-	-	+
SQD (10% v/v)	-	+	-	+	-
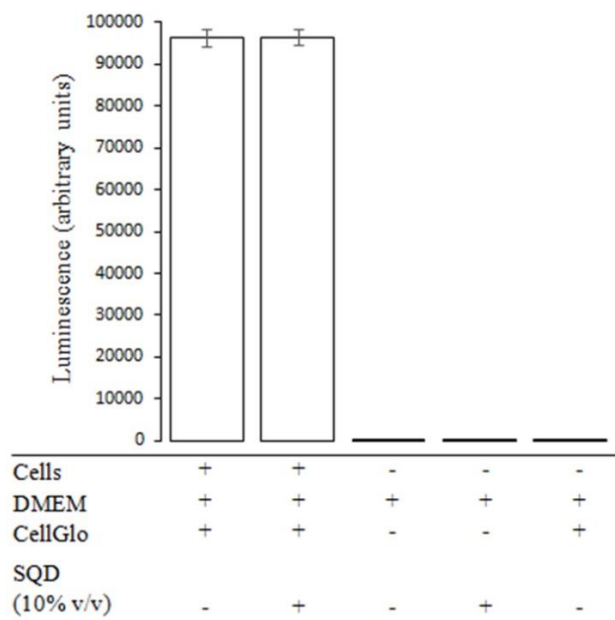
Figure 3-11. ATP-dependent viability assay

U2OS cells were assayed after treatment with 100 µg/mL urea-SQD-per (SQD) for one hour in high glucose DMEM, following the manufacturer's instructions (see methods). Plot shows mean luminescence, which correlates with cellular ATP levels. Errors bars indicate one standard deviation of the mean. Near-undetectable signal from DMEM only, DMEM + SQD, and DMEM + CellGlo reagent indicates the observed luminescence was solely due to detection of cellular ATP.

3.2.5 Conclusion

Using simple and environmentally friendly chemistry, we were able to synthesize two dyad systems coupling the SQDs of an average size of ~1.6 nm with 3,4,9,10-tetracarboxylic acid diimide (PDI) chromophore through N-propylurea or propylamine spacers. The chemical nature of the spacer has proven to exert a significant impact on the photophysical properties of the obtained dyad as confirmed by steady state and time-resolved spectroscopy measurements. The results confirmed the possibility to control the nature of the interaction throughout the backbone of the dyad by the change of the spacer used for coupling PDI to the SQDs. While the use of N-propylurea allowed photoinduced energy transfer (PET), the utilization of propylamine permitted photoinduced energy and/or electron transfer within the dyad. Furthermore, PL activity of the synthesized systems was investigated as a function of pH where Am-SQD-Per found to show negligible changes whereas Urea-SQD-Per was sensitive to pH changes. Moreover, *in vitro* fluorescent imaging of the human osteosarcoma U2OS and human embryonic kidney cells HEK293 cell lines showed promising results for bioimaging application.

3.3 Methods and materials

Chemicals

(3-Aminopropyl) triethoxysilane (99%, APTES), 1-[3-(trimethoxysilyl)propyl]urea (97%, UPTES), sodium citrate dihydrate (≥99%, citrate), and perylene-3,4,9,10-tetracarboxylic dianhydride (97%, PDA) were used without additional purification. All solvents were dried by passing through MB SPS-800 (MBraun) solvent purification system with water content below 15 ppm.

Methods

The XPS analyses were carried out with a Kratos Axis Nova spectrometer using a monochromatic Al K(alpha) source (15 mA, 14 kV). The TEM/HRTEM images were recorded using Libra 200 MC operated at 200 kV. The FTIR spectra were measured using a Nicolet 6700 FTIR spectrometer equipped with a smart iTR diamond horizontal attenuated total reflectance (ATR).

The UV–Vis absorption spectra were recorded using a Shimadzu UV-1800 double beam spectrophotometer with a 1cm path length quartz cuvette. Steady-state emission and excitation spectra were recorded on a Photon Technology International (PTI) spectrofluorometer equipped with a xenon short-arc lamp. All measurements carried out using Felix X32 PTI software for data collection and analysis at 298 K under ambient oxygen in methanol (MeOH).

Time-resolved emission spectra (TRES) and fluorescence lifetimes measurements were carried out using a PicoQuant Fluorescence lifetime system (Picoquant GmbH) equipped with a FluoTime 200 (Fluorescence Lifetime spectrometer), a TimeHarp 200 (Time-correlated Single Photon Counting (TCSPC) system), and a PDL800-B pulsed diode laser driver unit. Samples were excited using a 375 nm using a picoseconds laser diode head (LDH-P-C375). Instrument Response Function (IRF) found to be ~250 picosecond (ps) obtained from analysis of scattered light kinetic trace using LUDOX SM-30 colloidal silica solution at 375 nm. Fluorescence lifetimes were obtained from deconvolution of the kinetic traces of their solutions using global fluorescence decay data analysis software (Fluo Fit) supported by Picoquant GmbH. The TRES was recorded using an automated wavelength scanner and multichannel scaler (MCS) data collection under instrument software control. In this mode, the monochromator was controlled by a stepper motor and automated collection of spectrally resolved lifetime histograms. Data was collected in standard Integration Mode and saved in different blocks of memory for each wavelength. The collected data was then analyzed using FluoPlot software to construct the different emission spectra as function of delay time after excitation with the laser source.

Quatum yield measurements were carried out at 298 K in MeOH using 6-Aminochrysene (Φ_F = 18 %) as references. [62] Three different solutions for both sample and reference were used for the measurements. Concentrations were adjusted so as to have an absorbance of ~0.05 at the excitation wavelength and absorption spectra recorded five times for accuracy and error minimization.

Fluorescent imaging: Human U2OS osteosarcoma or HEK293 embryonic kidney cells were grown in 24-well plates in high glucose (4.5g/L) Dulbecco's modified Eagle medium

containing 3% penicillin and streptomycin and 10% fetal bovine serum (Gibco by Life Technologies). At 60-70% confluency, media was replaced with phosphate buffered saline (1 x PBS pH 7.4; Corning CellGro) and functionalized Urea-SQD-Per dissolved in PBS to a final concentration of 50 ug/mL and incubated for 1-1.5 hr. After incubation, cells were washed twice with PBS to remove excess Urea-SQD-per. Images were captured using an EVOL FL auto fluorescent microscope in GFP mode (excitation/bandwidth = 470/22, emission/bandwidth = 510/42) and phase mode at 20X magnification.

Cell viability assay: U2OS cells were seeded in equivalent densities in an opaque-walled 96-well plate and grown overnight in high glucose DMEM (4.5 g/L glucose, 10%FBS, 3% penicillin and streptomycin). Cellular viability was determined using a CellTiter-Glo 2.0 Luminescent Cell Viability Assay following the manufacturer's instructions (Promega). We incubated 6-wells with and without urea-SQD-Per dissolved in PBS to a final concentration of 100 ug/mL for 1 hour. As controls, we measured luminescence of media only, media + SQD (100ug/mL), and media + CellTiter Glo 2.0, each in triplicate. Luminescence readings were collected using a Synergy H1 microplate reader (BioTek).

Synthesis and purification of SQDs.

The SQDs were synthesized using a modified solution-based reduction method.[21] All experiments were performed under argon atmosphere using a schlenk line. In a typical experiment, 0.3 g of citrate was added to 10 ml of warm glycerol with vigorously stirring for 15 minutes till all citrate has been completely dissolved in glycerol. 2 ml of the silicon source (APTES) was then added dropwise to the solution, and the mixture was heated to 180 ºC in an oil bath for 3 hours under vigorous stirring. The product (Am-SQD) was then purified using a combination of centrifugation and dialysis against methanol (MWCO of 1 KDa, Spectra/Por® 6 Standard RC Pre-wetted Dialysis Tubing, diameter 29 mm). The previous procedures were repeated using UPTES as the silicon source to produce Urea-SQD.

Functionalization of SQDs.

An excess amount of PDA (2 g) was added to 2 ml of Am-SQD, and the mixture was then heated to 130 ºC for 5 hours under argon atmosphere. The product Am-SQD-Per was

extracted from the resulting thick red solid by methanol, and insoluble solid reactants were removed by gravity filtration. The filtrate was then concentrated using a rotatory evaporator and purified using dialysis against methanol. Similarly, the compound Urea-SQD-Per was prepared.

3.4 Supporting Information
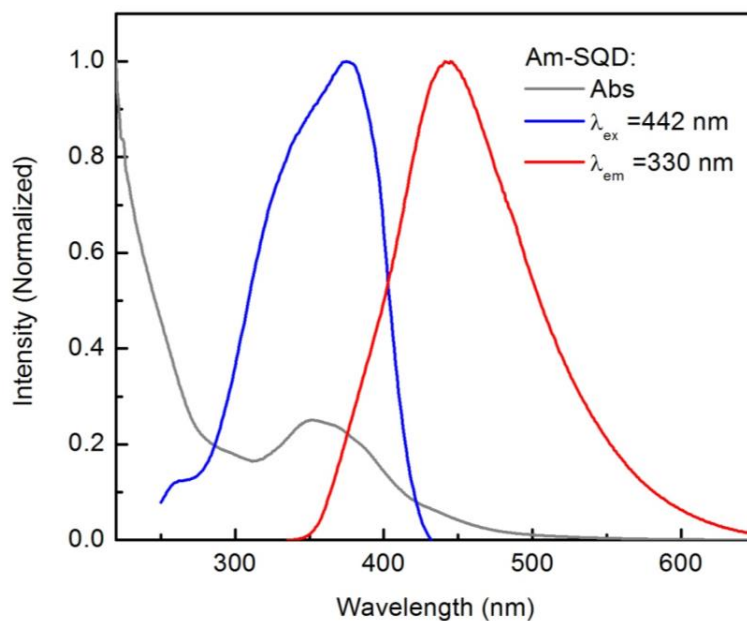
Figure 3-12. Absorption, excitation spectra and emission of Am-SQD (A) collected at room temperature in methanol (λ_{em} and λ_{ex} indicated on graph).
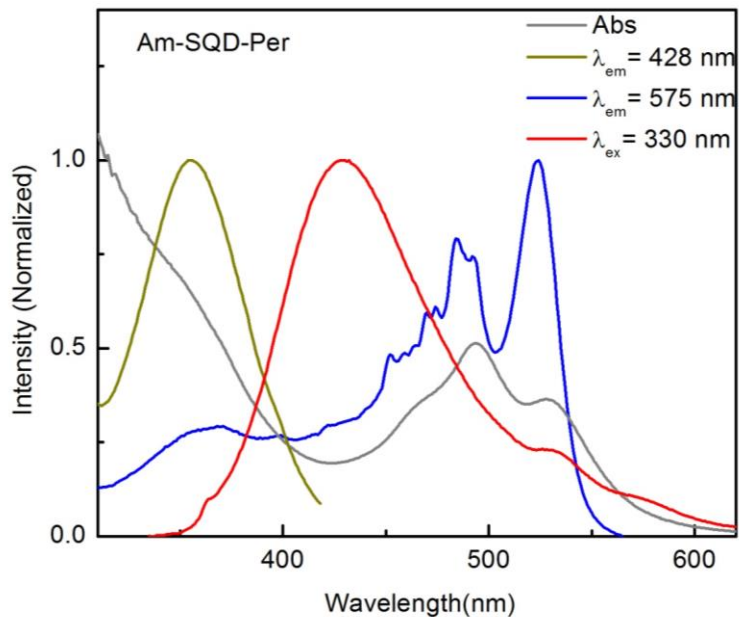
Figure 3-13. Absorption, excitation spectra and emission spectra of Am-SQD-Per (A) collected at room temperature in methanol (λ_{em} and λ_{ex} indicated on graph).
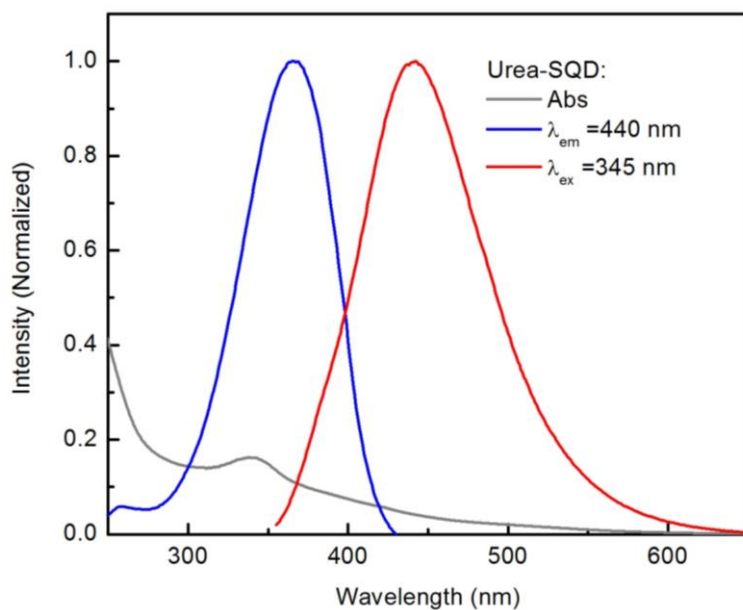
Figure 3-14. Absorption, excitation spectra and emission spectra of Urea-SQD (A) collected at room temperature in methanol (λ_{em} and λ_{ex} indicated on graph).
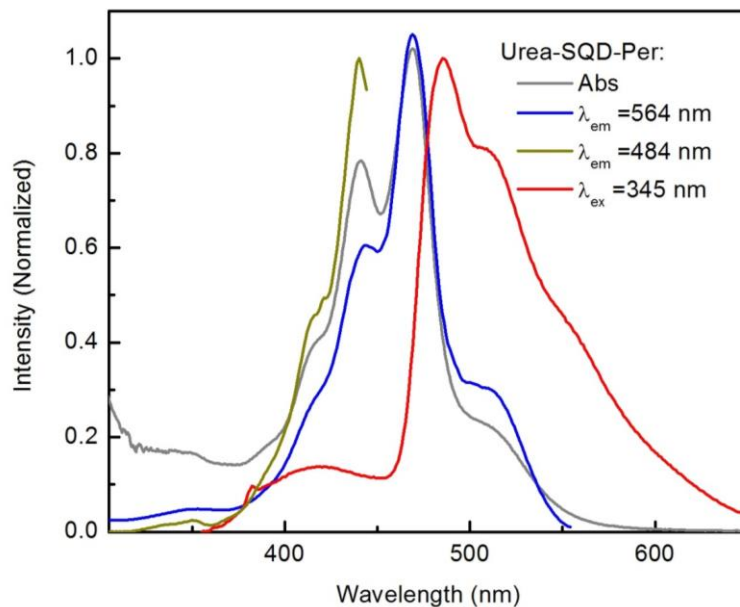
Figure 3-15. Absorption, excitation spectra and emission spectra of Urea-SQD-Per (A) collected at room temperature in methanol (λ_{em} and λ_{ex} indicated on graph).
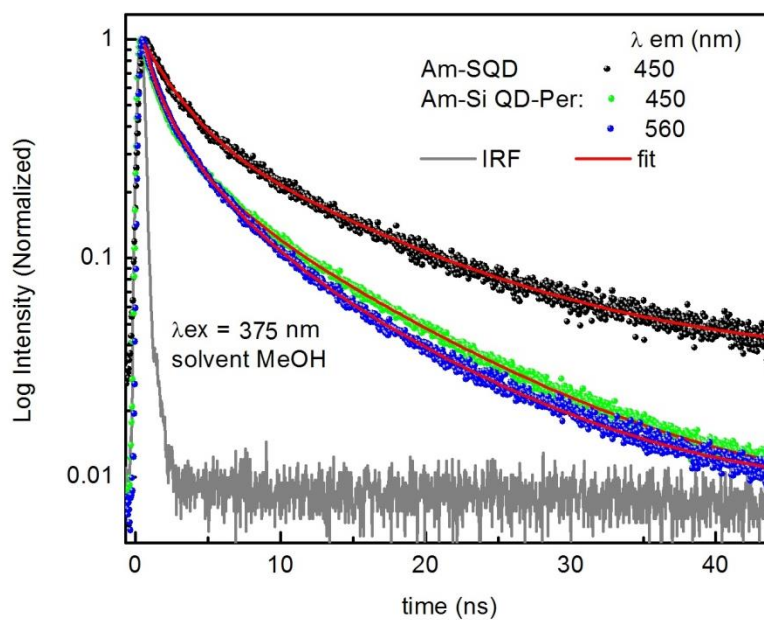
Figure 3-16. Kinetic traces of Am-SQD and Am-SQD-Per collected at room temperature in methanol (λ_{em} and λ_{ex} indicated on graph; IRF ≈ 250 ps).
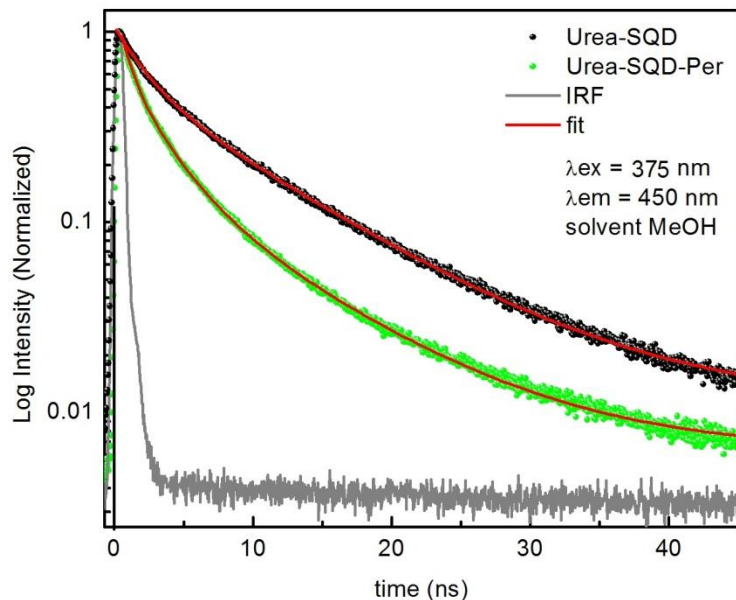
Figure 3-17. Kinetic traces of Urea-SQD and Urea-SQD-Per collected at room temperature in methanol (λ_{em} and λ_{ex} indicated on graph; IRF ≈ 250 ps).
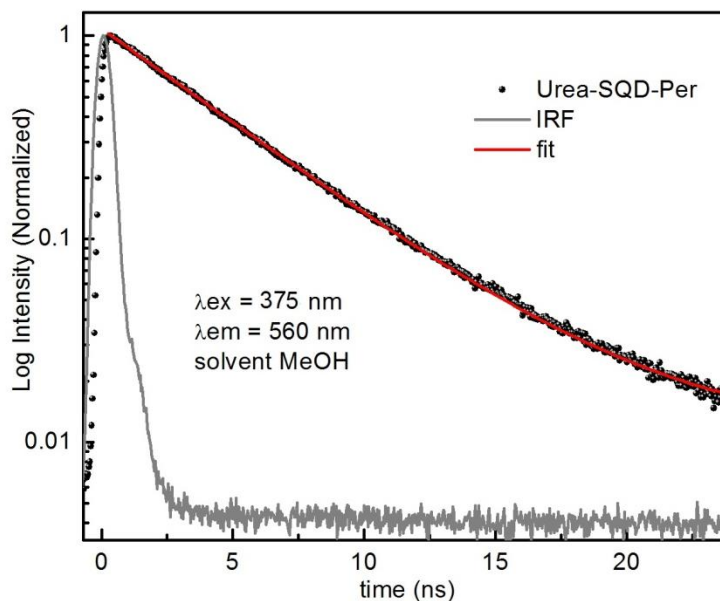
Figure 3-18. Kinetic traces of Urea-SQD-Per collected at room temperature in methanol (λ_{em} and λ_{ex} indicated on graph; IRF ≈ 250 ps).
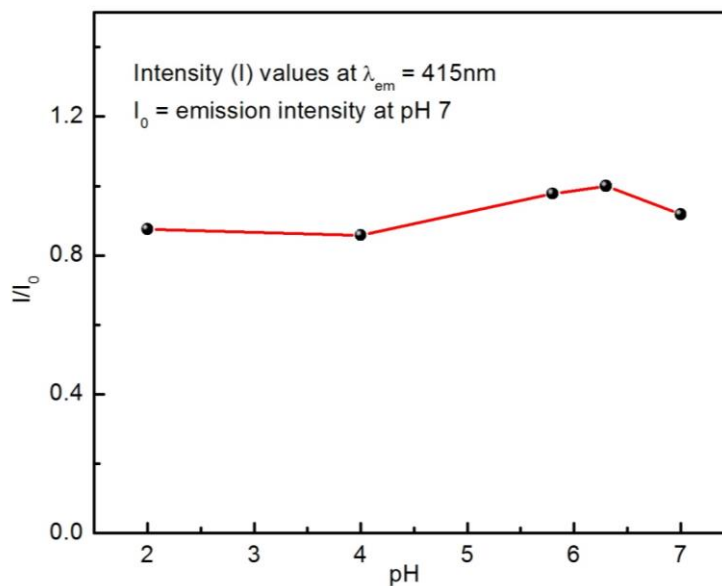
Figure 3-19. Relative emission intensity as a function of pH change for Am-SQD-Per aqueous solution using λ_{ex} = 330 nm.
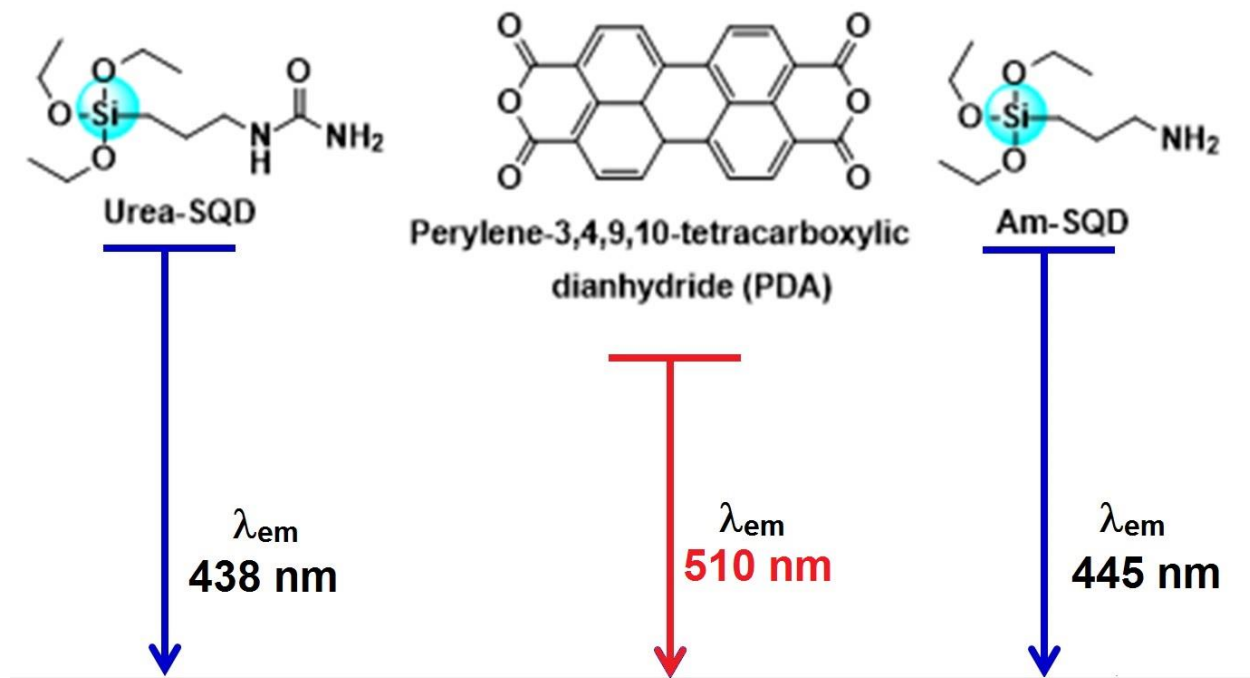
Figure 3-20. Relative energy level diagram as predicted from the emission wavelength collected at room temperature.
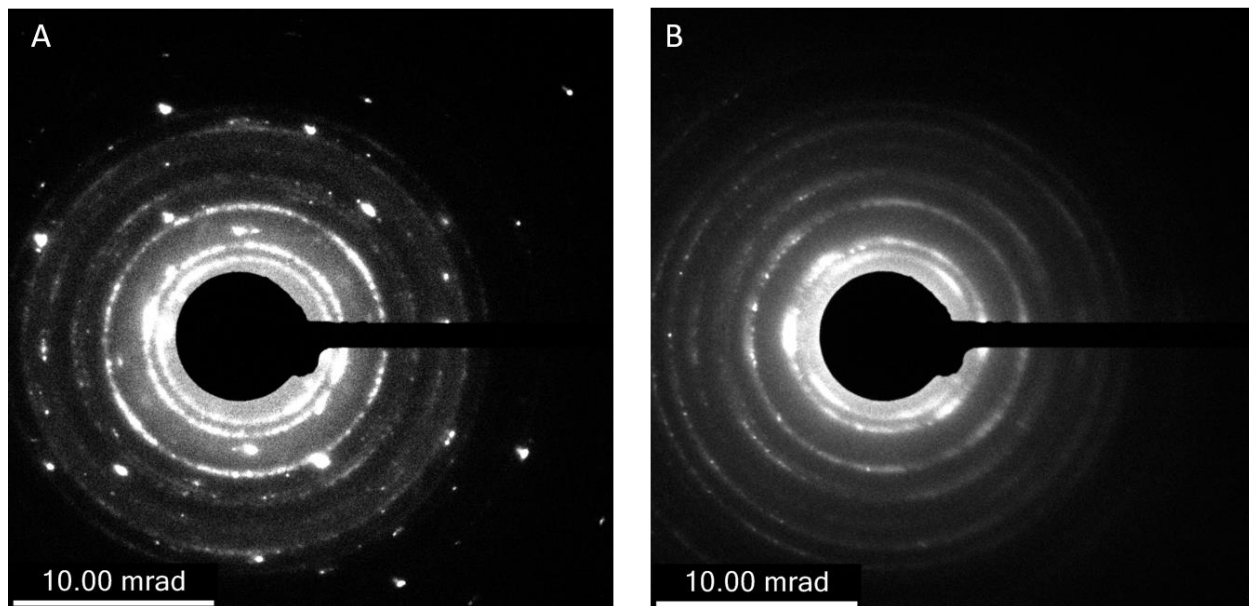
Figure 3-21. SAED pattern of Am-SQD-Per (A) and Urea-SQD-Per (B).

3.5 References

1.   Alivisatos, A. P. "Perspectives on the Physical Chemistry of Semiconductor Nanocrystals." <u>The Journal of Physical Chemistry</u> 100 (1996/01/01 1996): 13226-13239.

2.   Choi, Jonghoon; Zhang, Qin; Reipa, Vytas; Wang, Nam Sun; Stratmeyer, Melvin E; Hitchins, Victoria M; and Goering, Peter L. "Comparison of cytotoxic and inflammatory responses of photoluminescent silicon nanoparticles with silicon micron-sized particles in RAW 264.7 macrophages." <u>Journal of Applied Toxicology</u> 29 (2009): 52-60.

3.   Buriak, Jillian M. "Illuminating Silicon Surface Hydrosilylation: An Unexpected Plurality of Mechanisms." <u>Chemistry of Materials</u> 26 (2014/01/14 2014): 763-772.

4.   Ji, Xin; Wang, Wentao; and Mattoussi, Hedi. "Controlling the spectroscopic properties of quantum dots via energy transfer and charge transfer interactions: Concepts and applications." <u>Nano Today</u> 11 (2016): 98-121.

5.   Gonzalez, Christina M.; Iqbal, Muhammad; Dasog, Mita; Piercey, Davin G.; Lockwood, Ross; Klapotke, Thomas M.; and Veinot, Jonathan G. C. "Detection of high-energy compounds using photoluminescent silicon nanocrystal paper based sensors." <u>Nanoscale</u> 6 (2014): 2608-2612.

6.   Carvalho, Alexandra; Martsinovich, Natalia; Vieira, Ricardo; and Troisi, Alessandro. "Charge Injection Rates in Hybrid Nanosilicon–Polythiophene Bulk Heterojunction Solar Cells." <u>The Journal of Physical Chemistry C</u> 117 (2013/01/10 2013): 110-115.

7.   Maier-Flaig, Florian; Rinck, Julia; Stephan, Moritz; Bocksrocker, Tobias; Bruns, Michael; Kübel, Christian; Powell, Annie K.; Ozin, Geoffrey A.; and Lemmer, Uli. "Multicolor Silicon Light-Emitting Diodes (SiLEDs)." <u>Nano Letters</u> 13 (2013/02/13 2013): 475-480.

8.   Wen, Xiaoming; Zhang, Pengfei; Smith, Trevor A.; Anthony, Rebecca J.; Kortshagen, Uwe R.; Yu, Pyng; Feng, Yu; Shrestha, Santosh; Coniber, Gavin; and Huang, Shujuan. "Tunability Limit of Photoluminescence in Colloidal Silicon Nanocrystals." <u>Scientific Reports</u> 5 (07/22/online 2015): 12469.

9.   Mazzaro, Raffaello; Romano, Francesco; and Ceroni, Paola. "Long-lived luminescence of silicon nanocrystals: from principles to applications." <u>Physical Chemistry Chemical Physics</u> 19 (2017): 26507-26526.

10.   Abdelhameed, Mohammed; Martir, Diego Rota; Chen, Shalimar; Xu, William Z.; Oyeneye, Olabode O.; Chakrabarti, Subrata; Zysman-Colman, Eli; and Charpentier, Paul A. "Tuning the Optical Properties of Silicon Quantum Dots via

Surface Functionalization with Conjugated Aromatic Fluorophores." Scientific Reports 8 (2018/02/14 2018): 3050.

11.   Li, Qi; Luo, Tian-Yi; Zhou, Meng; Abroshan, Hadi; Huang, Jingchun; Kim, Hyung J.; Rosi, Nathaniel L.; Shao, Zhengzhong; and Jin, Rongchao. "Silicon Nanoparticles with Surface Nitrogen: 90% Quantum Yield with Narrow Luminescence Bandwidth and the Ligand Structure Based Energy Law." ACS Nano 10 (2016/09/27 2016): 8385-8393.

12.   Zhou, Tianlei; Anderson, Ryan T.; Li, Huashan; Bell, Jacob; Yang, Yongan; Gorman, Brian P.; Pylypenko, Svitlana; Lusk, Mark T.; and Sellinger, Alan. "Bandgap Tuning of Silicon Quantum Dots by Surface Functionalization with Conjugated Organic Groups." Nano Letters 15 (2015/06/10 2015): 3657-3663.

13.   Dung, Mai Xuan; Tung, Dao Duy; Jeong, Sohee; and Jeong, Hyun-Dam. "Tuning Optical Properties of Si Quantum Dots by π-Conjugated Capping Molecules." Chemistry – An Asian Journal 8 (2013): 653-664.

14.   Kang, Yimin; Najmaei, Sina; Liu, Zheng; Bao, Yanjun; Wang, Yumin; Zhu, Xing; Halas, Naomi J; Nordlander, Peter; Ajayan, Pulickel M; and Lou, Jun. "Plasmonic hot electron induced structural phase transition in a MoS2 monolayer." Advanced Materials 26 (2014): 6467-6471.

15.   Li, Bowen; Zu, Shuai; Zhou, Jiadong; Jiang, Qiao; Du, Bowen; Shan, Hangyong; Luo, Yang; Liu, Zheng; Zhu, Xing; and Fang, Zheyu. "Single-Nanoparticle Plasmonic Electro-optic Modulator Based on MoS2 Monolayers." ACS nano 11 (2017): 9720-9727.

16.   Yu, Ying; Ji, Ziheng; Zu, Shuai; Du, Bowen; Kang, Yimin; Li, Ziwei; Zhou, Zhangkai; Shi, Kebin; and Fang, Zheyu. "Ultrafast plasmonic hot electron transfer in Au nanoantenna/MoS2 heterostructures." Advanced Functional Materials 26 (2016): 6394-6401.

17.   Lacour, F; Guillois, O; Portier, X; Perez, H; Herlin, N; and Reynaud, C. "Laser pyrolysis synthesis and characterization of luminescent silicon nanocrystals." Physica E: Low-dimensional Systems and Nanostructures 38 (2007): 11-15.

18.   Xia, Bing; Wang, Bin; Shi, Jisen; Zhang, Wenyi; and Xiao, Shou-jun. "Engineering near-infrared fluorescent styrene-terminated porous silicon nanocomposites with bovine serum albumin encapsulation for in vivo imaging." Journal of Materials Chemistry B 2 (2014): 8314-8320.

19.   Sahu, Bibhuti Bhusan; Yin, Yongyi; Han, Jeon Geon; and Shiratani, Masaharu. "Low temperature synthesis of silicon quantum dots with plasma chemistry control in dual frequency non-thermal plasmas." Physical Chemistry Chemical Physics 18 (2016): 15697-15710.

20.	Pell, Lindsay E.; Schricker, April D.; Mikulec, Frederic V.; and Korgel, Brian A. "Synthesis of Amorphous Silicon Colloids by Trisilane Thermolysis in High Temperature Supercritical Solvents." Langmuir 20 (2004/08/01 2004): 6546-6548.

21.	Ye, Hong-Li; Cai, Shi-Jiao; Li, Si; He, Xi-Wen; Li, Wen-You; Li, Yu-Hao; and Zhang, Yu-Kui. "One-Pot Microwave Synthesis of Water-Dispersible, High Fluorescence Silicon Nanoparticles and Their Imaging Applications in Vitro and in Vivo." Analytical Chemistry 88 (2016/12/06 2016): 11631-11638.

22.	Wang, Zhenfeng; Zheng, Nannan; Zhang, Wenqiang; Yan, He; Xie, Zengqi; Ma, Yuguang; Huang, Fei; and Cao, Yong. "Self-Doped, n-Type Perylene Diimide Derivatives as Electron Transporting Layers for High-Efficiency Polymer Solar Cells." Advanced Energy Materials 7 (2017): 1700232.

23.	Dasog, Mita; Yang, Zhenyu; Regli, Sarah; Atkins, Tonya M.; Faramus, Angelique; Singh, Mani P.; Muthuswamy, Elayaraja; Kauzlarich, Susan M.; Tilley, Richard D.; and Veinot, Jonathan G. C. "Chemical Insight into the Origin of Red and Blue Photoluminescence Arising from Freestanding Silicon Nanocrystals." ACS Nano 7 (2013/03/26 2013): 2676-2685.

24.	Wu, Jinzhu; Dai, Jun; Shao, Yanbin; and Sun, Yanchun. "One-step synthesis of fluorescent silicon quantum dots (Si-QDs) and their application for cell imaging." RSC Advances 5 (2015): 83581-83587.

25.	Zhu, Baoya; Ren, Guojuan; Tang, Mingyu; Chai, Fang; Qu, Fengyu; Wang, Chungang; and Su, Zhongmin. "Fluorescent silicon nanoparticles for sensing Hg2+ and Ag+ as well visualization of latent fingerprints." Dyes and Pigments 149 (2018): 686-695.

26.	Sriramulu, Deepa; Reed, Ella Louise; Annamalai, Meenakshi; Venkatesan, Thirumalai Venky; and Valiyaveettil, Suresh. "Synthesis and Characterization of Superhydrophobic, Self-cleaning NIR-reflective Silica Nanoparticles." Scientific Reports 6 (11/08/online 2016): 35993.

27.	Wu, Fu-Gen; Zhang, Xiaodong; Kai, Siqi; Zhang, Mengyi; Wang, Hong-Yin; Myers, John N.; Weng, Yuxiang; Liu, Peidang; Gu, Ning; and Chen, Zhan. "One-Step Synthesis of Superbright Water-Soluble Silicon Nanoparticles with Photoluminescence Quantum Yield Exceeding 80%." Advanced Materials Interfaces 2 (2015): 1500360.

28.	Xu, Lan; Manda, Venkata Ramana; McNamara, Louis E.; Jahan, Muhammad P.; Rathnayake, Hemali; and Hammer, Nathan I. "Covalent synthesis of perylenediimide-bridged silsesquioxane nanoribbons and their electronic properties." RSC Advances 4 (2014): 30172-30179.

29.	Cuesta, A; Martinez-Alonso, A; Tascon, JMD; and Bradley, RH. "Chemical transformations resulting from pyrolysis and CO2 activation of Kevlar flocks." Carbon 35 (1997): 967-976.

30. Medeiros, HS; Pessoa, RS; Sagás, JC; Fraga, MA; Santos, LV; Maciel, HS; Massi, M; da Silva Sobrinho, AS; and da Costa, MEH Maia. "Effect of nitrogen content in amorphous SiCxNyOz thin films deposited by low temperature reactive magnetron co-sputtering technique." Surface and Coatings Technology 206 (2011): 1787-1795.

31. Annadhasan, M.; Kasthuri, J.; and Rajendiran, N. "Green synthesis of gold nanoparticles under sunlight irradiation and their colorimetric detection of Ni2+ and Co2+ ions." RSC Advances 5 (2015): 11458-11468.

32. Bhowmick, Deb Kumar; Stegemann, Linda; Bartsch, Manfred; Strassert, Cristian A.; and Zacharias, Helmut. "Fluorescence Properties of Perylene and Pyrene Dyes Covalently Linked to 6H-SiC(0001) and Silicate Surfaces." The Journal of Physical Chemistry C 120 (2016/02/18 2016): 3275-3288.

33. Khung, Y. L.; Ngalim, S. H.; Scaccabarozzi, A.; and Narducci, D. "Thermal and UV Hydrosilylation of Alcohol-Based Bifunctional Alkynes on Si (111) surfaces: How surface radicals influence surface bond formation." Scientific Reports 5 (06/12/online 2015): 11299.

34. David, Lamuel; Bhandavat, Romil; Barrera, Uriel; and Singh, Gurpreet. "Silicon oxycarbide glass-graphene composite paper electrode for long-cycle lithium-ion batteries." Nature Communications 7 (03/30/online 2016): 10998.

35. Wüsten, J; Ertl, Th; Lach, S; and Ziegler, Ch. "Post deposition purification of PTCDA thin films." Applied surface science 252 (2005): 104-107.

36. Damaceanu, Mariana-Dana; Rusu, Radu-Dan; Musteata, Valentina-Elena; and Bruma, Maria. "Insulating polyimide films containing n-type perylenediimide moieties." Polymer International 61 (2012): 1582-1591.

37. Czubanowski, M.; Schuster, A.; Akbari, S.; Pfnür, H.; and Tegenkamp, C. "Adsorbate induced refacetting: Pb chains on Si(557)." New Journal of Physics 9 (2007): 338.

38. Shiohara, Amane; Hanada, Sanshiro; Prabakar, Sujay; Fujioka, Kohki; Lim, Teck H.; Yamamoto, Kenji; Northcote, Peter T.; and Tilley, Richard D. "Chemical Reactions on Surface Molecules Attached to Silicon Quantum Dots." Journal of the American Chemical Society 132 (2010/01/13 2010): 248-253.

39. Le, Thu-Huong, and Jeong, Hyun-Dam. "The effects of electronic coupling between capping molecules and quantum dots on the light absorption and emission of octyl, styryl, and 4-ethynylstyryl terminated silicon quantum dots." Physical Chemistry Chemical Physics 16 (2014): 18821-18826.

40. Ahmed, M. E.; Goss, J. P.; Eyre, R. J.; Briddon, P. R.; and Taylforth, M. A. "Ab Initio Study of functionalized 1 nm Silicon Nanoparticles." Journal of Physics: Conference Series 245 (2010): 012046.

41.   Hua, Fengjun; Erogbogbo, Folarin; Swihart, Mark T.; and Ruckenstein, Eli. "Organically Capped Silicon Nanoparticles with Blue Photoluminescence Prepared by Hydrosilylation Followed by Oxidation." Langmuir 22 (2006/04/01 2006): 4363-4370.

42.   Wolkin, M. V.; Jorne, J.; Fauchet, P. M.; Allan, G.; and Delerue, C. "Electronic States and Luminescence in Porous Silicon Quantum Dots: The Role of Oxygen." Physical Review Letters 82 (01/04/ 1999): 197-200.

43.   Reboredo, Fernando A., and Galli, Giulia. "Theory of Alkyl-Terminated Silicon Quantum Dots." The Journal of Physical Chemistry B 109 (2005/01/01 2005): 1072-1078.

44.   Manning, Steven J.; Bogen, William; and Kelly, Lisa A. "Synthesis, Characterization, and Photophysical Study of Fluorescent N-substituted Benzo[ghi]perylene "Swallow Tail" Monoimides." The Journal of Organic Chemistry 76 (2011/08/05 2011): 6007-6013.

45.   Gao, Di; Aly, Shawkat M.; Karsenti, Paul-Ludovic; Brisard, Gessie; and Harvey, Pierre D. "Ultrafast energy and electron transfers in structurally well addressable BODIPY-porphyrin-fullerene polyads." Physical Chemistry Chemical Physics 19 (2017): 2926-2939.

46.   Aly, Shawkat Mohammed; Ho, Cheuk-Lam; Fortin, Daniel; Wong, Wai-Yeung; Abd-El-Aziz, Alaa S.; and Harvey, Pierre D. "Intrachain Electron and Energy Transfer in Conjugated Organometallic Oligomers and Polymers." Chemistry – A European Journal 14 (2008): 8341-8352.

47.   Ganguly, Tapan; Sharma, Devendra K.; Gauthier, Sylvain; Gravel, Denis; and Durocher, Gilles. "Strongly exothermic electron-transfer reaction in the excited singlet state of alkylcarbazole-polynitrofluorene and -polynitrofluorenone bichromophoric systems. 1. Correlation between the probability of charge separation, photoactivity, and picosecond laser photolysis studies on the photoinduced charge recombination of ion pair state produced in some media." The Journal of Physical Chemistry 96 (1992/04/01 1992): 3757-3766.

48.   Hernández, Laura I.; Godin, Robert; Bergkamp, Jesse J.; Llansola Portolés, Manuel J.; Sherman, Benjamin D.; Tomlin, John; Kodis, Gerdenis; Méndez-Hernández, Dalvin D.; Bertolotti, Sonia; Chesta, Carlos A.; Mariño-Ochoa, Ernesto; Moore, Ana L.; Moore, Thomas A.; Cosa, Gonzalo; and Palacios, Rodrigo E. "Spectral Characteristics and Photosensitization of TiO2 Nanoparticles in Reverse Micelles by Perylenes." The Journal of Physical Chemistry B 117 (2013/04/25 2013): 4568-4581.

49.   Wang, Fuling; Tang, Jianguo; Liu, Jixian; Wang, Yao; Wang, Rui; Niu, Lin; Huang, Linjun; and Huang, Zhen. "Synthesis and photoinduced electron transfer

characteristic of a bis (zinc porphyrin)-perylene bisimide array." <u>Journal of Physical Organic Chemistry</u> 24 (2011): 1101-1109.

50. Mahmood, Zafar; Xu, Kejing; Küçüköz, Betül; Cui, Xiaoneng; Zhao, Jianzhang; Wang, Zhijia; Karatay, Ahmet; Yaglioglu, Halime Gul; Hayvali, Mustafa; and Elmali, Ayhan. "DiiodoBodipy-Perylenebisimide Dyad/Triad: Preparation and Study of the Intramolecular and Intermolecular Electron/Energy Transfer." <u>The Journal of Organic Chemistry</u> 80 (2015/03/20 2015): 3036-3049.

51. Gómez, Rafael; Veldman, Dirk; Blanco, Raúl; Seoane, Carlos; Segura, José L.; and Janssen, René A. J. "Energy and Electron Transfer in a Poly(fluorene-alt-phenylene) Bearing Perylenediimides as Pendant Electron Acceptor Groups." <u>Macromolecules</u> 40 (2007/04/17 2007): 2760-2772.

52. Sachenko, A. V.; Sokolovsky, I. O.; Kaganovich, E. B.; and Manoilov, E. G. "Interpretation of exciton photoluminescence spectra in films with silicon quantum dots." <u>Ukr. Fiz. Zh.</u> 51 (// 2006): 800-804.

53. Rosso-Vasic, Milena; Spruijt, Evan; Popovic, Zoran; Overgaag, Karin; van Lagen, Barend; Grandidier, Bruno; Vanmaekelbergh, Daniel; Dominguez-Gutierrez, David; De Cola, Luisa; and Zuilhof, Han. "Amine-terminated silicon nanoparticles: synthesis, optical properties and their use in bioimaging." <u>Journal of Materials Chemistry</u> 19 (2009): 5926-5933.

54. Rosso-Vasic, Milena; De Cola, Luisa; and Zuilhof, Han. "Efficient Energy Transfer between Silicon Nanoparticles and a Ru-Polypyridine Complex." <u>J. Phys. Chem. C</u> 113 (// 2009): 2235-2240.

55. Bai, Hui; Chen, Qiang; Miao, Chang-Qing; Mu, Yue-Wen; Wu, Yan-Bo; Lu, Hai-Gang; Zhai, Hua-Jin; and Li, Si-Dian. "Ribbon aromaticity in double-chain planar BnH22- and Li2BnH2 nanoribbon clusters up to n = 22: lithiated boron dihydride analogues of polyenes." <u>Physical Chemistry Chemical Physics</u> 15 (2013): 18872-18880.

56. Huang, Chun; Barlow, Stephen; and Marder, Seth R. "Perylene-3,4,9,10-tetracarboxylic Acid Diimides: Synthesis, Physical Properties, and Use in Organic Electronics." <u>The Journal of Organic Chemistry</u> 76 (2011/04/15 2011): 2386-2407.

57. Harris, Rachel D.; Bettis Homan, Stephanie; Kodaimati, Mohamad; He, Chen; Nepomnyashchii, Alexander B.; Swenson, Nathaniel K.; Lian, Shichen; Calzada, Raul; and Weiss, Emily A. "Electronic Processes within Quantum Dot-Molecule Complexes." <u>Chemical Reviews</u> 116 (2016/11/09 2016): 12865-12919.

58. OhtaCurrent address: Center for Disease, Biology; Integrative Medicine, Faculty of Medicine The University of Tokyo Hongo Bunkyo-ku Tokyo Japan Seiichi; Yamura, Kentaro; InasawaCurrent address: Graduate School of, Bio-Applications; Systems Engineering, Tokyo University of Agriculture; Technology, Nakacho Koganei Tokyo Japan Susumu; and Yamaguchi, Yukio. "Aggregates of silicon

quantum dots as a drug carrier: selective intracellular drug release based on pH-responsive aggregation/dispersion." <u>Chemical Communications</u> 51 (2015): 6422-6425.

59.   Liu, Pingping; Na, Na; Huang, Lingyun; He, Dacheng; Huang, Changgang; and Ouyang, Jin. "The Application of Amine-Terminated Silicon Quantum Dots on the Imaging of Human Serum Proteins after Polyacrylamide Gel Electrophoresis (PAGE)." <u>Chemistry – A European Journal</u> 18 (2012): 1438-1443.

60.   Chatterjee, Surajit, and Mukherjee, Tushar Kanti. "Thermal luminescence quenching of amine-functionalized silicon quantum dots: a pH and wavelength-dependent study." <u>Physical Chemistry Chemical Physics</u> 17 (2015): 24078-24085.

61.   Georgiev, Nikolai I.; Sakr, Alaa R.; and Bojinov, Vladimir B. "Design and synthesis of novel fluorescence sensing perylene diimides based on photoinduced electron transfer." <u>Dyes and Pigments</u> 91 (2011/12/01/ 2011): 332-339.

62.   Mishra, A. K., and Dogra, S. K. "Excited state prototropism of 6-aminochrysene." <u>Journal of Photochemistry</u> 23 (1983/01/01/ 1983): 163-169.

Chapter 4   Impact of the Chemical Nature and Position of Spacers on Controlling the Optical Properties of Silicon Quantum Dots

This work was published in Physical Chemistry Chemical Physics

4.1   Introduction

Silicon Quantum Dots (SQDs) have garnered significant attention in the past decade due to their unique optical properties, including high stability against photobleaching and size-dependent photoluminescence.[1] Furthermore, SQDs have shown several advantages over their counterpart QDs, e.g. CdS, due to their excellent biocompatibility and biodegradability,[2] low-toxicity,[3] being environmentally friendly,[4] and the ease of their surface modification.[5] Thus, SQDs are promising candidates for various applications such as biosensing,[6] bioimaging,[7] photodynamic therapy,[8] photovoltaics, [9] and light-emitting diodes (LEDs).[10]

In addition to the advantages of SQDs, several challenges limit the wide applicability of SQDs, particularly due to their inferior quantum efficiency (quantum yield <10%).[11] In general, the optical properties of SQDs are greatly influenced by their surface oxidation which often leads to a reduction in their fluorescence quantum yield.[12] Additionally, the quantum yield for SQDs of 2 nm diameter drops significantly as the electrons in the higher excited states can be non-radiatively trapped by surface states, leading to a deviation from the quantum confinement effect.[13] Furthermore, SQDS usually show unstable photoluminescence and poor colloidal stability in an aqueous environment.[14] To overcome these issues, surface functionalization of SQDs with organic ligands can protect the surface from oxidation and improve their colloidal stability.[15,16]

Only a few studies in literature have reported the impact of ligands on the optical properties of SQDs.[7,17,18] Interestingly, the utilization of aromatic dyes as capping agents has shown some promising results as a means of improving the QE of SQDs due to the influence on the electronic communication between the SQDs and aromatic dye capping

agent.[7,15] [19,20] Thus, the chemical nature of the ligand plays a crucial role towards controlling the optical properties of SQDs.

This work reports the synthesis of SQDs using a facile solution-based reduction method. Different derivatives of triethoxy silane were used as the silicon source with sodium citrate dihydrate used as the reducing agent. The synthesis was carried out in the green solvent, glycerol, at ambient pressure and relatively high temperature (180 °C). This method has several advantages over other synthesis methods including: 1) its simplicity using a single step synthesis, 2) cost-effectiveness, 3) suitability for large-scale production, and 4) non-toxic starting materials. The synthesized SQDs were then functionalized with fluorescein dyes through several spacers. Three families of SQDs were covalently attached to fluorescein isothiocyanate (FITC) through the isothiocyanate spacer, while a fourth SQD family was attached to a fluorescein dye through the esterification of COOH in the phenyl component of the dye. Fluorescein dye was selected as the capping agent due to its interesting photophysical properties including high fluorescence QE, high extinction coefficients, low cost, and biocompatibility.[21,22] The functionalized SQDs were characterized using UV−Vis absorption spectroscopy, Fourier-transform infrared (FTIR) spectroscopy, high-resolution transmission electronic microscopy (HRTEM), and X-ray photoelectron spectroscopy (XPS), steady-state and times-resolved emission spectroscopy, and Transient Absorption spectroscopy (TA).

4.2 Experimental Section

Chemicals

3-Aminopropyl triethoxysilane (99%, APTES), 1-[3-(trimethoxysilyl)propyl] urea (97%, UPTES), [3-(2-aminoethylamino)propyl]trimethoxysilane (97%, DAPTMS), (3-iodopropyl) trimethoxysilane (≥95%, IPTMS), sodium citrate dihydrate (≥99%, citrate), glycerol (≥99.5%), fluorescein Isothiocyanate, isomer I (FITC), Fluorescein (FL), cesium carbonate (99.99%), N,N-dimethylformamide (99.8%, DMF) were obtained from Sigma-Aldrich Canada, and used as received.

Synthesis of SQDs

The synthesis and purification of SQDs was carried out as previously reported.[19] All synthesis procedures were performed under nitrogen using a schlenk line. In brief, 0.15 gm of sodium citrate was added to 5 ml of glycerol in a 50 ml round bottom flask, then heated to 60 ℃ until all citrate was dissolved in glycerol. Then, 1 ml of the silicon precursor (APTES) was added dropwise over 10 minutes, and the mixture was heated to 180 ℃ for 3 hours under vigorous stirring. The product (Am-SQD) was then purified using a combination of centrifugation and dialysis against ethanol (MWCO of 1 KDa, Spectra/Por®6 Standard RC Pre-wetted Dialysis Tubing, diameter 29 mm). The assemblies Urea-SQD and DiAm-SQD were synthesized in a similar manner using UPTES and DAPTMS as silicon sources.

Functionalization of SQDs

Functionalization of SQDs is shown in scheme 1. An excess amount of fluorescein isothiocyanate (FITC, 100 mg) was mixed with the purified Am-SQDs in 20 ml of anhydrous ethanol and the mixture was stirred for 24 hours in the dark. The functionalized SQDs were then purified to remove any excess FITC using dialysis against ethanol (MWCO of 1 KDa, Spectra/Por®6 Standard RC Pre-wetted Dialysis Tubing, diameter 29 mm) to give Am-SQD-Fl. The product was stored in ethanol for further characterization. Similarly, the dyads Urea-SQD-Fl and DiAm-SQD-Fl were prepared.

Synthesis of TMS-Fl and SQD-FL

The compound TMS-Fl was prepared according to a previously reported procedure.[23] In brief, fluorescein (FL, 1 mmol), IPTMS (3 mmol), and Cs_2CO_3 (3 mmol) were mixed in 30 ml of DMF, and the mixture was stirred at 60 ℃ for 24 hours. After cooling to room temperature, the insoluble Cs_2CO_3 was removed using gravity filtration. The unreacted IPTMS and DMF were then removed using a rotary evaporator to obtain a powder of TMS-Fl. The as-prepared TMS-Fl was used in the following step as the silicon source. Similar to the procedures mentioned above for the synthesis of SQDs, the compound SQD-FL was prepared.
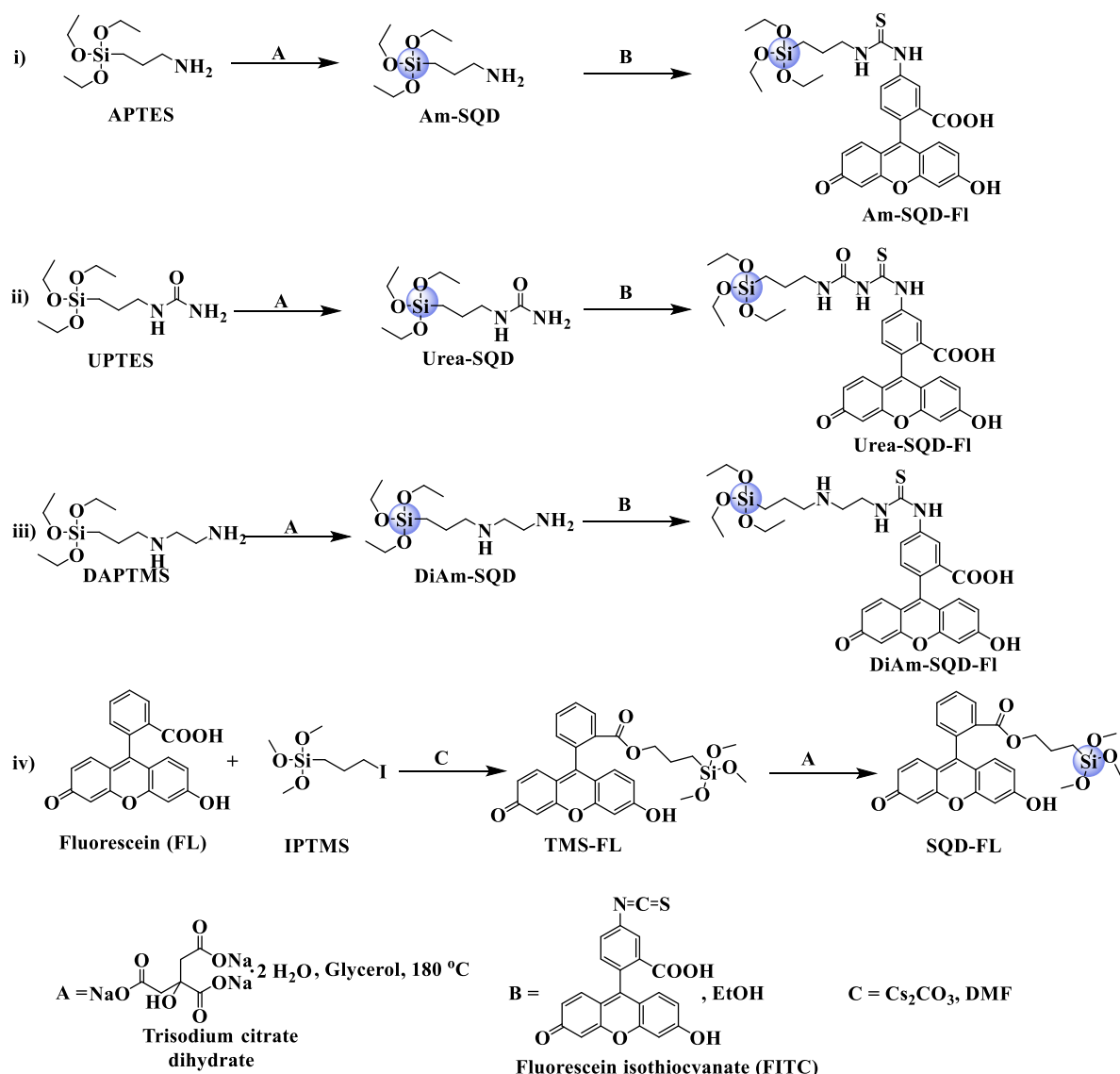
Scheme 1. Synthetic route of different assemblies of SQDs and their surface functionalization.

Methods

XPS analyses was performed with a Kratos Axis Nova spectrometer using a monochromatic Al K(alpha) source (15 mA, 14 kV). The TEM/HRTEM images were recorded using a Libra 200 MC operated at 400 kV. The FTIR spectra were collected using a Nicolet 6700 FTIR spectrometer equipped with a smart iTR diamond horizontal attenuated total reflectance (ATR). The UV–Vis absorption spectra were measured using

a Shimadzu UV-1800 double beam spectrophotometer with a 1 cm path length quartz cuvette. Steady-state emission and excitation spectra were recorded on a Photon Technology International (PTI) spectrofluorometer equipped with a Xenon short-arc lamp. All measurements were carried out using Felix X32 PTI software for data collection and analysis at 298 K under ambient oxygen in ethanol (EtOH). Time-resolved emission spectra (TRES) and fluorescence lifetimes measurements were carried out using a PicoQuant Fluorescence lifetime system (Picoquant GmbH) equipped with a FluoTime 200 (Fluorescence Lifetime spectrometer), a TimeHarp 200 (Time-correlated Single Photon Counting (TCSPC) system), and a PDL800-B pulsed diode laser driver unit. Samples were excited at 375 nm using a picoseconds laser diode head (LDH-P-C375). Instrument Response Function (IRF) was found to be around 350 picoseconds (ps) obtained from analysis of the scattered light kinetic trace using LUDOX SM-30 colloidal silica solution at 375 nm. Fluorescence lifetimes were obtained from deconvolution of the kinetic traces of their solutions using global fluorescence decay data analysis software (Fluo Fit) supported by Picoquant GmbH. The TRES was recorded using an automated wavelength scanner and multichannel scaler (MCS) data collection under instrument software control. In this mode, the monochromator was controlled by a stepper motor and automated collection of spectrally resolved lifetime histograms. Data was collected in standard Integration Mode and saved in different blocks of memory for each wavelength. The collected data was then analyzed using FluoPlot software to construct the different emission spectra as function of delay time after excitation with the laser source.

Fluorescence Quantum yield measurements were carried out at 298 K in EtOH; measurement of the quantum yield involved the comparison of very dilute solutions of the studied sample with a solution of approximately equal optical density using a standard reference compound of known quantum yield. The quantum yield of an unknown sample is related to that of a standard by the equation: $\Phi_u = [(A_s F_u n^2)/(A_u F_s n_0^2)]$; where A is the absorbance at a given excitation wavelength, F is the integrated emission area across the band, and n and n_0 are the refractive indexes of the solvent containing the unknown and standard, respectively. Measurements were carried out using 6-aminochrysene (Φ_F= 25%)[24,25] and fluorescein (Φ_F= 79%)[26] as references. Three different solutions for both sample and reference were used for measurements. Concentrations were adjusted to

have an absorbance of ~0.05 at the excitation wavelength, while the absorption spectra were recorded 5X for accuracy and error minimization.

The detailed experimental setup for Femtosecond Broadband TA Spectroscopy was described elsewhere. [27] In brief, the setup consists of a white-light continuum probe pulse generated by a 2-mm-thick sapphire plate and spectrally pump tunable fs pulses (240–2600 nm; a few μJ pulse energy) generated in an optical parametric amplifier (Newport Spectra-Physics). The pump and probe pulses were overlapped in a 2-mm-thick cuvette cell containing the sample solution. The transmitted probe light from the solution was collected and focused onto a broadband UV-Vis detector to monitor the transient absorbance change (ΔA). The sample solution was constantly stirred using a magnetic stirrer to ensure a fresh volume was available for each laser shot. To include the transient spectra from a few hundred fs to ns time delays after photoexcitation, a Helios detection system with time resolutions of 120 fs and detection limits of 5.5 ns was employed.

Fluorescent Imaging: Human cell lines (U2OS osteosarcoma bone cancerous cells) were maintained in Dulbecco's modified Eagle medium (DMED) containing 1% penicillin and streptomycin and 10% fetal bovine serum (WISENT). Cells were grown on coverslips up to approximately 80% confluence, then washed with 1 x PBS. Cells were fixed using 4% formaldehyde and stained as described elsewhere.[7] The cells were then treated with different families of SQDs dissolved in PBS to a final concentration of 50 ug/mL and incubated for 3 hrs. After incubation, the cells were washed twice with PBS to remove any excess SQDs. The cell nucleus was stained using DAPI (4′,6-Diamidine-2′-phenylindole dihydrochloride) while images were captured using an EVOS FL auto fluorescent microscope by GFP filter (excitation/bandwidth = 470/22, emission/bandwidth = 510/42) and phase mode at 20X magnification.

4.3 Results and Discussion

The synthesis of the SQDs and their surface functionalization was carried out as shown in scheme 1. APTES, UPTES, DAPTMS, and TMS-Fl were used as the silicon sources and were reduced using sodium citrate dihydrate. The synthesis of SQDs was carried out in glycerol as a high boiling functional solvent at atmospheric pressure and 180 °C with the

resulting SQDs purified by dialysis membrane and then functionalized with fluorescein dye to produce Am-SQD-Fl, Urea-SQD-Fl, DiAm-SQD-Fl, and SQD-FL.

4.3.1 Size and structure

Figure 4-1 presents the size distribution histograms, photographs of SQDs solutions under UV, TEM, and HR-TEM of the assemblies DiAm-SQD, Urea-SQDs, Am-SQDs, and SQD-FL. The TEM images indicate that the SQDs are semi-spherical without obvious agglomeration or aggregation. The size distribution histograms of the four SQDs assemblies showed that 97% of the particle's diameters ranged from 1 – 3 nm after analyzing more than 250 dots from different regions of the grid. The average diameters for the assemblies DiAm-SQD, Urea-SQDs, Am-SQDs, and SQD-FL are 1.7 ± 0.7, 1.8 ± 0.7, 1.8 ± 0.8, and 1.6 ± 0.6 nm, respectively. The HR-TEM images show a high crystallinity for the SQDs as indicated by the distinct lattice fringes with 0.30 nm interplanar spacing, which is consistent with the (111) plane of diamond silicon.[28] It should be mentioned that the rather low-quality visualization from TEM is well known due to the ultra-small dimensions of the SQDs as well as the small atomic weight of the silicon atom compared to the counterpart metallic or semiconductor quantum dots.[7,19,29,30]
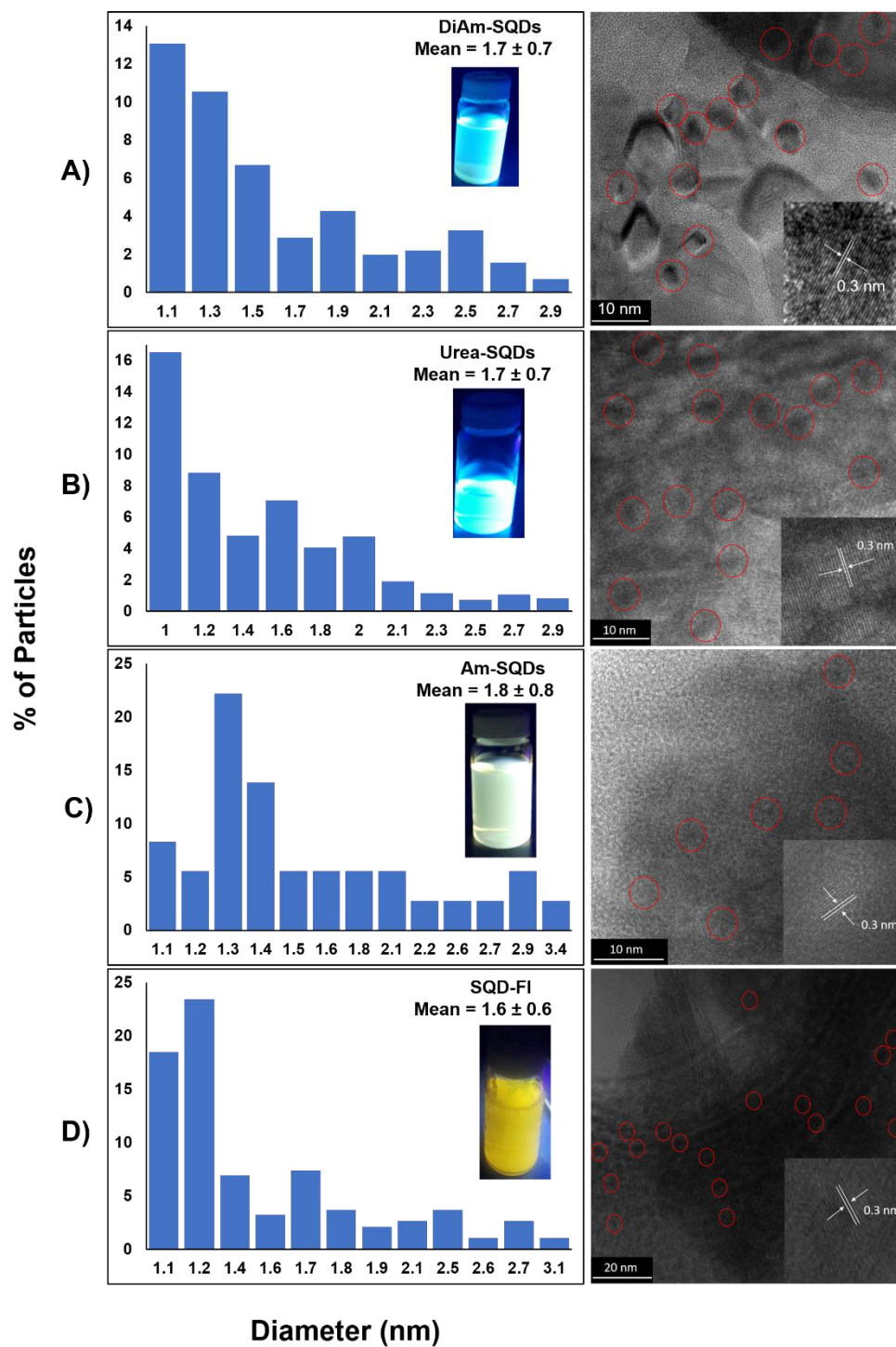
Figure 4-1. Diameter distribution with photographs of solutions under UV (365 nm) irradiation (left) and TEM together with HR-TEM (right) for the assemblies DiAm-SQDs(A), Urea-SQDs (B), Am-SQDs (C), and SQD-FL (D).

To confirm the binding of fluorescein dyes to the surface of the SQDs assemblies, both FTIR and XPS spectroscopy were carried out. Figure 4-2 shows the FTIR spectra for the Urea-SQD-Fl, DiAm-SQD-Fl, Am-SQD-Fl, and FITC dye as well as SQD-Fl and Fl dye. In figure 4-2(i), the broad peak at 3664 – 3004 cm^{-1} is attributed to the stretching vibration of hydroxyl groups (OH);[31] and the intense broad peak at 1000 – 1150 cm^{-1} is assigned to the stretching vibration of Si-O-Si.[32] The peak at 2985 – 2770 cm^{-1} is attributed to the C-H stretching vibration of methyl and methylene,[33] and the peak at 1735 cm^{-1} is assigned to the carbonyl group (C=O).[33] It is worth mentioning that the characteristic peak of the isothiocyanate group (N=C=S) at 2015 cm^{-1} in the FITC has completely disappeared in the spectra of Urea-SQD-Fl, DiAm-SQD-Fl, and Am-SQD-Fl.[33] This indicates successful binding of SQDs to the FITC dye. In figure 4-2(ii), the peaks at 3656 – 2985 cm^{-1}, 2981 – 2777 cm^{-1}, and 1025 cm^{-1} are assigned to the stretching vibration of hydroxyl group, methyl groups, and Si-O-Si, respectively. It is noted that the carbonyl stretching vibration in the Fl dye was observed at 1734 cm^{-1}, but that of SQD-FL was monitored at 1716 cm^{-1} which is attributed to interactions with the SQD surface.[34]
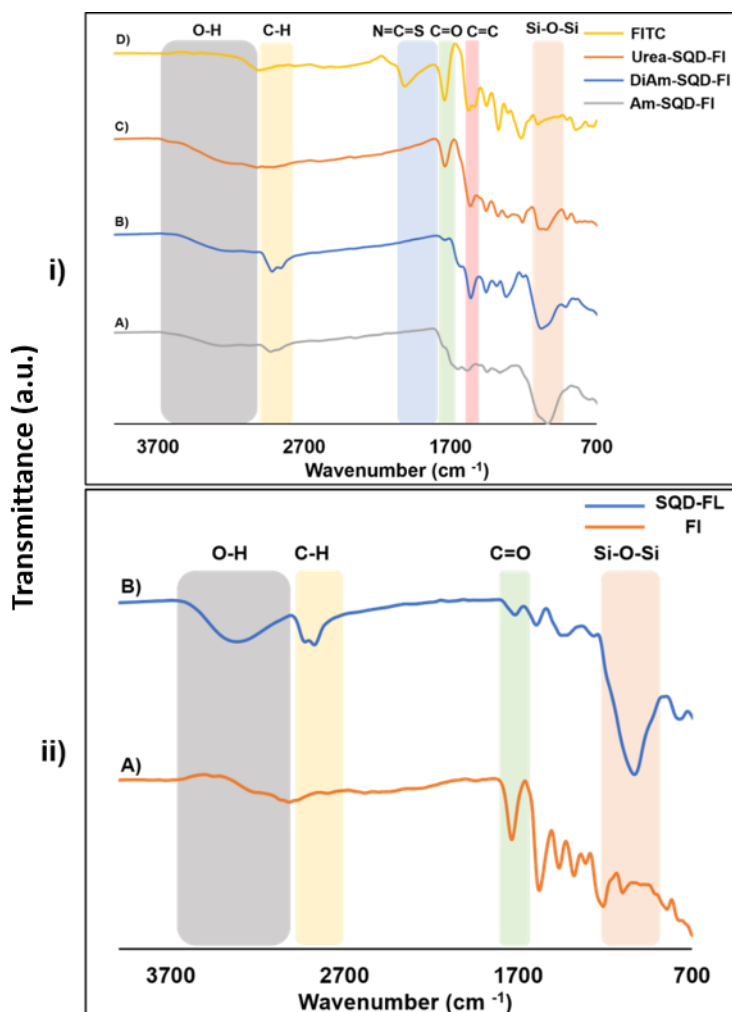
Figure 4-2. FTIR spectra of i) Am-SQD-Fl (A), DiAm-SQD-Fl (B), Urea-SQD-Fl (C) and FTIC(D); and ii) Fl (A) and SQD-FL (B).

XPS spectroscopy was performed in order to further confirm the binding of SQDs to fluorescein dyes via the examined linkers. Figure 4-3 presents the high resolution XPS spectra of C 1s and N 1s for the assemblies DiAm-SQD-Fl (A), Urea-SQD-Fl (B), and Am-SQD-Fl (C) as well as that of O 1s and C 1s for SQD-FL (D). The deconvoluted peaks of N 1s for Urea-SQD-Fl appeared at 400.1 and 401.8 eV; and that of Am-SQD-Fl appears at 400 and 401.7 eV, which can be assigned to the thiourea nitrogen species (NHC=SNH) and protonated amine species, respectively.[35] Similarly, the N 1s binding energies for DiAm-SQD-Fl appear at 399.6 and 400.6 eV which are attributed to the amine and thiourea nitrogen atom (NHC=SNH), respectively.[35]
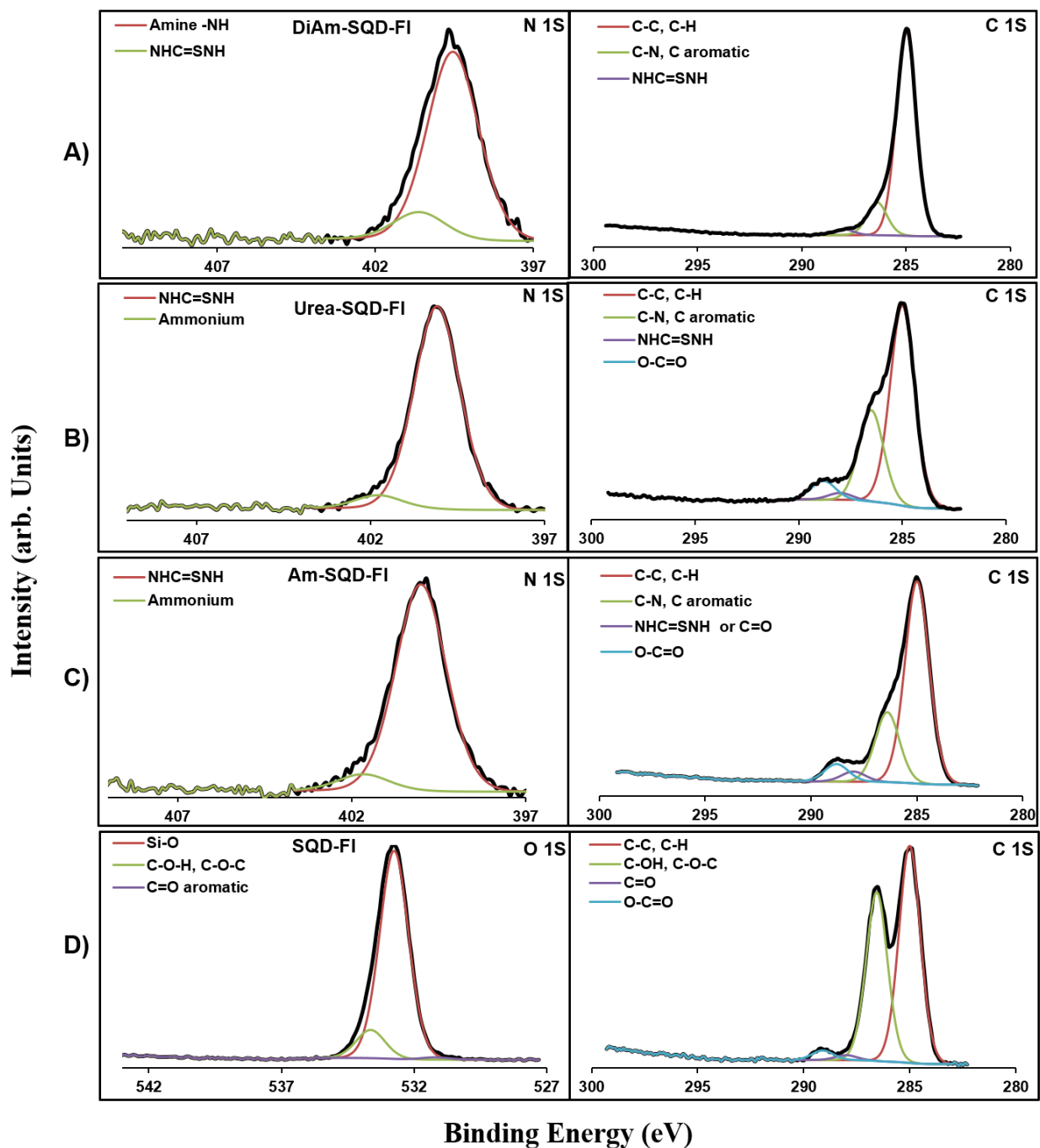
Figure 4-3. XPS Spectra of N 1s and C 1s for DiAm-SQD-Fl (A), Urea-SQD-Fl (B), Am-SQD-Fl (C); and O 1s and C 1s for SQD-FL (D).

The C 1s binding energy peaks appearing at 288, 286.4, 285 eV for the assemblies DiAm-SQD-Fl, Urea-SQD-Fl, and Am-SQD-Fl are assigned to the thiourea carbon species (NHC=SNH), C-N, and C-C or C-H bonding, respectively.[35] This provides confirmation

for the attachment of Am-SQDs, DiAm-SQD, and Urea-SQD to the FITC dye. The XPS spectrum of O 1s for the assemblies SQD-FL shows binding energy peaks at 533.6, 532.8, and 531.2 eV which are assigned to C-OH or C-O-C, Si-O, and C=O, respectively.[19] The C 1s peaks at 289.1, 288, 286.6, and 285 eV are attributed to O-C=O, C=O, C-OH or C-O, C-C or C-H, respectively.[19,35] The XPS results are consistent with the FTIR data, helping confirm the binding of SQDs to fluorescein dyes through the examined linkers.

4.3.2 Photophysical properties

In order to understand the nature of interaction between fluorescein dyes and SQDs assemblies, their photophysical properties including steady-state photoluminescence (PL) and excitation spectra, PL lifetime (τe), quantum efficiency (ΦPL), and femtosecond transient absorption (fs-TA) measurements were performed for the SQDs assemblies and their counterparts dyads Urea-SQD-Fl, DiAm-SQD-Fl, Am-SQD-Fl, and SQD-FL.

Steady-state photoluminescence

The two fluorophores in the current investigated dyad systems are SQDs and fluorescein dye (Fl). Both fluorophores are attached through different spacers that vary in chemical nature and length. Previous reports for SQDs of the same average size revealed that they are characterized with one broad emission spectrum covering the spectral range from 350 – 600 nm with a central emission band located at ~440 nm. [7] The PL for the SQDs within this average size usually shows a deviation from the spectral range predicted from the quantum confinement effect. This is due to the edge of the conduction band and the separation of the discrete states increasing, thus electrons can fill higher excited state levels.[36] The other counterpart fluorophore in these dyads is Fluorescein, which is an organic dye with well-known fluorescence properties and a relatively high photoluminescence quantum yield.[37] Typically, fluorescein shows a broad fluorescence spectrum over a spectral range of 500 - 600 nm, which is sensitive to the surrounding chemical environment.[38]

Steady-state photoluminescence (PL) spectra are given in Figure 4-4 (A), where the spectral profile reveals the presence of one main spectral band extended over the range of 480 - 650 nm in common for all dyads investigated. This band agrees in shape and position

with the fluorescence spectra reported for fluorescein. [37] The spectral profile in general exhibits a broad featureless emission band with central maxima at 515 nm for Am-SQD-Fl and 520 nm for both of Urea-SQD-Fl and DiAm-SQD-Fl. On the other hand, the PL for SQD-FL showed an extra shoulder at 545 nm in addition to the main maximum at 515 nm. The chemical linkage between SQDs and fluorescein takes place through the COO- group, rather than the isothiocyanate (-NCS) in the other three assemblies as shown in Scheme 1. The structure of fluorescein dye generally has two structural components, i.e. the benzene ring and the xanthene unit. Generally, substitution on the phenyl ring exerts a significant impact on the photophysics of the fluorescein. [38] [21] For some cases, substitution results in excited state deformation [38] while other cases lead to different isomer formation in solution. [21] Thus, the changes in PL spectra observed for SQD-FL can be attributed to excited-state deformation and/or isomer formation. Furthermore, the dyad DiAm-SQD-Fl shows an additional emission band detected over the range 400 - 480 nm with a central spectral maximum at 430 nm. This band was almost quenched for the rest of the investigated SQDs dyads. Further discussion in this regard is given in the time-resolved femtosecond transient absorption (fs-TA) section.

Nanosecond time-resolved PL traces were collected using time-correlated single photon counting (TCSPC) and the decay curves are given in Figure 4-4 (B). The estimated fluorescence lifetimes as obtained from deconvolution of the TCSPC curves are listed in Table 4-1. Kinetic traces for the PL decay signals of all dyads exhibited bi-exponential profiles except for the Am-SQD-Fl where the traces were fitted with a single exponential function. The PL decay traces reveal the existence of one long-lived lifetime together with another relatively shorter lifetime. The relatively long-lived component agrees with the fluorescence lifetime reported for fluorescein.[21] The short-lived lifetime component (~ 0.7 and ~ 0.6 ns for Urea-SQD-Fl and DiAm-SQD-Fl; respectively) is attributed to an additional process associated with intramolecular photoinduced electron transfer between the phenyl and xanthenes moieties of the fluorescein. [38] On the other hand, the mono-exponential decay observed with the Am-SQD-Fl kinetic trace is indicative of interruption for the intramolecular photo-induced electron transfer process. It should be pointed out that this process is dependent on the substitution of the phenyl group.[39]
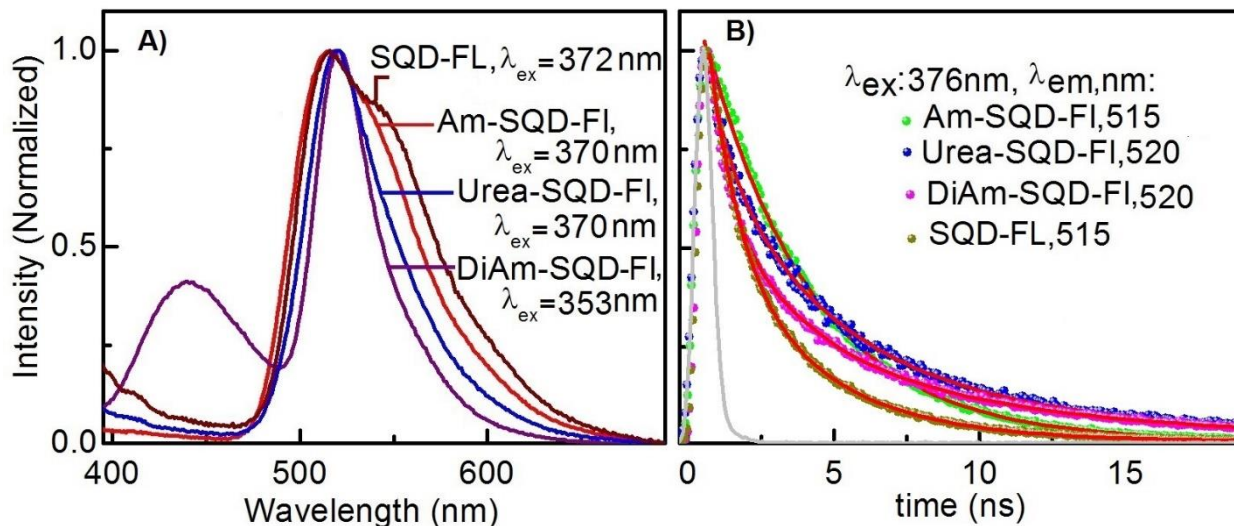
Figure 4-4. (A) Photoluminescence spectra of SQD-FL, Am-SQD-Fl, Urea-SQD-Fl, and DiAm-SQD-Fl in EtOH with λ_{ex} designated for each spectrum; and (B) time-resolved kinetic traces in EtOH using laser excitation at 376 nm with monitoring λ_{em} given at each trace. (IRF ≈ 350 ps, and red lines are fitted curves).

Photoluminescence quantum yield (PLQY) of the investigated assemblies were measured in EtOH using 6-aminochrysene (Φ_F = 18 %) as reference [40]; with the obtained values given in Table 4-1. These PLQY values are significantly improved compared to those previously reported SQDs based assemblies.[7] The higher values obtained for the Am-SQD-Fl are corroborated by the results obtained from the TCSPC curves, suggesting an interruption of the non-radiative intramolecular electron transfer. The measured quantum yields for the SQDs assemblies Urea-SQD, Am-SQD, and Di-Am-SQD were 16.5, 12.6, 23.6 %, respectively. The counterpart dyads showed a significant improvement in their quantum yields except for the DiAm-SQD-Fl and SQD-FL. The dyads Urea-SQD-Fl, Am-SQD-Fl, DiAm-SQD-Fl, and SQD-FL exhibited a quantum yield of 38.3, 64.7, 17.7, and 12.4 %, respectively. The PLQY for the SQD-FL was found to be the lowest, attributed to the non-radiative relaxation contribution resulting from the excited state deformation.

It is worth mentioning that the change in the overall quantum efficiencies in the dyad systems is impacted with the photoinduced energy and/or electron transfer. Hence, the QE of the dyad systems is different from that of the dye or SQDs individually.

The structure of Fl dye is composed of two parts namely the phenyl and xanthene sub-unit where an intramolecular photo-induced electron transfer (PET) operative between these two parts. Any Substitutes on the phenyl group changes redox potential of the phenyl group and consequently free energy change for the intramolecular PET which in turn is controlling the Fl photoluminescent quantum yield.[39] For the current investigated dyad assemblies, the overall quantum yields values reported have predominant contribution from the Fl especially for Am-SQD-Fl where almost quenching for the SQDs fluorescence was observed. Comparison between the three investigated dyads shows the overall quantum yield values to be in the order of: Am-SQD-Fl > Urea-SQD-Fl > DiAm-SQD-Fl. This order is in agreement with the increase of spacer length connecting SQDs and Fl which is expected to change the overall electron density on the phenyl group. In turn, this is expected to affect the free energy change for the intramolecular PET and consequently the overall quantum yield for the assembly. Thus, the dyad Am-SQD-Fl exhibited the highest quantum efficiency.

More interestingly, PLQY measurements repeated for samples stored at room temperature for almost a year revealed a high stability with only slight changes in the measured values, confirming photo-stability of the samples.

Table 4-1. PLQY and PL lifetime of the different samples measured in EtOH. The PL lifetime was extracted from time-correlated single photon counting (TCSPC) upon 376-nm excitation.

	%Quantum yield (%Φ)[a]	Fluorescence lifetime[b] (% Pre)[c]	
		λ_{em}, nm	τ, ns (% Pre)
Fl	-	515[d]	4.3 ± 0.1
FTIC	-	515[d]	3.9 ± 0.1
Urea-SQD	16.5	440	10.7 ± 0.2 (27%) 2.2 ± 0.1 (73%)
Am-SQD	12.6	440	10.0 ± 0.2 (35%) 2.0 ± 0.1 (65%)
DiAm-SQD	23.6	440	9.2 ± 0.1 (24%) 2.4± 0.1 (76%)

Urea-SQD-Fl	38.3	520	0.7±0.2 (60)
			3.7±0.2 (40)
Am-SQD-Fl	64.7	515	3.6±0.2
DiAm-SQD-Fl	17.7 (total):	440	0.6±0.2 (40)
	7.2 (SQD)		2.9±0.2 (40)
	10.4 (Fl)		10.1±0.2 (20)
		520	1.2±0.2 (47)
			4.1±0.2(53)
SQD-FL	12.4	515	1.3±0.2 (68)
			3.8±0.2(32)

[a] Reference used is 6-Aminochrysene and $\lambda_{ex} = 345$ nm.

[b] IRF ≈ 350 ps (from LUDOX SM-30 colloidal silica solution).

[c] pre-exponential weighting factor for the lifetime component.
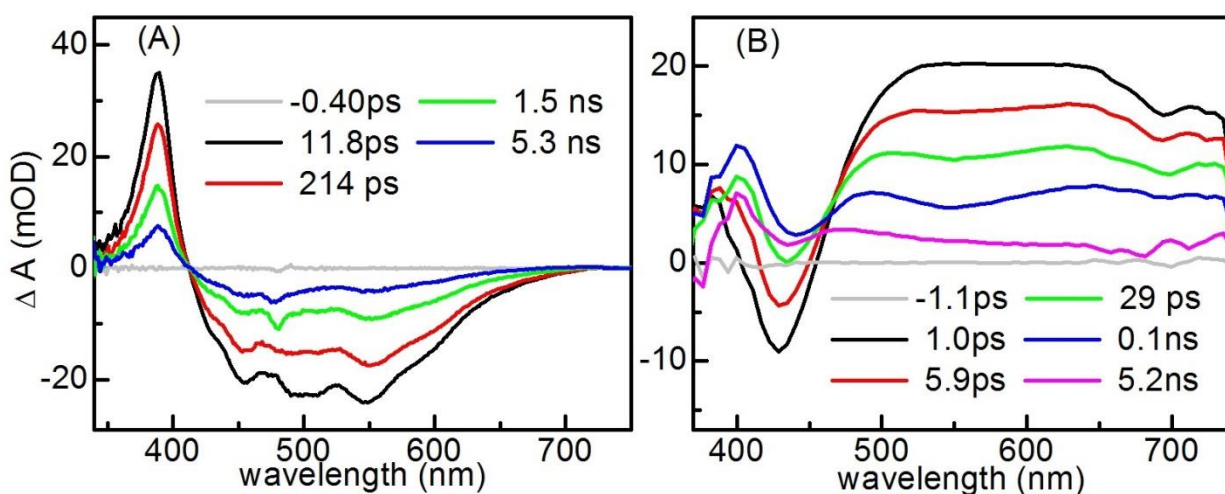
Figure 4-5. fs-TA spectra at different delay times in response to 475 nm (for Fl, A) and 350 nm (for Am-SQD, B) optical excitation.

In order to better understand the excited state in these assemblies upon photo-excitation, time-resolved laser spectroscopy was conducted using fs-TA measurements with broadband capabilities where excitation uses a 120 fs laser.[41,42] Figure 4-5 shows the fs-TA spectra of Fl (A) and Am-SQD (B) in response to 475 and 350 nm optical excitation; respectively. The fs-TA spectra for Fl revealed two signals, one as a positive absorption change referred to as a photo-induced excited state absorption (PIA), corresponding to S_1-S_n absorption. The other is a negative absorption change corresponding to ground-state

bleaching (GSB) due to depletion of the ground state population. The TA signal for the Am-SQD revealed one broad PIA with the dipping at 445 nm attributed to stimulated emission (SE); see SI for steady state of starting SQDs.

The collected fs-TA spectra and the kinetic traces for the investigated assemblies are given in Figure 4-6. In general, the fs-TA spectra exhibited similar spectral features in both PIA and GSB to the Fl signal, whereas the GSB for DiAm-SQD-Fl reflected the ground-state absorption and stimulated emission; see Figure 4-6 (A&B). Indeed, the very strong overlap between PIA, SE and GSB precludes precise confirmation about the nature of interaction on whether it is energy or electron transfer. By monitoring the changes in the kinetic traces, we can elucidate that the interaction is strongly dependent on the nature and the length of the spacer bridge and the position of attachment between the SQDs and Fl dye. Three different scenarios detected in the kinetic trace profiles are: while Urea-SQD-Fl exhibited the same profile as that for Fl; DiAm-SQD-Fl and SQD-FL showed a faster decay (see Table 4-2) whereas Am-SQD-Fl exhibited a slower decay monitored at 390 nm; see Figure 4-7 (A). Similarly, GSB recovery kinetics at 455 nm revealed the same trend with Urea-SQD-Fl having the same recovery kinetics as that of Fl while different kinetics detected are slower for Am-SQD-Fl and faster for SQD-FL. This strongly implies that energy transfer is the dominant mechanism for the Urea-SQD-Fl, while electron transfer is the more likely mechanism for Am-SQD-Fl and SQD-FL assemblies. This can be understood considering the change in GSB recovery in comparison to that of Fl, which can be assigned to a different charge recombination time for the formed charged radicals. This is in agreement with a previous report which indicated that the orientation of the phenyl group is almost perpendicular to the xanthene ring in the Fl molecule, leading to a significant trend for favoring the rate of electron transfer in both directions; i.e. charge separation and charge recombination.[43]
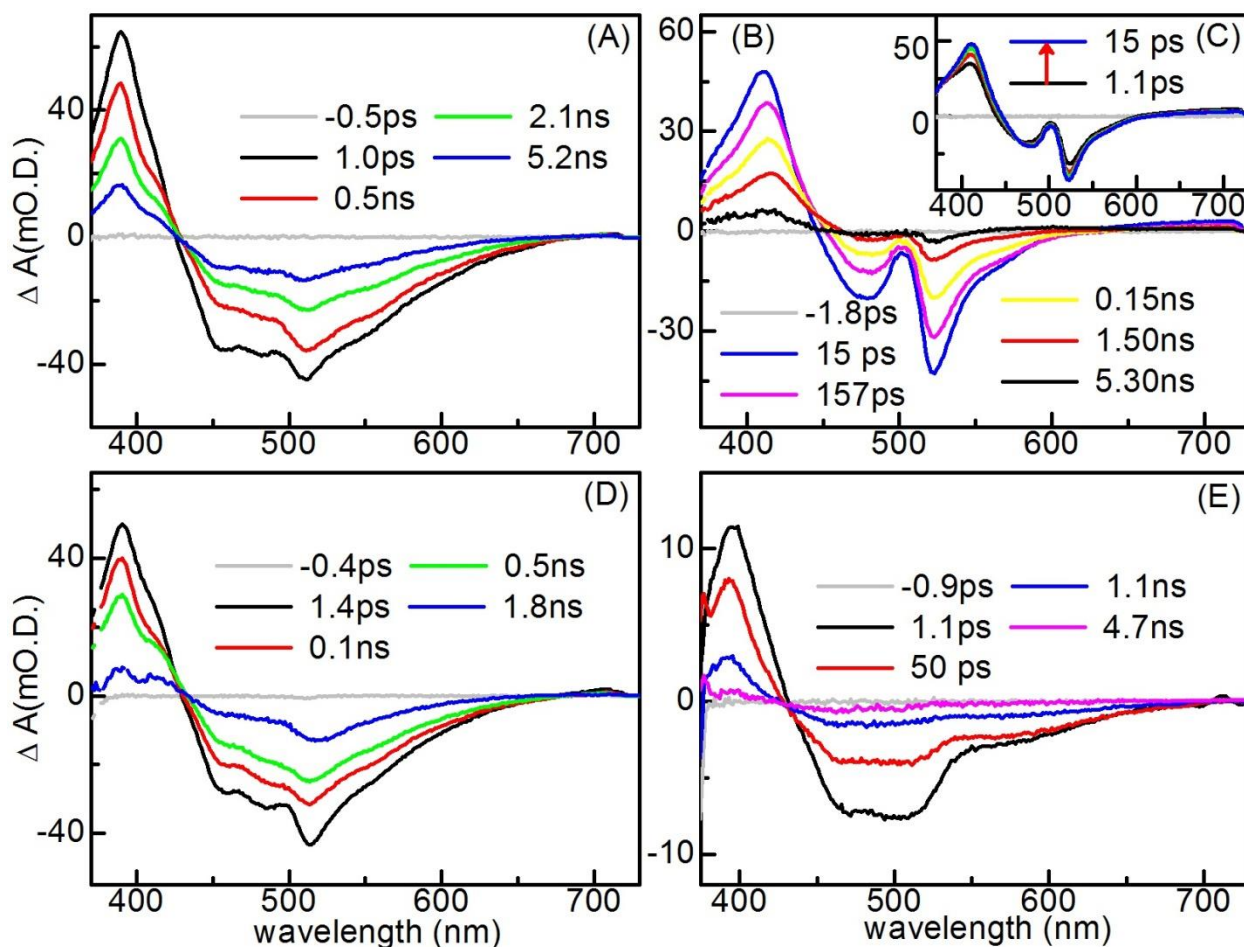
Figure 4-6. fs-TA spectra at different delay times in response to 350 nm optical excitation of Am-SQD-Fl (A), DiAm-SQD-Fl (B, inset showing rising signal over 15 ps (C)), Urea-SQD-Fl (D), and SQD-FL (E); in EtOH.

It is worth mentioning that it was not possible to obtain pure kinetic traces at GSB for DiAm-SQD-Fl due to the strong spectral overlap with SE. The different behavior detected for Urea-SQD-Fl may be due to hydrogen bond formation rendering the electron transfer less thermodynamically favorable; similar behavior was recently reported.[19] Interestingly, the recombination rates proceeded slower for Am-SQD-Fl than for SQD-FL. This allowed us to predict the stability of the formed radical ions regarding the position through which SQDs and Fl are connected. Furthermore, while kinetic traces of all three assemblies of Am-SQD-Fl, Urea-SQD-Fl and SQD-FL showed instant development within the temporal resolution of the laser (i.e. 120 fs) [44], kinetic traces for DiAm-SQD-Fl revealed a slower rising rate when the time constant extracted from the fitting was found

to be ~4 ps; see Figure 4-7 (B) inset. This is indicative of a slower electron transfer rate within this dyad assembly, attributed to elongation of the bridging spacer and the extra NH group as compared to Am-SQD-Fl.

These results indicate that the structure and/or position of the spacer significantly affects both the forward/backward rates of interaction. In this manner, the faster rates for SQD-FL are indicative of the assembly adopting the most favorite orientation for facilitating electron transfer. On the other hand for Am-SQD-Fl, the adopted orientation favors electron transfer while rendering the recombination less favorite as indicated by longer lifetime decays. As the length of the spacer between SQD and Fl in DiAm-SQD-Fl is longer, the rate for forward electron transfer becomes slower as confirmed by slower rates in the fs-TA kinetic traces. Finally, with incorporation of the hydrogen bond along the backbone of the spacing bridge, the interaction mainly proceeds through energy transfer as observed in Urea-SQD-Fl.

Table 4-2. Lifetimes obtained from fs-TA spectra in EtOH.

	t (ps)	
	GSB	EA
Urea-SQD-Fl	16.3±1.8 (18%) 219.1±26.2 (32%) 2632.2±361.7 (50%)	136.32±14.1 (27%) 2801.87±294 (73%)
Am-SQD-Fl	11.95±1.7 (22%) 197.3±49.7 (19%) 2697.6±365.6 (59%)	108.5±15.5 (23%) 2840±206.2 (77%)
DiAm-SQD-Fl	a	4.1±0.3 (rise) 229.8±33.4 (46%) 2128±513 (54%)
SQD-FL	2.2±0.2 (22%) 49.2±4.4 (21%) 817.2±40.2 (57%)	66.7±3.6 (39%) 1076.8±43.5 (61%)

[a] It was not possible to get the kinetic traces at GSB for DiAm-SQD-Fl due to the SE
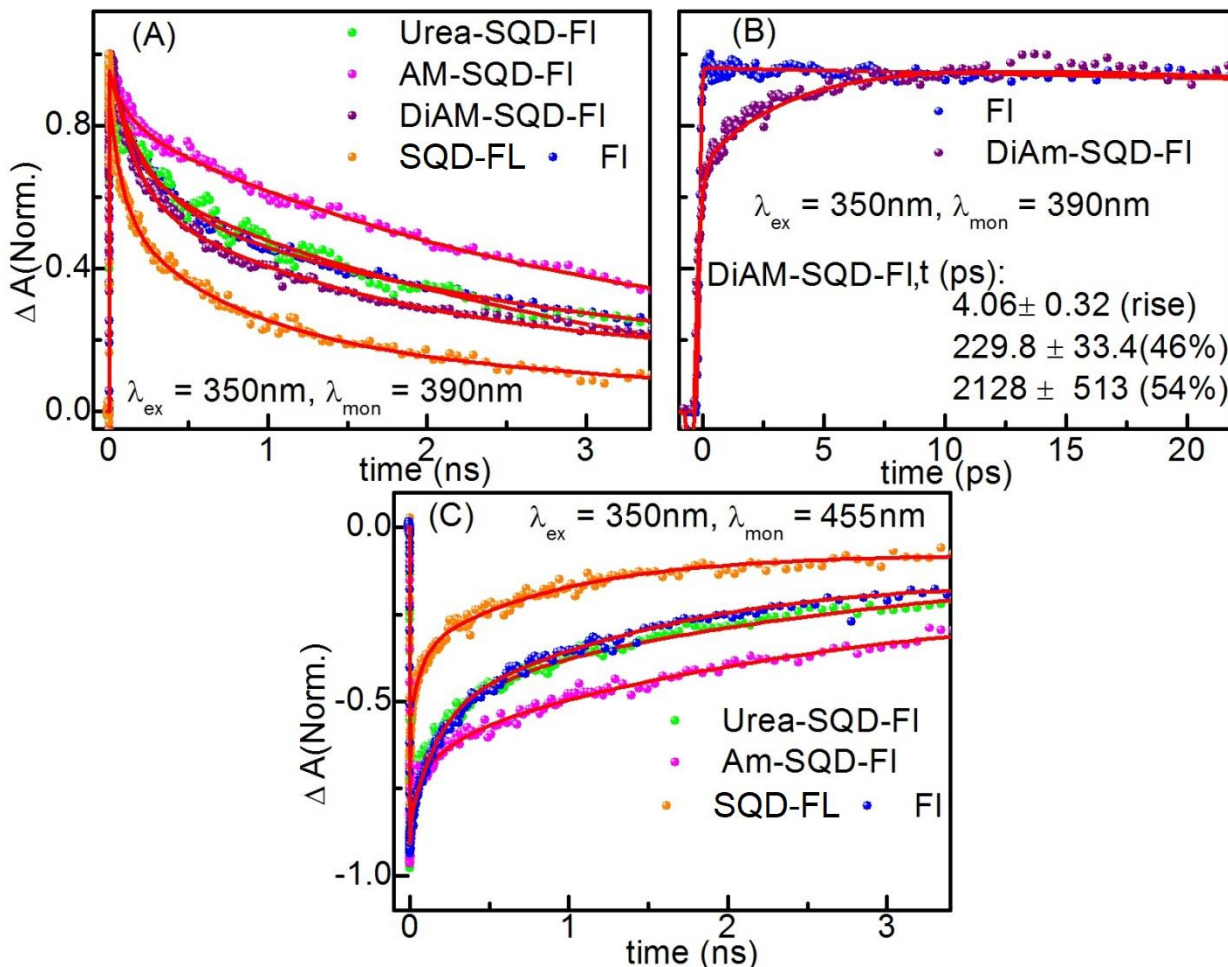
Figure 4-7. Kinetic traces collected from TA from ESA decay for all investigated assemblies (A), ESA rising time for DiAm-SQD-Fl (B), and GSB recovery (C). Exponential fitting traces are given with the red solid lines.

4.3.3 Effect of pH on steady-state fluorescence

Fluorescein derivatives are known to undergo changes in the nature of the photoactive species at different pH values [45]; thus it is important to investigate the effect of pH on the photoactivity of the current synthesized assemblies. Steady-state fluorescence was recorded at different pH values; as given in Figure 4-16. In general, the relative fluorescence intensity remained relatively stable across the pH range of 8.5-3.5. As the pH value decreased below 3.5, a sudden drop was detected for all investigated systems. Further increasing of the pH above 8.5 resulted in a decrease in the relative fluorescence intensity for all investigated assemblies, except SQD-FL. This agrees with the trend reported earlier

for fluorescein isothiocyanate in which the changes are assigned to different neutral and charged forms of the dye.[46] The decrease observed at pH values ≥ 8.5 is associated with the anionic forms of the dye being more predominant in solution. Deviation from this behavior was observed for SQD-FL where the relative intensity undergoes an increase for pH values beyond 8.5. This behavior is attributed to the use of the (COO-) group as the spacer between Fl and SQDs.

4.3.4 Fluorescent cellular imaging study

To demonstrate the suitability of the functionalized water-soluble SQDs for bioimaging applications, the SQDs assemblies were examined for in vitro fluorescent imaging of human osteosarcoma U2OS cell lines. Figure 4-8 shows the U2OS cells that were incubated with DiAm-SQD-Fl, Urea-SQD-Fl, Am-SQD-Fl, and SQD-FL, for which an excitation wavelength of 470 nm was utilized and the emission was monitored at 510 nm. The U2OS cell's nucleus was stained using DAPI dye. The control images, which involved no treatment for U2OS with SQDs, show no fluorescence and the overlay panel shows only a blue color for the DAPI-stained nucleus. Fluorescence imaging of U2OS cells with all 4 dyads of SQDs show bright green fluorescence. The efficient uptake of SQDs by U2OS cells demonstrates the potential utility of these quantum dots for bioimaging studies. It is worth mentioning that the overlay images for DiAm-SQD-Fl and Urea-SQD-Fl show non-distinguishable blue and green colors which can be assigned to the effectiveness of these dyads to stain both the cytoplasm and nucleus. On the other hand, the overlay images of Am-SQD-Fl and SQD-FL show clearly distinguishable blue and green colors which indicate their suitability to stain the cytoplasm only.

	Brightfield	**DAPI**	**Fluorescence**	**Overlay**
No SQDs	A	F	K	P
DiAm-SQD-Fl	B	G	L	Q
Urea-SQD-Fl	C	H	M	R
Am-SQD-Fl	D	I	N	S
SQD-FL	E	J	O	T
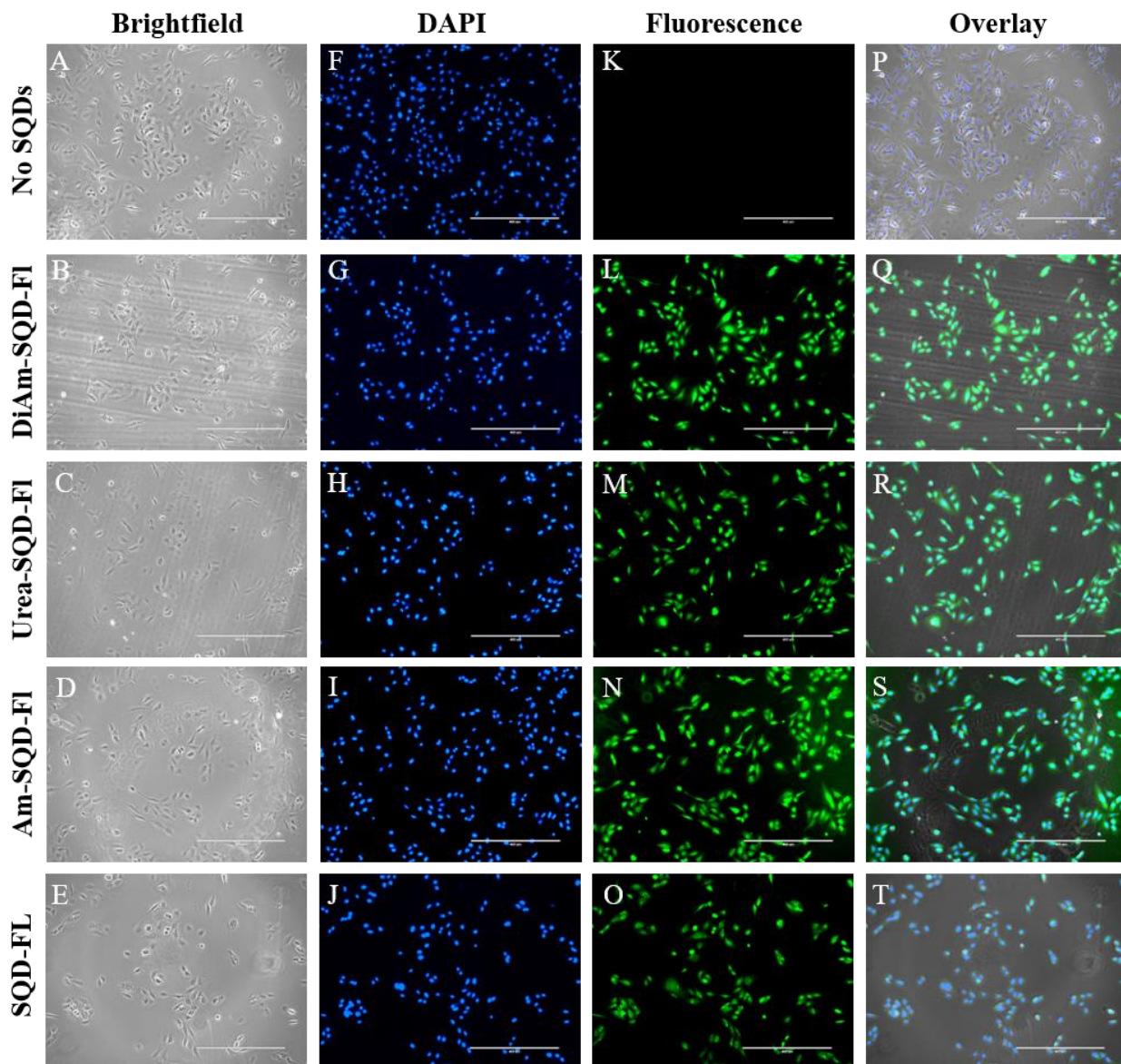
Figure 4-8. Brightfield (A - E), DAPI-stained (F-J), fluorescence (K-O), and overlay images (P-T) of U2OS cells for control sample (no SQDs added), DiAm-SQD-Fl, Urea-SQD-Fl, Am-SQD-Fl, and SQD-FL.

4.4 Conclusion

In this work, four assemblies of SQDs were covalently functionalized with fluorescein dyes through isothiocyanate (-NCS) and carboxyl (COO-) spacers. The utilization of the (-NCS) spacer led to a significant enhancement of the dyads PL quantum yield and showed a high stability of their optical properties for up to one year. The photophysical results revealed

that the nature and length of the spacer as well as the position of connection in these systems played a key role towards tuning their optical properties by controlling both the type and rate of interaction between the SQDs and the Fl dye capping agent. In the dyads SQD-FL, Am-SQD-Fl, and DiAm-SQD-Fl, the interaction between SQDs and Fl was found to mainly take place through electron transfer but at different rates depending on the orientation of the phenyl group comparing to the xanthene part of the Fl dye. Surprisingly, the communication between SQDs and Fl dye in Urea-SQD-Fl proceeds through energy transfer due to the incorporation of the hydrogen bond along the backbone of the spacing bridge. The PL activity of all four dyads were investigated as a function of pH where they were found to show negligible changes over the range 8.5 - 3.5. The dyads DiAm-SQD-Fl, Urea-SQD-Fl, Am-SQD-Fl, and SQD-FL showed promising results when used for fluorescent cellular imaging of human osteosarcoma U2OS which enables their use as fluorescence probes in bioimaging.

4.5   Supporting information
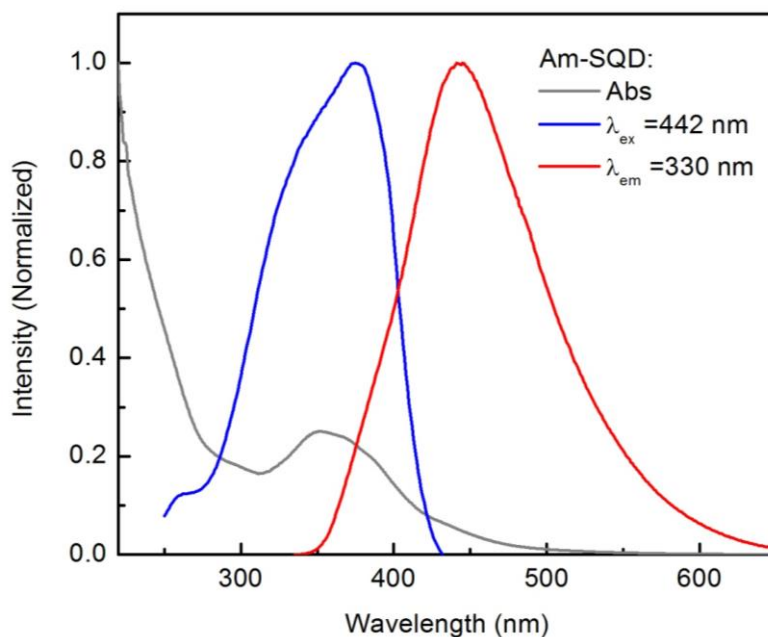
Figure 4-9. Absorption and excitation spectra of Am-SQD collected at room temperature; (λ_{em} and λ_{ex} indicated on graph).
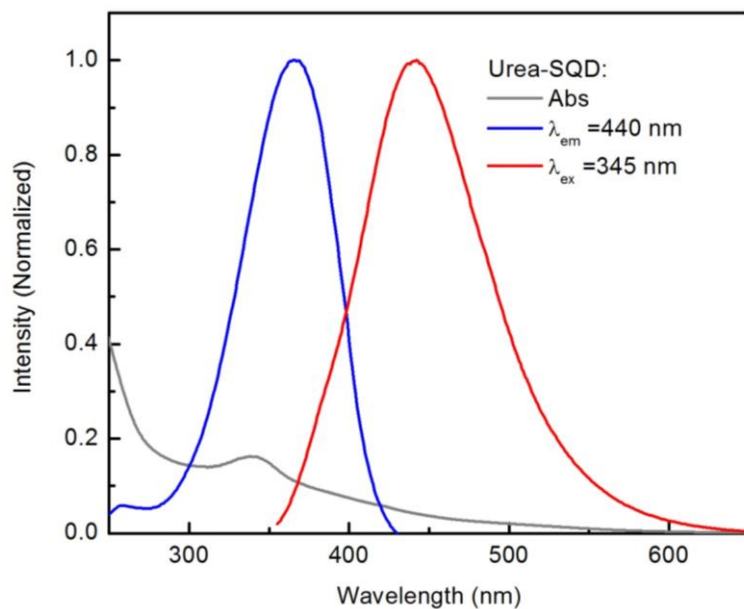
Figure 4-10. Absorption and excitation spectra of Urea-SQD collected at room temperature; (λ_{em} and λ_{ex} indicated on graph).
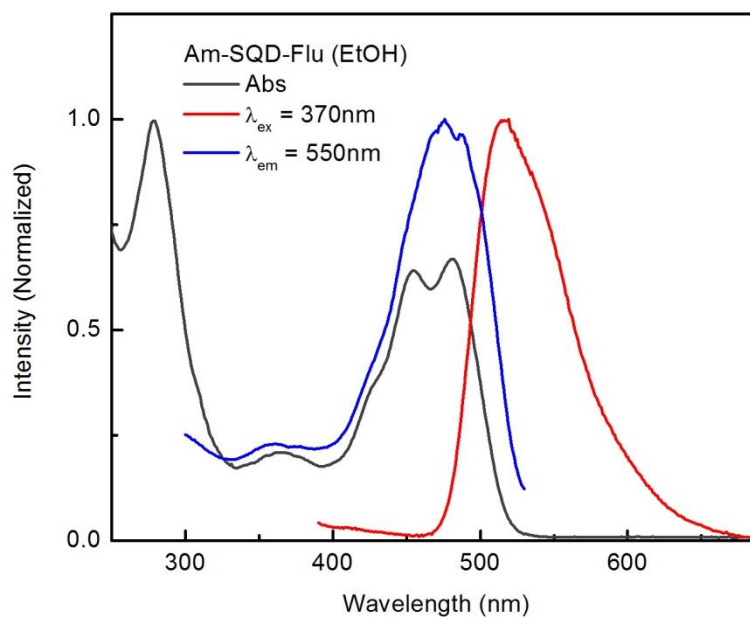
Figure 4-11. Absorption and excitation spectra of Am-SQD-Flu collected at room temperature; (λ_{em} and λ_{ex} indicated on graph).
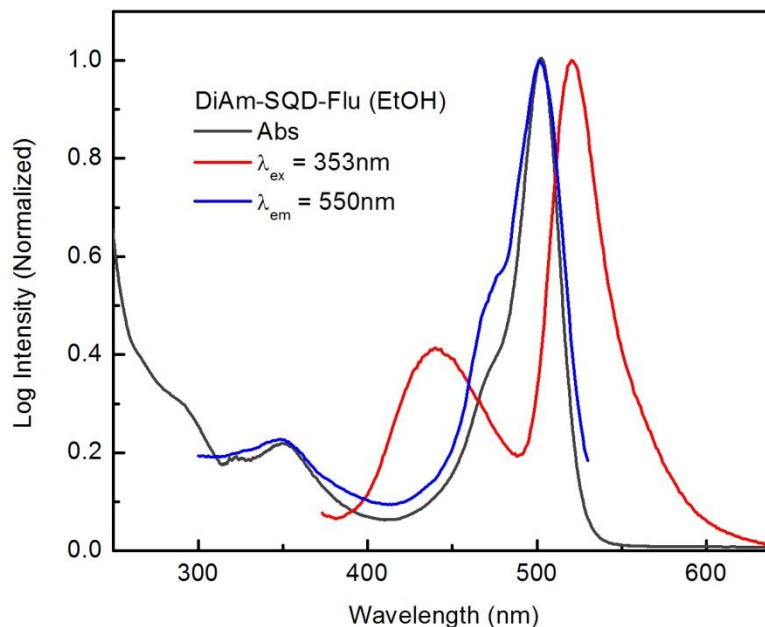
Figure 4-12. Absorption and excitation spectra of DiAm-SQD-Flu collected at room temperature; (λem and λex indicated on graph).
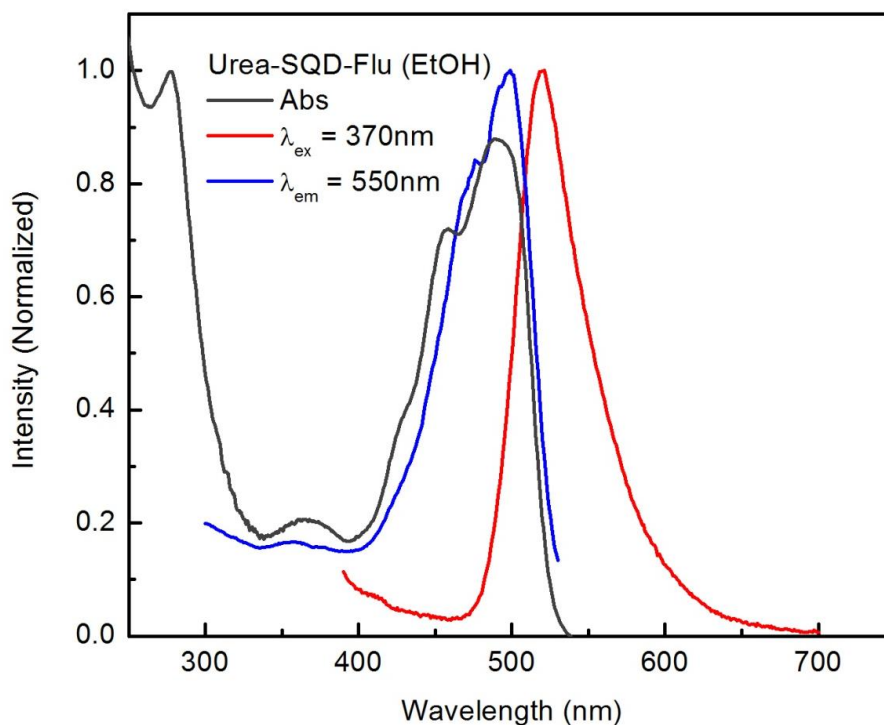
Figure 4-13. Absorption and excitation spectra of Urea-SQD-Flu collected at room temperature; (λem and λex indicated on graph).
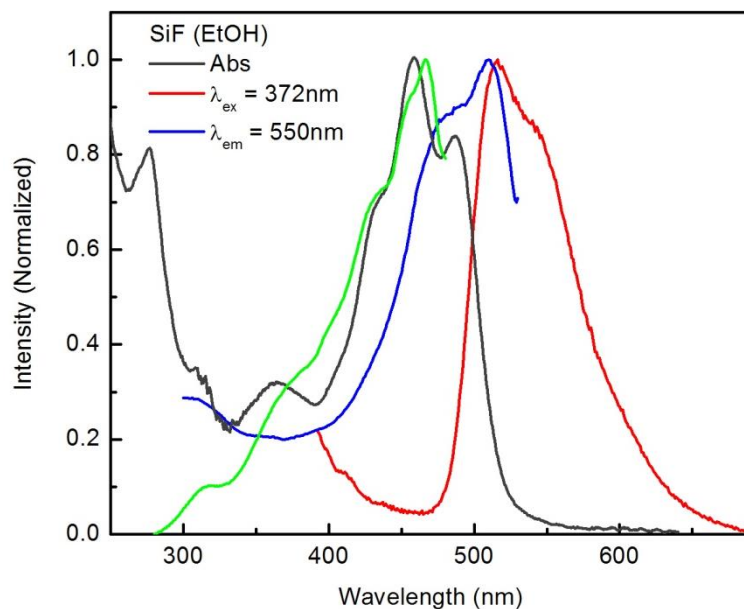
Figure 4-14. Absorption and excitation spectra of SQD-FL collected at room temperature; (λ_{em} and λ_{ex} indicated on graph).
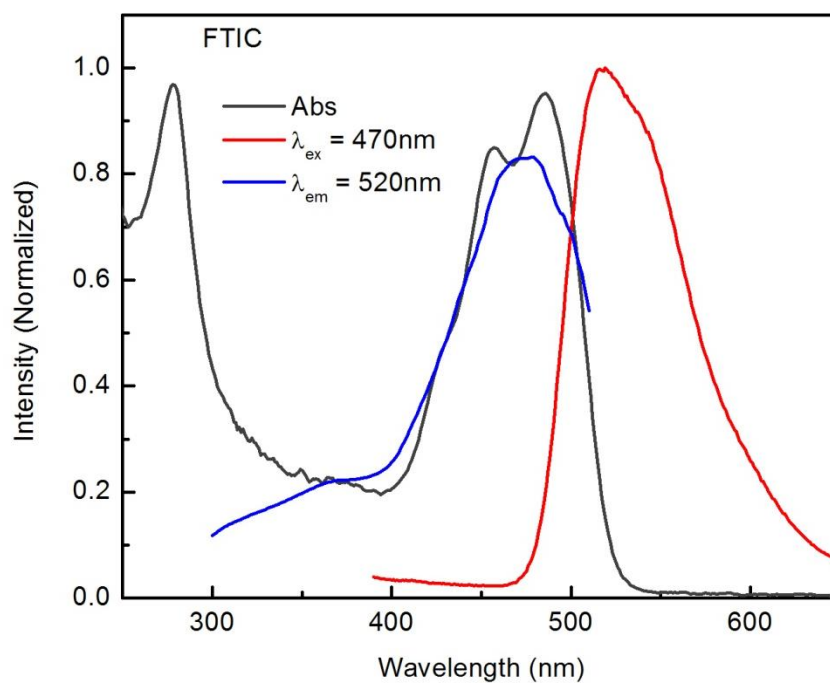
Figure 4-15. Absorption and excitation spectra of FTIC collected at room temperature; (λ_{em} and λ_{ex} indicated on graph).
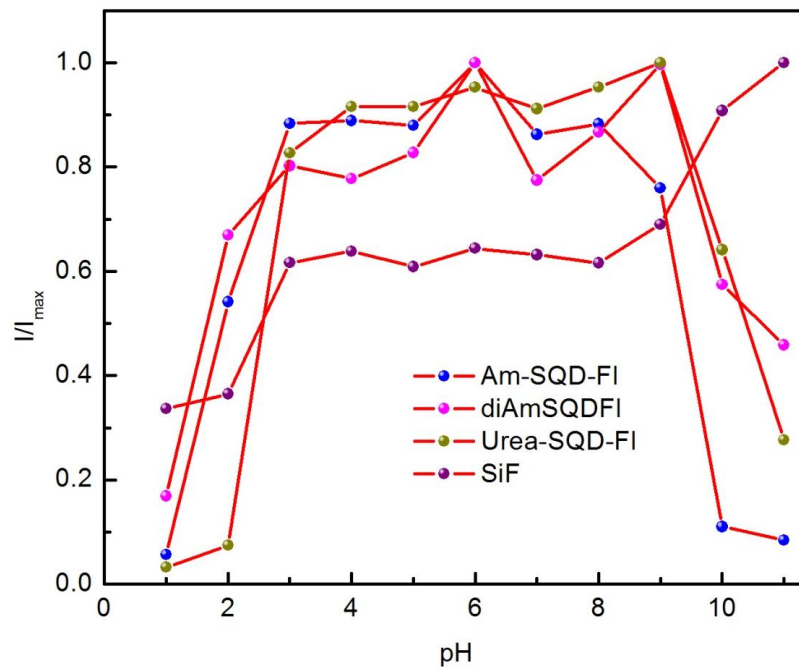
Figure 4-16. Relative fluorescence intensity changes at different pH values.

4.6 References

1. Cheng, Xiaoyu; Lowe, Stuart B; Reece, Peter J; and Gooding, J Justin. "Colloidal silicon quantum dots: from preparation to the modification of self-assembled monolayers (SAMs) for bio-applications." <u>Chemical Society Reviews</u> 43 (2014): 2680-2700.

2. Peng, Fei; Su, Yuanyuan; Zhong, Yiling; Fan, Chunhai; Lee, Shuit-Tong; and He, Yao. "Silicon nanomaterials platform for bioimaging, biosensing, and cancer therapy." <u>Accounts of chemical research</u> 47 (2014): 612-623.

3. Pramanik, Sunipa; Hill, Samantha K. E.; Zhi, Bo; Hudson-Smith, Natalie V.; Wu, Jeslin J.; White, Jacob N.; McIntire, Eileen A.; Kondeti, V. S. Santosh K.; Lee, Amani L.; Bruggeman, Peter J.; Kortshagen, Uwe R.; and Haynes, Christy L. "Comparative toxicity assessment of novel Si quantum dots and their traditional Cd-based counterparts using bacteria models Shewanella oneidensis and Bacillus subtilis." <u>Environmental Science: Nano</u> 5 (2018): 1890-1901.

4. Dohnalová, Kateřina; Poddubny, Alexander N.; Prokofiev, Alexei A.; de Boer, Wieteke D. A. M.; Umesh, Chinnaswamy P.; Paulusse, Jos M. J.; Zuilhof, Han; and Gregorkiewicz, Tom. "Surface brightens up Si quantum dots: direct bandgap-like size-tunable emission." <u>Light: Science &Amp; Applications</u> 2 (01/04/online 2013): e47.

5. Choi, Jonghoon; Zhang, Qin; Reipa, Vytas; Wang, Nam Sun; Stratmeyer, Melvin E; Hitchins, Victoria M; and Goering, Peter L. "Comparison of cytotoxic and inflammatory responses of photoluminescent silicon nanoparticles with silicon micron-sized particles in RAW 264.7 macrophages." <u>Journal of Applied Toxicology</u> 29 (2009): 52-60.

6. Zhang, Lei; Tang, ZhaoRong; and Dong, YongPing. "Silicon quantum dot involved luminol chemiluminescence and its sensitive detection of dopamine." <u>Analytical Methods</u> 10 (2018): 4129-4135.

7. Abdelhameed, Mohammed; Martir, Diego Rota; Chen, Shalimar; Xu, William Z; Oyeneye, Olabode O; Chakrabarti, Subrata; Zysman-Colman, Eli; and Charpentier, Paul A. "Tuning the optical properties of silicon quantum dots via surface functionalization with conjugated aromatic fluorophores." <u>Scientific reports</u> 8 (2018): 3050.

8. Ji, Xin; Wang, Wentao; and Mattoussi, Hedi. "Controlling the spectroscopic properties of quantum dots via energy transfer and charge transfer interactions: Concepts and applications." <u>Nano Today</u> 11 (2016): 98-121.

9. Carvalho, Alexandra; Martsinovich, Natalia; Vieira, Ricardo; and Troisi, Alessandro. "Charge Injection Rates in Hybrid Nanosilicon–Polythiophene Bulk

Heterojunction Solar Cells." The Journal of Physical Chemistry C 117 (2013/01/10 2013): 110-115.

10.   Maier-Flaig, Florian; Rinck, Julia; Stephan, Moritz; Bocksrocker, Tobias; Bruns, Michael; Kübel, Christian; Powell, Annie K.; Ozin, Geoffrey A.; and Lemmer, Uli. "Multicolor Silicon Light-Emitting Diodes (SiLEDs)." Nano Letters 13 (2013/02/13 2013): 475-480.

11.   Chen, Xueqian; Liu, Yang; and Ma, Qiang. "Recent advances in quantum dot-based electrochemiluminescence sensors." Journal of Materials Chemistry C 6 (2018): 942-959.

12.   He, Yao; Fan, Chunhai; and Lee, Shuit-Tong. "Silicon nanostructures for bioapplications." Nano Today 5 (2010): 282-295.

13.   Wen, Xiaoming; Zhang, Pengfei; Smith, Trevor A; Anthony, Rebecca J; Kortshagen, Uwe R; Yu, Pyng; Feng, Yu; Shrestha, Santosh; Coniber, Gavin; and Huang, Shujuan. "Tunability limit of photoluminescence in colloidal silicon nanocrystals." Scientific reports 5 (2015): 12469.

14.   Erogbogbo, Folarin; Yong, Ken-Tye; Roy, Indrajit; Xu, GaiXia; Prasad, Paras N.; and Swihart, Mark T. "Biocompatible Luminescent Silicon Quantum Dots for Imaging of Cancer Cells." ACS Nano 2 (2008/05/01 2008): 873-878.

15.   Li, Qi; Luo, Tian-Yi; Zhou, Meng; Abroshan, Hadi; Huang, Jingchun; Kim, Hyung J; Rosi, Nathaniel L; Shao, Zhengzhong; and Jin, Rongchao. "Silicon nanoparticles with surface nitrogen: 90% quantum yield with narrow luminescence bandwidth and the ligand structure based energy law." ACS nano 10 (2016): 8385-8393.

16.   Yang, Zhenyu; Iqbal, Muhammad; Dobbie, Alexander R; and Veinot, Jonathan GC. "Surface-induced alkene oligomerization: does thermal hydrosilylation really lead to monolayer protected silicon nanocrystals?" Journal of the American Chemical Society 135 (2013): 17595-17601.

17.   Wang, Lei; Li, Qi; Wang, Hai-Yu; Huang, Jing-Chun; Zhang, Ran; Chen, Qi-Dai; Xu, Huai-Liang; Han, Wei; Shao, Zheng-Zhong; and Sun, Hong-Bo. "Ultrafast optical spectroscopy of surface-modified silicon quantum dots: unraveling the underlying mechanism of the ultrabright and color-tunable photoluminescence." Light: Science &Amp; Applications 4 (01/30/online 2015): e245.

18.   Dasog, Mita; De los Reyes, Glenda B.; Titova, Lyubov V.; Hegmann, Frank A.; and Veinot, Jonathan G. C. "Size vs Surface: Tuning the Photoluminescence of Freestanding Silicon Nanocrystals Across the Visible Spectrum via Surface Groups." ACS Nano 8 (2014/09/23 2014): 9636-9648.

19.   Abdelhameed, Mohammed; Aly, Shawkat; Lant, Jeremy T.; Zhang, Xiaoran; and Charpentier, Paul. "Energy/Electron Transfer Switch for Controlling Optical

Properties of Silicon Quantum Dots." Scientific Reports 8 (2018/11/20 2018): 17068.

20. Mazzaro, Raffaello; Locritani, Mirko; Molloy, Jennifer K; Montalti, Marco; Yu, Yixuan; Korgel, Brian A; Bergamini, Giacomo; Morandi, Vittorio; and Ceroni, Paola. "Photoinduced processes between pyrene-functionalized silicon nanocrystals and carbon allotropes." Chemistry of Materials 27 (2015): 4390-4397.

21. Zhang, Xian-Fu; Zhang, Jianlong; and Liu, Limin. "Fluorescence properties of twenty fluorescein derivatives: lifetime, quantum yield, absorption and emission spectra." Journal of fluorescence 24 (2014): 819-826.

22. Sjöback, Robert; Nygren, Jan; and Kubista, Mikael. "Absorption and fluorescence properties of fluorescein." Spectrochimica Acta Part A: Molecular and Biomolecular Spectroscopy 51 (1995): L7-L21.

23. Ha, Shin-Woo; Camalier, Corinne E; Beck Jr, George R; and Lee, Jin-Kyu. "New method to prepare very stable and biocompatible fluorescent silica nanoparticles." Chemical Communications (2009): 2881-2883.

24. Mishra, AK, and Dogra, SK. "Excited state prototropism of 6-aminochrysene." Journal of photochemistry 23 (1983): 163-169.

25. Eaton, David F. "Reference materials for fluorescence measurement." Pure and Applied Chemistry 60 (1988): 1107-1114.

26. Topal, Sevinc Z; Ertekin, Kadriye; Topkaya, Derya; Alp, Serap; and Yenigul, Berrin. "Emission based oxygen sensing approach with tris (2, 2′-bipyridyl) ruthenium (II) chloride in green chemistry reagents: room temperature ionic liquids." Microchimica Acta 161 (2008): 209-216.

27. Mohammed, Omar F.; Xiao, Dequan; Batista, Victor S.; and Nibbering, Erik T. J. "Excited-State Intramolecular Hydrogen Transfer (ESIHT) of 1,8-Dihydroxy-9,10-anthraquinone (DHAQ) Characterized by Ultrafast Electronic and Vibrational Spectroscopy and Computational Modeling." The Journal of Physical Chemistry A 118 (2014/05/01 2014): 3090-3099.

28. Dasog, Mita; Yang, Zhenyu; Regli, Sarah; Atkins, Tonya M.; Faramus, Angelique; Singh, Mani P.; Muthuswamy, Elayaraja; Kauzlarich, Susan M.; Tilley, Richard D.; and Veinot, Jonathan G. C. "Chemical Insight into the Origin of Red and Blue Photoluminescence Arising from Freestanding Silicon Nanocrystals." ACS Nano 7 (2013/03/26 2013): 2676-2685.

29. Warner, Jamie H; Hoshino, Akiyoshi; Yamamoto, Kenji; and Tilley, Richard D. "Water-soluble photoluminescent silicon quantum dots." Angewandte Chemie International Edition 44 (2005): 4550-4554.

30.	Wu, Jinzhu; Dai, Jun; Shao, Yanbin; and Sun, Yanchun. "One-step synthesis of fluorescent silicon quantum dots (Si-QDs) and their application for cell imaging." RSC Advances 5 (2015): 83581-83587.

31.	Zhu, Baoya; Ren, Guojuan; Tang, Mingyu; Chai, Fang; Qu, Fengyu; Wang, Chungang; and Su, Zhongmin. "Fluorescent silicon nanoparticles for sensing Hg2+ and Ag+ as well visualization of latent fingerprints." Dyes and Pigments 149 (2018): 686-695.

32.	Rao, G Ranga. "Infrared reflection absorption study of water interaction with H-terminated Si (100) surfaces." Bulletin of Materials Science 27 (2004): 497-500.

33.	Jiang, Liqin; Li, Xuemin; Liu, Lingrong; and Zhang, Qiqing. "Cellular uptake mechanism and intracellular fate of hydrophobically modified pullulan nanoparticles." International journal of nanomedicine 8 (2013): 1825.

34.	Manhat, B. A. "Understanding the Emission from Semiconductor Nanoparticles." Portland State University, 2012.

35.	Graf, Nora; Lippitz, Andreas; Gross, Thomas; Pippig, Falko; Holländer, Andreas; and Unger, Wolfgang ES. "Determination of accessible amino groups on surfaces by chemical derivatization with 3, 5-bis (trifluoromethyl) phenyl isothiocyanate and XPS/NEXAFS analysis." Analytical and bioanalytical chemistry 396 (2010): 725-738.

36.	Wu, Fu-Gen; Zhang, Xiaodong; Kai, Siqi; Zhang, Mengyi; Wang, Hong-Yin; Myers, John N; Weng, Yuxiang; Liu, Peidang; Gu, Ning; and Chen, Zhan. "One-Step Synthesis of Superbright Water-Soluble Silicon Nanoparticles with Photoluminescence Quantum Yield Exceeding 80%." Advanced Materials Interfaces 2 (2015): 1500360.

37.	Forster, Leslie S., and Dudley, Daniel. "Luminescence of fluorescein dyes." J. Phys. Chem. 66 (// 1962): 838-840.

38.	Telore, Rahul; Chemate, Santosh; Padalkar, Vikas; and Sekar, Nagaiyan. "Novel Fluorescein-Based Fluorophores: Synthesis, Photophysics and Micro-Environmental Study." Journal of Fluorescence 25 (November 01 2015): 1835-1845.

39.	Zhang, Xian-Fu. "The effect of phenyl substitution on the fluorescence characteristics of fluorescein derivatives via intramolecular photoinduced electron transfer." Photochemical & Photobiological Sciences 9 (2010): 1261-1268.

40.	Mishra, A. K., and Dogra, S. K. "Excited state prototropism of 6-aminochrysene." Journal of Photochemistry 23 (1983/01/01/ 1983): 163-169.

41.	Sun, Jingya; Yu, Weili; Usman, Anwar; Isimjan, Tayirjan T.; Dgobbo, Silvano; Alarousu, Erkki; Takanabe, Kazuhiro; and Mohammed, Omar F. "Generation of

Multiple Excitons in Ag2S Quantum Dots: Single High-Energy versus Multiple-Photon Excitation." <u>The Journal of Physical Chemistry Letters</u> 5 (2014/02/20 2014): 659-665.

42. Aly, Shawkat M.; Parida, Manas R.; Alarousu, Erkki; and Mohammed, Omar F. "Ultrafast electron injection at the cationic porphyrin–graphene interface assisted by molecular flattening." <u>Chemical Communications</u> 50 (2014): 10452-10455.

43. Zhang, Haiping; Zhou, Yalin; Zhang, Manhua; Shen, Tao; Xiang, Junfeng; and Feng, Juan. "Nanosecond time-resolved studies of long-lived photoinduced charge separation in the dyad fluorescein–anthraquinone–methyl ester adsorbed on TiO2 colloids." <u>Journal of Colloid and Interface Science</u> 263 (2003/07/15/ 2003): 669-673.

44. El-Ballouli, Ala'a O.; Alarousu, Erkki; Bernardi, Marco; Aly, Shawkat M.; Lagrow, Alec P.; Bakr, Osman M.; and Mohammed, Omar F. "Quantum Confinement-Tunable Ultrafast Charge Transfer at the PbS Quantum Dot and Phenyl-C61-butyric Acid Methyl Ester Interface." <u>Journal of the American Chemical Society</u> 136 (2014/05/14 2014): 6952-6959.

45. Orte, Angel; Crovetto, Luis; Talavera, Eva M.; Boens, Noeel; and Alvarez-Pez, Jose M. "Absorption and emission study of 2',7'-difluorofluorescein and its excited-state buffer-mediated proton exchange reactions." <u>J. Phys. Chem. A</u> 109 (// 2005): 734-747.

46. Ma, Li Ying; Wang, Huai You; Xie, Hui; and Xu, Li Xiao. "A long lifetime chemical sensor: study on fluorescence property of fluorescein isothiocyanate and preparation of pH chemical sensor." <u>Spectrochimica acta. Part A, Molecular and biomolecular spectroscopy</u> 60 (2004/07// 2004): 1865-1872.

Chapter 5 Controlling the Surface-defect-state Photoluminescence in Ultra-Small Silicon Quantum Dots Via Spacers

5.1 Introduction

Silicon Quantum Dots (SQDs) have recently attracted a considerable attention as excellent candidates for a variety of applications such as bioimaging,[1] photodynamic therapy,[2] biosensing,[3] photovoltaics,[4] and light-emitting diodes (LEDs).[5] This is due to their unique optical properties including broad absorption spectra, size-dependent tunable emission,[6] and high stability against photobleaching.[7] Furthermore, SQDs have excellent biocompatibility and biodegradability,[8] very low cytotoxicity,[9] and versatile surface functionalization capability.[10]

Generally, the size-tunable emission of SQDs is attributed to the quantum confinement effect where the photoluminescence is red- or blue-shifted when the size of SQDs increases or decreases, respectively.[11] However, a deviation from this behavior was observed for ultra-small SQDs of a size smaller than ~2 nm in which the PL originates from surface relevant states.[12] Interestingly, the functionalization of such SQDs surface with capping agents was shown to play a vital role toward controlling their optical properties rather than the size of particles.[13] Moreover, the utilization of aromatic dyes capping agent has shown some potential to impact the optical properties of SQDs, enhances their photostability, and prevents them from agglomeration and aggregation.[14]

Despite a few reports in literature of aromatic fluorophores covalently attached to the surface of SQDs as a means to control their optical properties,[15,16,17] there is still a lack of understanding of factors that impact the interaction of the aromatic fluorophores with the electronic wave functions of SQDs which in turn influence the electronic structure of SQDs. The length and chemical nature of the utilized spacer that connect SQDs with the aromatic dye as well as its attachment position with the fluorophore are among these factors that need more investigations. This may impact the resulting optical properties of SQDs including a red/blue shift in the PL, affect their emission quantum yield (QY) and lifetime

(τ_f) as a result of a photoinduced energy and/or electron transfer between the dye and SQDs.[17,18]

In this work, we report the synthesis of SQDs using a facile one-pot synthetic method. Three derivatives of triethoxysilane were used as silicon sources and sodium citrate dihydrate was used as the reducing agent. The synthesis was performed in glycerol green solvent at normal pressure and relatively high temperature (180 °C). This synthetic method is advantageous over others due to its simplicity, large-scale suitability, non-toxic starting materials, and low cost. The resulting SQDs were then functionalized with two derivatives of rhodamine dye, rhodamine B Isothiocyanate (RITC) and rhodamine 6G (R6G). The SQDs assemblies were attached to the RITC through the isothiocyanate group (-NCS), while they were linked to R6G through the carboxylate group in the phenyl component of the dye. Rhodamine dyes have been chosen for this study due to their superior photochemical and photophysical properties including large absorption coefficients, high fluorescent quantum yields, and excellent photostability.[19,20] The resulting functionalized SQDs were characterized using UV−Vis absorption spectroscopy, Fourier-transform infrared (FTIR) spectroscopy, high-resolution transmission electronic microscopy (HRTEM), and X-ray photoelectron spectroscopy (XPS), steady-state and times-resolved emission spectroscopy, and femtosecond Transient Absorption spectroscopy (fs-TA).

5.2   Experimental Section

Chemicals

3-Aminopropyl triethoxysilane (99%, APTES), 1-[3-(trimethoxysilyl)propyl] urea (97%, UPTES), [3-(2-aminoethylamino)propyl]trimethoxysilane (97%, DAPTMS), sodium citrate dihydrate (≥99%, citrate), glycerol (≥99.5%), Rhodamine B Isothiocyanate (RITC), Rhodamine 6G (R6G), and absolute ethanol. All solvents were dried by passing through MB SPS-800 (MBraun) solvent purification system with water content below 15 ppm.

Synthesis of SQDs

The synthesis of different assemblies of SQDs were carried out following a solution-based reduction route as shown in scheme 1.[21] All synthesis procedures were performed under nitrogen atmosphere using a schlenk line. In a typical experiment, 0.6 gm of sodium citrate dihydrate was added to 20 ml of warm glycerol in a 50 ml round bottom flask, and the mixture was heated with vigorously stirring for 20 mins till all citrate has been completely dissolved. 4 ml of the silicon source (APTES) was added dropwise over 10 minutes, and the mixture was then heated to 180 ºC for 3 hours. The color of the solution turns into yellow due to the formation of Am-SQD. The assemblies Am-SQD was then purified using a combination of centrifugation and dialysis against ethanol (MWCO of 1 KDa, Spectra/Por®6 Standard RC Pre-wetted Dialysis Tubing, diameter 29 mm). The assemblies Urea-SQD and DiAm-SQD were similarly synthesized using UPTES and DAPTMS.

Functionalization of SQDs

1) Synthesis of Am-SQD-RITC, Urea-SQD-RITC, and DiAm-SQD-RITC

An excess amount of Rhodamine B Isothiocyanate (RITC, 100 mg) was mixed with the purified Am-SQD in 20 ml of anhydrous ethanol using 50 ml round bottom flask, and the mixture was vigorously stirred in dark for 24 hours. The resulting product was purified to remove any excess unreacted RITC using dialysis against ethanol (MWCO of 1 KDa, Spectra/Por®6 Standard RC Pre-wetted Dialysis Tubing, diameter 29 mm) to give Am-SQD-RITC. The product was stored in ethanol for further characterization. Similarly, the dyads Urea-SQD-RITC and DiAm-SQD-RITC were prepared.

2) synthesis of Am-SQD-R6G, Urea-SQD-R6G, and DiAm-SQD-R6G

Rhodamine 6G was dissolved in 20 ml of anhydrous ethanol (R6G, 100 mg), and the assemblies Am-SQD were added. The mixture was refluxed for 8 hours under nitrogen atmosphere.[22] After cooling to room temperature, the product Am-SQD-R6G was

purified using dialysis against ethanol. The dyads Urea-SQD-R6G and DiAm-SQD-R6G were prepared in a similar manner.
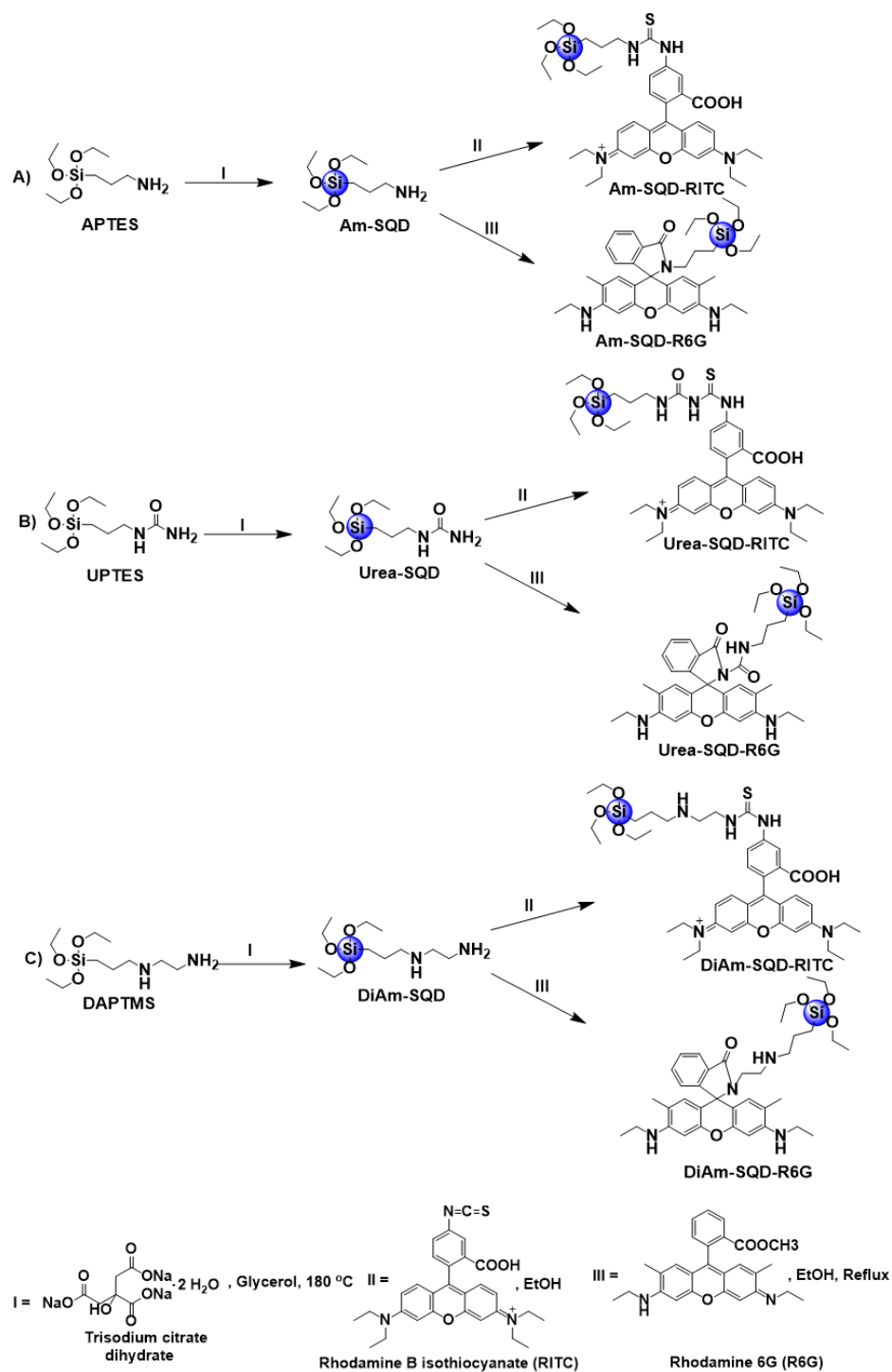
Scheme 1. Synthetic routes for A) Am-SQD-RITC and Am-SQD-R6G; B) Urea-SQD-RITC and Urea-SQD-R6G; C) DiAm-SQD-RITC and DiAm-SQD-R6G.

Methods

XPS spectra were collected using a Kratos Axis Nova spectrometer using a monochromatic Al K(alpha) source (15 mA, 14 kV). The TEM and HRTEM images were measured using a Libra 200 MC operated at 400 kV. The FTIR spectroscopy were performed using a Nicolet 6700 FTIR spectrometer equipped with a smart iTR diamond horizontal attenuated total reflectance (ATR). The UV–Vis absorption spectra were collected using a Shimadzu UV-1800 double beam spectrophotometer with a 1 cm path length quartz cuvette. Steady-state emission and excitation spectra were measured on a Photon Technology International (PTI) spectrofluorometer equipped with a Xenon short-arc lamp. All measurements were carried out using Felix X32 PTI software for data collection and analysis at room temperature under ambient oxygen in ethanol (EtOH). Fluorescence lifetime measurements were performed using a PicoQuant Fluorescence lifetime system (Picoquant GmbH) equipped with a FluoTime 200 (Fluorescence Lifetime spectrometer), a TimeHarp 200 (Time-correlated Single Photon Counting (TCSPC) system), and a PDL800-B pulsed diode laser driver unit. Samples were excited at 372 nm using a picoseconds laser diode head (LDH-P-C375). Fluorescence lifetimes were obtained from deconvolution of the kinetic traces of their solutions using global fluorescence decay data analysis software (Fluo Fit) supported by Picoquant GmbH.

Fluorescence Quantum yield measurements were carried out at room temperature in EtOH; measurement of the quantum yield involved the comparison of very diluted solutions of the studied sample with a solution of approximately equal optical density using a standard reference compound of known quantum efficiency. The quantum yield of an unknown sample is related to that of a standard by the equation: $\Phi_u = [(A_s F_u n^2)/(A_u F_s n_0^2)]$; where A is the absorbance at a given excitation wavelength, F is the integrated emission area across the band, and n and n_0 are the refractive indexes of the solvent containing the unknown and standard, respectively.[23] Measurements were carried out using 6-aminochrysene (Φ_F= 25%)[24] [24] and fluorescein (Φ_F= 79%)[25] as references. Three different solutions for both sample and reference were used for measurements. Concentrations were adjusted to have an absorbance of ~0.05 at the excitation wavelength, while the absorption spectra were recorded 5X for accuracy and error minimization.

The detailed experimental setup for Femtosecond Broadband TA Spectroscopy was described elsewhere.[26] In brief, the setup consists of a white-light continuum probe pulse generated by a 2-mm-thick sapphire plate and spectrally pump tunable fs pulses (240–2600 nm; a few μJ pulse energy) generated in an optical parametric amplifier (Newport Spectra-Physics). The pump and probe pulses were overlapped in a 2-mm-thick cuvette cell containing the sample solution. The transmitted probe light from the solution was collected and focused onto a broadband UV-Vis detector to monitor the transient absorbance change (ΔA). The sample solution was constantly stirred using a magnetic stirrer to ensure a fresh volume was available for each laser shot. To include the transient spectra from a few hundred fs to ns time delays after photoexcitation, a Helios detection system with time resolutions of 120 fs and detection limits of 5.5 ns was employed.

5.3 Results and Discussion

SQDs were synthesized following a solution-based reduction route as shown in scheme1. The starting materials APTES, UPTES, DAPTMS were utilized as silicon sources and were reduced by sodium citrate dihydrate at atmospheric pressure and 180 °C. The functionalization of SQDs was done using rhodamine isothiocyanate and rhodamine 6G to produce Am-SQD-RITC, DiAm-SQD-RITC, Urea-SQD-RITC, Am-SQD-R6G, DiAm-SQD-R6G, Urea-SQD-R6G.

5.3.1 Size and Structure

Figure 5-1 shows the TEM, HR-TEM, and size distribution of DiAm-SQD, Urea-SQD, and Am-SQD. The size distributions indicate that the average diameter of DiAm-SQD, Urea-SQd, and Am-SQD is 1.7 ± 0.7, 1.8 ± 0.7, and 1.8 ± 0.8 nm, respectively, after the analysis of more than 250 dots from different regions of the grid. The high crystallinity of different assemblies of SQDs is shown in the HR-TEM images which is evidenced by the distinct lattice fringes with 0.30 nm interplanar spacing. This is in a good agreement with the (111) plane of diamond structured silicon.[27] It should be mentioned that the low resolution of both TEM and HR-TEM images is assigned to the extreme small diameters of SQDs in addition to the low atomic weight of silicon compared to metallic or semiconductor quantum dots.[14,28,29,30]
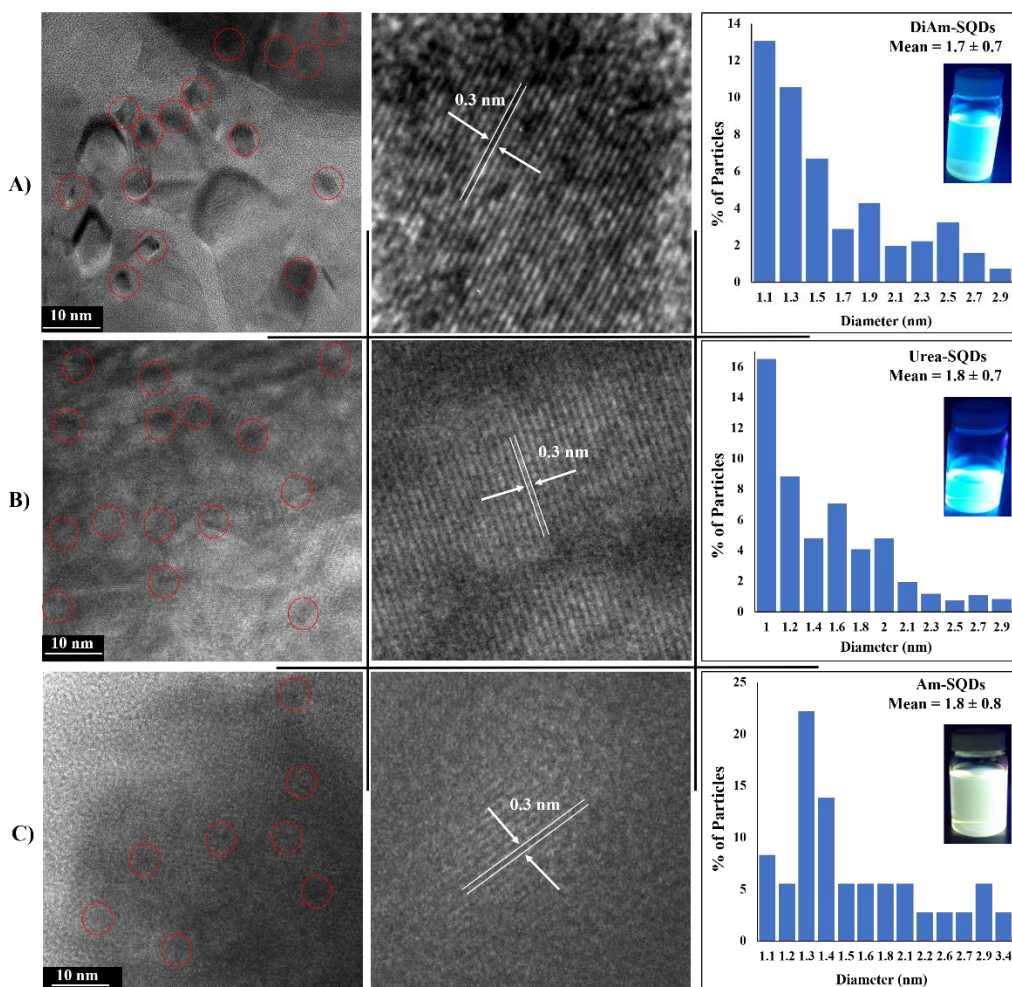
Figure 5-1. TEM (left), HR-TEM (middle), and diameter distribution with photograph of solution under UV irradiation (right) for DiAm-SQD (A), Urea-SQD (B), and Am-SQD (C).

To confirm aromatic fluorophores binding to different SQDs assemblies, both FTIR and XPS spectroscopy were carried out. Figure 5-2 (A) shows the FTIR spectra for Urea-SQD-R6G, DiAm-SQD-R6G, Am-SQD-R6G, and R6G. The broad band at $3567 – 3093$ cm^{-1} is attributed to the stretching vibration of hydroxyl (OH) band,[31] and the intense peak at 1024 cm^{-1} is assigned to the Si-O-Si stretching.[32] The peaks at $2992 – 2795$ cm^{-1} correspond to the –CH stretching vibrations of the alkyl groups and spacers.[33] It is worth mentioning that the characteristic band at 1711 cm^{-1} of the carbonyl C=O stretching mode of the carboxylate group of the R6G is absent in the three dyads.[34] Furthermore, a new peak appeared at the wavenumber of 1658 cm^{-1} which is attributed to the carbonyl (C=O)

vibrations of amide group [35] in the dyads Urea-SQD-R6G, DiAm-SQD-R6G, and Am-SQD-R6G. This indicates the success binding of SQDs to R6G. Figure 5-2 (B) presents the FTIR spectra for Urea-SQD-RITC, DiAm-SQD-RITC, Am-SQD-RITC, and RITC. The bands at 3693 – 3159, 2994 – 2793, and 1031 cm^{-1} are attributed to stretching vibrations of OH, -CH, and Si-O-Si, respectively. The characteristic peak at 2015 cm^{-1} of the isothiocyanate (N=C=S) [36] of the RITC disappeared in the dyads Urea-SQD-RITC, DiAm-SQD-RITC, and Am-SQD-RITC. This confirms the attachment of SQDs to RITC dye.
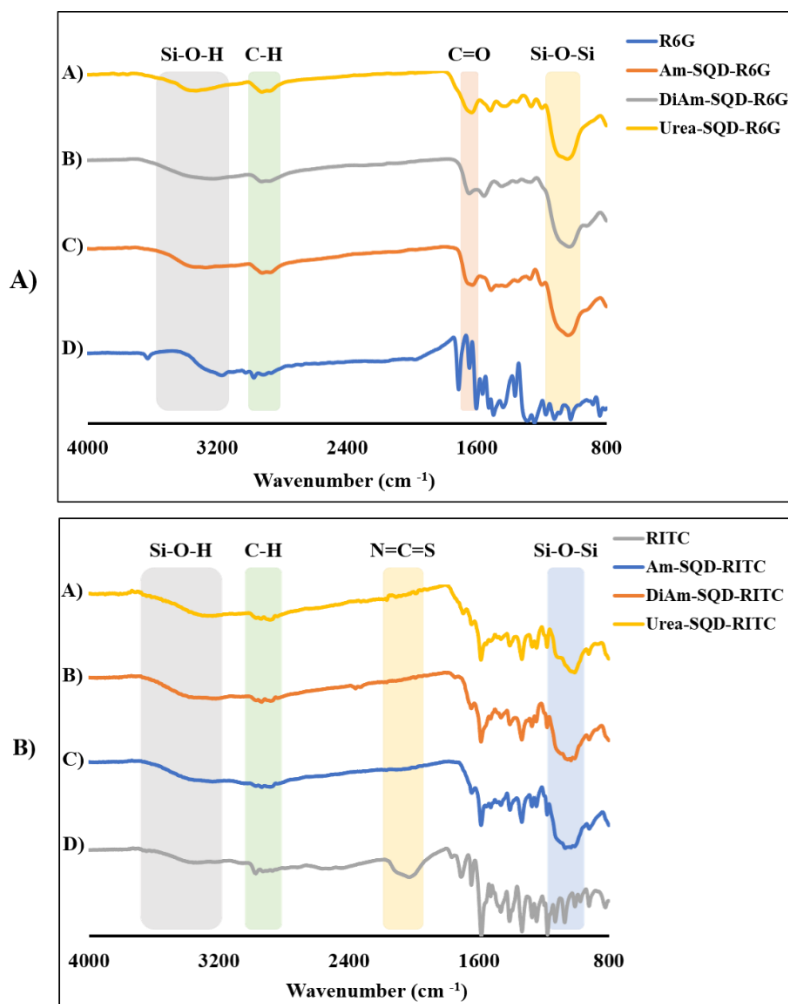
Figure 5-2. FTIR spectra of A) Urea-SQD-R6G (A), DiAm-SQD-R6G (B), Am-SQD-R6G (C), and R6G (D); and B) Urea-SQD-RITC (A), DiAm-SQD-RITC (B), Am-SQD-RITC (C), and RITC (D).

To further confirm the attachment of SQDs to RITC and R6G dyes, XPS spectroscopy was performed. Figure 5-3 displays the high resolution XPS of N 1s, C 1s, and O 1s for Am-SQD-RITC, DiAm-SQD-RITC, Urea-SQD-RITC, Am-SQD-R6G, DiAm-SQD-R6G, Urea-SQD-R6G. The deconvoluted peaks of N 1s centered at 401.4 and 399.7 eV for Am-SQD-RITC, 401.6 and 399.9 eV for DiAm-SQD-RITC, 401.3 and 399.7 eV for Urea-SQD-RITC are attributed to protonated amine species and thiourea nitrogen species (NHC=SNH), respectively.[37] The C 1 s binding energy peaks for Am-SQD-RITC, DiAm-SQD-RITC, and Urea-SQD-RITC 288.8, 287.8, 286.6, 286.1, and 284.8 eV are assigned to COOH, NHC=SNH, C=N, C-N, and C-H/C-C, respectively.[37] The deconvoluted peak of N 1s for Am-SQD-R6G, DiAm-SQD-R6G, and Urea-SQD-R6G centered at 399.5, 399.7, and 399.8 eV, respectively, is assigned to amidic carbonyl (N-C=O).[28,38] XPS spectrum of O 1s shows multiple components at 533.7, 532.3, and 531 eV for Am-SQD-R6G; 533.5, 532.1, and 530.8 eV for DiAm-SQD-R6G; 533.9, 532.4, and 530.8 eV for Urea-SQD-R6G. These peaks are assigned to C-OH/C-O-C, Si-O, and N-C=O, respectively. [28,39,40] The XPS data are consistent with FTIR data, providing clear evidence for successful functionalization of SQDs with RITC and R6G.
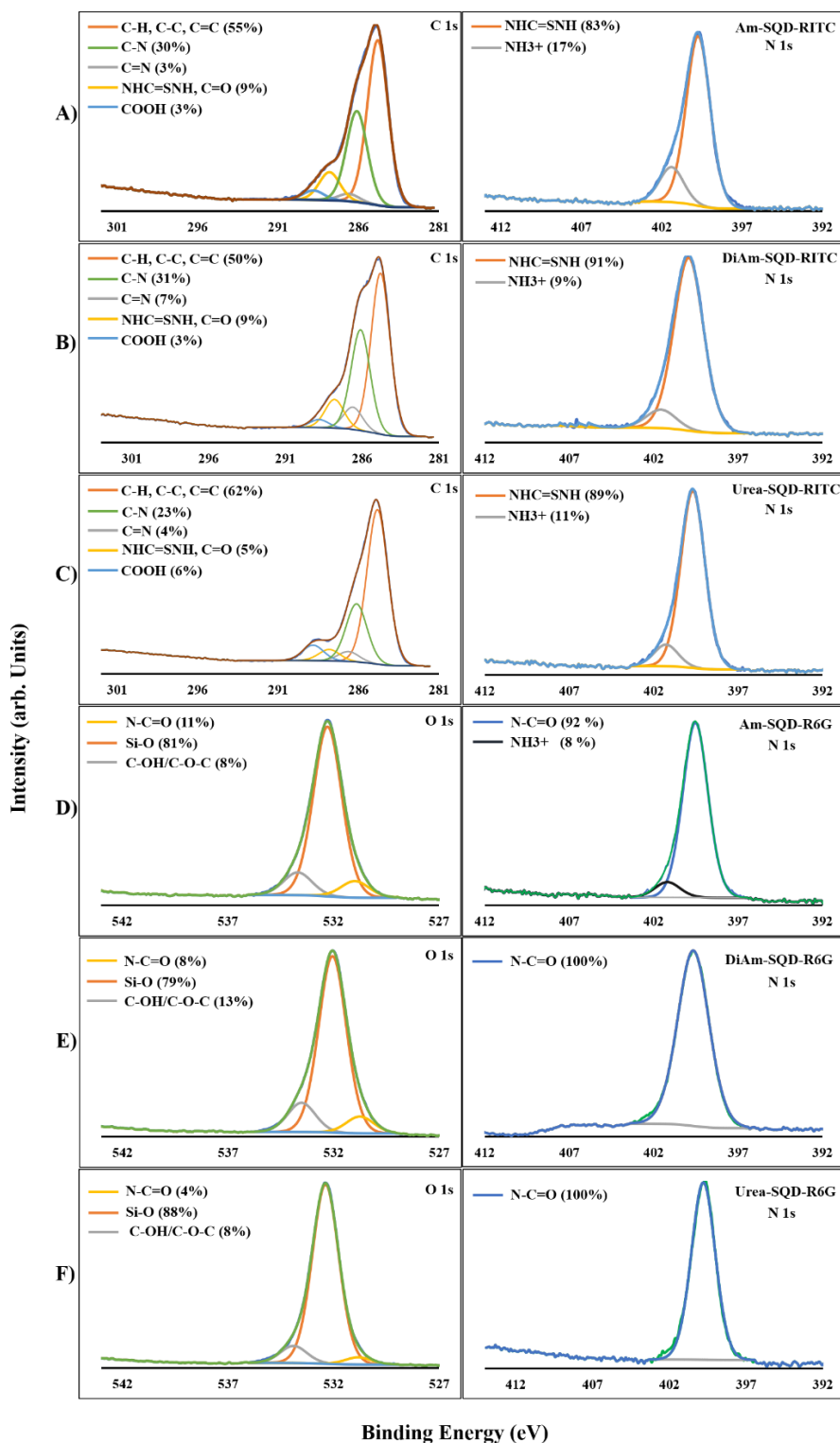
Figure 5-3. XPS Spectra of N 1s and C 1s for Am-SQD-RITC (A), DiAm-SQD-RITC (B), Urea-SQD-RITC (C); and N 1s and O 1s for Am-SQD-R6G (D), DiAm-SQD-R6G (E), Urea-SQD-R6G (F).

5.3.2 Photophysical properties

In order to understand the nature of interaction between rhodamine dyes and SQDs assemblies as well as the impact of spacer on the optical properties of SQDs, their photophysical properties including steady-state photoluminescence (PL) and excitation spectra, PL lifetime (τe), quantum efficiency (ΦPL), and femtosecond transient absorption (fs-TA) measurements were carried out for the SQDs assemblies and their counterparts dyads Am-SQD-RITC, DiAm-SQD-RITC, Urea-SQD-RITC, Am-SQD-R6G, DiAm-SQD-R6G, Urea-SQD-R6G.

Steady-state photoluminescence measurements: Steady-state fluorescence, photoluminescent (PL) excitation, and absorption spectra of the investigated SQD/R6G and SQD/RITC families are given in Figure 5-4. Fluorescence spectra were collected with excitation at absorption of the SQDs for both series of assemblies. The PL spectra for SQD/R6G family reveal a dual emission signature of both SQDs and R6G fluorophore over the spectral range of 400-500 [14,28] and 500-650 nm, respectively [41,42]. Additionally, the PL maxima of the SQDs in the dyads Am-SQD-R6G, Urea-SQD-R6G, and DiAm-SQD-R6G were blue-shifted to 430, 435, 444 nm, respectively, compared to their counterpart SQDs. The fluorescence spectra reveal a maximum contribution of R6G fluorescence in the dyad Am-SQD-R6G while contribution becomes relatively weaker for Urea-SQD-R6G; whereas fluorescence spectra of Diam-SQD-R6G reveals minor contribution from R6G; see Figure 5-4 (A-C). This is assigned to different efficiencies of energy and/or electron transfer interaction between the SQDs and R6G dye in the dyad assemblies. On the other hand, SQD/RITC family is mainly revealing fluorescence of the organic dye with almost a complete quench of the SQDs fluorescence. This indicates a more efficient interaction, i.e. energy and/or electron transfer, involved in SQD/RITC as compared to SQD/R6G; see Figure 5-4 (D-F). Moreover, a variation in the relative contribution of the two fluorophores in the collected fluorescence spectra indicates that energy and/or electron transfer efficiency is dependent on the spacer nature between the SQDs and organic dye. Furthermore, the PL quantum efficiency measurements (Φ) for SQD/R6G family increase in the order of Diam-SQD-R6G > Am-SQD-R6G > Urea-SQD-R6G, while that for SQD/RITC family increase in the order of Urea-SQD-RITC > Diam-

SQD-RITC > Am-SQD-RITC; see Table 5-1. Comparison between obtained quantum yield values for Urea-SQD-R6G with that for Urea-SQD-RITC indicate that the interaction in the preceding systems is of more energy waste nature i.e. more contribution of electron transfer in the interaction. The change in quantum yield values can be attributed to change in degree of intramolecular photoinduced electron transfer (PET) between the phenyl group and xanthenes ring of the organic dye. [43,44] This interruption of the PET can be a consequent of electron density change along with different spacer and/or different types of interactions with SQDs. Interestingly, the PL quantum efficiency measurements performed for the dyad samples stored at room temperature for at least one year revealed a high photostability for these samples.
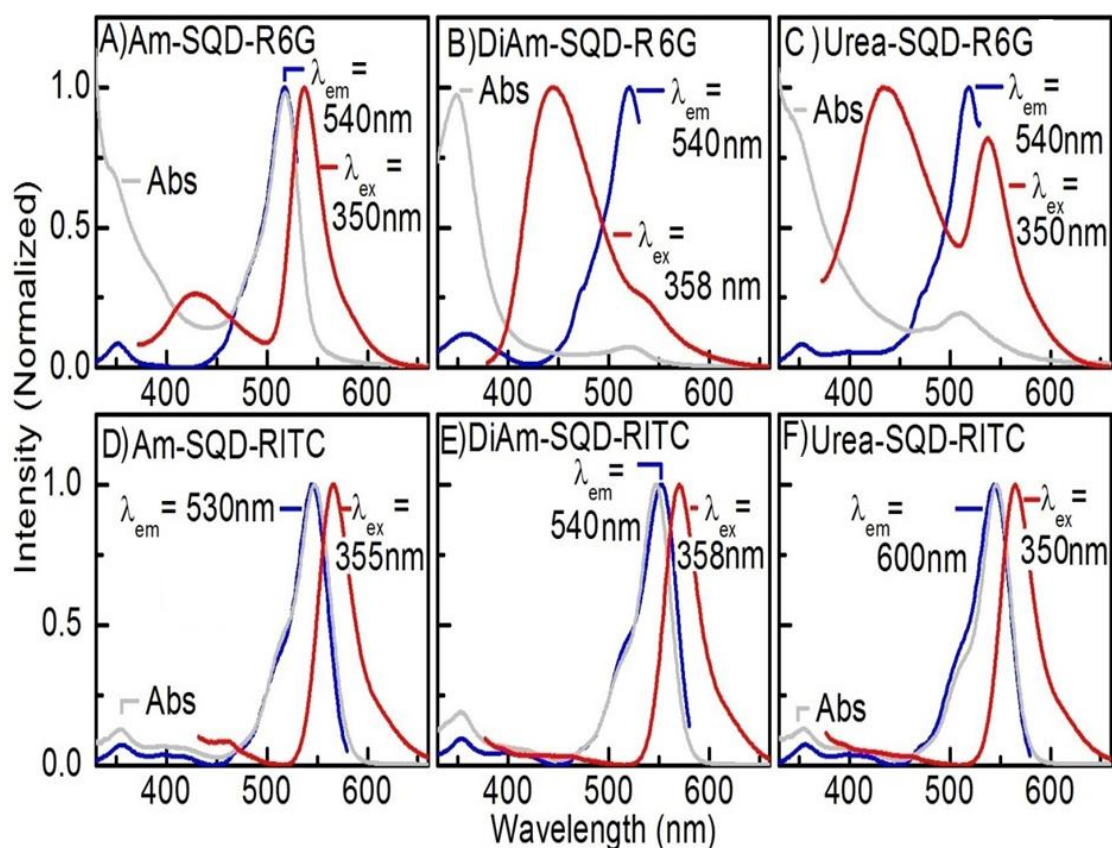

Figure 5-4. Fluorescence (red), PL excitation (blue) and absorption (grey) of: A) Am-SQD-R6G, B) Diam-SQD-R6G, C) Urea-SQD-R6G, D) Am-SQD-RITC, E) Diam-SQD-RITC, and F) Urea-SQD-RITC in EtOH. (λ_{ex} and λ_{em} used for PL spectra are given on curves).

Time Correlated Single Photon Counting (TCSPC): TCSPC measurements were carried out to estimate the fluorescence lifetime for the investigated SQDs assemblies and dyads (see Table 5-1); whereas fluorescence decay curves are given in supporting information. Fluorescence lifetimes monitored at the emission wavelength corresponding to SQDs (i.e. 440 nm) was found to be shorter for SQD/R6G family than their counterpart SQDs. Fluorescence lifetime decay curves of SQDs assemblies were fitted to bi-exponential kinetic whereas for SQD/R6G family, the decay curves found to best fit to three component exponent kinetic equation. The extra component detected in kinetic profile of the dyad assemblies can be attributed to photo-induced energy and/or electron transfer interaction. This allows estimating the rate of energy and/or electron transfer to be in the order of Am-SQD-R6G > Urea-SQD-R6G > Diam-SQD-R6G. Moreover, fluorescence lifetime curves monitored at the emission of R6G were found to be almost the same for both of Am-SQD-R6G and Diam-SQD-R6G; whereas shorter fluorescence lifetime obtained in case of Urea-SQD-R6G. This can be understood considering different nature of interaction involved in Urea-SQD-R6G i.e. more charge separation involved. Indeed, this is in line with the low quantum yield value obtained for Urea-SQD-R6G which supports the suggested involvement of charge-separation energy wasting process; i.e. radical pair formation. This could be due to the possibility of hydrogen bond formation which is in favorite of electron transfer. [28] On the other hand for SQD/RITC assemblies the almost complete quench of emission bands corresponding to SQD precluded the estimation of SQD lifetime in dyad assemblies. Yet, fluorescence lifetimes from decay curves monitored at emission wavelength corresponding to RITC fluorescence are given in Table 5-1 whereas the TCSPC decay curves are given in supporting information. The estimated lifetimes for RITC in dyad assemblies showed almost the same values as those for RITC alone (within experimental error); see Table 5-1.

Table 5-1. PLQY and PL lifetime of the different samples measured in EtOH. The PL lifetime was extracted from time-correlated single photon counting (TCSPC) upon 376-nm excitation.

	Φ	λ_{em} (nm)	τ_f (ns)
Am-SQD	16.0	440	9.97 ± 0.2 (35%)
			2.03 ± 0.1 (65%)
Diam-SQD	42.0	440	9.15 ± 0.1 (24%)
			2.39 ± 0.1 (76%)
Urea-SQD	13.8	440	10.68 ± 0.2 (27%)
			2.22 ± 0.1 (73%)
RITC	33.9	515	3.9 ± 0.1
Am-SQD-R6G	26.8	425	0.59 ± 0.2 (74%)
			2.16 ± 0.1 (21%)
			6.50 ± 0.33 (5%)
		535	2.59 ± 0.10 (62%)
			6.02 ± 0.12 (38%)
Diam-SQD-R6G	28.5	450	1.61 ± 0.1 (48%)
			5.35 ± 0.5 (44%)
			16.50 ± 0.8 (8%)
		540	2.22 ± 0.10 (59 %)
			6.56 ± 0.10 (41%)
Urea-SQD-R6G	8.1	435	0.91 ± 0.2 (66%)
			3.43 ± 0.2 (26%)
			10.35 ± 0.8 (8%)
		540	3.48 ± 0.10
Am-SQD-RITC	17.8	560	2.83 ± 0.10
Diam-SQD-RITC	22.9	560	0.46 ± 0.10 (74%)
			3.31 ± 0.10 (26%)
Urea-SQD-RITC	25.9	560	3.47 ± 0.10

<u>Femtosecond transient absorption (fs-TA) spectroscopy.</u> In order to better understand the kinetics encountering the excited state in these systems upon photoexcitation, time-resolved laser spectroscopy was conducted using femtosecond transient absorption (fs-TA) measurements with broadband capabilities. Details of the experimental set up can be found elsewhere. [45,46] The fs-TA spectra of Am-SQD-R6G and time dependent absorption change of assemblies monitored at both photo-induce excited state absorption (PIA) decay

and ground state bleach (GSB) recovery are given in Figure 5-5 and supporting information.

Figure 5-5. fs-TA spectra at different delay times in response to 350 nm optical excitation of Am-SQD-R6G (A), kinetic traces for absorbance change (B) and (C) (monitoring wavelengths are given on graph; fit in red); in EtOH.

Table 5-2. Lifetime of the different assemblies as obtained from fs-TA kinetic traces.

	λ_{mon} (nm)	τ_f (ps)
Am-SQD-R6G	650	0.54 ± 0.08 (44%)
		25.47 ± 4.06 (22%)
		305.20 ± 26.80 (34%)
Diam-SQD-R6G	620	4.48 ± 0.98 (26%)
		50.30 ± 12.20 (52%)
		565.20 ± 83 (22%)
Urea-SQD-R6G	535	< 0.12 (80%)
		4.38 ± 0.69 (10%)
		130.90 ± 19.10 (10%)

Kinetic traces collected at the PIA change for SQD/R6G assemblies compared to free R6G are shown in Figure 5-5(B). From the kinetic traces and the estimated lifetimes given in Table 5-2 it is clear that kinetic decay traces for excited-state absorption R6G in the dyad assemblies exhibited an extra faster lifetime component compared to free R6G. For both of Am-SQD-R6G and DiAm-SQD-R6G kinetic traces initially reflected this fast component at the early delay times whereas kinetic traces exhibited almost the same kinetic decay profile of free R6G over extended delay times. For Urea-SQD-R6G the magnitude of the faster component is clearly predominating the kinetic trace in distinguish difference to the other two dyads namely Am-SQD-R6G and DiAm-SQD-R6G. Considering the aforementioned mechanism of interaction to be both energy and electron transfer, we can confidently assign this to major contribution of electron transfer for Urea-SQD-R6G. Due to the strong spectral overlap observed along investigated spectrum range, it was not possible to observe charge separated ion signature. Yet, from kinetics of GSB recovery, see Figure 5-5 (C), kinetic traces collected at 535 nm corresponding to R6G ground-state absorption is longer for SQD/R6G family than those for R6G alone. This is in favorite of involvement of charge separation/recombination affecting the ground-state recovery kinetics for R6G in the SQD/R6G family. It is worth to mention here that GSB kinetic trace for DiAm-SQD-R6G was not possible to obtain due to stimulated emission from SQDs over same spectral range. Thus, it allows us to confidently suggest the involvement of photo-induced electron transfer in the interaction in the investigated SQD/R6G family without excluding the contribution of energy transfer. It is expected to be both mechanism operative with the photo-induced electron transfer to be more predominant in Urea-SQD-R6G. On the other hand for SQD/RITC family, the fs-TA spectrum was predominated by the GSB of RITC; see Figure 5-6. Thus, it was difficult to monitor the TA signal for excited state absorption either for SQD or RITC over the investigated spectral range. Yet, kinetic traces associated with GSB recovery clearly reveal faster kinetics for the assemblies as compared to the organic dye alone. The faster kinetic associated with GSB recovery in SQD/RITC dyad assemblies can strongly argue in favorite of charge separation/recombination affecting the ground-state recovery rates for the dyad assemblies. Clearly GSB recovery rates observed for SQD/RITC assemblies are faster than the free organic dye (RITC); in difference with the behavior observed for SQD/R6G where GSB

recovery rates found to be slower than the organic dye (R6G); see Figure 5-5 C. Thus, it allows us to anticipate the structure differences between the counter parts organic dyes in these two dyad assemblies plays an important role in stabilizing the charge-separated radicals.
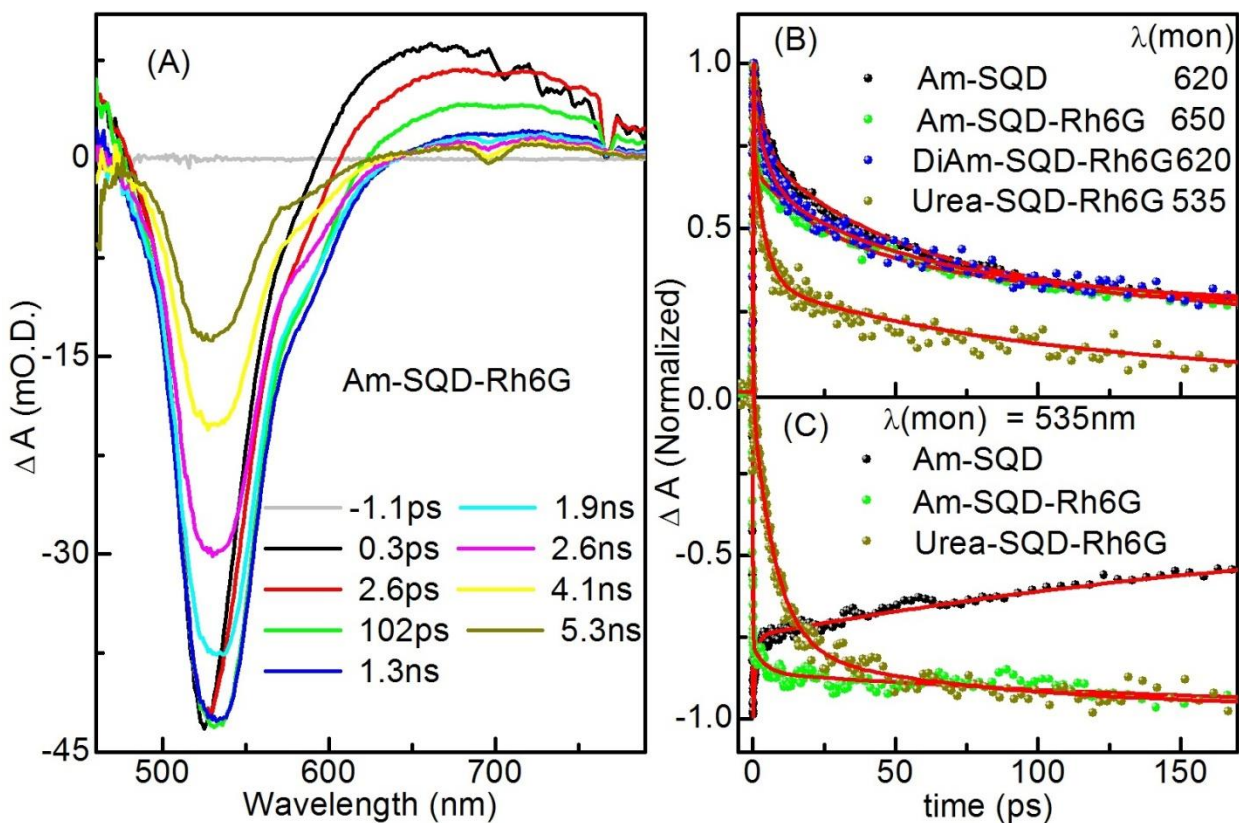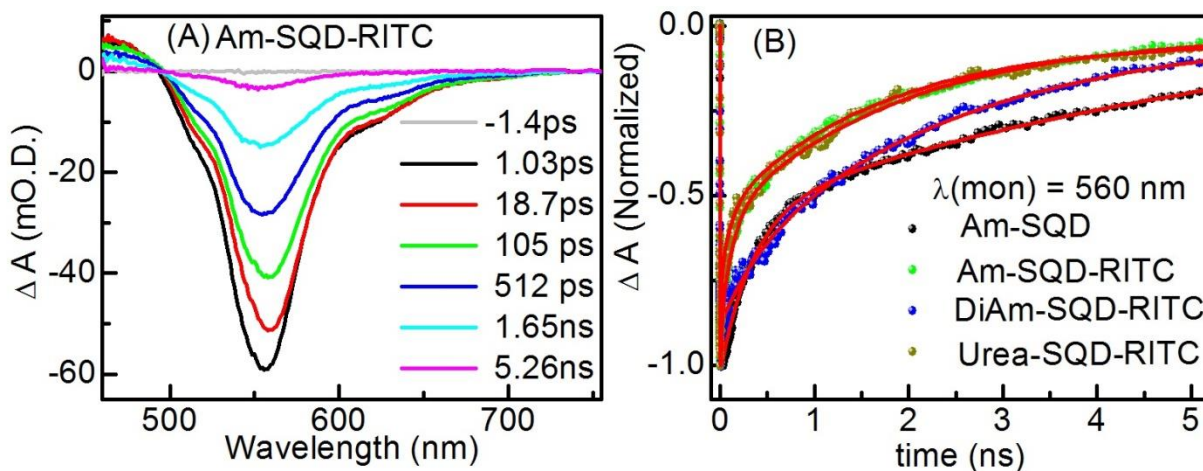

Figure 5-6. fs-TA spectra at different delay times in response to 350 nm optical excitation of Am-SQD-RITC (A), kinetic traces for absorbance change (B) (monitoring wavelengths are given on graph; fit in red); in EtOH.

5.3.3 Conclusion

In summary, we have synthesized two families of SQDs, SQD/R6G and SQD/RITC, covalently functionalized with rhodamine 6G and rhodamine B isothiocyanate via the carbonyl and thiourea groups in the phenyl part of the dye using three different spacers. The photoluminescence of the SQD/R6G family showed a dramatic variation of the relative intensity of the dual emission peaks, while that of SQD/RITC family presented a single emission peak with a complete quench of the SQDs fluorescence. Interaction within the investigated dyads was found to be operative via photo-induced energy and/or electron transfer. Charge separation confirmed from fs-TA measurements where charge recombination found to be dependent on the spacer as well as position of connection with the organic dye. Slower rates for charge recombination, as confirmed from GSB recovery, was obtained for SQD/R6G whereas faster rates obtained for SQD/RITC. Moreover, rates for forward interaction in SQD/R6G found to be in the order of Urea-SQD-R6G > Am-SQD-R6G > DiAm-SQD-R6G.

5.3.4 Supporting information
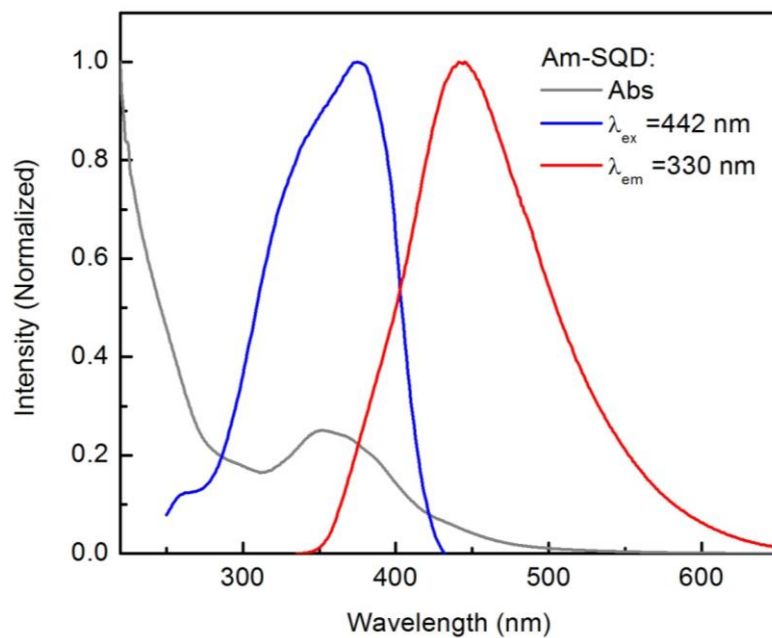
Figure 5-7. Absorption and excitation spectra of Am-SQD collected at room temperature; (λ_{em} and λ_{ex} indicated on graph).
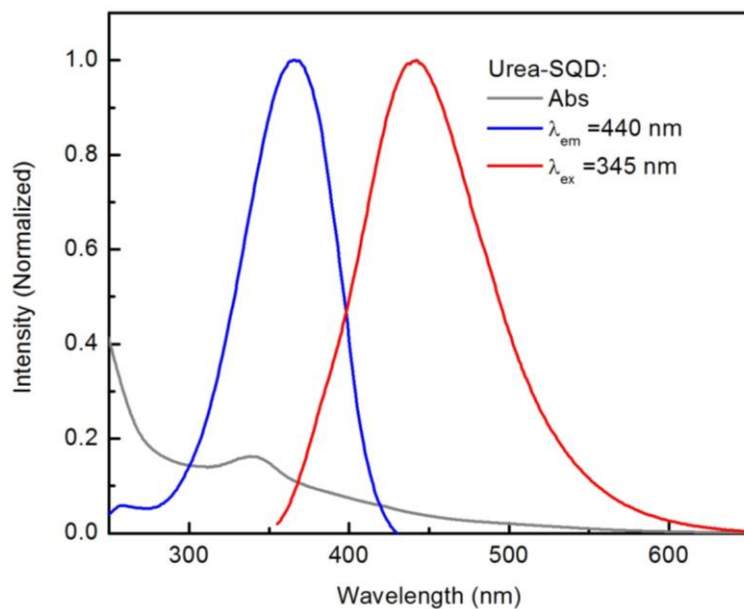
Figure 5-8. Absorption and excitation spectra of Urea-SQD collected at room temperature; (λ_{em} and λ_{ex} indicated on graph).
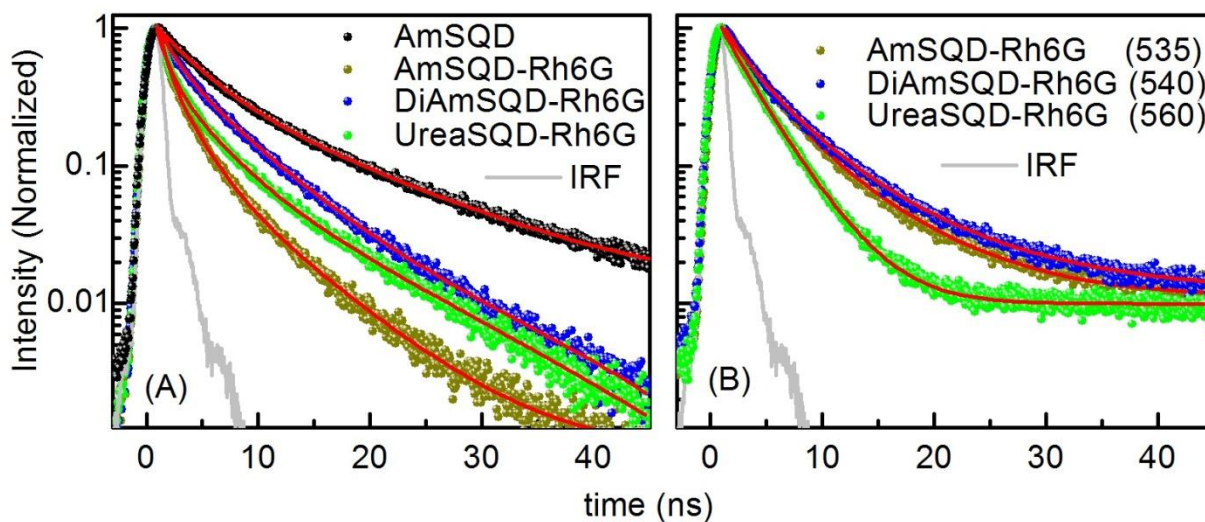
Figure 5-9. TCSPC decay curves collected with λ_{ex} = 372 nm and monitored at (A) λ_{em} = 450 nm and (B) λ_{em} given between brackets.
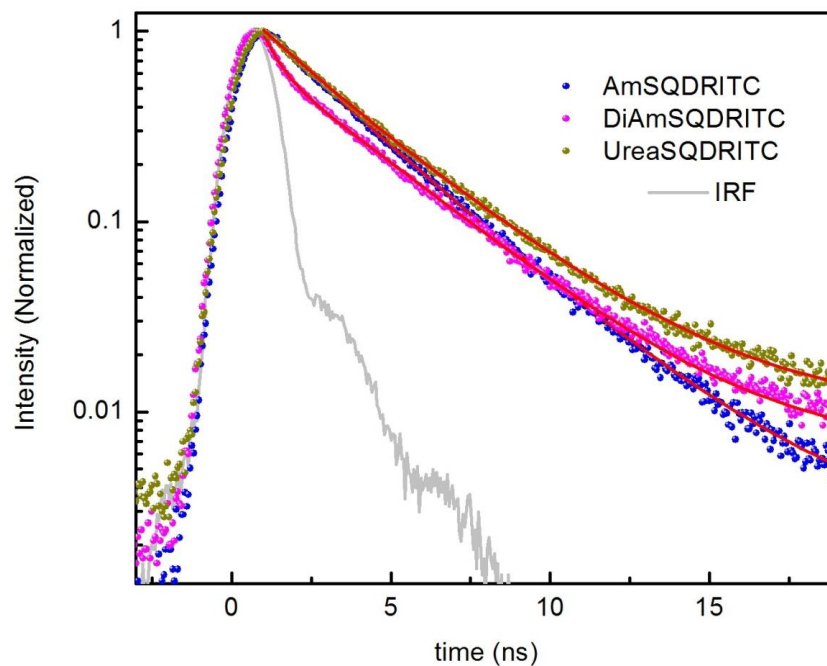
Figure 5-10. TCSPC decay curves collected with λ_{ex} = 372 nm and monitored at λ_{em} = 560 nm.
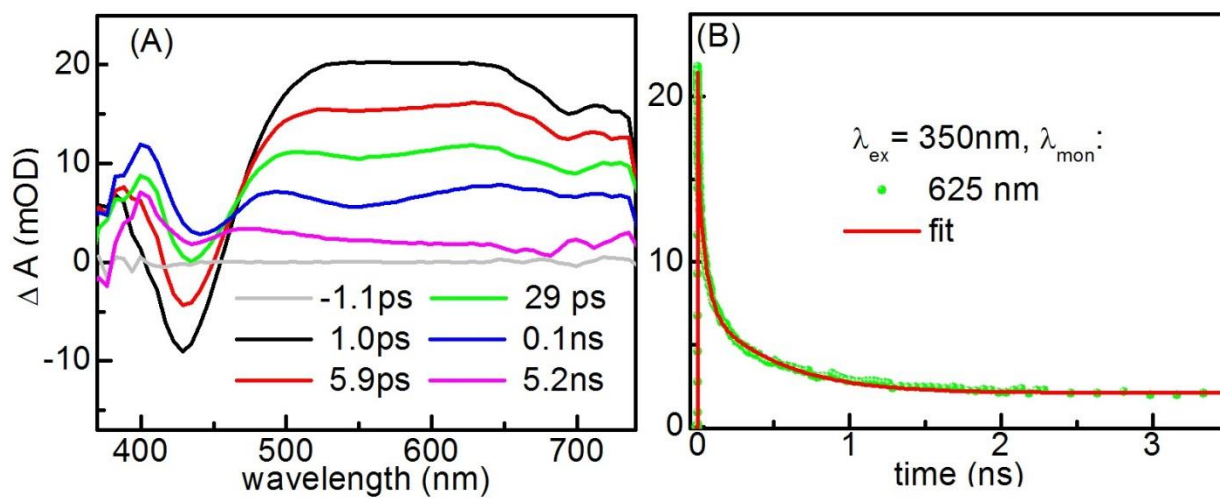
Figure 5-11. fs-TA spectra at different delay times in response to 350 nm optical excitation (A) and absorbance change kinetic traces (B) for Am-SQD.
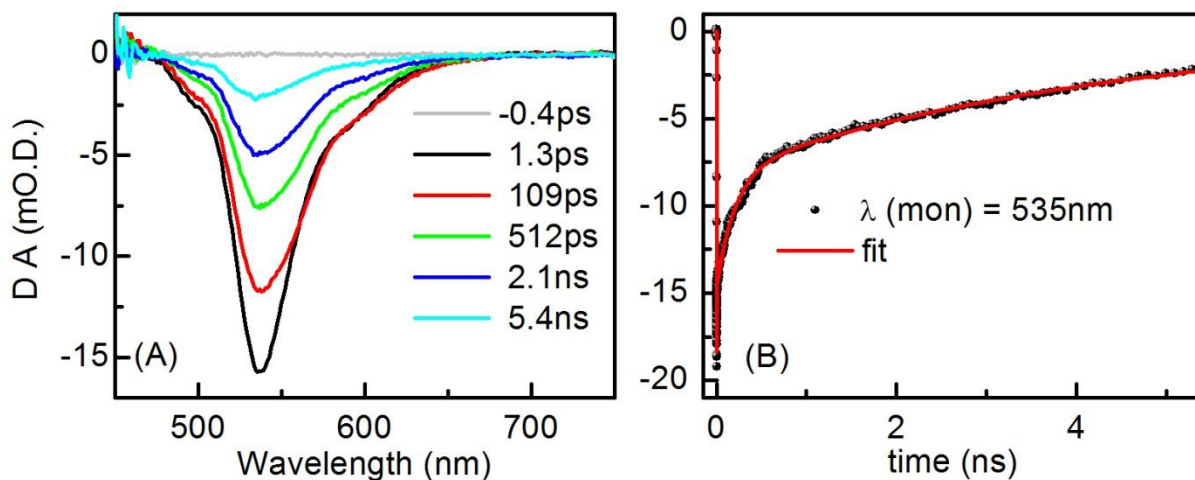
Figure 5-12. fs-TA spectra at different delay times in response to 520 nm optical excitation (A) and absorbance change kinetic traces (B) for R6G.
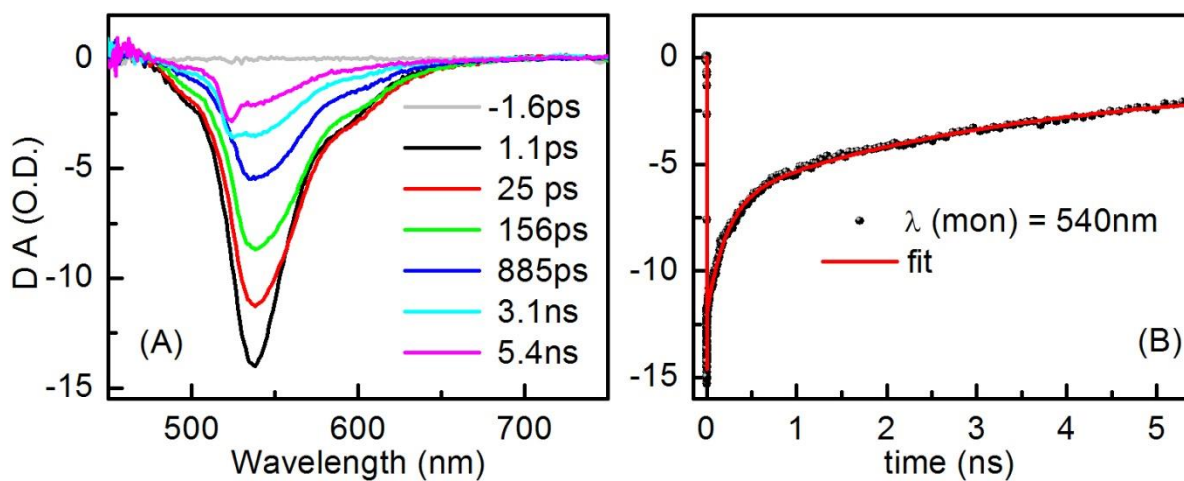
Figure 5-13. fs-TA spectra at different delay times in response to 520 nm optical excitation (A) and absorbance change kinetic traces (B) for RITC.
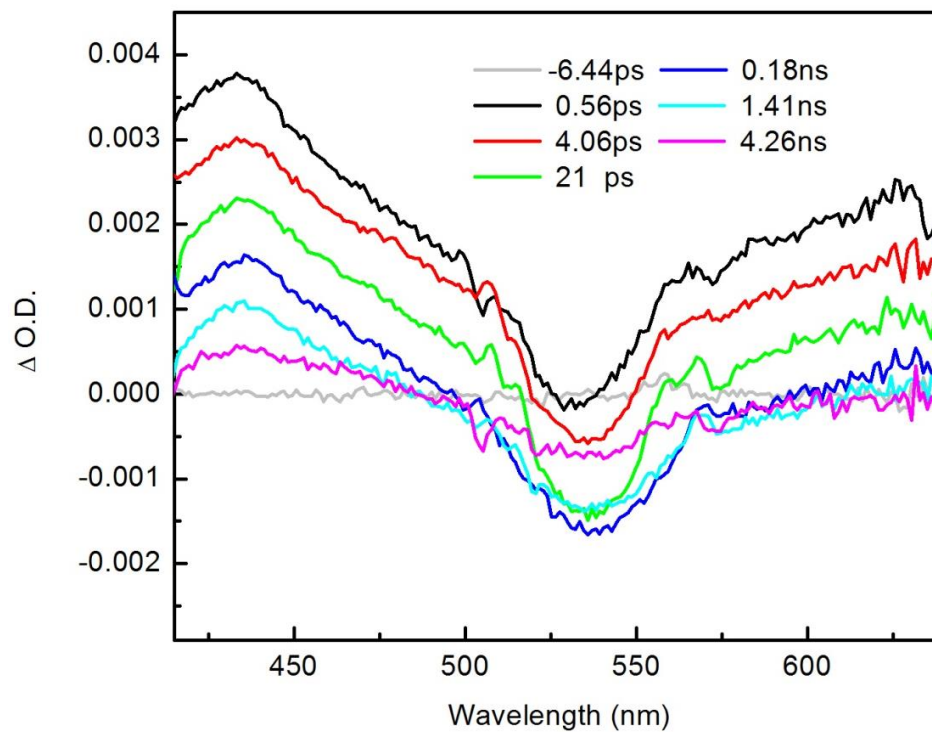
Figure 5-14. fs-TA spectra at different delay times in response to 350 nm for Urea-SQD-Rh6G.
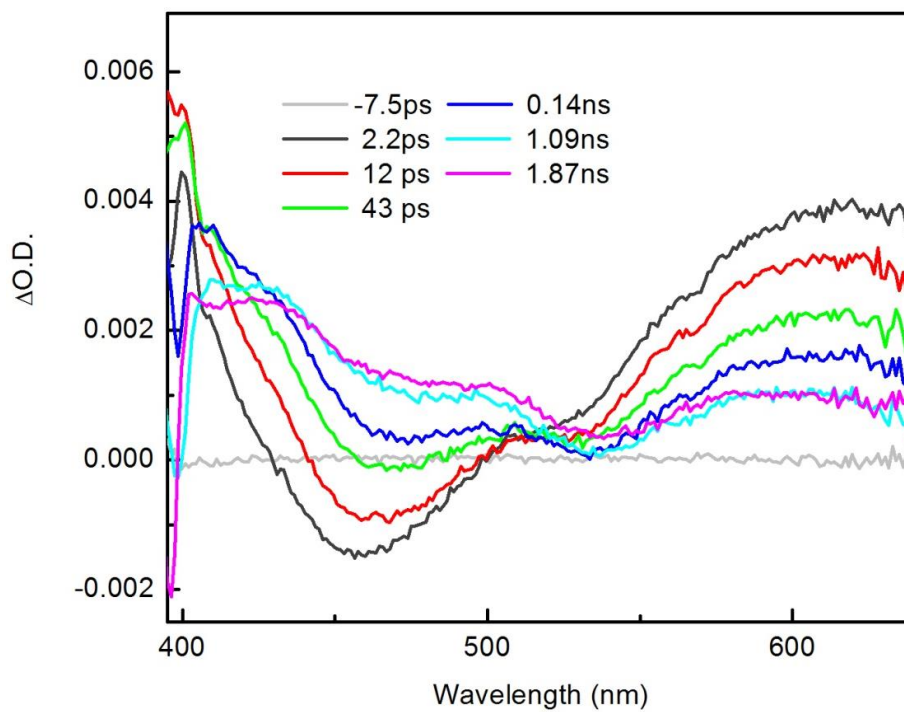
Figure 5-15. fs-TA spectra at different delay times in response to 350 nm for DiAm-SQD-Rh6G.
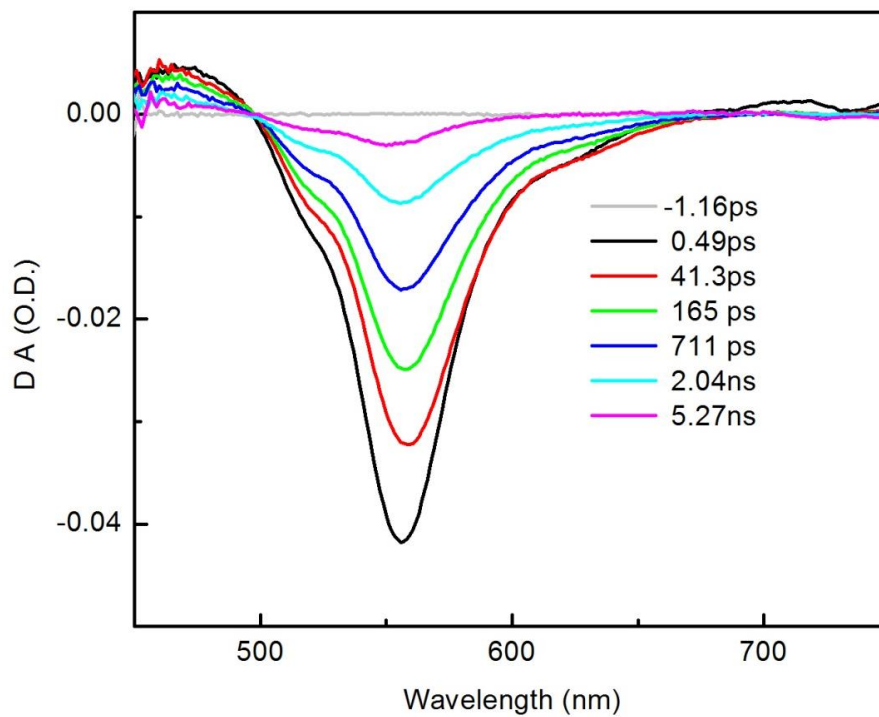
Figure 5-16. fs-TA spectra at different delay times in response to 350 nm for Urea-SQD-RhITC.
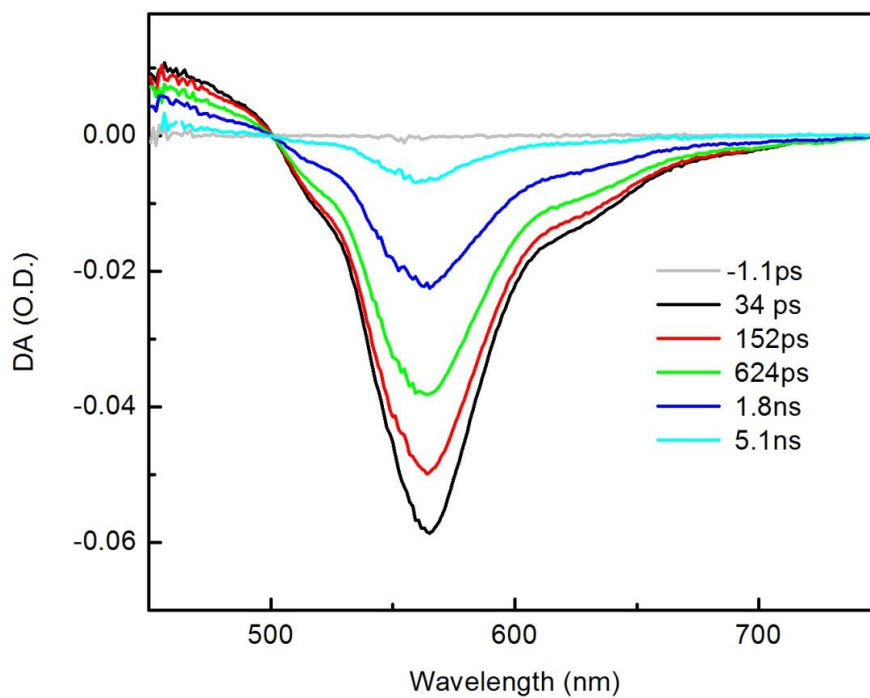
Figure 5-17. fs-TA spectra at different delay times in response to 350 nm for DiAm-SQD-RhITC.

5.4 References

1. Zheng, Xiaohui; Zhang, Dingfang; Fan, Zexuan; Huang, Zusheng; Mao, Hongju; and Ma, Yunfei. "One-step hydrothermal synthesis of ultrabright water-soluble silicon nanoparticles for folate-receptor-mediated bioimaging." <u>Journal of Materials Science</u> 54 (July 01 2019): 9707-9717.

2. Ji, Xin; Wang, Wentao; and Mattoussi, Hedi. "Controlling the spectroscopic properties of quantum dots via energy transfer and charge transfer interactions: Concepts and applications." <u>Nano Today</u> 11 (2016): 98-121.

3. Zhang, Lei; Tang, ZhaoRong; and Dong, YongPing. "Silicon quantum dot involved luminol chemiluminescence and its sensitive detection of dopamine." <u>Analytical methods</u> 10 (2018): 4129-4135.

4. Carvalho, Alexandra; Martsinovich, Natalia; Vieira, Ricardo; and Troisi, Alessandro. "Charge Injection Rates in Hybrid Nanosilicon–Polythiophene Bulk Heterojunction Solar Cells." <u>The Journal of Physical Chemistry C</u> 117 (2012): 110-115.

5. Maier-Flaig, Florian; Rinck, Julia; Stephan, Moritz; Bocksrocker, Tobias; Bruns, Michael; Kübel, Christian; Powell, Annie K; Ozin, Geoffrey A; and Lemmer, Uli. "Multicolor silicon light-emitting diodes (SiLEDs)." <u>Nano letters</u> 13 (2013): 475-480.

6. Alivisatos, A. P. "Perspectives on the Physical Chemistry of Semiconductor Nanocrystals." <u>The Journal of Physical Chemistry</u> 100 (1996/01/01 1996): 13226-13239.

7. Zhong, Yiling; Peng, Fei; Bao, Feng; Wang, Siyi; Ji, Xiaoyuan; Yang, Liu; Su, Yuanyuan; Lee, Shuit-Tong; and He, Yao. "Large-scale aqueous synthesis of fluorescent and biocompatible silicon nanoparticles and their use as highly photostable biological probes." <u>Journal of the American Chemical Society</u> 135 (2013): 8350-8356.

8. Erogbogbo, Folarin; Yong, Ken-Tye; Roy, Indrajit; Xu, GaiXia; Prasad, Paras N; and Swihart, Mark T. "Biocompatible luminescent silicon quantum dots for imaging of cancer cells." <u>ACS nano</u> 2 (2008): 873-878.

9. Pramanik, Sunipa; Hill, Samantha KE; Zhi, Bo; Hudson-Smith, Natalie V; Wu, Jeslin J; White, Jacob N; McIntire, Eileen A; Kondeti, VS Santosh K; Lee, Amani L; and Bruggeman, Peter J. "Comparative toxicity assessment of novel Si quantum dots and their traditional Cd-based counterparts using bacteria models Shewanella oneidensis and Bacillus subtilis." <u>Environmental Science: Nano</u> 5 (2018): 1890-1901.

10. Choi, Jonghoon; Zhang, Qin; Reipa, Vytas; Wang, Nam Sun; Stratmeyer, Melvin E; Hitchins, Victoria M; and Goering, Peter L. "Comparison of cytotoxic and inflammatory responses of photoluminescent silicon nanoparticles with silicon micron-sized particles in RAW 264.7 macrophages." Journal of Applied Toxicology 29 (2009): 52-60.

11. Park, Nae-Man; Choi, Chel-Jong; Seong, Tae-Yeon; and Park, Seong-Ju. "Quantum Confinement in Amorphous Silicon Quantum Dots Embedded in Silicon Nitride." Physical Review Letters 86 (02/12/ 2001): 1355-1357.

12. Wen, Xiaoming; Zhang, Pengfei; Smith, Trevor A; Anthony, Rebecca J; Kortshagen, Uwe R; Yu, Pyng; Feng, Yu; Shrestha, Santosh; Coniber, Gavin; and Huang, Shujuan. "Tunability limit of photoluminescence in colloidal silicon nanocrystals." Scientific reports 5 (2015): 12469.

13. Li, Qi; Luo, Tian-Yi; Zhou, Meng; Abroshan, Hadi; Huang, Jingchun; Kim, Hyung J; Rosi, Nathaniel L; Shao, Zhengzhong; and Jin, Rongchao. "Silicon nanoparticles with surface nitrogen: 90% quantum yield with narrow luminescence bandwidth and the ligand structure based energy law." ACS nano 10 (2016): 8385-8393.

14. Abdelhameed, Mohammed; Martir, Diego Rota; Chen, Shalimar; Xu, William Z; Oyeneye, Olabode O; Chakrabarti, Subrata; Zysman-Colman, Eli; and Charpentier, Paul A. "Tuning the optical properties of silicon quantum dots via surface functionalization with conjugated aromatic Fluorophores." Scientific reports 8 (2018): 3050.

15. Medintz, Igor L, and Mattoussi, Hedi. "Quantum dot-based resonance energy transfer and its growing application in biology." Physical Chemistry Chemical Physics 11 (2009): 17-45.

16. Bae, Yoonjung; Lee, Doh C; Rhogojina, Elena V; Jurbergs, David C; Korgel, Brian A; and Bard, Allen J. "Electrochemistry and electrogenerated chemiluminescence of films of silicon nanoparticles in aqueous solution." Nanotechnology 17 (2006): 3791.

17. Sommer, Anja; Cimpean, Carla; Kunz, Michael; Oelsner, Christian; Kupka, Hans J; and Kryschi, Carola. "Ultrafast excitation energy transfer in vinylpyridine terminated silicon quantum dots." The Journal of Physical Chemistry C 115 (2011): 22781-22788.

18. Locritani, Mirko; Yu, Yixuan; Bergamini, Giacomo; Baroncini, Massimo; Molloy, Jennifer K; Korgel, Brian A; and Ceroni, Paola. "Silicon nanocrystals functionalized with pyrene units: efficient light-harvesting antennae with bright near-infrared emission." The journal of physical chemistry letters 5 (2014): 3325-3329.

19. Lu, Hua; Qi, Shulin; Mack, John; Li, Zhifang; Lei, Jianping; Kobayashi, Nagao; and Shen, Zhen. "Facile Hg2+ detection in water using fluorescent self-assembled

monolayers of a rhodamine-based turn-on chemodosimeter formed via a "click" reaction." Journal of Materials Chemistry 21 (2011): 10878-10882.

20. Saha, Sukdeb; Mahato, Prasenjit; Baidya, Mithu; Ghosh, Sudip K.; and Das, Amitava. "An interrupted PET coupled TBET process for the design of a specific receptor for Hg2+ and its intracellular detection in MCF7 cells." Chemical Communications 48 (2012): 9293-9295.

21. Ye, Hong-Li; Cai, Shi-Jiao; Li, Si; He, Xi-Wen; Li, Wen-You; Li, Yu-Hao; and Zhang, Yu-Kui. "One-Pot Microwave Synthesis of Water-Dispersible, High Fluorescence Silicon Nanoparticles and Their Imaging Applications in Vitro and in Vivo." Analytical Chemistry 88 (2016/12/06 2016): 11631-11638.

22. Kim, Hyungjoo; Rao, Boddu Ananda; Jeong, Jaemyeng; Angupillai, Satheshkumar; Choi, Joon Sig; Nam, Jin-Oh; Lee, Chang-Soo; and Son, Young-A. "A rhodamine scaffold immobilized onto mesoporous silica as a fluorescent probe for the detection of Fe (III) and applications in bio-imaging and microfluidic chips." Sensors and Actuators B: Chemical 224 (2016): 404-412.

23. Eaton, David F. "Reference materials for fluorescence measurement." Pure and Applied Chemistry 60 (1988): 1107-1114.

24. Mishra, AK, and Dogra, SK. "Excited state prototropism of 6-aminochrysene." Journal of photochemistry 23 (1983): 163-169.

25. Topal, Sevinc Z; Ertekin, Kadriye; Topkaya, Derya; Alp, Serap; and Yenigul, Berrin. "Emission based oxygen sensing approach with tris (2, 2′-bipyridyl) ruthenium (II) chloride in green chemistry reagents: room temperature ionic liquids." Microchimica Acta 161 (2008): 209-216.

26. Mohammed, Omar F; Xiao, Dequan; Batista, Victor S; and Nibbering, Erik TJ. "Excited-state intramolecular hydrogen transfer (ESIHT) of 1, 8-Dihydroxy-9, 10-anthraquinone (DHAQ) characterized by ultrafast electronic and vibrational spectroscopy and computational modeling." The Journal of Physical Chemistry A 118 (2014): 3090-3099.

27. Dasog, Mita; Yang, Zhenyu; Regli, Sarah; Atkins, Tonya M; Faramus, Angelique; Singh, Mani P; Muthuswamy, Elayaraja; Kauzlarich, Susan M; Tilley, Richard D; and Veinot, Jonathan GC. "Chemical insight into the origin of red and blue photoluminescence arising from freestanding silicon nanocrystals." Acs Nano 7 (2013): 2676-2685.

28. Abdelhameed, Mohammed; Aly, Shawkat; Lant, Jeremy T.; Zhang, Xiaoran; and Charpentier, Paul. "Energy/Electron Transfer Switch for Controlling Optical Properties of Silicon Quantum Dots." Scientific Reports 8 (2018/11/20 2018): 17068.

29. Warner, Jamie H; Hoshino, Akiyoshi; Yamamoto, Kenji; and Tilley, Richard D. "Water-soluble photoluminescent silicon quantum dots." Angewandte Chemie International Edition 44 (2005): 4550-4554.

30. Wu, Jinzhu; Dai, Jun; Shao, Yanbin; and Sun, Yanchun. "One-step synthesis of fluorescent silicon quantum dots (Si-QDs) and their application for cell imaging." RSC Advances 5 (2015): 83581-83587.

31. Zhu, Baoya; Ren, Guojuan; Tang, Mingyu; Chai, Fang; Qu, Fengyu; Wang, Chungang; and Su, Zhongmin. "Fluorescent silicon nanoparticles for sensing Hg2+ and Ag+ as well visualization of latent fingerprints." Dyes and Pigments 149 (2018): 686-695.

32. Rao, G Ranga. "Infrared reflection absorption study of water interaction with H-terminated Si (100) surfaces." Bulletin of Materials Science 27 (2004): 497-500.

33. Jiang, Liqin; Li, Xuemin; Liu, Lingrong; and Zhang, Qiqing. "Cellular uptake mechanism and intracellular fate of hydrophobically modified pullulan nanoparticles." International journal of nanomedicine 8 (2013): 1825.

34. Mathew, Aneesh; Parambadath, Surendran; Barnabas, Mary Jenisha; Song, Hyun Jin; Kim, Jae-Sung; Park, Sung Soo; and Ha, Chang-Sik. "Rhodamine 6G assisted adsorption of metanil yellow over succinamic acid functionalized MCM-41." Dyes and Pigments 131 (2016): 177-185.

35. Machovič, V; Lapčák, L; Havelcová, M; Borecká, L; Novotná, Mi; Novotná, Ma; Javůrková, I; Langrová, I; Hájková, Š; and Brožová, A. "Analysis of European Honeybee (Apis Mellifera) Wings Using ATR-FTIR and Raman Spectroscopy: A Pilot Study." Scientia Agriculturae Bohemica 48 (2017): 22-29.

36. Sinigaglia, Giulietta; Magro, Massimiliano; Miotto, Giovanni; Cardillo, Sara; Agostinelli, Enzo; Zboril, Radek; Bidollari, Eris; and Vianello, Fabio. "Catalytically active bovine serum amine oxidase bound to fluorescent and magnetically drivable nanoparticles." International journal of nanomedicine 7 (2012): 2249.

37. Graf, Nora; Lippitz, Andreas; Gross, Thomas; Pippig, Falko; Holländer, Andreas; and Unger, Wolfgang ES. "Determination of accessible amino groups on surfaces by chemical derivatization with 3, 5-bis (trifluoromethyl) phenyl isothiocyanate and XPS/NEXAFS analysis." Analytical and bioanalytical chemistry 396 (2010): 725-738.

38. Damaceanu, Mariana-Dana; Rusu, Radu-Dan; Musteata, Valentina-Elena; and Bruma, Maria. "Insulating polyimide films containing n-type perylenediimide moieties." Polymer International 61 (2012): 1582-1591.

39. Annadhasan, M.; Kasthuri, J.; and Rajendiran, N. "Green synthesis of gold nanoparticles under sunlight irradiation and their colorimetric detection of Ni2+ and Co2+ ions." <u>RSC Advances</u> 5 (2015): 11458-11468.

40. Cuesta, A; Martinez-Alonso, A; Tascon, JMD; and Bradley, RH. "Chemical transformations resulting from pyrolysis and CO2 activation of Kevlar flocks." <u>Carbon</u> 35 (1997): 967-976.

41. Zehentbauer, Florian M.; Moretto, Claudia; Stephen, Ryan; Thevar, Thangavel; Gilchrist, John R.; Pokrajac, Dubravka; Richard, Katherine L.; and Kiefer, Johannes. "Fluorescence spectroscopy of Rhodamine 6G: Concentration and solvent effects." <u>Spectrochimica Acta Part A: Molecular and Biomolecular Spectroscopy</u> 121 (2014/03/05/ 2014): 147-151.

42. Selanger, K. A.; Falnes, J.; and Sikkeland, T. "Fluorescence lifetime studies of Rhodamine 6G in methanol." <u>The Journal of Physical Chemistry</u> 81 (1977/10/01 1977): 1960-1963.

43. Zhang, Xian-Fu; Zhang, Jianlong; and Liu, Limin. "Fluorescence properties of twenty fluorescein derivatives: lifetime, quantum yield, absorption and emission spectra." <u>Journal of fluorescence</u> 24 (2014): 819-826.

44. Zhang, Xian-Fu. "The effect of phenyl substitution on the fluorescence characteristics of fluorescein derivatives via intramolecular photoinduced electron transfer." <u>Photochemical & Photobiological Sciences</u> 9 (2010): 1261-1268.

45. Aly, Shawkat M.; Parida, Manas R.; Alarousu, Erkki; and Mohammed, Omar F. "Ultrafast electron injection at the cationic porphyrin–graphene interface assisted by molecular flattening." <u>Chemical Communications</u> 50 (2014): 10452-10455.

46. Sun, Jingya; Yu, Weili; Usman, Anwar; Isimjan, Tayirjan T.; Dgobbo, Silvano; Alarousu, Erkki; Takanabe, Kazuhiro; and Mohammed, Omar F. "Generation of Multiple Excitons in Ag2S Quantum Dots: Single High-Energy versus Multiple-Photon Excitation." <u>The Journal of Physical Chemistry Letters</u> 5 (2014/02/20 2014): 659-665.

Chapter 6   General discussion and conclusions

The novelty of this work stems from being the first study to utilize and investigate surface states as a means to control the physical, optical and photophysical properties of ultra-small silicon quantum dots (SQDs). Ultra-small SQDs, are usually of size less than 2 nm, deviate from the quantum confinement effect. Thus, their surface functionalization would play a key role toward controlling their optical properties including a change in their photoluminescence, quantum efficiency, fluorescence lifetimes, and photostability. This is due to the interaction of the ligands with the electronic wave function of SQDs which in turn influence the electronic structure of SQDs.

First, we have synthesized and investigated three families of SQDs (ranging from 1.7–2.1 nm) covalently functionalized with phenanthrene, pyrene, and perylene fluorophores through a vinyl spacer. The photophysical measurements of these SQDs provided clear evidence for an efficient energy transfer from the aromatic dyes to the core of the SQDs in which Förster energy transfer is the likely mechanism. The emission color was red-shifted by 69 and 65 nm when perylene and phenanthrene were used as capping agents, while pyrene fluorophore led to a blue-shift by 50 nm, compared to their counterpart model SQDs. The QE was moderately enhanced by up to 10%. Therefore, the functionalization of SQDs surface with aromatic ligands via a conjugated spacer is an efficient strategy to tune the optical properties and improve the QE of SQDs. Interestingly, SQDs functionalized with pyrene and perylene fluorophores were of low toxicity and showed promising results when used for the bioimaging of cervical cancerous HeLa cells.

The next study of my thesis investigated the impact of spacer on directing the optical properties of SQDs. Two SQDs assemblies of 1.6 nm average diameter were synthesized and functionalized with perylene-3,4,9,10-tetracarboxylic acid diimide (PDI) fluorophore via non-conjugated spacers. The spacers utilized in this study were N-propylurea and propylamine. The photophysical characterization revealed an efficient energy and/or electron transfer between the SQDs and PDI dye based on the type of the utilized spacer. Energy transfer was confirmed to be the predominant process when propylurea spacer was used, while the propylamine spacer secured an electron transfer process. To illustrate

functionality, both SQDs families were proven to be nontoxic and efficient for fluorescent imaging of embryonic kidney HEK293 cells and human bone cancerous U2OS cells.

Despite of the suitability of the utilized fluorophores and spacers mentioned above to control the optical properties of SQDs due to the photoinduced energy and/or electron transfer processes, it was not possible to enhance the QE of SQDs significantly. Thus, we have investigated other types of spacers that vary in chemical nature, length, and attachment position with the dye.

In the third study, we synthesized and studied four different assemblies of SQDs, ranging from 1.6 – 1.8 nm, and functionalized them with fluorescein dyes through isothiocyanate (-NCS) and carboxylate (COO-) spacers in the *para* and *ortho* position of the benzene ring of the fluorescein dye, respectively. The photophysical measurements showed that the isothiocyanate spacer enabled a significant enhancement in the QE of the SQDs assemblies by up to 65%. Interestingly, both spacers allowed to extend the photostability of SQDs assemblies for at least one year. Additionally, energy and/or electron transfer processes were confirmed to be operative in these systems. The type and rate of interaction between the SQDs and the aromatic dye in these four systems were determined to be dependent on the type of ligand and connection position with the dye which impact the orientation of the phenyl group comparing to the xanthene part of the dye. The presented SQDs dyads here showed promising results for fluorescent cellular imaging of human osteosarcoma U2OS cells.

Finally, we have synthesized and investigated two families of SQDs (1.8 average diameter), and functionalized their surface using rhodamine b isothiocyanate and rhodamine 6G to produce SQD/RITC and SQD/R6G families. The photophysical studies of the SQD/R6G family showed a dual emission peak in which SQDs emission maxima were blue-shifted compared to their SQDs counterparts, while they were completely quenched in SQD/RITC family. This is due to the contribution of energy and/or electron transfer in these systems. Moreover, the rate of the resulting interaction in these dyads of each family varied significantly depending on the type and length of the utilized spacers. Interestingly, these dyads showed photostability for over one year.

In conclusion, several factors can be utilized to control the optical properties of SQDs rather than changing their size to overcome challenges related to the deviation from the quantum confinement effect for ultra-small quantum dots. This includes: 1) type of aromatic dye capping agent; 2) chemical nature and length of spacer; and 3) attachment position with the aromatic dye.

6.1 Future Work

We are now aiming to develop a biocompatible, highly selective and sensitive activatable fluorescent imaging probes to enable the in vivo and in vitro detection of several species of bacteria and viruses. The probe must be able to produce a photophysical change upon the exposure to specific bacteria/viruses such as absorption/emission spectral shift or a change in the QE. The rapid clearance, biocompatibility, and biodegradability of the fluorescent imaging probes are desired to demonstrate its suitability for potential clinical applications.

Based on our understanding now on how different factors impact the optical properties of SQDs, I am proposing two approaches to design an activatable fluorescent imaging probes which are activated in response to specific biomolecular recognition or environmental changes in real time.

1) Inhibitor-SQDs approach. This approach depends on the attachment of SQDs to a specific bacterial or viral inhibitor. The inhibitors-loaded SQDs will selectively bind to the targeted bacteria or virus, and consequently will lead to the aggregation of SQDs on the microorganisms. Thus, they would affect the optical properties capability of these SQDs such as change in their absorption/ photoluminescence and QE. Quantum Dots aggregation usually leads to a shift in the absorption/emission wavelength (usually red shift) and a decrease in the absorption/emission intensity.[1] Here, the NIR-absorbing and emitting SQDs are ideal candidates for biomedical applications due to their excellent optical properties and biocompatibility.[2]
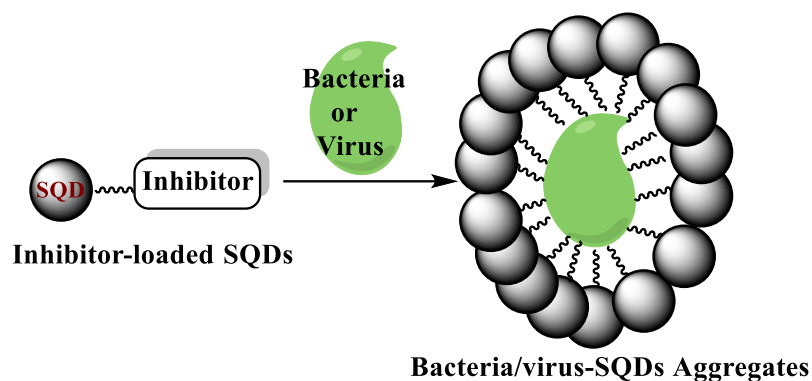
Figure 6-1. Inhibitor-SQDs approach.

2) SQDs-Peptide-Fluorophore Approach. This approach is dependent on the utilization of sensitive and selective peptides that respond in a certain way upon the exposure to different types of bacteria and viruses. The peptide here acts as a bridge to connect SQDs to the organic dye fluorophore to produce the SQDs-Peptide-Fluorophore probe. The proposed probe is composed of a bacteria/virus-specific peptide linker connected into red-absorbing/emitting SQDs and aromatic dye at each terminal side. The overall optical properties of this probe are expected to be induced by an energy and/or electron transfer process between the SQDs and the organic dye when connected through peptides. Thus, the optical properties of the dyad system will be different from that of the individual SQDs and aromatic fluorophores. Upon the exposure to the bacterial/viral-specific peptidases, the peptide linker will cleave leading to the release of the SQDs and aromatic dye. As a result, the probe will be activated and a change in the fluorescence ratiometric signals for both fluorophores (SQDs and aromatic dye) will be detected.
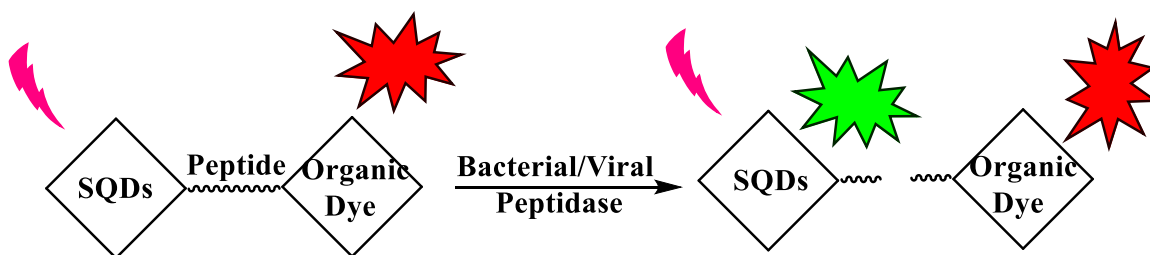
Figure 6-2. SQDs-Peptide-Fluorophore Approach.

6.2 References

1. Poderys, Vilius; Matulionyte, Marija; Selskis, Algirdas; and Rotomskis, Ricardas. "Interaction of water-soluble CdTe quantum dots with bovine serum albumin." <u>Nanoscale Res Lett</u> 6 (2011): 9.

2. Chinnathambi, Shanmugavel, and Shirahata, Naoto. "Recent advances on fluorescent biomarkers of near-infrared quantum dots for in vitro and in vivo imaging." <u>Science and technology of advanced materials</u> 20 (2019): 337-355.

Curriculum Vitae

Name: Mohammed Abdelhameed

Post-secondary   Assiut University
Education and   Assiut, Egypt
Degrees: 2005-2009; B.Sc. in Chemistry

Sherbrooke University
Sherbrooke, Quebec, Canada
2011-2014; M.Sc. in Chemistry

University of Western Ontario
London, Ontario, Canada
2015-2019; Ph.D. in Chemical & Biochemical Engineering

Honours and Awards:
2019: Best Presenter in the Three Minute Thesis competition (3MT) in the department of Chemical Engineering.
2018: Ontario Graduate Scholarship (OGS).
May 2015 – April 2019: Western Graduate Research Scholarship.
September 2011 – June 2014: Graduate Research Scholarship at University of Sherbrooke.

Related Work Experience
1. Teaching Assistant for:
09/2018 - 12/2018: Organic Chemistry course (CBE 2206); **01/2018 – 04/2018:** Energy and Society course (CBE 4485); **09/2017 - 12/2017:** Heat Transfer course (CBE 3322); **09/2016 – 04/2017:** Chemical Engineering Project Course (CBE 4415).
2. Research Assistant
09/2010-08/2011: Assiut University, Egypt

Publications:

1- **Abdelhameed, M.,** Aly, S., Maity, P., Manni, E., Mohammed, O. F., Charpentier, P. C., *Controlling Surface-defect-state Photoluminescence in Ultra-Small Silicon Quantum Dots Via Spacers, To be* submitted to ACS Nano.

2- **Abdelhameed, M.,** Aly, S., Maity, P., Kazi, F., Mohammed, O. F., Charpentier, P. C., *Impact of the Chemical Nature and Position of Spacers on Controlling the Optical Properties of Silicon Quantum Dots, Accepted in PCCP.*

3- **Abdelhameed, M.,** Aly, S., Lant, J., Zhang, X. & Charpentier, P. (2018), *Energy/Electron Transfer Switch for Controlling Optical Properties of Silicon Quantum Dots,* Scientific Reports, 8 (17068).

4- **Abdelhameed, M.,** Martir, D, Chen, S., Xu, W., Oyeneye, O., Chakrabarti, S., Zysman-Colman, E. & Charpentier, P. (2018), *Tuning the Optical Properties of Silicon Quantum Dots via Surface Functionalization with Conjugated Aromatic Fluorophores,* Scientific Reports, 8 (3050) <u>Top 100 in Chemistry in 2018</u>.

5- **Abdelhameed, M.,** Langlois, A., Fortin, D., Karsenti, P.-L., & Harvey, P. D. (2014) *A drastic substituent effect on the emission properties of quinone diimine models and valuable insight into the excited states of emeraldine,* Chemical Communications, 50 (11214).

6- **Abdelhameed, M.,** Langlois, A., Karsenti, P.-L., Richeter, S., Ruppert, R., & Harvey, P. D. (2014), *Ultrafast energy transfer in a Pd(ii)-bridged bisporphyrin dyad*, Chemical Communications, 50 (14609).

7- **Abdelhameed, M.,** Karsenti, P.-L., Langlois, A., Lefebvre, J.-F., Richeter, S., Ruppert, R., & Harvey, P. D. (2014), *Unexpected Drastic Decrease in the Excited-State Electronic Communication between Porphyrin Chromophores Covalently Linked by a Palladium(II) Bridge,* Chemistry – A European Journal, 20 (12988).

8- **Mohammed Abdelhameed** *Charge and Energy Transfer in Porphyrin Dyads And Oligomers,* (2014), Université de Sherbrooke.

9- Xu, H.-J., Bonnot, A., Karsenti, P. L., Langlois, A., **Abdelhameed, M**., Barbe, J.-M., Gros, C. and Harvey, P. (2014), Antenna *effects in truxene-bridged BODIPY triarylzinc(II)porphyrin dyads: evidence for a dual Dexter–Förster mechanism,* Dalton Trans., **43** (8219).

10- Soliman, A., **Abdelhameed, M.,** Zysman-Coleman, E. and Harvey, P. (2013), *Monitoring the On/Off Switching of the Electronic Communication in Diethynyl platinum(II)-bridged Dyads Using Triplet Energy Transfer,* Chemical Communications, 49 (5544).

Conference Papers

1- ACS Fall 2019 National Meeting & Exposition in San Diego, CA, August 25 - 29, 2019. Impact of spacers on controlling the optical properties of silicon quantum dots: Fluorescein dyad. **Mohammed Abdelhameed**, Devin Machin, Paul Charpentier

2- ACS Fall 2019 National Meeting & Exposition in San Diego, CA, August 25 - 29, 2019. Role of spacers towards directing the interactions in silicon quantum dots: Fluorescein dyads. **Mohammed Abdelhameed**, Shawkat Aly, Devin D Machin, Paul Charpentier

3- 1st National conference: Converging on Nanomanufacturing, Canada, September 25-26, 2017. Biomedical Applications of Silicon Quantum Dots. **Mohammed Abdelhameed** and Paul Charpentier.

4- 100th Canadian Chemistry Conference, Toronto, Canada, May 28 - June 1, 2017. Silicon Quantum Dots: Towards Fluorescent Cellular Imaging Applications. **Mohammed Abdelhameed** and Paul Charpentier.

5- 9th CSACS, Concordia University, Canada, September 12th, 2013. Di(imine(tetraarylzinc(II)porphyrin))di-α-(amine (tetraarylzinc(II) porphyrin)) quinone as a Model for Conjugated and Unconjugated Porphyrin Dye Polymers. **Mohammed Abdelhameed** and Pierre D. Harvey.

6- 5e Colloque annuel du CQMF, Canada, November 2nd, 2012. Synthesis, Characterization and Photophysical Properties of Bridged Organometallic Dyads. Tripler Energy Transfers in a [Ir]+-[Pt]-(Zn(II)porphyrin) species. **Mohammed Abdelhameed**, Ahmed Soliman, Eli Zysman- Colman, Pierre D. Harvey.